

A Perspective on Conventional High-Temperature Superconductors at High Pressure: Methods and Materials

José A. Flores-Livas^a, Lilia Boeri^b, Antonio Sanna^c, Gianni Profeta^d, Ryotaro Arita^{e,f}, Mikhail Eremets^g

^aDepartment of Physics, Universität Basel, Klingelbergstr. 82, 4056 Basel, Switzerland

^bDepartment of Physics, Sapienza Università di Roma, Italy

^cMax-Planck Institute of Microstructure Physics, Weinberg 2, 06120 Halle, Germany

^dDipartimento di Fisica Università degli Studi di L'Aquila and SPIN-CNR, I-67100 L'Aquila, Italy

^eDepartment of Applied Physics, Hongo Bunkyo-ku, 113-8656, Japan

^fRIKEN Center for Emergent Matter Science, 2-1 Hirosawa, Wako, 351-0198, Japan

^gMax-Planck Institute for Chemistry, Hahn-Meitner-Weg 1 55128 Mainz, Germany

Abstract

Two hydrogen-rich materials: H_3S and LaH_{10} , synthesized at *megabar* pressures have revolutionized the field of superconductivity by providing a first glimpse into the solution for the hundred-year-old problem of room-temperature superconductivity. The mechanism governing these exceptional superconductors is the *conventional* electron-phonon coupling. Here, we describe recent advances in experimental techniques, superconductivity theory and first-principles computational methods, which made this discovery possible. The aim of this work is to provide an up-to-date compendium of the available results on superconducting hydrides and explain the synergy of different methodologies that led to the extraordinary discoveries in the field. Furthermore, in an attempt to evidence empirical rules governing superconductivity in binary hydrides under pressure, we discuss general trends in electronic structure and chemical bonding. The last part of the Review introduces possible strategies to optimize pressure and transition temperatures in conventional superconducting materials. Directions for future research in areas of theory, computational methods and high-pressure experiments are proposed, in order to advance our understanding of superconductivity.

Keywords: High-pressure chemistry, Hydrides, Conventional superconductivity, Density-functional theory, Structure prediction

Contents

1	Introduction	2		
2	Experimental methods: High pressure Physics	6		
2.1	The diamond anvil cell	7		
2.1.1	Diamond anvils	7		
2.1.2	Gasket preparation	8		
2.1.3	Pressure measurements	9		
2.1.4	Low-temperature loading	9		
2.2	Superconductivity in sulfur-hydrogen compounds	10		
2.2.1	Sample preparation	12		
2.2.2	Raman measurements	12		
2.2.3	Electrical measurements	12		
2.2.4	Measurements in magnetic field	13		
2.3	Superconductivity in PH_x and LaH_x Hydrides .	14		
3	Theoretical Methods for superconductivity	15		
3.1	Phonons and electron phonon coupling	15		
3.1.1	Phonons	15		
3.1.2	Density Functional Theory	15		
3.1.3	Electron-phonon interaction	16		
3.1.4	Anharmonic effects	16		
3.1.5	Dielectric Screening in Metals	18		
3.2	Formalism for conventional superconductivity .	19		
3.2.1	BCS theory	19		
			3.2.2	Éliashberg Theory 20
			3.2.3	Morel-Anderson theory 22
			3.2.4	Empirical models for Tc 22
			3.3	Density functional theory for superconductors . 23
			3.3.1	SCDFT Hamiltonian and OGK theorem 23
			3.3.2	The Kohn-Sham system 24
			3.3.3	Electron-phonon interaction 25
			3.3.4	Plasmon-Assisted Superconductivity . . 26
4	Computational methods for structural prediction	26		
4.1	<i>Ab-initio</i> crystal structure prediction	26		
4.1.1	Potential energy surface	27		
4.1.2	Methods to explore structures	27		
4.2	Convex hull and phase diagrams	31		
4.3	First principles calculations	33		
5	Trends on hydrides under pressure	36		
5.1	Periodic table of binary hydrides	37		
5.1.1	Superconducting hydrides	37		
5.1.2	Non-superconducting hydrides	39		
5.2	Overview of selected hydrides	39		
5.2.1	Palladium hydride	40		
5.2.2	Phosphorus hydride	42		
5.2.3	Sulfur hydride	43		
5.2.4	Lanthanum hydride	45		
5.2.5	Elemental hydrogen at HP	47		

5.3	Summary	47
6	Discussion and Perspectives	49
6.1	Chemical space of hydrides	49
6.2	Optimizing T_c and pressure in hydrides	50
6.3	Searches on other superconductors	51
6.4	Theoretical and experimental outlook	52
7	Conclusions	53

1. Introduction

A new era of superconductivity was initiated by the discovery of high-temperature conventional superconductivity in H_3S [1] and LaH_{10} [2, 3]. These major breakthroughs were enabled by an unprecedented synergy between high-pressure experiments, theoretical methods and computational tools, which are likely to bring many new discoveries in coming years. This Review is meant to offer an up-to-date perspective on the new, exciting field of high-temperature conventional superconductivity in hydrides at high pressure.

When, the Nobel laureate V. L. Ginzburg was asked “*What problems of physics and astrophysics seem now to be especially important and interesting?*”, *Room-temperature Superconductivity* and *Metallic Hydrogen* appeared as number two and three on his list [4, 5]. Both problems had challenged and fascinated solid-state physicists for almost a century and appeared still unsolvable. Thirty years later the picture has changed and a path towards their solution has been elucidated, bringing to a common ground: the high pressure hydrides.

That hydrogen could exhibit a *metallic solid* phase was speculated by Wigner and Huntington [6] in mid 30’s and the possibility that a metallic solid-hydrogen could exhibit superconductivity close to, or even higher than, room temperature was discussed by Neil Ashcroft and independently, Vitaly Ginzburg [7, 8] in late 60’s. However only recently, thanks to advances in theoretical and experimental techniques, it has been possible to make the crucial step from general arguments of plausible, to predictions and observations. In 2017 a (still controversial) report of a solid metallic phase has appeared in literature [9]. The observed critical pressure is consistent to that predicted by the most accurate available theoretical calculations i.e. 400 GPa [10]. Although, this pressure is still challenging to reach in laboratories, it is common in the core of celestial bodies, as now it is well established [11] that a large portion of Jupiter’s core is formed by hydrogen in a *metallic liquid state*.

At lower pressure an alternative route to high temperature hydrogenic superconductivity has been found through the idea of *chemical precompression* of the hydrogen sub-lattice in hydride materials [12, 13]. As a consequence, in 2018, a new record of superconducting transition temperature (T_c) of $-23^\circ C$ [2, 3] was reported in a hydrogen-rich solid, LaH_{10} . Superconductivity at room temperature, which is conventionally set at 300 K ($27^\circ C$), is only $50^\circ C$ away.

What makes solid hydrogen and high-pressure hydrides different from previously-known superconductors? In contrast to previous record-holders superconductors, cuprates and Fe-based superconductors, where the high T_c are most likely due to a complex interplay between charge, spin and orbital fluctuation and lattice vibrations (vibrations), superconductivity in hydrides is described by the *conventional* theory for superconductivity. What is different, however, are the superconducting parameters that determine critical temperatures, that are exceptional compared to all previously study compounds. This is due to the extreme pressure that allows to stabilize chemical environments which would not exist spontaneously at ambient pressure (*forbidden chemistry*).

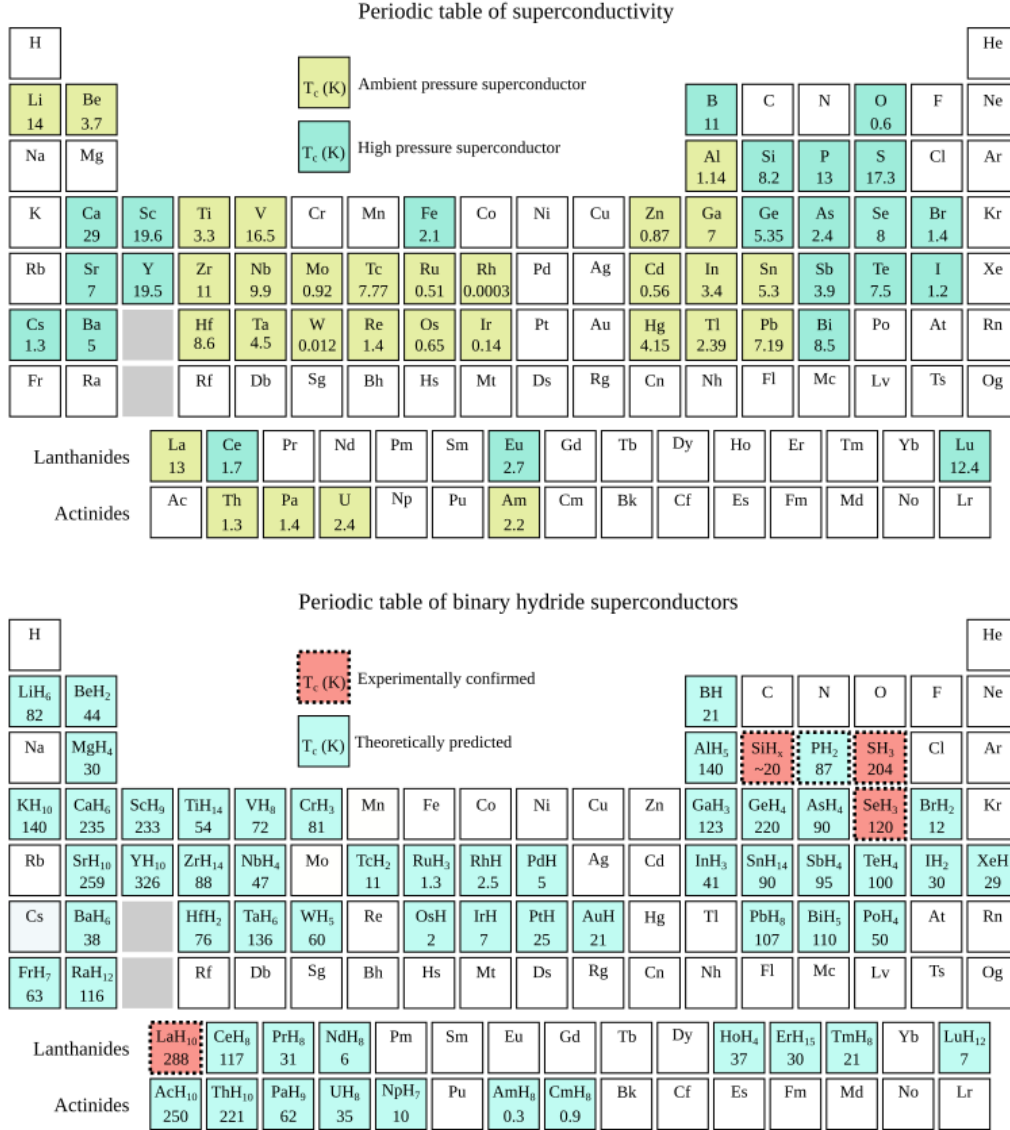


Figure 1: Top: Periodic table of superconducting elements (experimental transition temperature of superconductivity, T_c) is indicated. Bottom: Periodic table of superconducting binary hydrides (0–300 GPa). Theoretical predictions are indicated in blue and experimental results in red.

Before delving longer into the problem of superconductivity, we briefly introduce a few key concepts and definitions related to pressure, which will be one of the key actors of this Review. Pressure (p) is a thermodynamic quantity which plays an important role in modifying the properties of substances; for example, it can turn most semiconductors into metals. In this Review, we will distinguish two regimes: the first, *high-pressure*, extends from 1 to 100 gigapascals (GPa); the second, *megabar pressure*, from 100 GPa to the teraPascal range (1,000 GPa or 1 TPa). For comparison, 1 GPa is equivalent to 10,000 bar, or 9869 atmospheres. Thus, a pressure of 100 GPa (1 Mbar) equals roughly one million times the atmospheric pressure. Pressures in the megabar range are typically found in the interior of the planets: for example, the pressure in the core of the Earth ranges from 330 to 360 GPa [14], while that in Jupiter's core is estimated to be above 1 TPa.

In order to understand how a solid can change when it is subject to megabar pressures, let us consider a substance that is compressed at 200 GPa (2 Mbar). In most solids, this would correspond to a volume reduction of a factor of 1.5. The volume reduction can be drastically larger for gases [15], for instance, the volume of solid hydrogen is reduced by 10 times [16]. One can also estimate the free-energy change of the system induced by such a compression. For this range of pressures, the pV term in the Gibbs free-energy, $G = E + pV - TS$ can be of the order of 10 eV per two atoms, i.e. it can easily exceed the bond energy of any chemical bond at zero pressure [17, 18, 19]. In other words meaning, in the megabar range of pressures the order of chemical bonds may be drastically altered or even new bonds may be formed. These arguments can provide a first hint on how high pressure may produce materials with physical and chemical properties different from ambient pressure and hence

help to shed light on problems like the search for room temperature superconductivity.

The quest for room-temperature superconductivity is a rather old one. The first ever measured superconductor, found by H. K. Onnes in 1911 [20], was mercury (Hg), an elemental substance that possesses a very low- $T_c \sim 4.2$ K. Such low temperatures require helium cooling which is rather expensive, while exploiting the characteristic properties of superconductors (vanishing resistivity, perfect diamagnetism) for large scale applications would require materials with a substantially larger T_c . More than a century have passed and the field have continuously evolved delivering materials with higher and higher T_c s. However, the evolution has not been at a constant rate; for more than 60 years (1911-1975), the maximum critical temperature was slowly increased with a rate of ~ 0.3 K/year, until a maximum T_c of 23.2 K was measured in an alloy of Nb and Ge (Nb_3Ge) [21].

Higher values of T_c seemed impossible to achieve that even in 1972 Cohen and Anderson postulated that a hard limit of 25 K must exist for conventional superconductors [22]. This idea was based on several misconceptions on material properties and stability limits, and seemed to be supported experimentally by not being able to measure a higher T_c . It had a long-lasting impact and it was detrimental to progress on the field for decades. It was definitely disproven at the turn of the 21st century by three important discoveries: I) superconductivity at 39 K in MgB_2 [23], II) high- T_c superconductivity at 203 K in H_3S [1], III) and near room-temperature superconductivity at 250 K in LaH_{10} [2, 3] – High- T_c cuprates, discovered in 1986 (max $T_c=133$ K [24]), and iron-based superconductors, discovered in 2006 (Ref. [25, 26] max $T_c=100$ K), technically do not contradict the Cohen-Anderson limit, since superconductivity is not of conventional electron-phonon interaction.

Empirical arguments such as the Cohen-Anderson limit (and former Matthia's rules [27]), became obsolete once accurate methods for calculating electron-phonon spectra of materials from first-principles became available towards the end of the 90's [28].

Indeed, the lack of a predictive theory for superconductivity was probably the main limiting factor to the discovery of new superconductors in the last century. In 1966, Ted Geballe, after discovering a new record compound, with a record T_c of 20 K, evidenced that "there is no theory whatsoever for high-transition temperature of a superconductor" [29]. This statement is founded by a misconception and do not reflect the evolution of the field. In fact, a fully mature microscopic theory of superconductivity had been already since the 60's. The BCS theory of superconductivity (1957) states that electrons in *conventional* superconductors are pairwise coupled via excitations of bosonic character such as phonons (lattice vibrations) [30]. The BCS theory assumes an instantaneous interaction between electrons and enables us to describe quantitatively only a few, low-temperature superconductors. On the other hand, its strong-coupling diagrammatic extension developed in the 60's, i.e. Migdal-Éliashberg theory [31], succeeded in explaining experimental data for all superconductors known at the time, assuming a phonon-mediated interaction between

electrons. However, at the time, Migdal-Éliashberg theory was essentially a semi-phenomenological theory, because its basic ingredient, i.e. the electron-phonon spectral function, could not be estimated *a priori* for a given material, but only indirectly extracted from experiments. Thus, one could describe at that time, to a great accuracy an existing superconductor but not predict whether a given material would be a good (high T_c) or bad (low T_c) superconductor.

The situation has definitely changed in this century, thanks to the development of quantitative methods for superconductivity, based on Density Functional Theory [32, 33, 34]. To understand how accurate and reliable current theoretical methods for conventional superconductors are, let us look at the periodic table of superconductivity (top) in Fig. 1. Colored in yellow are elements showing superconductivity at ambient pressure and colored in blue are elements showing superconductivity under pressure. If one used computational-theoretical methods on these 53 superconducting elements to estimate the value of T_c and compares it with the experimental value, one would find that the deviation is less 1 K% [34]. This accuracy was possible thanks to years of developments in the field of superconductivity and computational methods.

A big leap in this direction came from the report of a T_c of 39 K in MgB_2 in 2001 [23]. Although its critical temperature was not spectacular, compared to the record T_c of the cuprates, MgB_2 posses several aspects which had a major impact on the future development of the field: i) superconductivity is of conventional (electron-phonon) origin; ii) T_c is distinctively higher than the Cohen-Anderson limit; iii) from a material perspective, MgB_2 is chemically very simple and differs from the best conventional superconductors known until that time, which all contained heavy transition metals, such as vanadium or niobium. Being formed by magnesium and boron, two of the lightest elements of the periodic table, MgB_2 was a rare example of covalent metal [35] in which (relatively) high- T_c superconductivity could be obtained exploiting high phonon frequencies and large electron-phonon matrix elements.

Superconductivity arising from light-element based compounds was not new or particularly original idea. In fact, from a purely technical point of view, Migdal-Éliashberg theory does not pose an upper or lower bound of temperature for the emergence of superconductivity and even suggests compounds with light elements as the most obvious candidates for conventional superconductivity. Indeed, metallic hydrogen had been proposed to be a high- T_c superconductor as early as 1968. However, experience had shown that at ambient pressure most light-element compounds are insulating, while conventional superconductivity requires a good metallic ground state. Metallic hydrides at ambient pressure, which were extensively studied during the 70's, on what we call the *first hydride rush* in Fig. 2, achieved maximum T_c 's around 16.6 K, i.e. falling just below the Cohen-Anderson limit.

Covalent metals like MgB_2 are extremely rare at ambient pressure but, as we have seen, megabar pressures can strongly modify the properties of materials and in particular induce an insulator-to-metal transition in many substances. In 2004, Neil Ashcroft realized that the progress in high-pressure techniques,

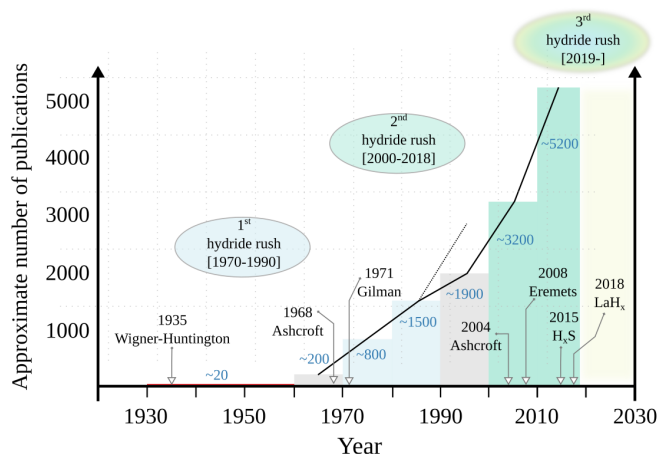


Figure 2: Approximate number of publications in the field of hydrides per decade. The first hydride rush took place right after Ashcroft’s and Ginzburg’s prediction of high- T_c superconductivity in hydrogen at the end of the 60’s [7, 8]. The second hydride rush started at the dawn of the 2000’s and the third is starting now (2019) with the discovery of LaH₁₀ [2, 3] and will continue through the following decade. The expected number of publications in the field by the year 2030 is 10,000.

compared to the 70’s was such, that covalent hydrides could now be compressed to pressure so high to make them metallic, realizing an effective chemical precompression of the hydrogen sublattice [12]. Although history proceeded otherwise, we believe that the origins of ‘chemical precompression’ dates back to 1971, when J. Gilman studied the possibility of making a new form of hydrogen in a metallic state through preparation of a covalent compound, LiH₂F under pressure [13].

The *second hydride rush* (see Fig. 2) started at the dawn of the 2000’s and was characterized by an extremely fast progress. The first metallic covalent hydride, SiH_x was metallized in 2008 [36]; the first high- T_c high-pressure hydride, H₃S with a record T_c of 203 K was discovered in 2015 [1] and LaH₁₀ with a T_c of 250 K came three years later [2, 3]. Furthermore, the breakthrough discoveries of H₃S and LaH₁₀, followed a completely different circumstance from all previous superconductor discoveries, i.e. they were the result of precise experimentation guided by accurate theoretical predictions – a full account of the circumstances is given in Sec. 2.

How did this change of perspective occur? We mentioned previously that the possibility of predicting accurate critical temperatures (T_c) from first principles played a major role. Equally crucial was the development of computational tools to predict crystal structures and phase diagrams of materials under given thermodynamical conditions, which was one of the most pressing open challenges for theoretical material design [37].

To have an idea of the rapid progress in the field of superconductivity in high-pressure hydrides enabled by theoretical/computational methods for superconductivity and crystal structure prediction, the reader is urged to take a look at the lower panel of Fig. 1, the periodic table of superconducting binary hydrides, which collects existing theoretical predictions. For each element, we show only compositions with the highest- T_c predicted in the range of 0 to 300 GPa (see Appendix for

information on references). We count only 61 superconducting binary hydrides but to compile this table many different pressures and compositions were analyzed, accounting to at least ten times as many distinct compounds. In red, we highlight those elements that form a hydride for which a superconducting transition under pressure has been experimentally measured (silicon, sulfur, selenium, phosphorus, lanthanum). Note that all measurements and predictions reported in the table were performed in the last ten years, and most of them in the last five.

Compared to the progress in the last century, the rate of material discovery in the last ten years is impressive. Given the complexity of high-pressure experiments compared to theoretical calculations, it is not surprising that predictions largely outnumber experimental realizations. For those hydrides where superconductivity has actually been measured, the agreement between theory and experiments is remarkably good (see Sec. 5). This makes of predictions extremely valuable, since they allow to focus experimental research on specific, pin-pointed chemical compositions and in some cases they also suggest favorable thermodynamic conditions. Undoubtedly, we are currently witnessing the beginning of a new era of superconductivity. Hydrogen-rich materials are perhaps the most promising materials to deliver exciting discoveries in the field of superconductivity, having already provided glimpses onto room-temperature superconductivity ($T_c = -23^\circ\text{C}$). Our periodic table of superconducting binary hydrides shows that predictions of even higher T_c exist. Furthermore, the phase space left to explore is huge: ternary, quaternary and complex hydrides are still unexplored. A *third hydride rush* is likely to open at this point and will reserve many more surprises.

Fig. 2 summarizes the progress of the field of ‘hydrides’, from mid 30’s (Wigner-Huntington’s paper) to 2019. The ordinate axis (y) shows the approximate number of publications per decade (see Appendix for details). Although, it is technically very challenging to filter the exact number articles, these numbers serve as a good estimate of size and importance of the field. Between 1930 to 1960 the number of published articles related to superconducting or metallic hydrides is of the order of few tens. By the 70’s this number has increased to several hundreds publications and it doubled during the 80’s (*first hydride rush*). The research on hydride-superconductors was eclipsed at the end of the 80’s by the discovery of unconventional high- T_c cuprates [38]. Consequently, during the 90’s the number of publications did not grow as expected (≈ 3000) and the field survived because hydrides appeared in other research context, predominantly as energy materials. It was eventually revived at the beginning of 2000’s thanks to maturity of high pressure techniques and by Gilman-Ashcroft’s bold idea of chemical precompression [13]. More recently (2008-2018) the high pressure hydride research was fueled by the experimental work of Eremets and collaborators (*second hydride rush*). The discovery of LaH₁₀ will likely trigger the (*third hydride rush*) on the field: from the current publication rate we can estimate that 10,000 publications will be published by the end of 2030.

Although unveiling a new, potentially huge class of high- T_c superconductors is extremely exciting, the identification of new routes for material discovery opened by highly accurate predic-

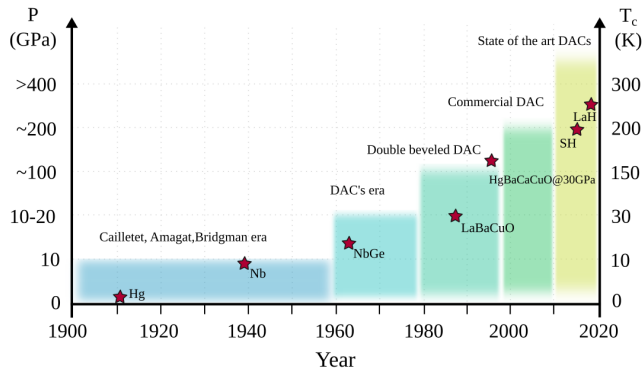


Figure 3: Landmarks of maximum pressure are depicted by coloured areas (left y-axis) achieved per year: from early stages (Bridgman era) to the revolutionizing use of diamond as anvil in late 50's to the state-of-the-art DACs. In the same context, stars (right y-axis) shows the evolution of transition temperature of superconductivity for representative materials that shaped the landscape of superconductivity.

tions has a much deeper meaning. This work is consecrated to review these theoretical tools, experimental techniques and methodologies that permitted to extend the range of pressures. These aspects have been overlooked in recent reviews in this field (see for instance Ref. [39, 40, 41, 42, 43, 44, 45]).

The structure of the Review is as follows. Sec. 2 reviews the most important developments in experiments including high-pressure techniques. In Sec. 3, we describe theoretical methods that made possible to understand the mechanism of superconductivity at various levels and approximations. The computational tools that are currently used to predict crystal structures and phase diagrams of hydrides and in general materials are discussed in Sec. 4.

The primary goal of this Review to analyze the past, present and future on the field of superconducting hydrides under pressure. In Sec. 5 we compiled a large number of studies, predictions and experimental results on these systems and analyzed representative examples of different classes of hydrides to understand their electronic structure and superconductivity features. Finally, in Sec. 6, perspectives are presented and different questions are addressed: how vast is the chemical space of hydrides? What are the best strategies to optimized hydrides under pressure? i.e. decrease pressure and maximize T_c ? Are there other systems, where similarly to high-pressure hydrides, high- T_c conventional superconductivity could be realized? The last part is consecrated to discuss what we believe are the future developments necessary in experimental techniques, theoretical models and computational tools to tackle the challenges ahead. It is the wish and hope of the authors that the Review will serve as reference point for this exciting and rapidly-changing field.

2. Experimental methods: High pressure Physics

High-pressure physics in its contemporary form started at the beginning of the 20th century with the pioneering work of Cailliet, Amagat and Bridgman [46]. The field has then evolved

through the last century, racing to reach higher and higher pressures with a rate that, as shown in Fig. 3, is surprisingly parallel to the increase of the maximum critical temperatures in superconductors.

Bridgman's heavy, metal-made and gross anvils dominated high pressure experiments for almost fifty years until a new era started in 1959 when diamond was used for the first time as an anvil by Wier, Van Valkenburg, Bunting and Lippincott [47]. This experiment introduced the diamond anvil cell (DAC) and marked the beginning of an era that will radically change the landscape of high pressure [48]. Not only because higher pressures were allowed, although limited to about 20 GPa in these early devices, but also because the new device permitted to have *in-situ* characterization with spectroscopic techniques (being diamond transparent to a wide range of the electromagnetic spectrum).

A further advancement in DACs took place in 1978 when Mao-Bell [49] introduced beveled diamond anvils, cracking the limit of 100 GPa static pressure. The full maturity of the DAC technology has been reached in the mid-90s with the raise of commercial DACs. These have introduced a large array of characterization techniques and transformed the DAC from an exotic device, available only in a handful of centers world-wide, to a universal tool accessible to standard laboratories. By the year 2000s, pressures up to 200 GPa could be reached routinely and a number of applications had been published, improving significantly our understanding of matter under extreme compression [50, 51]

One of the first accomplishment of systematic investigations at high pressure has been to map the structural phase transformation and emergence of superconductivity in elements under strong compression [52, 53, 54, 55]. Among the first studies showing that the rules of chemistry change with applied pressure in unexpected ways, was the study of a simple diatomic molecules, oxygen, which was of particular interest because it shows magnetism at low temperatures. Under pressures exceeding 95 GPa, solid molecular oxygen becomes metallic [56] and superconducting with T_c of 0.6 K [57].

At ambient pressure there are 29 elemental superconductors in the periodic table, none of which is an alkali metal [58]. The first alkali metal discovered to become superconducting under pressure was Cs [59], followed years later by Li [60, 61, 62, 63]. In fact, years later Li was confirmed to be a superconductor at ambient pressure but at mere 0.4 mK [64]. Alkali metals are exemplary free-electron systems and it is surprising and yet counter-intuitive that under pressure they exhibit marked deviations from free-electron behaviour, whereas one would expect that with pressure bands should widen and gaps close, leading in general to an ubiquitous metallic behaviour [65, 66, 67]. Alkali metals represented a fertile ground of research for scientist in late 90's to early 2000's to study the exotic chemistry under pressure, and superconductivity is still one of their most fascinating properties.

Among Group-V elements, for instance boron is particularly interesting: in 2001 with the report of T_c of 11.2 K at 250 GPa it set a record pressure for both electrical conductivity studies and investigations of superconductivity in dense matter [68]. Ca is

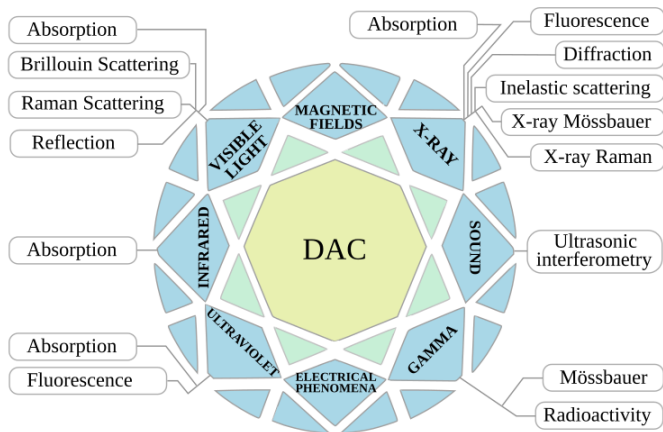


Figure 4: Diamond anvil cell (DAC) is a universal tool essential to high pressure physics that can be combined with large number of spectroscopy techniques and *in situ* characterization of electrical and magnetic properties.

the element with the highest ever measured T_c that under pressure reaches 29 K [69, 70]. Interestingly, yttrium possesses also a high- T_c at substantially lower pressures [71]. Other elements that show superconductivity upon compression are phosphorus [72, 73, 74], which at ambient conditions exhibit a complex phase diagram [75, 76, 77, 78] and under pressure shows a more simpler cubic structure [79, 80]. Other elements that undergo a long sequence of phase transformations are chalcogens [81] (sulfur [82, 83, 84] and selenium [85, 86], carbon [87, 88], rubidium [89], barium [90, 91] and rhenium [92] to name a few [55].

Arguably, one of the most interesting surprises of high pressure chemistry/physics [93, 94] of materials has been the discovery that superconductivity becomes *more common* under pressure, and occurs with substantially higher critical temperatures [39, 40, 41, 42, 43]. After this brief compendium of selected examples of high-pressure phase-transformation and emergence of superconductivity in the elements, we explain in the following details on techniques and devices that made possible these discoveries.

2.1. The diamond anvil cell

The diamond anvil cell represents the icon [95, 96] of high pressure research. In order to keep the pace with science progress in other fields, its design and capabilities are continuously improving, attaining higher pressures and deeper levels of characterization [97, 98]. This tool allows to study matter at extreme conditions of density, which have implications for planetary, biology, chemistry and materials science [99, 100]. Fig. 4 summarizes the characterization techniques that can be combined with DAC. These cover a broad range of spectroscopy techniques [101, 102] and probes [103, 104, 105] including magnetic fields [106, 107, 108]. In addition modern DACs allow for synthesis and *in-situ* characterization within temperature range from milli to thousands Kelvin [109, 110, 100]. The working principle of a DAC used in high-pressure experiments is very simple: the sample is placed in-between two diamond

surfaces and squeezed. However, in more elaborated experiments, a DAC can have a large number of interacting parts and minuscule components. In its essence, a diamond anvil cell consists of a body of the cell (base of the cell, piston, cap with screws for increasing pressure and springs to control separation), anvil seats, diamond anvils, and a gasket. All these components are illustrated in Fig. 5. In particular the diamond geometry and the gasket are the crucial parts for the performance of the device. These will be discussed in the following sections, together with other key aspects such as pressure measurements and loading.

2.1.1. Diamond anvils

As the name indicates, diamonds are the principal components in DACs. Diamond is known as the hardest material to occur naturally. This material is perfect to serve as an anvil also because it provides a window to observe the sample and study its properties with electromagnetic radiation from the far IR to the UV. In fact, diamond is transparent to nearly all visible electromagnetic radiation (with weak absorption in the infrared range) and in the UV up to 220 nm (corresponding to its 5.5 eV band gap). There is in principle no lower limit for the frequencies of the radiation. The features of the DAC strongly depend on the properties of the diamonds used as anvils. Diamonds can be categorized by a) their origin (natural or synthetic), b) the amount and type of impurities and c) the diamond cut or shape of the culet (see right panel in Fig. 5). Natural diamonds are formed deep within the Earth below the core mantle at depths of 140 Km, while synthetic diamonds can be synthesized in laboratories at pressure of 10 GPa and temperatures in excess of 2500 °C (HPHT). Additionally, diamonds can also be grown with chemical vapor deposition (CVD) process from plasma at reduced pressures. Interestingly, diamonds from all three sources can be used in high-pressure experiments. Synthetic diamonds (both HPHT and CVD) can be grown very pure, i.e. flawless. Such defect-free synthetic diamonds are typically useful for IR studies as they have very low absorption, as well as for Raman studies as they have low or negligible luminescence. On the other hand, synthetic diamonds are currently the hardest known material.

Irrespective of the source, all diamonds are classified by the amount and character of impurities. In fact diamond can currently be doped only with small-size ions, such as H, Li, B, N, etc. The main impurity found in natural diamonds is nitrogen, the so-called NV-center. Boron can be also relatively easily incorporated experimentally in diamond, but boron-doped diamonds are rare in nature (they are known for its blue-pristine colour, which found mainly use in jewelry industry). Within the nitrogen-doped diamonds, there are two major type of families, distinguished by the number of nitrogen per million particles. Type-I contain nitrogen inclusions of more than 10 particles per million (ppm) and type-II (high purity) contain less than 10 ppm. On the other hand, synthetic diamonds contain impurities of Ni, Co or Fe, which are used as catalysts. As for CVD diamonds, they often contain H as impurity derived from the reactive hydrogen content plasma.

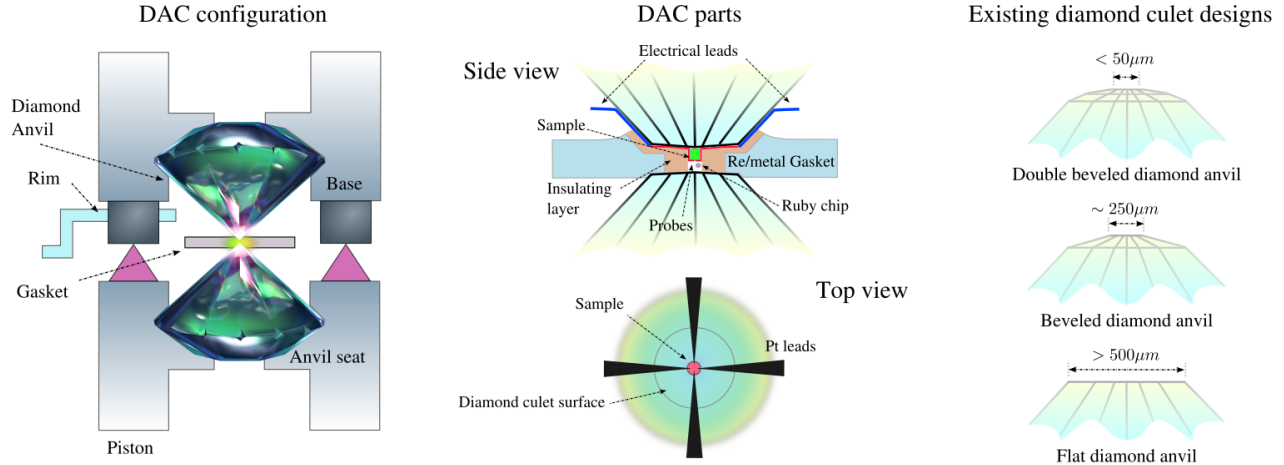


Figure 5: Left: schematic of DAC including anvil seats, gasket and pistons. Center: detailed design of a DAC for transport measurements under pressure. Right: types of diamond culets used for high pressure experiments. All drawings are not at scale.

Fig. 5 (center) shows in detail the essential parts that compose a DAC. Although its operating principle is simple and consists in bringing together two diamond surfaces, it requires highly precise machinery that work at micrometer accuracy. Piston-cylinder parts (left panel in Fig. 5) are crucial to pressurize and to control applied pressure and since diamond is a very brittle material it can be easily damaged during operation. Especially, any contact between the surfaces (diamond culet) should be avoided. Another crucial component are the anvil seats, these are made of a strong material because they are typically loaded with more than 1000 kG forces, which produce significant stress at the contact with the diamond anvils. Usually these seats are made from tungsten carbide, although for X-ray measurements, where a large aperture is crucial, seats can be made of boron nitride which is transparent to X-rays.

The first models of DAC used flat seats, until Boehler [111] introduced seats with conical support that offer great advantage over their former counterparts. They have a larger aperture for optical and X-ray measurements and diamonds are better protected once loaded (they are supported from the sides and not destroyed completely). Over years, mastering the cutting of diamonds in novel shapes and developments in surface (culet) preparation make it possible to expand the use of DAC to electrical and magnetic characterization at static pressures well above 200 GPa [112, 113, 114, 115, 116].

The future in DAC foresees many more developments, mainly on two fronts: I) focus ion beam techniques will play a fundamental role in DAC, permitting to sculpt futuristic micro-anvils ($< 20\mu\text{m}$) which will extend the range of pressure well above the 400 GPa, the ceiling pressure for one-stage DAC. Recently, micromilling gem-quality diamond tips shaped in toroidal form have been shown to greatly extend the accessible pressure up to ~ 550 to 600 GPa on DACs [117, 118, 119]. II) thanks to the advancements on characterization techniques such as new X-ray sources in synchrotron and X-ray free electron lasers, producing much brighter, sub- μm -beams will enable the study of compression volumes of only tenths of picolitres [116].

2.1.2. Gasket preparation

In the first DAC design, back in 1958, the sample was directly compressed between the two diamonds. It was in 1962 that Van Vakenbourg introduced the gasket in the high-pressure DAC technique. A gasket is a piece of metal sheet with a drilled hole for sample loading that brings a number of advantages: it allows to have a better control of the sample; it protects the diamonds from direct contact that may cause them to crack; it helps to develop a more homogeneous gradient of pressure across the sample by confining it in a relatively small area; it allows the possibility to add a chemical inert gas or a liquid as pressure transmitting medium (PTM), leading to near-hydrostatic conditions. In addition the gasket gives the possibility to load the DAC not only with solid samples, but also with samples that are gaseous at room pressure, like in the case of hydrides. The thickness of the gasket also plays a role in certain experiments, for instance on gaseous samples that are very compressible. A great number of experimentation has to be carried out before finding the ideal compromise between size and anvil geometry, specially culet sizes to find an ideal gasket thickness.

For electrical measurements it is necessary to introduce an insulating layer between the electrodes and the metallic gasket. The preparation of electrodes for electrical measurements is a crucial step in all high-pressure experiments. As alluded above the preparation of the insulating gasket and making of wires is not a standardized procedure and relies more on a trial-and-error approach. As a matter of fact different group have mastered their own approach to achieve the same experimental conditions.

In terms of electrodes for electrical measurements there are three different approaches. I) Manually crafted electrodes: for culets of than $100\mu\text{m}$ wide, the best compromise is to prepare electrodes made of platinum strips or other metallic foil and carefully place it in the DAC. This relatively simple approach was first introduced by Mao-Bell [120] and Shimizu et al. [61]. A clear disadvantage of this method is represented by the constraints on the size of the culet and of the measured sam-

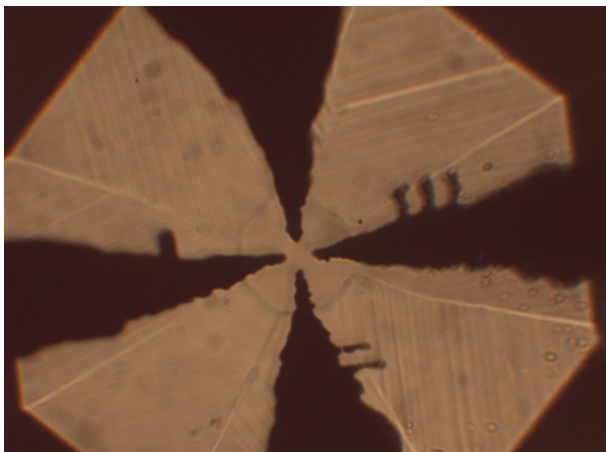


Figure 6: Micrograph taken using optical microscopy showing in detail the sputtered electrodes in DAC prepared for high pressure measurement in hydrogen-sulfide.

ple. Although it requires many attempts before the tiny strip by hand can be placed inside a culet of around $20\text{--}30\text{ }\mu\text{m}$, this approach has been shown to pay-off, see Eremets et al. [121]. II) Focused ion beam lithography: this is a more appropriate method for creating electrodes in tiny spaces. The technique consists of shaping metallic electrodes directly on the diamond surface with the aid of focused ion beam ultra-thin lithography. Recently, Rotundu et al. [122] have shown the capabilities of lithography and the possibility of reaching pressure of up to 240 GPa . The main advantage of this approach is the precision and control of the electrodes, while focused ion beam does not have practical limitations on the size of the culet. Deposition of the electrodes with this technique can provide precision down to 20 nm . It has been also shown that the created electrodes can sustain an indentation of the metal gasket. Unfortunately, this technique has a very high cost which makes it inaccessible to most laboratories. III) Sputtered electrodes: a third method is to sputter metals (Ti, Al, Ta, etc) to form ohmic contacts directly on the diamond culet. This technology has been proven to be robust and has worked since the pioneering works of Das [123], Evan [124], and Werner [125]. In practice the electrodes are made with the aid of a mask with four slits which cover the diamond culet. In some of the experiments in which one of us (ME) reported superconductivity in the H-S systems (see Sec. 2.2) a mask of aluminum foil was used. The diamond surface was first ion-etched for $30\text{--}40$ seconds and subsequently sputtered to form ohmic contacts.

After this, metal contacts must be covered with gold or platinum to protect electrodes from oxidation. In our experiments, see in detail the electrodes in final assembling in a DAC in Fig. 6, the resistance in the electrodes is about $100\text{ }\Omega$ which is suitable for detecting any change upon temperature. The sputtered electrodes can be connected externally outside the DAC with copper wires, platinum foil or silver paint. It is important to mention that the sputtered electrodes adhere conveniently to the surface of diamond, however, they last a maximum of 2 to 4 weeks, after this period resistivity increases dramatically.

2.1.3. Pressure measurements

The most reliable procedure to measure pressures in the megabar region is to determine the volume of a known material and use their equation of state (EoS). The EoS of simple metals or other FCC compounds (NaCl, Au, Pt, Re) have been determined from shock-wave experiments and are a reliable pressure scale. The main disadvantage of this method is that it requires a X-ray measurements typically at synchrotron sources. In the low-pressure regime a much more convenient technique for experimentation is to determine the pressure using the luminescence of ruby chips. This technique was first introduced by Forman et al. [126] using a small ruby. The sharp-line (R-line) luminescence of ruby shift under pressure was calibrated against EoS and found to move constantly up to 100 GPa with high reproducibility. As ruby is chemically inert and micrometer-size it can produce a good signal. This technique has been a real breakthrough in the high-pressure community and made possible to conduct high pressure experiments with DAC in standard laboratories without accessing X-ray sources.

To estimate the pressure beyond the 100 GPa limit alternative methods are used. For long time it has been known that the Raman spectrum of the diamond anvil itself changes with pressure. While, theoretically, the Raman peak evolution of carbon structures is well documented [127]. Hanfland and Sayassen [128] reported in 1985 that the high-frequency diamond edge has a linear dependence on the pressure, up to 300 kbar (0.3 GPa). Back in those days, they concluded that this shift would be hardly used for determination of pressure mainly because the stresses at the tip of the loaded anvils are highly nonuniform and strongly depend on the geometry of the anvils, gasket etc. However, the accumulated experience showed that in fact the pressure dependence of the diamond edge is surprisingly universal and can be used for a reliable estimation of pressure. This pressure scale was introduced in 2003 by one of us (ME) [129] and subsequently extended for pressures up to 410 GPa by Akahama et al. [130, 131]. Akahama also extended the study and analyzed differently orientations in diamonds, the typical $[0001]$ of the anvil axis but also $[0111]$ and $[0110]$ [132]. This scale became important for determination of pressure at the megabar range of pressures.

2.1.4. Low-temperature loading

A large number of interesting systems in the hydride family are gases at ambient temperature which complicates the loading of sample into DAC. A special loading procedure is then required for H_2S , PH_3 and LaH_2 , and we describe it in the following. To prevent decomposition during loading, it is necessary to perform it at low temperatures. For this the diamond anvil cell is placed into a cryostat and cooled down (with liquid He), to a temperature where most of the samples transform to their liquid phase. The left panel in Fig. 5 shows the inlet (rim) that introduces the gas into the chamber through a capillary. At room temperature, the piston is moved close to the base at a distance about $100\text{ }\mu\text{m}$ between the two anvils. Before loading, the air from this space should be pumped out through capillaries. To close any possible leaks at low temperature, the pistons are moved closer to the base up to a distance of about

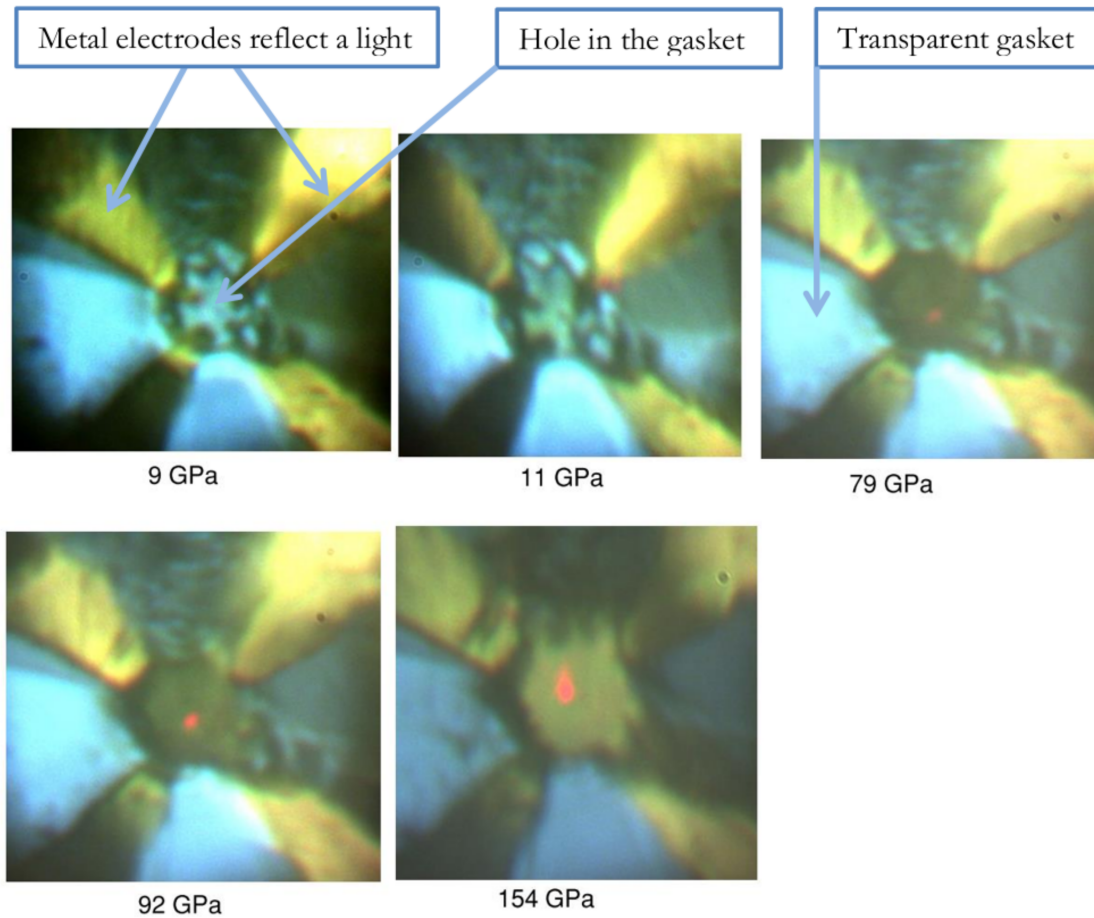


Figure 7: Micrographs taken using optical microscopy during the transformation of the sample upon compression. Images are obtained with transmitting and reflective light simultaneously. Blue parts indicate the optically transparent gasket. Yellow represents a reflection from the metal electrodes. The sample is transparent at 9 GPa. Darkening begins at about 11 GPa and the sample become opaque at pressure between 30–40 GPa. Weak reflection (on set of metallicity) starts to appear at 79 GPa. Reflection of the sample becomes comparable with electrodes reflection at about 150 GPa.

20-50 microns between anvils. At temperatures lower than the boiling point, gaseous samples are put into the rim where they become liquid and completely fill the space inside the rim, including the hole in the gasket. After this the sample can be clamped between the anvils and the gasket.

2.2. Superconductivity in sulfur-hydrogen compounds

In condensed matter and solid state physics, a substantial amount of research in the field of high pressure (post-Bridgman era) was triggered by the tantalizing idea of metallizing hydrogen (Wigner-Huntington [6] transition) which dates back to the mid 30's. The metallization of hydrogen is seen as the *holy-grail* of high pressure research and has been a compelling subject of interest for many scientists, ranging from experimental chemists and physicists [133, 134, 135, 9, 136, 137, 10], to theoreticians [138, 139, 140, 141]. However, despite the great advancement in high pressure-techniques and tools, the metallization of hydrogen in its solid phase has proved to be challenging [142, 143, 144, 145, 146, 147, 148, 149, 150, 151, 152].

The landscape in the field changed in 2004, when Ashcroft suggested chemically precompressed hydrogen-rich materials [12] as an alternative route to decrease the tremendous pressure necessary to metalize hydrogen. Eremets et al.[153] successfully proved the principle correct in 2008 by metallizing silane (SiH_4). Although subsequent studies attributed these results to probable decomposition or the existence of other stoichiometries [154, 155, 156, 157, 158, 159], this work remains the first solid evidence of superconductivity in chemically precompressed hydrides at high pressure.

Serendipity discovery of H_xS superconductors. *It is the wish of one of the authors (M.E.) to provide an accurate description of the context and circumstances that lead to the measurements of 190-200 K superconductivity in sulfur hydrides. Very often in scientific conferences, seminars, talks and practically in 90 % of the publications that followed this discovery, the events are described in wrong chronology.*

In fact, this important discovery was driven by serendipity much more than it is currently believed. Back in 2013-2014 my former PhD student, A. Drozdov, and myself started exper-

iments on H_2S following ideas proposed by Li et al. [160], on the possibility of metallization and superconductivity in dense hydrogen sulfide. This prediction seemed simple to verify experimentally, since highly pure liquid/gas of H_2S are almost freely available. Within one month of experiments we measured a $T_c \sim 55 \text{ K}$, a major result for those days, which was in agreement with the theoretical prediction that we were following. I would like to add as a side note, that at the time many shared a skeptical opinion about the possibility of achieving high- T_c in hydrides, and even doubted the driving mechanism for superconductivity.

Coming back to the main story-line, we continued with our experiments and surprisingly, with each experiment carried out we observed higher and higher T_c s (25, 60, 80 and then 120 K). A sudden decrease of resistivity at temperatures around 190 K occurred close to 150 GPa in one of our samples; we were blown away. This disheveled situation, which had not been predicted by theory, turned out to be more complicated to disentangle. We knew that it will be hard pass this result by plotting a resistivity drop at 200 K. The community is plagued by many claims of high- T_c materials, most of them of doubtful nature.

Therefore, we did not publish our first result but rather spent about 8 months complicating our experiments in order to understand the reason for such scattered values of T_c . Our main goal was to find a reliable and reproducible thermodynamic path to obtain T_c s of 190 K. This value was clearly at odds with Yanming Ma's group original prediction [160].

We came up with the guess that sulfur, known for its supervalency, could in principle bound more hydrogen atoms than in H_2S and presumably our samples have transformed to another hydride (H_4S or H_6S). We were preparing the manuscript and solving the issues on the isotope effect when Duan's paper appeared on line on November 10th, 2014 [161]. We uploaded our work to arXiv on December 1st, 2014 [162]. It is important to remark that in the version submitted to arXiv, we (M.E. et al.) kept our own original interpretation and that Duan's paper did not influenced our work in any aspect, perhaps only by accelerating our arXiv submission.

Note that, the calculated T_c amazingly coincided with our result. Computational and theoretical scientists linked immediately our observed superconductivity with the $\text{Im}\bar{3}\text{m}$ predicted structure. At that time, it was not obvious that the experimental and theoretical phases coincided, since we did not have X-ray data of the high- T_c samples. The almost simultaneous appearance of experimental and theoretical works tremendously accelerated the understanding of the T_c in this compound. We believe that the special circumstances surrounding the rush raised by a material with such a high T_c that saw within few weeks a theoretical and an experimental manuscript on the same subject, spread a rumor that the prediction of Duan's was first and our experiment followed, however that was clearly not the case.

In this section, we will briefly review some key aspects of the experimental work on sulfur hydride, focus on the emergence of superconductivity at high pressure. The phase diagram of hydrogen sulfide was first studied by Shimizu et al. [163] back in 1995, by Sakashita et al. [164] in 1997 and revisited by Fujihisa et al. [165] in 2004. H_2S is a typical molecular compound with

a rich phase diagram. Infrared studies under pressure show that hydrogen sulfide transforms to a metal at pressures of about 96 GPa [164]. The transformation is complicated by the partial dissociation of H_2S and the appearance of elemental sulfur at pressure larger than 27 GPa at room temperature. In principle one could attribute the metallization of hydrogen sulfide to disassociation in H and elemental sulfur, the later known to become metallic above 95 GPa [86]. It is worth mentioning that before 2014 there were no experiments or studies reported on hydrogen sulfide above 100 GPa.

Thanks to the advent of computational tools to explore energetically-stable crystal structures under pressure (see Sec. 4), this material was revisited by Li et al. [160]. Unexpectedly, the authors showed stable, metallic phases of H_2S , for pressures above 100 GPa, with superconducting temperatures of the order of $\sim 80 \text{ K}$ at 160 GPa. Most importantly, they showed that elemental decomposition into sulfur is highly unlikely, in apparent contradiction with previous experiments. To address this apparent disagreement between theory and experiment, back in 2014 we performed a series of experiments in order to stabilize the predicted phases of H_2S under pressure.

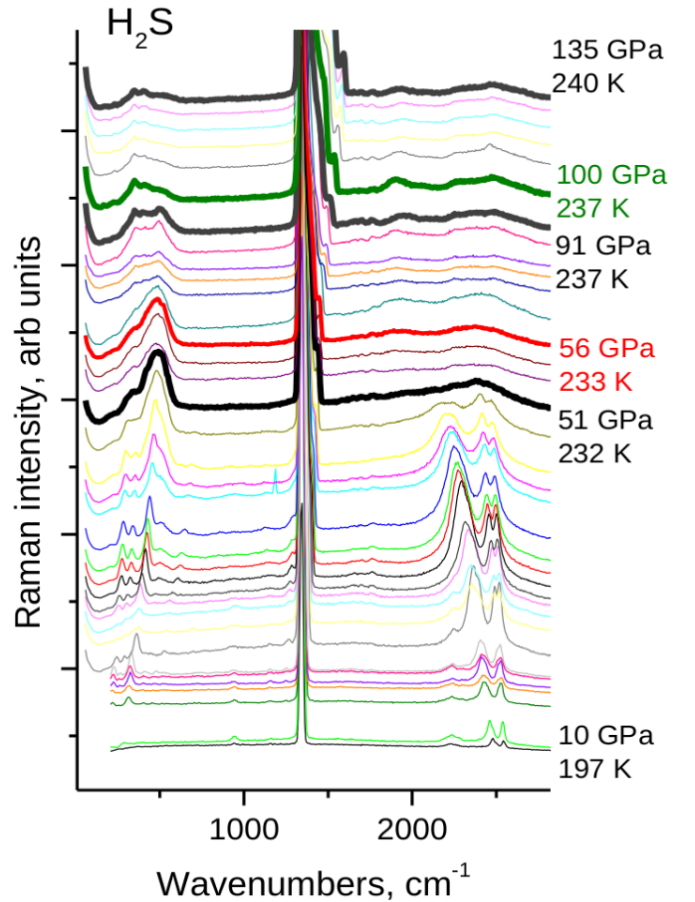


Figure 8: Spectra of sulfur hydride at increasing pressure at 230 K. Spectra are shifted with respect to each other for comparison. Phase transformation occurring at 51 GPa is marked by the disappearance the characteristic vibron peaks in the 2,100 – 2,500 (wave-numbers).

2.2.1. Sample preparation

In the H_2S experiments [1], the loading occurred in a cryostat at temperatures where hydrogen sulfide is liquid. The DAC was placed into a cryostat and cooled down to 191-213 K (within the temperature range of liquid H_2S) and then the H_2S gas was inserted in the chamber through a capillary into the rim around the diamond anvil where it liquified. H_2S and D_2S gases of 99,5% and 97% purity, respectively were used for all experiments. The filling of the chamber is monitored visually and the sample is identified by measuring Raman spectra (see Fig. 8). After clamping the DAC, the system was heated to 220 K to evaporate the rest of H_2S , and then pressure was increased typically at this temperature. Pressure remained stable during the cooling within a 5 GPa deviation. It was found [1] that the low-temperature loading procedure seems to be required to prepare samples with high- T_c . For instance, if H_2S was loaded at room temperature, only sulfur was detected in Raman and X-ray scattering.

Fig. 7 shows different images taken using optical microscopy during the transformation of the sample upon compression. These images are obtained with transmitting and reflecting light simultaneously. In pictures, blue parts indicate the optically transparent gasket and yellow areas show reflection from the metal electrodes. Clearly the sample is transparent at 9 GPa, it starts darkening at about 11 GPa and then becomes fully opaque at pressures between 30–40 GPa. Hints of weak reflections, a possible onset of metallicity appear at 79 GPa. Reflection from the sample becomes comparable with the electrodes above 150 GPa.

2.2.2. Raman measurements

The 632.8 nm line of a He-Ne laser was used originally to probe the Raman spectra of hydrogen sulfide and to determine pressure. The Raman spectrometer was equipped with a nitrogen-cooled CCD and notch filters. The pressure was determined by a diamond edge scale as previously described [129] at room and low temperatures. Ultra-low luminescence synthetic diamond anvils allowed us to record the Raman spectra at high pressures in the metallic state.

Fig. 8 condenses a series of spectra taken at different conditions of pressure and temperature. For pressure above 50 GPa, the molecular characteristic vibrations of hydrogen sulfide considerably diminish. Above this pressure only a broad band at 1900 cm^{-1} remains. Vibron modes disappeared in D_2S at a higher pressure of about 100 GPa. In general the Raman spectra of hydrogen sulfide is complex and hard to analyze due to different factors: I) the decomposition in elemental phases occurs in some cases (vibration of sulfur appear at low frequencies ($600\text{--}200\text{ cm}^{-1}$)). One could also see that annealing at room temperature produced stronger sulfur peaks, while operating the sample close to 200 K diminished the peaks considerably. II) In contrast to the clear evidence of the presence of elemental sulfur, peaks belonging to elemental hydrogen (vibrons) were never observed despite the use of the ultra-low luminescence synthetic diamond anvils. Above 80 GPa a new phase appeared, which persisted up to 150 GPa in the metallic state. At 160 GPa

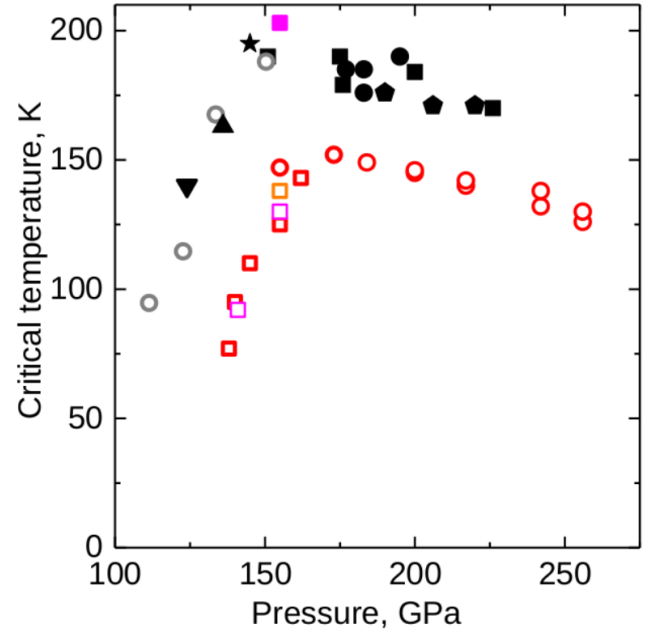


Figure 9: Summary of critical temperatures of superconductivity upon pressure, solid shapes shows for sulfur hydride (H_xS) and open shapes represent sulfur deuteride (D_xS). Only data on annealed samples is shown. The highest measured T_c is 203 K.

the Raman spectrum disappears, likely because of a transformation to the β -Po phase [1]. In this figure, the Raman spectra of sulfur hydride is also shown after the release of pressure from 208 GPa at room temperature. The spectrum is much more intense than those of sulfur in the metallic state at high pressures with a non-confirmed evidence of phase transition at ~ 180 GPa.

2.2.3. Electrical measurements

In the original experiment, electrical measurement of resistivity were conducted using a four-probe Van der Pauw configuration with Tantalum electrodes sputtered on the diamond. Currents between 10 to $10,000\text{ }\mu\text{A}$ were probed by a Keithley 6220 current source and voltage was measured by a Keithley 2000 multimeter. Electrical measurements were also reproduced by the PPMS6000 Quantum Design physical property device. The insulating gasket was prepared from either Teflon, NaCl or CaSO_4 as these materials do not react with H_2S . To check a possible contribution of the diamond surface to the conductivity a configuration with a pair of electrodes on one diamond and another pair on the second diamond anvil was prepared, similarly to the technique reported in Ref. [135]. Temperature cycles were at slow rate of $\sim 1\text{ K/min}$ which allowed the system to reach thermal equilibrium between measurements.

All the samples started to conduct above pressures of ~ 50 GPa. At this pressure, samples behaves as a semiconductor, shown by the temperature dependence of the resistance and by the presence of a pronounced photoconductivity. At 90-100 GPa, the resistance drops further and the temperature dependence shows a metallic behaviour, confirmed by the absence of photoconductive response. It is noticeable that during the

cooling of the sample for pressures above 100 GPa the resistance dropped abruptly by three orders of magnitude indicating a transition to the superconducting state. Further increasing of pressure, resulted in consistently higher values of T_c . Fig.9 shows a summary of critical temperatures of superconductivity under pressure for sulfur hydride H_xS and sulfur deuteride (D_xS) samples. The highest measured T_c is 203 K. A clear isotope effect, i.e. a shift of the T_c to lower temperatures in the case of sulfur deuteride points towards a phonon-assisted mechanism of superconductivity. The BCS theory gives dependence of critical temperature on the atomic mass M as $T_c \propto M^{-\beta}$, for which experimentally we found $\beta = 0.3$ at 175 GPa. For further details see A. Drozdov thesis work [166] and Ref.[1].

2.2.4. Measurements in magnetic field

To prove the actual occurrence of superconductivity it is not sufficient to measure a drop in the electrical resistance; the isotope effect is also not conclusive because it may or not be present. To guarantee that superconductivity indeed occurs, the most important signature which has to be present is the the expulsion of magnetic field (Meissner effect) below T_c .

In the original work on H_xS , magnetic susceptibility measurements were performed using the MPMS Quantum Design setup. In order to carry out this type of complicated measurements, a specialized miniature non-magnetic cell made of Cu:Ti alloy working up to 200 GPa had to be designed (see Drozdov et al. [1, 166]). The first series of experiments consisted on performing resistivity measurements upon variable magnetic field, which confirmed the shifting of T_c as function of magnetic field (roughly, a shift of 60 K in the 0-7 Tesla). Furthermore, magnetic susceptibility was recorded as function of temperature for sulfur hydride at pressure of 155 GPa in a the zero-field-cooled (ZFC) and 20 Oe field cooled (FC) modes.

Fig. 10 shows the temperature dependence of the magnetization of sulfur hydride at 155 GPa in a the zero-field-cooled (ZFC) and 20 Oe field cooled (FC) modes. The ZFC curve demonstrates a rather sharp transition from the diamagnetic to the paramagnetic state which could be classified as a superconducting one. The onset temperature is $T_c = 203$ K. For comparison, the superconducting step obtained for sulfur hydride from electrical measurements at 145 GPa is depicted in red color. Furthermore, the superconducting transition with $T_c = 203$ K was confirmed by the magnetization $M(H)$ measurements at different temperatures. The clear diamagnetism in the Meissner phase is responsible for the initial decrease of the magnetization until the first critical field H_{c1} of 300 Oe is attained. Afterwards, a subsequent increase of the magnetization as the external field increases is explained by the penetration of magnetic vortices which confirms the assignment of H_3S to the hard Type-II superconductors. As the sign of the field change reverses, the magnetic flux in the Shubnikov state remains trapped, and the returning branch of the magnetic cycle runs above the direct one leading to the irreversibility of the magnetization curve. Hysteric behavior of the magnetization becomes more clearly visible as temperature decreases.

Moreover, in-depth detailed characterization of magnetization curves evidenced hysteresis confirmed a type-II supercon-

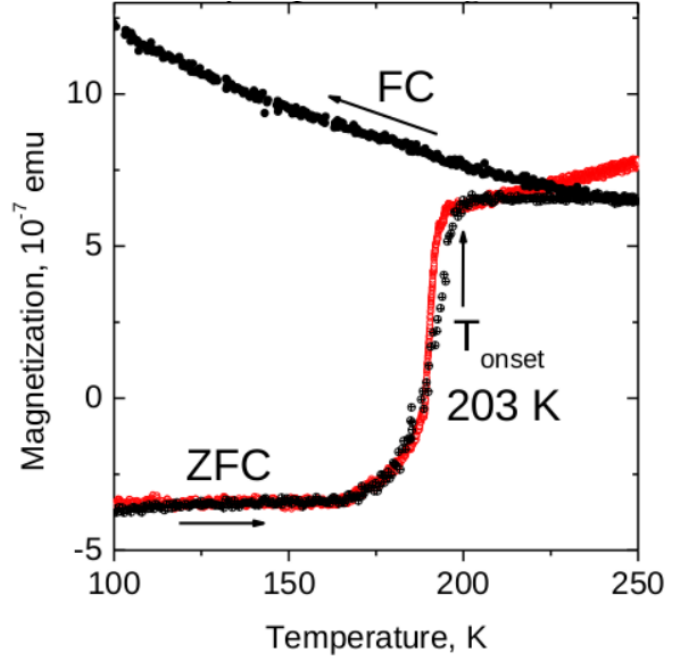


Figure 10: Temperature dependence of the magnetization of sulfur hydride at 155 GPa in zero-field cooled (ZFC) and 20 Oe field cooled (FC) modes (black circles). The onset temperature is $T_c = 203$ K. For comparison, the superconducting step obtained for sulfur hydride from electrical measurements at 145 GPa is shown by red circles.

ductor (not shown). Magnetic hysteresis measurements were performed using a subtraction of a background which was determined in the normal state at $T = 250$ K. The magnetization curves however are distorted by obvious paramagnetic impurities, often present in many other superconductors. We reported the first critical field $H_{c1} \sim 300$ Oe, estimated roughly from where the magnetization deviates from the linear behavior. At higher fields, magnetization increases due to the penetration of magnetic vortices.

We have summarized the key points on the first experimental evidence of superconductivity in sulfur hydride and evidenced the record-breaking temperature of 203 K, using both electrical resistance and magnetic measurements. However, as discussed in the following sections (Sec.5) hydride-sulfide possesses a rather complex phase diagram on which different compositions and structure phases emerge. Decomposition from the original H_2S loaded in our experiments to H_3S upon pressure is likely to occur. Experimental measurements of X-ray data by Einaga et al. [167] show that the superconducting phase is in good agreement with theoretically predicted hexagonal and body-centred cubic (bcc) structure and coexists with elemental sulfur. Nevertheless, phase mixture is also a possible scenario, since precipitation of elemental sulfur upon the decomposition could be expected [165] and we measured T_c of sulfur at significantly lower temperatures (< 20 K). Another expected product of the decomposition of H_2S is hydrogen. However, the body of experimental evidence does not support this scenario, since the strong characteristic vibrational stretching mode of the H_2 molecule is absent in Raman measurements. A complicated

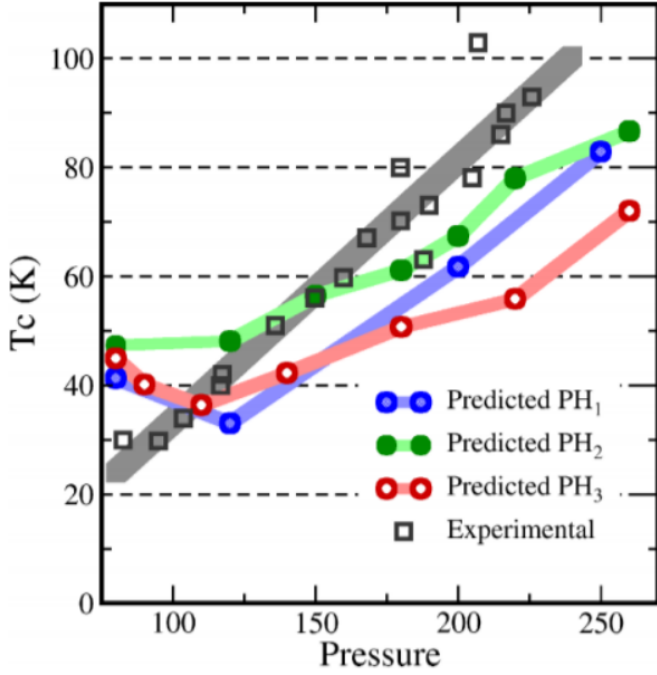


Figure 11: SCDFD calculated critical temperatures T_c for P-H composition as function of pressure as presented in Ref. [168]. Experimental values of T_c extracted from Drozdov et al. [169] are shown in black squares.

path of transformation is thus likely to happen to account for hydrogen-rich compositions. The key features of this superconductor and other hydrogen-rich compositions will be addressed in detail with the aid of theoretical and computation methods in Sec. 5-6.

2.3. Superconductivity in PH_x and LaH_x Hydrides

Sulfur-hydride it is not an isolated example of conventional high- T_c superconductivity at high pressures [170, 167, 171, 172, 173, 174, 175]. In fact, in less than a year after the discovery of superconductivity in sulfur hydride [1], Drozdov have reported high- T_c superconductivity in a second hydrogen-rich compound at extreme pressures: resistivity measurements on phosphine (PH_3) show that the samples, which are semiconducting at ambient pressure, metallize above 40 GPa and become superconducting at around 80 GPa, exhibiting a maximum T_c of 100 K at about 200 GPa [169]. However, in the original publication the composition responsible of the superconducting phase and its crystal structure, nor the mechanism responsible for T_c were addressed.

Analogies with the superconducting sulfur-hydride, which was obtained from a H_2S precursor, suggest that the superconductivity in the P-H system is of conventional nature, but that the composition of the superconducting phase might be different from the original PH_3 stoichiometry. To shed light on this matter, we used *ab initio* techniques to map out the high-pressure phase diagram of the P-H binary system by exploring the compositional and configurational space of PH_n with sophisticated structure prediction methods, and estimated the superconducting properties of the most promising phases (sum-

marized in Fig. 11). Interestingly, theoretical studies reported all the high-pressure binary phases of P and H as metastable with respect to elemental decomposition in the pressure range 100-300 GPa. However, critical temperatures of the three phases closest to the convex hull (PH , PH_2 , and PH_3) reproduce to a good approximation the experimental values. Possible ways to reconcile our results with experiments are addressed in Sec. 5.

The finding of superconductivity in the H-S system at 200 K under pressure and later in P-H, stimulated a large part of the community to explore in other systems, in the so-called *superhydrides* to search for even higher values of T_c . A substantial amount of computational studies have been published and in some of them spectacular values close or above room temperature have been predicted [176, 177]. Many other systems have been theoretically proposed to form *superhydrides*, reviving also the interest in structural transformations of individual elements and their tendency to form metallic structures [63, 178, 54, 179, 74]. Experimentally, superconductivity in hydrides under pressure has been confirmed to occur (ordered by date): I) SiH_x , $T_c \sim 17$ K [153, 159], II) $BaReH_9$, $T_c = 7$ K [180], III) SH_x , $T_c = 203$ K [1, 106], IV) PH_3 , $T_c = 100$ K [169] and more recently in v) LaH_x , $T_c \sim 250$ K [181, 3]. For compressed hydrides not showing superconductivity see Sec. 5.1.2.

Less than one year ago (2018), the work on H-rich compositions in the La-H system set a new superconducting record, since it represents the first measurement of T_c near room temperature. The first lanthanum superhydride was synthesized under pressure above 160 GPa and upon heating to 1000 K. The X-ray data indicated that the stoichiometry corresponds to LaH_{10+x} ($-1 < x < 2$) which is close to the predicted high- T_c LaH_{10} [182]. In 2018, Somayazulu et al. [3] measured the temperature dependence of the resistivity of La heated with NH_3BH_3 as hydrogen source under similar pressure and observed a drop in the resistance at ~ 260 K upon cooling and 248 K upon warming the sample which was assigned to the superconducting transition of LaH_{10+x} ($-1 < x < 2$). In their original claim, they also observed a series of resistance anomalies at temperatures as high as 280 K. However, neither a zero resistance state nor additional confirmations (like the Meissner effect or isotopic effects or the effect of an external magnetic field on the transition temperature) was provided. Simultaneously, an independent research measured a superconducting transition $T_c \sim 215$ K in LaH_x [183] and subsequently a T_c 250 K [181].

Apart from setting a new T_c record, high-pressure experiments in the La-H system played also a major role in establishing methods to control the high-pressure synthesis of materials. This is a crucial point, since many –if not all– of the structures observed in high-pressure experiments are metastable phases [185] (i.e. out of thermodynamic equilibrium). Consequently, many of the HP phases cannot be recovered to ambient conditions. This translates into one of the greatest challenges when using high pressures in practical applications [186]. Different strategies to help the stabilization of HP-materials have been proposed; a major role is played by the precise control of thermodynamic conditions [187, 188, 178, 74, 189, 190]. The case of La-H represents a step towards mastering this control

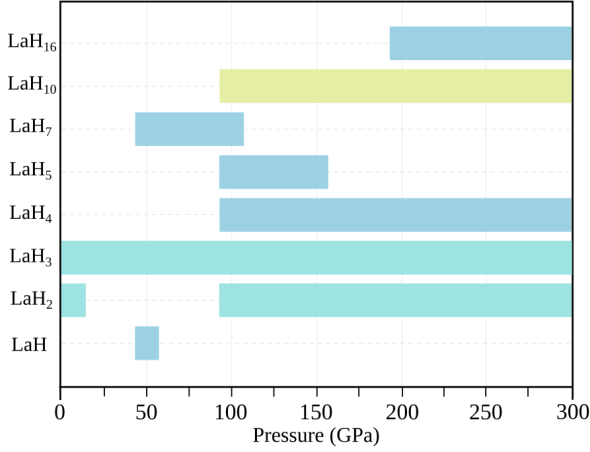


Figure 12: Summary of stable compositions calculated in La-H under pressure. Bars for different compositions mark the range of stability for several compositions estimated from convex hull construction (see Ref. [184]).

of thermodynamic conditions: For the unique route followed by Geballe et al. [191], Somayazulu et al. [3] and Drozdov et al. [183, 181] the key factor that played a role in ensuring a successful synthesis was: temperature. The stable compositions measured by experiments were accessed using pulsed laser heating, starting from different initial constituents: in Geballe and Somayazulu work's ammonia borane was used as hydrogen source and elemental lanthanum as a starting material, Drozdov et al. used (LaH₂ + H₂) as source materials. In both experiments, and independently of the P-T path followed, an elevated temperature was necessary to access compositions having the highest T_c.

We conclude this section of the Review, with the firm belief that in coming years we will witness measurements of even higher T_c, at room temperature (300 K) or possibly above. In fact, theory (Migdal-Éliashberg) [31, 192, 193]) predicts no upper limit for the critical temperature [194].

3. Theoretical Methods for superconductivity

3.1. Phonons and electron phonon coupling

3.1.1. Phonons

The basic assumption which allows the calculation of vibrational properties in solids is the *Born-Oppenheimer approximation* [195]. This consists in a decoupling of electronic and lattice degrees of freedom, the latter arising from the solution of the Schrödinger equation:

$$\left[-\sum_i \frac{\hbar^2}{2M_i} \nabla_i^2 + E(\mathbf{R}) \right] \Phi(\mathbf{R}) = \varepsilon \Phi(\mathbf{R}) \quad (1)$$

where $\mathbf{R} = \{\mathbf{R}_i\}$ are the nuclear coordinates, M_i are nuclear masses and $E(\mathbf{R})$ the fixed-ion energy of the whole system, which defines the Born-Oppenheimer energy surface. $E(\mathbf{R})$ is the ground state eigenvalue of the electronic Hamiltonian:

$$H_{BO} = \frac{-\hbar^2}{2m} \sum_i \nabla_i^2 + \frac{e^2}{2} \sum_{i \neq j} \frac{1}{|\mathbf{r}_i - \mathbf{r}_j|} + V_{\mathbf{R}}(\mathbf{r}) + E_N(\mathbf{R}) \quad (2)$$

being

$$V_{\mathbf{R}}(\mathbf{r}) = -\sum_{i,h} \frac{Z_h e^2}{|\mathbf{r}_i - \mathbf{R}_h|} \quad (3)$$

$$E_N(\mathbf{R}) = \frac{e^2}{2} \sum_{i \neq j} \frac{Z_i Z_j}{|\mathbf{R}_i - \mathbf{R}_j|} \quad (4)$$

where Z_h are the atomic numbers of the ions, E_N their bare electrostatic energy and V the electron ion interaction. This approximation neglects possible electronic transitions induced by the ionic motion. Furthermore, within the Born-Oppenheimer approximation the nuclear interaction is assumed to be instantaneous.

At the equilibrium geometry the forces acting on each nuclei [first derivative of $E(\mathbf{R})$] are zero. The diagonalization of the Hessian matrix of $E(\mathbf{R})$ gives the phonon frequencies in the *harmonic approximation*, according to the relation:

$$\det \left| \frac{1}{\sqrt{M_i M_j}} \frac{\partial^2 E(\mathbf{R})}{\partial \mathbf{R}_i \partial \mathbf{R}_j} - \omega^2 \right| = 0. \quad (5)$$

That in terms of periodic displacements from equilibrium can be rewritten [195] as:

$$\det \left| \frac{1}{\sqrt{M_i M_j}} \tilde{C}_{st}^{\alpha\beta}(\mathbf{q}) - \omega^2(\mathbf{q}) \right| = 0, \quad (6)$$

where

$$\tilde{C}_{st}^{\alpha\beta}(\mathbf{q}) = \frac{\partial^2 E}{\partial u_s^{\alpha}(\mathbf{q}) \partial u_t^{\beta}(\mathbf{q})}, \quad (7)$$

and $u_s^{\alpha}(\mathbf{q})$ are the normalized displacement of the atom s in the cartesian direction α modulated along the crystal by a wavevector \mathbf{q} . Phononic eigenvalues and eigenvectors are obtained by diagonalizing $\tilde{C}_{st}^{\alpha\beta}(\mathbf{q}) / \sqrt{M_i M_j}$ also called *Dynamical Matrix*.

3.1.2. Density Functional Theory

Due to its excellent cost/accuracy ratio, density functional theory (DFT) is the method of choice for the calculations of electronic and lattice properties of materials [196]. In particular is the universally used approach to compute, from first principles, the dynamical matrix in Eq. 7.

DFT is most conveniently used through the Kohn and Sham (KS) construct [197], a subsidiary system of non interacting electrons that reproduces exactly the density of the fully interacting system. This Kohn-Sham system is obtained by the solution of the Schrödinger equation:

$$H_s \psi_n(\mathbf{r}) \equiv -\left(\frac{\hbar^2}{2m} \nabla^2 + v_s(\mathbf{r}) \right) \psi_n(\mathbf{r}) = \epsilon_n \psi_n(\mathbf{r}) \quad (8)$$

where the effective potential v_s is to be computed self-consistently and reads:

$$v_s(\mathbf{r}) = v_{ex}(\mathbf{r}) + e^2 \int \frac{\rho(\mathbf{r}')}{|\mathbf{r} - \mathbf{r}'|} + v_{xc}(\mathbf{r}) \quad (9)$$

where $v_{ex}(\mathbf{r})$ is the potential due to the bare nuclei, the second term on the right hand side is the Hartree potential and v_{xc} is the functional derivative of $E_{xc}[\rho]$ with respect to the electronic density. $E_{xc}[\rho]$ is a universal (non material dependent) functional of the density; a central object in DFT and for which many good approximations exist [198, 199, 200]. The electronic density is obtained by occupying the solutions of Eq. 8, $\psi_n(\mathbf{r})$, with the lowest eigenvalues (ϵ_n) according to the Pauli principle:

$$\rho(\mathbf{r}) = 2 \sum_{n=1}^{N/2} |\psi_n(\mathbf{r})|^2, \quad (10)$$

For a metallic system the occupation of the states are smeared around the Fermi level, with a distribution function $S_\sigma(\epsilon)$:

$$\rho(\mathbf{r}, \epsilon) = \sum_n S_\sigma(\epsilon) |\psi_n(\mathbf{r})|^2. \quad (11)$$

S can be chosen as a Fermi distribution mimicking a fictitious electronic temperature to stabilize numerical calculations and speed up numerical convergence for the sampling of the Brillouin zone.

Within this scheme, the total energy of the system is also accessible and is expressed as:

$$\begin{aligned} E[\rho] &= 2 \sum_n S_\sigma(\epsilon) \epsilon_n - \frac{e^2}{2} \int \frac{\rho(\mathbf{r})\rho(\mathbf{r}')}{|\mathbf{r} - \mathbf{r}'|} d\mathbf{r}d\mathbf{r}' \\ &+ E_{xc}[\rho] - \int \rho(\mathbf{r})v_{xc}(\mathbf{r})d\mathbf{r}. \end{aligned} \quad (12)$$

This equation allows us to directly compute the dynamical matrix and the phonon spectrum by performing numerical derivatives through small finite displacements of the atoms. However in the linear response regime, when anharmonic effects are negligible, it is more convenient to study phonons as infinitesimal perturbations and therefore compute Eq. 7 in the linear response regime, by means of density functional perturbation theory (DFPT) applied to the phononic perturbation [195, 201, 202]. A great advantage of this method consists in its capability to treat perturbation of whatever wavelength without the need to simulate the lattice distortion on a unit cell commensurate with the \mathbf{q} -vector of the phonon.

3.1.3. Electron-phonon interaction

Up to now we have included the effect of phonons only within the adiabatic principle introduced with the Born Oppenheimer approach. This means that we neglected any electron-phonon (el-ph) scattering process and assumed that electrons respond smoothly to the ionic motion. Due to the small phonon energies (10 ÷ 100 meV) these scatterings are possible only inside a small (of the order of the Debye energy) window around E_F , and this is why very accurate phonons (that depend on the whole valence charge density) can be obtained from the unperturbed electronic structure [202]. On the other hand, important properties such as normal state resistivity or superconductivity, depend strongly on el-ph interactions. Both these properties in fact arise from elemental processes in which an electron with momentum \mathbf{k} emits (absorbs) a phonon of wavevector \mathbf{q} and

goes in a state of wavevector $\mathbf{k} + \mathbf{q}$. To develop a theory for superconductivity we need a coupling factor for this process.

The basic idea for calculating this coupling factor is to consider the phonon *dressed* with the electronic charge that adiabatically moves, as a perturbing potential that introduces a transition probability between KS eigenstates. This potential takes the form:

$$\Delta V = \sum_i \eta_i \frac{\partial v_s(\mathbf{r})}{\partial \eta_i} \quad (13)$$

where η_i is the position operator for the i -th atom. Passing to phonon coordinates:

$$\eta_i = \sum_{\mathbf{q}} \sqrt{\frac{\hbar}{2M_i\omega_{\mathbf{q}v}}} e^{i\mathbf{q}\cdot\mathbf{R}_i^0} (b_{\mathbf{q}}^\dagger - b_{\mathbf{q}}) \quad (14)$$

where \mathbf{R}_i^0 are the unperturbed lattice positions and $b_{\mathbf{q}}^\dagger b_{\mathbf{q}}$ are the phonon raising and lowering operators. If we calculate the expectation value of the above operator in a process in which a single phonon is created or absorbed we get a coupling:

$$g_{m\mathbf{k}+\mathbf{q},n\mathbf{k}}^v = \sqrt{\frac{\hbar}{2\omega_{\mathbf{q}v}}} \langle \psi_{m\mathbf{k}+\mathbf{q}} | \Delta v_s^{\mathbf{q}v} e^{i\mathbf{q}\cdot\mathbf{r}} | \psi_{n\mathbf{k}} \rangle \quad (15)$$

where $\Delta v_s^{\mathbf{q}v} e^{i\mathbf{q}\cdot\mathbf{r}}$ is the finite variation in the self consistent potential corresponding to a phonon displacement of wavevector \mathbf{q} and mode index v . From the computational point of view the matrix element appearing in the above equation must be normalized to one unit cell, then we separate the potential into a phase $e^{i\mathbf{q}\cdot\mathbf{r}}$ that cancels out with that of the wavefunctions and a periodic part $\Delta v_s^{\mathbf{q}v}$ that we evaluate in a unit cell. The electron-phonon interaction of the Kohn-Sham system therefore is described by the Hamiltonian:

$$\begin{aligned} \tilde{H}_{e-ph} &= \sum_{mn\sigma} \sum_{v\mathbf{k}\mathbf{q}} g_{m\mathbf{k}+\mathbf{q},n\mathbf{k}}^v \sum_{\sigma} \psi_{\sigma m\mathbf{k}+\mathbf{q}}^\dagger \psi_{\sigma n\mathbf{k}} (b_{v\mathbf{q}} + b_{v-\mathbf{q}}^\dagger) \\ &= \sum_{v\mathbf{q}} \sqrt{\frac{\hbar}{2\omega_{\mathbf{q}v}}} \int d^3r \Delta V_{scf}^{\mathbf{q}v}(\mathbf{r}) \psi_{\sigma}^\dagger(\mathbf{r}) \psi_{\sigma}(\mathbf{r}) (b_{v\mathbf{q}} + b_{v-\mathbf{q}}^\dagger) \end{aligned} \quad (16)$$

where $\psi_{\sigma n\mathbf{k}}^\dagger$ and $\psi_{\sigma n\mathbf{k}}$ are creation and destruction operators for Kohn-Sham states and $b_{v\mathbf{q}}$ is a phonon field operator. This electron phonon interaction for the Kohn-Sham states is by construction an approximation of the true electron phonon interaction. It is valid while the spectrum of the Kohn-Sham system remains a good approximation to the real quasi-particle spectrum of the material. Whenever this is not the case, one has to rely on perturbation approaches [203].

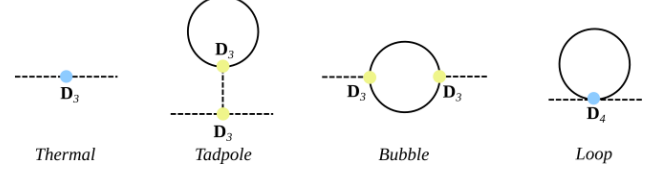
3.1.4. Anharmonic effects

The harmonic theory of lattice vibrations discussed so far is based on the expansion of the Born-Oppenheimer (BO) energy surface [204] to the second order around the ionic equilibrium positions [205]. It assumes that the amplitude of atomic displacements from equilibrium are relatively small and is useful to predict well defined non-interacting quasiparticles, i.e.

phonons, with infinite lifetime and temperature independent energy spectrum. Harmonic lattice vibration has proven to be exceptionally good in describing vibrational properties for many simple and complex materials, specially as a first approximation to obtain insights in frequency spectra in solids. However, by construction this approximation breaks due to anharmonic effects. Anharmonic effects, i.e., effects due to higher orders in the energy surface expansion, that introduce interaction between phonons, thus finite scattering rates and finite lifetimes. Systems containing light mass atoms, showing strong displacements, phonon softening, quantum effects, as present in hydrides under pressure also lead to perfect scenarios of strong anharmonicity.

The most intuitive approach and historically the first introduced was to consider higher-order terms in the potential expansion as a small perturbation of the harmonic potential [206, 207]. Perturbative approaches, however are restricted to conditions in which the displacements of the atoms are within the range in which higher-order terms are considerably smaller than the harmonic potential. Unfortunately, there are handful of situations in which perturbative approach are clearly not suitable, for example, when light atoms such as hydrogen are present (see case of PdH by Errea et al. [208]), or when the system is close to a dynamical instability (a phase transition) as in H_3S [209].

Several approaches have been developed to deal with this problem, these can be classified into two large categories: the one that relies on molecular dynamics (MD), and the one that relies on self-consistent field theory. Anharmonic effects at a non-perturbative level are treated within *ab-initio* molecular dynamics (AIMD) methods [210, 211, 212, 213]. These approaches are computationally expensive since they require long simulation times to converge re-normalized phonon energies. Another intrinsic limitation is that because they are based on Newtonian dynamic, limiting their application to temperatures above the Debye temperature. Path-integral molecular dynamics [214] overcome this situation by incorporating the quantum character of atomic vibrations, however at cost of increasing the computational load. To overcome the aforementioned limitations in AIMD methods, several DFT-based methods have recently been developed for treating anharmonic effects in solids non-perturbatively, which rely on the vibrational self-consistent-field theory [215, 216] and the self-consistent phonon (SCP) theory [217, 218, 219, 207, 220], which can incorporate the effect of lattice anharmonicity at the mean-field level. In these methods, anharmonic phonon frequencies are calculated through the construction of effective harmonic force constants obtained self-consistently by repeatedly calculating atomic forces in supercells with suitably chosen atomic configurations. In these self-consistent field approaches, anharmonic corrections are computed by a diagrammatic approach on which the diagrammatic expansion is cut at finite order [221, 222, 223, 224]. Second order self-energies and leading terms are,



Dashed lines represent the free phonon propagator and solid points are vertices involving three or four phonons. The first term in the above mentioned quasi-harmonic effects comes from the thermally expanded lattice, which is less relevant at low temperature. The second contribution is a Hartree type diagram in which phonons are coupled with the average phononic distortion. Whenever Wyckoff positions are locked by symmetry this term becomes identically zero [225, 226]. This perturbation approach has the undeniable beauty that anharmonic effects are clearly seen and connected to a clear physical picture of interacting phonons and phonon decay. In fact, the loop diagram involving four phonon processes is related to D_4 , while the bubble diagram is, like the tadpole, related to D_3 and unlike the other terms is not Hermitian and contributes to the phonon line-width [220, 221]. However the perturbative expansion is only valid if anharmonicity is weak, an approximation that may very well fail for hydrides. Different *degrees* of anharmonicity in solids are exemplified in Fig. 13. Two distinct cases are distinguished: weak as in cases of thermal expansion and volume effects and strong anharmonicity, for which harmonic lattice instabilities are *cured* by anharmonic processes, like in the case of hydrides under pressure.

An approach to deal with strong anharmonicity (as is the case in hydride superconductors) is the Self-consistent harmonic approximation (SCHA) which dates back to 1955 and developed by Hooton [217]. The theory starts from the true anharmonic free energy:

$$\mathcal{F}_H[\rho] = \text{Tr}[\rho H] + \frac{1}{\beta} \text{Tr}[\rho \ln \rho] \quad (17)$$

with β the inverse temperature, \mathcal{H} the ionic Hamiltonian and ρ is a density matrix. The main idea of the SCHA is to use a variational principle, the Gibbs-Bogoliubov (GB) principle, in order to approximate the free energy of the true ionic Hamiltonian with the free energy calculated with a trial harmonic density matrix for the same system. For the Gibbs principle $\mathcal{F}_H[\rho]$ is minimized by the equilibrium density matrix ρ_H such that:

$$\mathcal{F}_H[\rho] \geq \mathcal{F}_H[\rho_H] \quad (18)$$

The above minimization can be performed restricting the search for ρ_H to a set of density matrices from the support Harmonic Hamiltonian H_{Harm} . That is particularly convenient because the auxiliary system consists of non-interacting phonons:

$$H_{Harm} = E_0[\mathbf{x}^0] + \frac{1}{2} \sum_j \mathbf{p}_j^2 + \frac{1}{2} \sum_j \omega_j^2 \mathbf{q}_j^2 \quad (19)$$

where \mathbf{x}^0 , \mathbf{p}_j , ω_j and \mathbf{q}_j are the vibration centers, momenta, frequencies and coordinates of the modes (j) to be optimized. Clearly this reduces to the harmonic problem in absence of

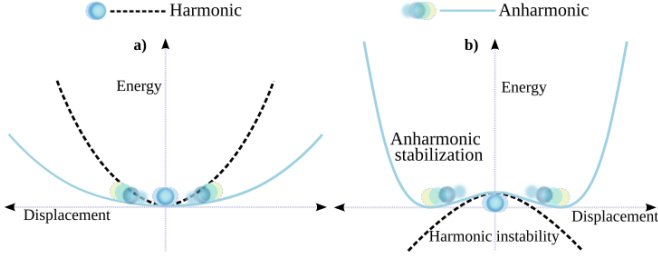


Figure 13: Possible scenarios of weak a) and strong b) anharmonicity. Harmonic vibration in left panel lead to strong softening and wrong determination of frequencies. In right panel the potential is harmonic unstable, that is stabilized via anharmonicity.

anharmonicity but otherwise can have different frequencies, modes and also vibration centers from the harmonic one. However, the computational cost of the SCHA is relatively high because at each self consistent iteration in the minimization over ρH_{harm} expensive high order derivative of the energy surface are required. This problem has been recently tackled by Errea-Calandra-Mauri by introducing a stochastic approach to sample the energy surface [208, 223].

In particular, in the stochastic self-consistent harmonic approximation (SSCHA) the free energy is explicitly minimized by using a conjugate gradient algorithm with respect to the independent coefficients of the trial harmonic potential. In the SSCHA, the free energy and its gradient are evaluated through averages computed with stochastic sampling of the configuration space and the importance sampling technique. In that way, the (approximated but nonperturbative) anharmonic free energy of the system is directly accessible. The stochastic approach is particularly suited to be used in conjunction with *ab initio* calculations, and it has been employed to study thermal anharmonic effects in several compounds such as hydrides.

The most recent inclusion in the methods to treat anharmonicity is the presented by Tadano and Tsuneyuki that implemented a Green's function self-consistent phonons [224]. This deterministic method considers the potential energy of an interacting nuclear system U as a Taylor expansion with respect to the atomic displacement as: $U - U_0 = U_2 + U_3 + U_4 + \dots$,

All the anharmonic terms U_n ($n > 2$) are neglected in harmonic calculations. Anharmonic terms can be treated as a perturbation, H' , of the non-interacting Hamiltonian H_0 as: $H = H_0 + H' \approx H_0 + H_3 + H_4$. Higher orders can be omitted when are negligible compared to cubic and quartic terms. The diagrammatic includes the loop-diagram (discussed before) that is computed not from the harmonic phonon propagator but self-consistently with the loop-dressed phonon propagator. Polarization vectors can either be kept fixed to their harmonic form or updated as well including some-off diagonal contributions to the loop self-energy in the harmonic base. Unlike SSCHA this implementation requires the knowledge of computationally expensive and numerically difficult anharmonic force constants. A problem that was solved by adopting a modern compressed sensing approach [227], exploiting the fact that force constants are a sparse set [228, 229]. The practical applications of these self-consistent field methods will be reviewed in Section 5, as

they are fundamental to successfully characterize the superconducting state of hydrides under pressure.

3.1.5. Dielectric Screening in Metals

Condensation of Cooper pairs via an attractive lattice interaction is universally accepted to be the microscopic mechanism of conventional superconductors. Electron-phonon interaction, in spite of being quite weak with respect to the direct Coulomb electron-electron repulsion, becomes dominant at very low energy (within the Debye frequency). Still, Coulomb forces are in action and are extremely important in the formation of the superconducting state as they partially balance the phononic mediation reducing the overall coupling and with it, the critical temperature.

Unlike the electron-phonon coupling this (screened) Coulomb interaction turns out to have an integrated effect that is usually weakly material dependent. At first glance and trusting this consolidated evidence, the calculation of Coulomb interactions can be avoided. As discussed in Sec. 3.2.4, its role is largely covered by the use of an adjustable/semi empirical μ_c^* parameter. Nevertheless Coulomb interactions can be actually included from first principles. As we will discussed later in Sec. 3.3, these enter the superconducting problem in the form of a screened effective interaction, formally equivalent to the GW approximation [230, 231] in Nambu space [232].

Screening can be reliably computed in the framework of the random phase approximation (RPA) or within time dependent DFT (TD-DFT) [233, 196]. The resulting interaction has a simple and intuitive form:

$$w(\mathbf{r}, \mathbf{r}_1, \omega) = \int d^3 r_2 \frac{\epsilon^{-1}(\mathbf{r}_2, \mathbf{r}_1, \omega)}{|\mathbf{r} - \mathbf{r}_2|}. \quad (20)$$

where the direct Coulomb repulsion is screened by the inverse dielectric function ϵ^{-1} . The interaction usually enters the superconducting problem in the form of its scattering matrix elements between Kohn-Sham electrons:

$$W_{n\mathbf{k}, n'\mathbf{k}'}(\omega) \equiv \int d^3 r d^3 r_1 \psi_{n\mathbf{k}}^*(\mathbf{r}) \psi_{n'\mathbf{k}'}(\mathbf{r}) w(\mathbf{r}, \mathbf{r}_1, \omega) \psi_{n'\mathbf{k}'}^*(\mathbf{r}_1) \psi_{n\mathbf{k}}(\mathbf{r}_1). \quad (21)$$

The average of $W_{n\mathbf{k}, n'\mathbf{k}'}(0)$ at the Fermi level ($\epsilon_{\mathbf{k}} = \epsilon_{\mathbf{k}'} = E_F$) multiplied by the density of states is known as μ the Coulomb potential parameter. As will be discussed in Sec.3.2.3, μ_c^* is derived from μ by considering the retardation effect [234].

The dynamical dependence ω , becomes relevant where significant retardation effects in the screening process occur. Due to the fast nature of Coulomb forces, the dynamical part of the interaction is often negligible, justifying the common use of a static approximation. Nevertheless, under certain conditions some materials may feature strong plasmonic effects (see for instance the work of Akashi et al. [235] in Li under pressure). Further theoretical details on plasmon effects will be addressed in Sec. 3.3.

It is important to observe at this point that, since the interaction is computed in a GW type of approximation, some

Coulomb effects as paramagnetic spin fluctuations can not be described in this approach, as these require spin effects that can not be described unless the vertex is included in the self energy. However these type of interactions are not relevant to the physics of hydrides superconductors as they only occur in the proximity of magnetic phase transitions [236, 237, 238].

3.2. Formalism for conventional superconductivity

3.2.1. BCS theory

The theory of Bardeen, Cooper and Schrieffer (BCS) [30] has been the first theory of superconductivity able to explain the microscopic nature of the superconducting state. BCS is perhaps one of the most successful theories in condensed matter physics and although, its predictive power is limited, compared to modern *ab-initio* methods, it is still today an essential theoretical and computational framework for the characterization and the understanding of superconducting materials.

BCS theory assumes the following Hamiltonian for the superconducting electrons:

$$H = H_0 + H_{\text{int}} \quad (22)$$

$$H_0 = \sum_{\mathbf{k}\sigma} \epsilon_{\mathbf{k}} c_{\mathbf{k}\sigma}^\dagger c_{\mathbf{k}\sigma} \quad (23)$$

$$H_{\text{int}} = - \sum_{\mathbf{k}\mathbf{k}'} V_{\mathbf{k}\mathbf{k}'} (c_{-\mathbf{k}'\downarrow}^\dagger c_{\mathbf{k}'\uparrow}^\dagger) (c_{\mathbf{k}\uparrow} c_{-\mathbf{k}\downarrow}) \quad (24)$$

where $c_{\mathbf{k}\sigma}$ and $c_{\mathbf{k}\sigma}^\dagger$ are creation and annihilation operator for the Bloch-wave with a wavevector \mathbf{k} and spin σ , respectively. $V_{\mathbf{k}\mathbf{k}'}$ are matrix elements of the leading superconducting interaction. Under the assumption of a momentum independent phononic coupling it can be written as:

$$V_{\mathbf{k},\mathbf{k}'} = -V\theta(\hbar\omega_D - |\epsilon_{\mathbf{k}}|)\theta(\hbar\omega_D - |\epsilon_{\mathbf{k}'}|) \quad (25)$$

where ω_D is the Debye frequency. BCS solved this model by an ansatz for the many body wavefunction and found an exact solution. The same can be achieved following Gor'kov [239, 240, 241] and solving for the Green's function:

$$G(\mathbf{k}, \tau) = -\langle T_\tau c_{\mathbf{k}\sigma}(\tau) c_{\mathbf{k}\sigma}^\dagger(0) \rangle \quad (26)$$

where the imaginary-time dependence of the operators are defined as $X(\tau) = \exp(H\tau)X\exp(-H\tau)$ and T_τ denotes time ordered product, and the expectation value of physical quantity A is calculated as:

$$\langle A \rangle = \frac{\text{Tr}(\exp(-\beta H)A)}{\text{Tr}(\exp(-\beta H))}. \quad (27)$$

G satisfies the equation of motion

$$\left(-\frac{d}{d\tau} - \epsilon_{\mathbf{k}}\right) G(\mathbf{k}, \tau) = \delta(\tau) - \sum_{\mathbf{k}'} V_{\mathbf{k}\mathbf{k}'} \langle T_\tau c_{-\mathbf{k}\downarrow}^\dagger(\tau) c_{\mathbf{k}'\uparrow}(\tau) c_{-\mathbf{k}'\downarrow}(\tau) c_{\mathbf{k}\uparrow}^\dagger(0) \rangle \quad (28)$$

That can be solved by introducing the mean-field approximation:

$$\langle T_\tau c_{-\mathbf{k}\downarrow}^\dagger(\tau) c_{\mathbf{k}'\uparrow}(\tau) c_{-\mathbf{k}'\downarrow}(\tau) c_{\mathbf{k}\uparrow}^\dagger(0) \rangle \rightarrow F(\mathbf{k}, \tau) F^*(\mathbf{k}, \tau) \quad (29)$$

with the definition of the anomalous Green's function:

$$F(\mathbf{k}, \tau) = -\langle T_\tau c_{\mathbf{k}'\uparrow}(\tau) c_{-\mathbf{k}'\downarrow}(0) \rangle$$

This leads to:

$$G(\mathbf{k}, i\omega_n) = \frac{-i\omega_n - \epsilon_{\mathbf{k}}}{\omega_n^2 + E_{\mathbf{k}}^2}$$

$$F(\mathbf{k}, i\omega_n) = \frac{\Delta_{\mathbf{k}}^*}{\omega_n^2 + E_{\mathbf{k}}^2}$$

where $\omega_n = (2n + 1)\pi k_B T$ are the Matsubara points,

$$E_{\mathbf{k}}^2 \equiv \epsilon_{\mathbf{k}}^2 + |\Delta_{\mathbf{k}}|^2 \quad (30)$$

and the function $\Delta_{\mathbf{k}}$:

$$\Delta_{\mathbf{k}} \equiv \sum_{\mathbf{k}'} V_{\mathbf{k}\mathbf{k}'} F(\mathbf{k}', 0) \quad (31)$$

clearly carries the meaning of a (superconducting) gap and satisfies the self-consistent BCS equation:

$$\Delta_{\mathbf{k}} = \frac{1}{\beta} \sum_{\mathbf{k}'} \sum_{n=-\infty}^{\infty} \frac{V_{\mathbf{k}\mathbf{k}'} \Delta_{\mathbf{k}'}}{\omega_n^2 + E_{\mathbf{k}}^2} = \sum_{\mathbf{k}'} \frac{V_{\mathbf{k}\mathbf{k}'} \Delta_{\mathbf{k}'}}{2E_{\mathbf{k}'}} \tanh\left(\frac{E_{\mathbf{k}'}}{2k_B T}\right) \quad (32)$$

If one assumes the gap function to be isotropic: $\Delta_{\mathbf{k}} = \Delta \neq 0$, then the gap equation (32) allows to extract the following limits:

1. For $T \rightarrow 0$ and $V N_F \ll 1$

$$\Delta \sim 2\hbar\omega_D \exp\left(\frac{-1}{V N_F}\right) \quad (33)$$

where E_F is the density of states at the Fermi level.

2. For $T \sim T_c$, then $\Delta \rightarrow 0$, one obtains:

$$T_c = 1.13\omega_D \exp\left(\frac{-1}{V N_F}\right) \quad (34)$$

By comparing (33) and (34), we find the universal BCS ratio:

$$\frac{2\Delta}{T_c} \sim \frac{4}{1.13} \sim 3.54 \quad (35)$$

The main drawback of BCS theory is that the pairing interaction between electrons assumed in Eq. 3.2.1 is an instantaneous effective field, while, as we will see from the *ab-initio* density-functional framework, the true nature of the phononic pairing of Sec. 3.1.3 and Coulomb interactions of Sec. 3.1.5 is dynamical. The intrinsic timescale should be taken into account to achieve a quantitative accuracy by means of many-body perturbation theory including explicitly the lattice degrees of freedom.

3.2.2. Éliashberg Theory

Éliashberg theory is a many body perturbation approach to superconductivity. In a modern perspective it can be seen as a GW_0 approximation applied in presence of a superconducting proximity effect field and including in the screened interaction (W_0) both Coulomb and phonon propagators. The derivation follows similar steps as in Sec. 3.2.1, where instead of a model BCS pairing the interactions are computed *ab-initio*.

The starting Hamiltonian H is one of interacting electrons and ions, in which the lattice dynamics is decoupled and the electron-phonon coupling is described within the Kohn-Sham theory as defined in Sec. 3.1.3. The decoupling procedure will be discussed in more detail in the framework of density functional theory for superconductors in Sec. 3.3, here to set up the Éliashberg perturbative approach, H is split in a zero-order approximation H_0 plus an interaction part H_I . A convenient choice for the zero order Hamiltonian includes the coupling with the external field, H_{ext} , and the Kohn-Sham Hamiltonian entering in Eq. 8:

$$H_s = \sum_{\sigma} \int d\mathbf{r} \psi_{\sigma}^{\dagger}(\mathbf{r}) \left[-\frac{\nabla^2}{2} + v_s(\mathbf{r}) - \mu \right] \psi_{\sigma}(\mathbf{r}), \quad (36)$$

while everything else (see also Sec. 3.3) goes into H_I . So:

$$H_0 = H_s + H_{ext} \quad (37)$$

$$H_I = H_{ee} + \tilde{H}_{e-ph} - H_{DC} \quad (38)$$

where the last term (as in conventional GW theory) removes extra xc effects already included in H_s therefore avoiding any *double counting*:

$$H_{DC} = \sum_{\sigma} \int d\mathbf{r} \psi_{\sigma}^{\dagger}(\mathbf{r}) v_s(\mathbf{r}) \psi_{\sigma}(\mathbf{r}). \quad (39)$$

Unfortunately conventional many body perturbation theory [242] can not be directly applied to $H_0 + H_I$ because the superconducting condensation H_{ext} should contain a proximity field [243, 232] (see also sec: 3.3.1):

$$H_{\Delta_{ext}} = \int d^3r d^3r' \Delta_{ext}^*(\mathbf{r}, \mathbf{r}') \psi_{\uparrow}(\mathbf{r}) \psi_{\downarrow}(\mathbf{r}') + h.c. \quad (40)$$

that introduces extra processes forbidden in a particle conserving theory.

In the Nambu-Gor'kov formalism one defines two new electronic field operators:

$$\tilde{\psi}(\mathbf{r}) = \begin{pmatrix} \psi_{\uparrow}(\mathbf{r}) \\ \psi_{\downarrow}^{\dagger}(\mathbf{r}) \end{pmatrix} \quad (41)$$

$$\tilde{\psi}^{\dagger}(\mathbf{r}) = \begin{pmatrix} \psi_{\uparrow}^{\dagger}(\mathbf{r}) & \psi_{\downarrow}(\mathbf{r}) \end{pmatrix}. \quad (42)$$

that still obey Fermionic commutation rules. With these two-component fields $\tilde{\psi}$ one can rewrite H_0 and H_I as:

$$H_0 = \int d\mathbf{r} \tilde{\psi}^{\dagger}(\mathbf{r}) \tilde{H}_0(\mathbf{r}, \mathbf{r}') \tilde{\psi}(\mathbf{r}') \quad (43)$$

$$H_I = \int d\mathbf{r} \tilde{\psi}^{\dagger}(\mathbf{r}) \left[\sum_{\mathbf{v}\mathbf{q}} \sqrt{\frac{\hbar}{2\omega_{\mathbf{q}\mathbf{v}}}} \int d\mathbf{r}' \Delta V_{scf}^{\mathbf{q}\mathbf{v}}(\mathbf{r}) \tilde{\sigma}_3 b_{\mathbf{v}\mathbf{q}} - \tilde{\sigma}_0 v_s(\mathbf{r}) \right] \tilde{\psi}(\mathbf{r}) + \frac{1}{2} \int d\mathbf{r} d\mathbf{r}' [\tilde{\psi}^{\dagger}(\mathbf{r}) \tilde{\sigma}_3 \tilde{\psi}(\mathbf{r}')] \frac{1}{|\mathbf{r} - \mathbf{r}'|} [\tilde{\psi}^{\dagger}(\mathbf{r}') \tilde{\sigma}_3 \tilde{\psi}(\mathbf{r})]. \quad (44)$$

where $\tilde{\sigma}_3$ is the Pauli matrix $\begin{pmatrix} 1 & 0 \\ 0 & -1 \end{pmatrix}$ and \tilde{H}_0 is defined as:

$$\tilde{H}_0(\mathbf{r}, \mathbf{r}') = \begin{pmatrix} \left[-\frac{\nabla^2}{2} + v_s(\mathbf{r}) - \mu \right] \delta(\mathbf{r} - \mathbf{r}') & \Delta_{ext}(\mathbf{r}, \mathbf{r}') \\ \Delta_{ext}^*(\mathbf{r}, \mathbf{r}') & -\left[-\frac{\nabla^2}{2} + v_s(\mathbf{r}) - \mu \right] \delta(\mathbf{r} - \mathbf{r}') \end{pmatrix} \quad (45)$$

The Hamiltonian in this new form does not features source terms for the field $\tilde{\psi}$ any longer, therefore the perturbation expansion for H_I will have exactly the same contributions (diagrams) as in conventional perturbation theory. The difference is that Green's functions and self energy will have a 2×2 matrix structure and vertices will carry the extra $\tilde{\sigma}_3$ terms [232].

\tilde{G} is obtained by solving of the Dyson equation, that is:

$$\tilde{G}(\mathbf{r}, \mathbf{r}', \omega_i) = \tilde{G}_0(\mathbf{r}, \mathbf{r}', \omega_i) + \tilde{G}_0(\mathbf{r}, \mathbf{r}', \omega_i) \tilde{\Sigma}(\mathbf{r}, \mathbf{r}', \omega_i) \tilde{G}(\mathbf{r}, \mathbf{r}', \omega_i) \quad (46)$$

Where $\tilde{G}_0(\mathbf{r}, \mathbf{r}', \omega_i)$ is the Green's function corresponding to the non interacting Hamiltonian H_0 .

Like in GW theory [230, 231] it is possible to increase the order of the approximation by dressing propagators and Green's functions (the phonon propagator is already dressed as it is computed externally) therefore defining the following approximation:

$$\tilde{\Sigma} = \underbrace{\text{diagram with wavy line}}_{\tilde{\Sigma}_{xc}} + \text{diagram with dashed line} - \tilde{\Sigma}_{DC} \quad (47)$$

where $\tilde{\Sigma}_{DC}$ is simply $\tilde{\tau}_3 v_{xc}$. This approximation neglects vertex corrections, this assumption can be justified for the phonon interaction by the same argument given by Migdal for the normal state [244, 240]. The absence of vertex corrections in the Coulomb vertex instead neglects the most important magnetic contributions to the superconducting pairing [232, 238].

The computational cost to pay for the approximation above mentioned is still relatively expensive. By looking at the Coulomb diagram, it corresponds to a self consistent GW approach in a 2×2 Nambu-Gor'kov space. It is better instead rely on the same approximations discussed in Sec. 3.3.3, assuming that electronic states are already well described by the Kohn-Sham Hamiltonian and neglect inter-band hybridization. The self energy is the same of Eq. 47, but the diagonal part of the second diagram is removed together with $\tilde{\Sigma}_{DC}$ (that was inserted in the first place to avoid the double counting of xc terms). In addition the Coulomb interaction in Eq. 3.1.5 can be taken to be static.

In the basis of the Kohn-Sham states (ψ_{nk}) this self energy then takes the form:

$$\tilde{\Sigma}_{nk}(\omega_i) = -\frac{1}{\beta} \sum_j \sum_{\mathbf{m}\mathbf{q}'} \left\{ \tilde{\sigma}_3 \tilde{G}_{nk}(\omega_i) \tilde{\sigma}_3 \sum_{\mathbf{v}} g_{nk, \mathbf{m}\mathbf{k}+\mathbf{q}}^{\mathbf{v}} D_{\mathbf{q}\mathbf{v}}^{ij} + \tilde{G}_{nk}(\omega_i) \circ \tilde{\sigma}_1 W_{nk, \mathbf{m}\mathbf{k}+\mathbf{q}} \right\} \quad (48)$$

where ω_i are the Matsubara frequencies, $\tilde{\sigma}_1$ is the Pauli matrix $\begin{pmatrix} 0 & 1 \\ 1 & 0 \end{pmatrix}$, $D_{\mathbf{q}\mathbf{v}}^{ij} = -2\omega_{\mathbf{v}\mathbf{q}} / \left[(\omega_i - \omega_j)^2 + \omega_{\mathbf{v}\mathbf{q}}^2 \right]$ is the phonon

propagator, \circ is the element-wise product and W the screened Coulomb interaction. $\bar{G}_{nk}(\omega_i)$ is the Nambu-Gor'kov Green's function that in momentum space is:

$$\bar{G}_{nk}(\omega_i) = \int_0^\beta d\tau e^{-i\omega_i(\tau-\tau')} \int d\mathbf{r}\mathbf{r}' \varphi_{nk}^*(\mathbf{r}) \bar{G}(\tau\mathbf{r}, \tau'\mathbf{r}') \varphi_{nk}(\mathbf{r}') \quad (49)$$

and is the solution of the Dyson equation:

$$\bar{G}_{nk}(\omega_i) = \bar{G}_{0nk}(\omega_i) + \bar{G}_{0nk}(\omega_i) \bar{\Sigma}_{nk}(\omega_i) \bar{G}_{nk}(\omega_i) \quad (50)$$

where $\bar{G}_{0nk}(\omega_i)$ is the Green's function corresponding to the non-interacting Hamiltonian H_0 . The above equations is the central result of the Éliashberg theory of superconductivity. Their solution is achieved by first expanding this matrix equation into Pauli matrices and separating it into components. The decomposition leads to a intuitive form for $G_{nk}(\omega_i)$ which reads as:

$$\begin{pmatrix} i\omega_i Z_{nk}(\omega_i) + [\xi_{nk} + \mathbb{X}_{nk}(\omega_i)] & \phi_{nk}(\omega_i) \\ \phi_{nk}(\omega_i) & i\omega_i Z_{nk}(\omega_i) - [\xi_{nk} + \mathbb{X}_{nk}(\omega_i)] \end{pmatrix} \frac{1}{[i\omega_i Z_{nk}(\omega_i)]^2 - [\xi_{nk} + \mathbb{X}_{nk}(\omega_i)]^2 - \phi_{nk}^2(\omega_i)} \quad (51)$$

where \mathbb{X} (not to be confused with the superconducting order parameter) shifts the non-interacting energies, Z behaves as a mass term and $\Delta = \phi/Z$ is the function giving the superconducting gap (this interpretation is evident by analytically continuing \bar{G} to the real frequency axis ($i\omega_i \rightarrow \omega$)). Δ , \mathbb{X} and Z are now scalar functions and can usually be assumed to be real valued¹. The set of equations satisfied by these functions are the Éliashberg equations [31, 246]. Owing to their computational cost, due to the presence of nested Matsubara and momentum integrations these are usually solved by imposing extra approximations. In particular on the Coulomb interactions that will be discussed in Sec. 3.2.3. Neglecting for the moment the Coulomb term in the expression of the self-energy, its component form reads:

$$Z_{\mathbf{k}}(i\omega_i) = 1 - \frac{1}{\beta} \sum_{mq\nu, j} [|g_{nk, m\mathbf{k}+q}|^2 D_{\nu q}^{ij}] \frac{i\omega_j Z_{m\mathbf{k}+q}(i\omega_j)}{i\omega_i \Theta_{m\mathbf{k}+q}(i\omega_j)} \quad (52)$$

$$\mathbb{X}_{nk}(i\omega_i) = \frac{1}{\beta} \sum_{mq\nu, j} [|g_{nk, m\mathbf{k}+q}|^2 D_{\nu q}^{ij}] \frac{\mathbb{X}_{m\mathbf{k}+q}(i\omega_j) + \epsilon_{m\mathbf{k}+q}}{\Theta_{m\mathbf{k}+q}(i\omega_j)}$$

$$\Delta_{nk}(i\omega_i) = \frac{1}{\beta} \sum_{mq\nu, j} [|g_{nk, m\mathbf{k}+q}|^2 D_{\nu q}^{ij} + W_{nk, m\mathbf{k}+q}] \frac{\Delta_{m\mathbf{k}+q}(i\omega_j)}{\Theta_{m\mathbf{k}+q}(i\omega_j)},$$

where $\Theta_{m\mathbf{k}+q}$ is the denominator of Eq. 51.

The position of the Fermi level is determined by calculating the number of particles per unit cell:

$$1 - \frac{2}{\beta} \sum_{\mathbf{k}, i\omega_j} \frac{\mathbb{X}_{nk}(i\omega_j) + \epsilon_{nk}}{\Theta_{nk}(i\omega_j)}.$$

¹One can show that for the Hamiltonian Eq. 71, the Δ , Z and \mathbb{X} functions satisfy a set of equations with real coefficients. Note that complex solutions can be found as in the famous three crystal experiment [245], however, this situation is rather unusual and is generally neglected.

As mentioned above, due to the nested Matsubara and BZ summation those equations are cumbersome and numerically expensive to solve. A recent attempt by Sano et al. [247] for a full solution on a realistic system (H_3S) evidenced its complexity. In particular the BZ summation is troublesome because it requires at the same time to perform a very careful integration in \mathbf{k} around the Fermi level, and the high energy integration to converge the Coulomb contribution (technically it extends to energies up to several Rydberg). Two approximations that are conventionally use to overcome this difficulty are:

1. to replace the Coulomb interaction by an effective one that acts only near the Fermi level.
2. to assume that the only relevant \mathbf{k} dependence is through ϵ_{nk} .

The first approximation has been extensively used by Giustino and coworkers to develop an anisotropic Éliashberg approach [192]. The second approximation is used in Ref. [193]. In the following, we focus only on a combined approximation in which both are performed at the same time

Isotropic Approximation. Éliashberg equations are simplified enormously by replacing any \mathbf{k} -dependence on the coupling kernels with its energy ϵ_{nk} . At the same time one assume that all interactions, including the Coulomb interaction can be replaced by their Fermi surface average. This leads to the simpler form of Eqs. 52:

$$\begin{aligned} Z(i\omega_i) &= 1 + \frac{\pi}{\omega_i \beta} \sum_j \frac{\omega_j}{\sqrt{\omega_j^2 + \Delta^2(i\omega_j)}} \lambda(i\omega_j - i\omega_i) \\ \Delta(i\omega_i) Z(i\omega_i) &= \frac{\pi}{\beta} \sum_j \frac{\Delta(i\omega_j)}{\sqrt{\omega_j^2 + \Delta^2(i\omega_j)}} [\lambda(i\omega_j - i\omega_i) - \mu] \end{aligned} \quad (53)$$

where

$$\lambda(i\omega_i - i\omega_j) = \int \frac{2\omega\alpha^2 F(\omega)}{(\omega_i - \omega_j)^2 + \omega^2} d\omega,$$

with

$$\alpha^2 F(\omega) = \frac{1}{N_{E_F}} \sum_{kq, \nu} |g_{nk, m\mathbf{k}+q, \nu}|^2 \delta(\epsilon_{nk}) \delta(\epsilon_{m\mathbf{k}+q}) \delta(\omega - \omega_{q\nu}), \quad (54)$$

where N_{E_F} is the density of states (DOS) at the Fermi level. In this approximation, the Fermi shift function \mathbb{X} becomes zero. In Eq. 53 the entire role of the Coulomb interactions is eventually assumed by the single number μ defined as the average of $W_{nk, m\mathbf{k}+q}$ at the Fermi level, times N_{E_F} itself. This approximation will be discussed in the next section.

By assuming that Δ is small enough (near T_c), one can derive a linearized form of the Éliashberg equations:

$$Z(i\omega_i) = 1 + \frac{\pi}{\omega_i \beta} \sum_j \lambda(i\omega_j - i\omega_i) \frac{\omega_j}{|\omega_j|} \quad (55)$$

$$\Delta(i\omega_i) Z(i\omega_i) = \frac{\pi}{\beta} \sum_j \frac{\Delta_g(i\omega_j)}{|\omega_j|} [\lambda(i\omega_j - i\omega_i) - \mu] \quad (56)$$

particularly useful to compute T_c .

3.2.3. Morel-Anderson theory

Coulomb interactions, as discussed in Sec. 3.1.5, play a major role in the mechanism of phonon-driven superconductors. In Eqs. 53 and Eqs. 56 the role of Coulomb interactions has been collapsed to a single quantity μ . This is because μ is usually finite and almost constant in the energy range of $\sim \epsilon_F$, the Fermi energy. In consequence, one can safely drop any energy dependence of μ and assume that λ is finite (attractive) only when $i\omega_j - i\omega_i$ is small, practically below a cutoff frequency ω_c . For high frequencies, we can also assume that $\Delta(i\omega_i)$ is constant ($= \Delta^\infty$) and $\lambda = 0$. Then the linearized gap equation for low frequencies is simplified as,

$$\begin{aligned} \Delta(i\omega_i) &= \frac{\pi}{\beta Z(i\omega_i)} \sum_{|\omega_j| < \omega_c} \frac{\Delta(i\omega_j)}{|\omega_j|} (\lambda(i\omega_j - i\omega_i) - \mu) \\ &- \mu \Delta^\infty \frac{\pi}{\beta Z(i\omega_i)} \sum_{\omega_c < |\omega_j| < \epsilon_F} \frac{1}{|\omega_j|} \end{aligned} \quad (57)$$

Since we can assume that $Z(i\omega_i) = 1$ (that is, the mass renormalization effect due to the electron-phonon coupling is absent for large ω_i),

$$\Delta_g^\infty = -\mu \frac{\pi}{\beta} \sum_{|\omega_j| < \omega_c} \frac{\Delta(i\omega_j)}{|\omega_j|} - \mu \Delta^\infty \frac{\pi}{\beta} \sum_{\omega_c < |\omega_j| < \epsilon_F} \frac{1}{|\omega_j|}$$

In the limit of low temperature, replacing the summation with integration, this gives

$$\Delta^\infty = - \left(\mu \frac{\pi}{\beta} \sum_{|\omega_j| < \omega_c} \frac{\Delta_g(i\omega_j)}{|\omega_j|} \right) / (1 + \mu \log(\epsilon_F/\omega_c)) \quad (58)$$

If we plug Eq. 58 into Eq. 57, we obtain

$$\Delta(i\omega_i) = \frac{\pi}{\beta Z(i\omega_i)} \sum_{|\omega_j| < \omega_c} \frac{\Delta(i\omega_j)}{|\omega_j|} (\lambda(i\omega_j - i\omega_i) - \mu_c^*) \quad (59)$$

where

$$\mu_c^* = \frac{\mu}{1 + \mu \log(\epsilon_F/\omega_c)} \quad (60)$$

which, for all practical reasons we call the pseudo-Coulomb potential. Moreover, if we assume that $\lambda(i\omega_j - i\omega_i)$ is constant

$$\lambda \equiv \lambda(0) = 2 \int \frac{\alpha^2 F(\omega)}{\omega^2} d\omega \quad (61)$$

for $|\omega_j| < \omega_D$ and $Z = 1 + \lambda$, Eq. 59 becomes

$$(1 + \lambda) \Delta(i\omega_i) = (\lambda - \mu_c^*) \sum_j \frac{\Delta(i\omega_j)}{[2j + 1]}. \quad (62)$$

When ω_i dependence on Δ can be neglected, Eq. 59 is further simplified as

$$\frac{1 + \lambda}{\lambda - \mu_c^*} = \sum_{i=0}^{\omega_D/2\pi T_c - 1/2} \frac{1}{i + 1/2} \quad (63)$$

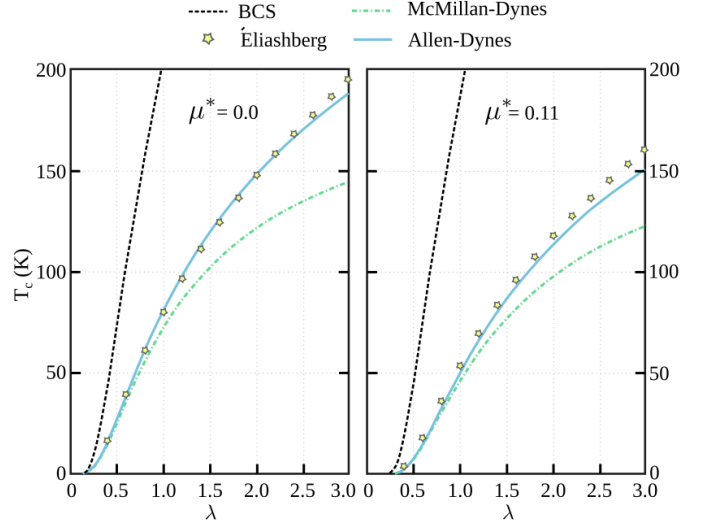


Figure 14: Superconducting critical temperatures calculated with the BCS equation, the solution of the Éliashberg equations, the McMillan-Dynes formula [249] and the Allen-Dynes parameterization [250]. The phononic coupling used in this model is an Einstein mode coupling at 60 meV of energy ($\omega_{log} = 60$ meV ~ 596 K)

which once solved gives an analytically estimation for T_c :

$$T_c = 1.13 \omega_D \exp \left(- \frac{1 + \lambda}{\lambda - \mu_c^*} \right) \quad (64)$$

By comparing this expression with the obtained with BCS weak coupling theory,

$$T_c = 1.13 \omega_D \exp \left(- \frac{1}{\lambda} \right), \quad (65)$$

we see that the mass enhancement effect ($Z = 1 + \lambda$) and the effect of the Coulomb repulsion ($\lambda - \mu_c^*$) both suppressing superconductivity, appearing in the numerator and denominator of the exponent, respectively.

3.2.4. Empirical models for T_c

Equation (64), as it stands is not reliably accurate for predictions, but it can be greatly improved by introducing extra parameters to be fitted to the solution of the Éliashberg equations (Eq. 56). This procedure was introduced by McMillan in 1968 [248] that used, as a reference, the experimental phonon spectral function of Nb for different scaling and μ_c^*/λ ratios. He obtained the so-called McMillan equation for T_c , which depends on a small number of simple parameters:

$$T_c = \frac{\omega_D}{1.45} \exp \left[- \frac{1.04(1 + \lambda)}{\lambda - \mu_c^*(1 + 0.62\lambda)} \right]$$

In 1972 Dynes [249] modified the prefactor to $\omega/1.20$ instead of $\omega_D/1.45$. Subsequently, in 1975, Allen and Dynes [250] performed a thorough analysis on the dependence of T_c on material properties (λ , μ^* , phonon spectrum) and this equation was re-parameterized in a slightly different form:

$$T_c = \frac{\omega_{log}}{1.2} \exp \left[- \frac{1.04(1 + \lambda)}{\lambda - \mu_c^*(1 + 0.62\lambda)} \right] \quad (66)$$

where, instead of the Debye energy, a logarithmic average is introduced:

$$\omega_{\log} = \exp \left[\frac{2}{\lambda} \int \log(\omega) \frac{\alpha^2 F(\omega)}{\omega} d\omega \right]. \quad (67)$$

This term corrects for the low energy phonons that are relevant for the superconducting pairing. The McMillan equation in Allen-Dynes form (66) is the most widely used approach for the calculation of the superconducting critical temperature from first principles. One of the aspects that makes it so accurate, in spite of its formal simplicity, is that in this parameterization the μ_c^* results to be largely material independent with a typical value of 0.11. Note that this universality of μ_c^* is only valid for the McMillan formula. In the original Éliashberg equations the value of μ_c^* is linked to the cutoff frequency ω_c and it should be computed from equation 60: Its value may differ significantly from 0.11.

The McMillan approach starts to deviate from the Éliashberg formulation at very strong coupling ($\lambda > 1.5$), above which it tends to saturate underestimating the true critical temperature. In this regime a more accurate approach was introduced by Allen and Dynes [250] involving the additional parameter:

$$\omega_2 = \left\{ \frac{2}{\lambda} \int \omega \alpha^2 F(\omega) d\omega \right\}^{\frac{1}{2}}. \quad (68)$$

and the prefactor

$$f = \left\{ 1 + \left[\frac{\lambda}{2.46 (1 + 3.8\mu^*)} \right]^{\frac{3}{2}} \right\}^{\frac{1}{3}} \times \left\{ 1 + \frac{(\omega_2/\omega_{\log} - 1)\lambda^2}{\lambda^2 + 3.31(1 + 6.3\mu^*)(\omega_2/\omega_{\log})} \right\}, \quad (69)$$

that multiply the right hand side of Eq. (66):

$$T_c = f \frac{\omega_{\log}}{1.2} \exp \left[-\frac{1.04(1 + \lambda)}{\lambda - \mu_c^*(1 + 0.62\lambda)} \right]. \quad (70)$$

This extended form of the McMillan equation (Allen-Dynes 2) is very accurate (see Fig. 14) and for conventional isotropic superconductors predicts critical temperatures that are usually identical to those obtained by the solution of the Éliashberg equations.

3.3. Density functional theory for superconductors

Density functional theory for superconductors (SCDFT) is an extension of DFT to account for the very peculiar symmetry breaking that occurs in a superconductor [30, 243]. Proposed in 1988 [32] by Oliveira, Gross and Kohn was later revisited and extended [251, 33, 34] to merge with the multi-component DFT of Kreibich and Gross [252] to include nuclear motion. This version of SCDFT has been extremely successful in predicting superconductivity in a wide variety of materials [253, 254] and proved especially useful for the investigation of superconductivity in high pressure environments [173].

3.3.1. SCDFT Hamiltonian and OGK theorem

The starting point of SCDFT is the non relativistic Hamiltonian for interacting electrons and nuclei subjected to external fields:

$$H = H_e + H_{en} + H_n + H_{ext}, \quad (71)$$

where e stands for electrons, n for nuclei and ext for external fields. The electronic Hamiltonian reads as:

$$H_e = \sum_{\sigma} \int d^3r \psi_{\sigma}^{\dagger}(\mathbf{r}) \left[-\frac{1}{2} \nabla^2 - \mu \right] \psi_{\sigma}(\mathbf{r}) + \frac{1}{2} \sum_{\sigma\sigma'} \int d^3r d^3r' \psi_{\sigma}^{\dagger}(\mathbf{r}) \psi_{\sigma'}^{\dagger}(\mathbf{r}') \frac{1}{|\mathbf{r} - \mathbf{r}'|} \psi_{\sigma'}(\mathbf{r}') \psi_{\sigma}(\mathbf{r}) \quad (72)$$

with ψ the electronic field operators and μ the chemical potential.

Nuclei need to be considered explicitly (not just as source of an external potential like in conventional DFT [255]) because in electron-phonon driven superconductors the ion dynamics provides an essential part of the superconducting coupling:

$$H_n = - \int d^3R \Phi^{\dagger}(\mathbf{R}) \frac{\nabla^2}{2M} \Phi(\mathbf{R}) \quad (73)$$

$$+ \frac{1}{2} \int d^3R d^3R' \Phi^{\dagger}(\mathbf{R}) \Phi^{\dagger}(\mathbf{R}') \frac{Z^2}{|\mathbf{R} - \mathbf{R}'|} \Phi(\mathbf{R}') \Phi(\mathbf{R})$$

$$H_{en} = - \sum_{\sigma} \int d^3R d^3r \psi_{\sigma}^{\dagger}(\mathbf{r}) \Phi^{\dagger}(\mathbf{R}) \frac{Z}{|\mathbf{R} - \mathbf{r}|} \Phi(\mathbf{R}) \psi_{\sigma}(\mathbf{r}) \quad (74)$$

where Φ are ionic field operator, M the mass of the nuclei and Z the atomic number (for simplicity we consider monoatomic systems).

The Hamiltonian needs to include an external symmetry breaking field [243] that for singlet superconductivity can be chosen as:

$$H_{A_{ext}} = \int d^3r d^3r' A_{ext}^*(\mathbf{r}, \mathbf{r}') \psi_{\uparrow}(\mathbf{r}) \psi_{\downarrow}(\mathbf{r}') + h.c. \quad (75)$$

In addition, one should also add an external field coupling with the electronic density:

$$H_{V_{ext}} = \int d^3r v_{ext}(\mathbf{r}) \sum_{\sigma} \psi_{\sigma}^{\dagger}(\mathbf{r}) \psi_{\sigma}(\mathbf{r}) \quad (76)$$

and an (different) external field that couples with the nuclei:

$$H_{W_{ext}} = \int \left[\prod_j d^3R_j \Phi^{\dagger}(\mathbf{R}_j) \Phi(\mathbf{R}_j) \right] W_{ext}(\{\mathbf{R}_i\}). \quad (77)$$

In its modern form [33, 34], SCDFT is based on the three densities:

$$\rho(\mathbf{r}) = \text{Tr} \left[\varrho_0 \sum_{\sigma} \psi_{\sigma}^{\dagger}(\mathbf{r}) \psi_{\sigma}(\mathbf{r}) \right] \quad (78)$$

$$\chi(\mathbf{r}, \mathbf{r}') = \text{Tr} [\varrho_0 \psi_{\uparrow}(\mathbf{r}) \psi_{\downarrow}(\mathbf{r}')] \quad (79)$$

$$\Gamma(\{\mathbf{R}_i\}) = \text{Tr} \left[\varrho_0 \prod_j \Phi^{\dagger}(\mathbf{R}_j) \Phi(\mathbf{R}_j) \right] \quad (80)$$

where ϱ_0 is the grand canonical density matrix.

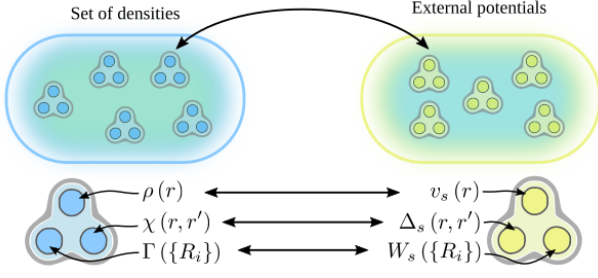


Figure 15: Illustration to show the Oliveira-Gross-Kohn (OGK) theorem that guarantees a one-to-one mapping between the set of densities (ρ, χ, Γ) onto external potentials (v, Δ, W) in SCDFT.

A recent paper by Schmidt et al. [256] have evidenced the problem of non-interacting (v, Δ) -representability of the superconducting densities in SCDFT. Indeed, this work proved that at zero temperature it seems that such a non-interacting system does not exist. Also showed, that in the limit of weakly correlated systems SCDFT still provides reliable results. They proposed a reduced density matrix functional theory for superconductors [257] and proved the existence of a Kohn-Sham system at finite temperature and corresponding Bogoliubov-de Gennes-like single particle equation.

The SCDFT generalization of the Hohenberg-Kohn theorem [255] (at finite temperature [258]) states:

1. There is a one-to-one mapping between the set of densities $\rho(\mathbf{r}), \chi(\mathbf{r}, \mathbf{r}'), \Gamma(\{\mathbf{R}_i\})$ onto the set of external potentials $v_{ext}(\mathbf{r}), \Delta_{ext}(\mathbf{r}, \mathbf{r}'), W_{ext}(\{\mathbf{R}_i\})$
2. There is a variational principle so that it exists a functional Ω that:

$$\begin{aligned} \Omega[\rho_0, \chi_0, \Gamma_0] &= \Omega_0 \\ \Omega[\rho, \chi, \Gamma] &> \Omega_0 \quad \text{for} \quad \rho, \chi, \Gamma \neq \rho_0, \chi_0, \Gamma_0 \end{aligned} \quad (81)$$

where ρ_0, χ_0, Γ_0 are the ground state densities and Ω_0 the grand canonical potential.

The fact that all observable are functionals of the densities and that H is the sum of internal interactions (Eq. 71) and couplings with external fields (Eq. 75 + Eq. 76 + Eq. 77) allows $\Omega[\rho, \chi, \Gamma]$ to be written as:

$$\begin{aligned} \Omega[\rho, \chi, \Gamma] &= F[\rho, \chi, \Gamma] + \int d^3r v_{ext}(\mathbf{r}) \rho(\mathbf{r}) \\ &+ \int \Gamma(\{\mathbf{R}_i\}) W_{ext}(\{\mathbf{R}_i\}) \prod_j d^3R_j \\ &+ \int d^3r d^3r' \Delta_{ext}^*(\mathbf{r}, \mathbf{r}') \chi(\mathbf{r}, \mathbf{r}') + c.c. \end{aligned} \quad (82)$$

that defines the universal functional $F[\rho, \chi, \Gamma]$.

3.3.2. The Kohn-Sham system

As for conventional DFT, it is useful to introduce the Kohn-Sham system [197], a non-interacting system whose free energy

is minimized by the the same densities of the physical (interacting) one, under the three external potentials:

$$\begin{aligned} v_s(\mathbf{r}) &= v_{ext}(\mathbf{r}) + v_H(\mathbf{r}) + v_{xc}(\mathbf{r}) \\ \Delta_s(\mathbf{r}, \mathbf{r}') &= \Delta_{ext}(\mathbf{r}, \mathbf{r}') + \Delta_{xc}(\mathbf{r}, \mathbf{r}') \\ W_s(\{\mathbf{R}_i\}) &= W_{ext}(\{\mathbf{R}_i\}) + W_H(\{\mathbf{R}_i\}) + W_{xc}(\{\mathbf{R}_i\}). \end{aligned} \quad (83)$$

The subscript H stands for Hartree terms and xc are the exchange-correlation potentials obtained by a functional derivative of the xc functional of the theory $F_{xc}[\rho, \chi, \Gamma]$, that can be obtained from perturbation theory [33, 34].

The electronic part of the Kohn-Sham equations are then derived by diagonalizing the Kohn-Sham Hamiltonian with a Bogoljubov-Valating transformation [259, 243]:

$$\psi_\sigma(\mathbf{r}) = \sum_i \left[u_i(\mathbf{r}) \gamma_{i\sigma} - \text{sgn}(\sigma) v_i(\mathbf{r}) \gamma_{i\sigma}^\dagger \right] \quad (84)$$

leading to the diagonalization conditions:

$$\begin{aligned} \left[-\frac{\nabla^2}{2} + v_s(\mathbf{r}) - \mu \right] u_i(\mathbf{r}) + \int \Delta_s(\mathbf{r}, \mathbf{r}') v_i(\mathbf{r}') d^3r' &= E_i u_i(\mathbf{r}) \\ - \left[-\frac{\nabla^2}{2} + v_s(\mathbf{r}) - \mu \right] v_i(\mathbf{r}) + \int \Delta_s^*(\mathbf{r}, \mathbf{r}') u_i(\mathbf{r}') d^3r' &= E_i v_i(\mathbf{r}) \end{aligned} \quad (85)$$

that are the electronic Kohn-Sham equation for SCDFT. Their mathematical form is well known in superconductivity literature as Bogoljubov-deGennes (BdG) equations [243] which are mostly used, within the BCS model, to describe superconducting structures in real space. In SCDFT, these equations become exact for the calculation of the total energy and the normal $(\rho(\mathbf{r}))$ and anomalous $(\chi(\mathbf{r}, \mathbf{r}'))$ densities:

$$\rho(\mathbf{r}) = 2 \sum_i \left[|u_i(\mathbf{r})|^2 f(E_i) + |v_i(\mathbf{r})|^2 f(-E_i) \right] \quad (86)$$

$$\chi(\mathbf{r}, \mathbf{r}') = \sum_i u_i(\mathbf{r}) v_i^*(\mathbf{r}') f(-E_i) - v_i^*(\mathbf{r}) u_i(\mathbf{r}') f(E_i). \quad (87)$$

In the absence of superconductivity, both χ and Δ are zero and the Kohn-Sham equation 85 and 86 become the usual Kohn-Sham equations of conventional DFT:

$$\left[-\frac{\nabla^2}{2} + v_s(\mathbf{r}) - \mu \right] \varphi_{nk}(\mathbf{r}) = \xi_{nk} \varphi_{nk}(\mathbf{r}). \quad (88)$$

This form is slightly more general because it would still include the full effect of temperature and ionic motion since it is still coupled with the ion dynamics via the potentials in Eq. 83.

Transformation to momentum space

Eq. 88 can be solved in the superconducting state (i.e. keeping the non-zero χ in the functional $v_s[\rho, \chi, \Gamma]$) and the corresponding eigenfunctions $\varphi_{nk}(\mathbf{r})$ can be used as a basis set to express the BdG equations in \mathbf{k} space. Introducing the expansion:

$$u_i(\mathbf{r}) = \sum_{nk} u_{i,nk} \varphi_{nk}(\mathbf{r}) \quad (89)$$

$$v_i(\mathbf{r}) = \sum_{nk} v_{i,nk} \varphi_{nk}(\mathbf{r}) \quad (90)$$

$$\Delta_s(\mathbf{r}, \mathbf{r}') = \sum_{nn'kk'} \Delta_{s,nn'kk'} \varphi_{nk}(\mathbf{r}) \varphi_{n'k'}(\mathbf{r}') \quad (91)$$

that when inserted into Eq. 85 and using the orthogonality of the basis set gives:

$$\begin{aligned}\xi_{nk} u_{i,nk} + \sum_{n'k'} \Delta_{s,nn'kk'} v_{i,n'k'} &= E_i u_{i,nk} \\ -\xi_{nk} v_{i,nk} + \sum_{n'k'} \Delta_{s,nn'kk'}^* u_{i,n'k'} &= E_i v_{i,nk}\end{aligned}\quad (92)$$

which is a form of the BdG equations particularly useful for introducing approximations. At this stage, the problem to solve is still very complicated and can not be tackled without introducing approximations. The key approximation is to decouple as much as possible the many degrees of freedom (and densities) of the problem:

1. Decouple electrons from ions separating static and dynamic part of the interaction, including the latter in a perturbative fashion.
2. Decouple the high energy chemical scale (responsible for bonding) from low energy pairing interactions (responsible for superconductivity).

3.3.3. Electron-phonon interaction

The problem of correlated electron-nuclear dynamics is enormously complex, however for systems close to equilibrium, theoretical methods are able to describe accurately and efficiently the nuclear dynamics and electron-phonon coupling [195, 260, 203]. A key approximation is to ignore the effect of superconductivity on the lattice dynamics and on the electron-phonon interaction. As the superconducting transition is usually of type-II, this approximation is exact near the critical temperature, where the superconducting density becomes infinitesimally small. This allow us to use the lattice dynamics of the normal state as in Sec. 3.1.

The step one needs to perform, out of computational convenience, is to approximate the dynamic part of H_{en} with \tilde{H}_{e-ph} defined in Sec. 3.1.3. This step can be certainly justified empirically by its success in many practical applications [261, 195, 202] but is theoretically less rigorous. The most compelling justification is that if the Kohn-Sham band structure is close to the interacting one, so will likely be its response to a lattice motion. Clearly if Kohn-Sham bands are far off from the interacting ones (like in strongly correlated systems) then use of Kohn-Sham electron-phonon coupling is expected to be a poor approximation.

Band decoupling approximation

The electronic BdG Kohn-Sham equations 92, can be further simplified by assuming that the superconducting condensation is a small perturbation on the non-superconducting system. As already pointed out in the previous subsection, since the superconducting transition is of second order, the assumption becomes exact close to T_c therefore it would not affect the estimation of T_c itself.

This assumption implies that the superconducting transition will not induce a structural one, therefore $\Delta_s(\mathbf{r}, \mathbf{r})$ should keep the original lattice periodicity and the quantum number \mathbf{k} in

Eq. 88 must be maintained [251, 262]. In other words, the summations in equation Eq. 89,90 should only run over the band index n and not over \mathbf{k} .

The summation over n means that the superconducting transition can still induce *hybridization* between different bands corresponding to the same \mathbf{k} -point. However, unless bands are degenerate (or close to degeneracy with respect to the energy scale set by Δ_s that is of the order 10 meV), this hybridization must be extremely small. Therefore, apart from anomalous cases, one can introduce a second and stronger approximation by ignoring this superconductivity induced band hybridization effect. Eq. 89,90 reduce to:

$$u_i(\mathbf{r}) \equiv u_{nk}(\mathbf{r}) = u_{nk} \varphi_{nk}(\mathbf{r}) \quad (93)$$

$$v_i(\mathbf{r}) \equiv v_{nk}(\mathbf{r}) = v_{nk} \varphi_{nk}(\mathbf{r}),$$

that implies $\Delta_{s,nn'kk'} \rightarrow \delta_{nk,n'k'} \Delta_{s,nk}$.

Inserting Eq. 93 into Eq. 92 one can formally solve these equations obtaining:

$$u_{nk} = \frac{1}{\sqrt{2}} \text{sgn}(E_{nk}) e^{\phi_{nk}} \sqrt{1 + \frac{\xi_{nk}}{|E_{nk}|}} \quad (94)$$

$$v_{nk} = \frac{1}{\sqrt{2}} \sqrt{1 - \frac{\xi_{nk}}{|E_{nk}|}} \quad (95)$$

with $e^{\phi_{nk}} = \Delta_s(n\mathbf{k}) / |\Delta_s(n\mathbf{k})|$ and $E_{nk} = \pm \sqrt{\xi_{nk}^2 + |\Delta_s(n\mathbf{k})|^2}$. While the densities in Eq. 86,87 take on the simple form:

$$\rho(\mathbf{r}) = \sum_{nk} \left[1 - \frac{\xi_{nk}^2}{|E_{nk}|} \tanh\left(\frac{\beta |E_{nk}|}{2}\right) \right] |\varphi_{nk}(\mathbf{r})|^2 \quad (96)$$

$$\chi(\mathbf{r}, \mathbf{r}') = \frac{1}{2} \sum_{nk} \frac{\Delta_s(n\mathbf{k})}{|E_{nk}|} \tanh\left(\frac{\beta |E_{nk}|}{2}\right) \varphi_{nk}(\mathbf{r}) \varphi_{nk}^*(\mathbf{r}') \quad (97)$$

The entire superconducting problem is now reduced to the construction of the matrix elements of the Kohn-Sham potential $\Delta_s(n\mathbf{k})$ that are obtained by the solution of the equation:

$$\Delta_{xc} = \frac{\delta F_{xc}[\rho, \chi[\Delta_s, \rho, \Gamma], \Gamma]}{\delta \chi}. \quad (98)$$

Several approximations for F_{xc} have been proposed and tested [34, 263, 264, 235, 265], and all lead to a BCS-like form of the equation above:

$$\begin{aligned}\Delta_s(n\mathbf{k}) &= \mathcal{Z}(n\mathbf{k}) \Delta_s(n\mathbf{k}) \\ &+ \frac{1}{2} \sum_{n'k'} \mathcal{K}(n\mathbf{k}, n'\mathbf{k}') \frac{\tanh\left(\frac{\beta}{2} E_{n'k'}\right)}{E_{n'k'}} \Delta_s(n'\mathbf{k}')\end{aligned}\quad (99)$$

Where the two kernels \mathcal{K} and \mathcal{Z} depend on the chosen F_{xc} functional and contain all the key information about electronic states, electron-electron and electron-phonon coupling. The main strength of the theory is its low computational cost, as compared to Green's function methods, mainly because the gap equation 99, while being fully dynamical and including strong coupling effects, does not involve cumbersome Matsubara integration (all the complexity is absorbed in the process of functional construction). This means that the equation can

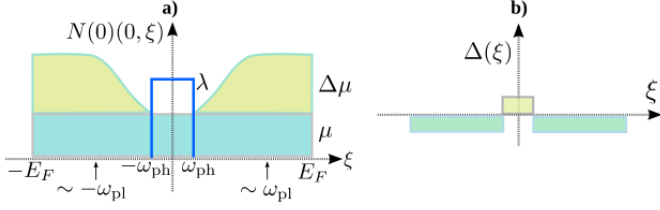


Figure 16: Schematic illustration on the energy dependence of a) the kernel \mathcal{K} and b) the gap function Δ in the SCDFT equation.

be easily solved in its full \mathbf{k} resolution and in a full energy window. Therefore, all anisotropic effects as well as high energy Coulomb interactions can be included in a fully *ab-initio* fashion, including the pairing induced by exchange of spin-fluctuations [238, 266].

3.3.4. Plasmon-Assisted Superconductivity

The consequences of electron-electron interaction in superconductors have been extensively studied [237], beyond the approximations discussed in Sec. 3.1.5, for instance to include magnetic effects in cuprates and Fe-superconductors. Beyond these, there is a Coulomb effect that often is overlooked, the plasmon mechanism, that exploits the dynamical structure of the screened Coulomb interaction represented by the frequency-dependent dielectric function $\epsilon(\omega)$ [267, 268, 269, 270].

In the theoretical treatment presented so far, we have neglected the Matsubara-frequency dependence of the screened Coulomb interaction W (eq. 3.1.5). However it has been argued that the dynamical structure in W can influence or even enhance superconductivity. Takada was the first to show that superconductivity could emerge in the electron-gas model even in the absence of phonon-mediated attractive interaction [267]. A natural theoretical background to treat on an equal footing the phonon-mediated interaction and dynamical screened Coulomb interaction is the *ab initio* density functional theory for superconductors as presented by Akashi et al. [235, 265] in full detail.

To give a simplified physical picture of the plasmon mechanism we will consider here a simplified model. Let us divide the kernel \mathcal{K} of the SCDFT gap eq. 99 into the contributions of the electron-phonon coupling \mathcal{K}^{eph} and the Coulomb interaction \mathcal{K}^{ee} :

$$\mathcal{K}(n\mathbf{k}, n'\mathbf{k}') = \mathcal{K}^{\text{eph}}(n\mathbf{k}, n'\mathbf{k}') + \mathcal{K}^{\text{ee}}(n\mathbf{k}, n'\mathbf{k}').$$

For \mathcal{K}^{eph} , it is finite and attractive within the a phonon energy ω_{ph} , but it becomes negligibly small for high energy states. Thus it can be approximated as:

$$N_{E_F} \mathcal{K}^{\text{eph}}(n\mathbf{k}, n'\mathbf{k}') = \begin{cases} -\lambda & (\xi_{n\mathbf{k}}, \xi_{n'\mathbf{k}'} < \omega_{\text{ph}}) \\ 0 & (\text{otherwise}) \end{cases}$$

On the other hand \mathcal{K}^{ee} , has large energy range. Adopting the simplified Morel-Anderson theory of Sec. 3.2.3

$$N_{E_F} \mathcal{K}^{\text{ee}}(n\mathbf{k}, n'\mathbf{k}') = \mu.$$

This situation is schematically shown in Fig. 16. As was discussed in Sec. 3.2.3, the sign of Δ is different for a low ξ and a high ξ , so that the scattering due to μ between high energy states and low energy states becomes effectively attractive. Let us now consider the frequency dependence of W or ξ dependence of \mathcal{K}^{ee} . Since the screening effect on W is less effective, \mathcal{K} is large for high energy states ($\Delta\mu$ in Fig. 16). Here, $\Delta\mu$ gives an additional attractive interaction between low energy states and high energy states in the SCDFT gap equation (eq. 99) so that T_c is enhanced. This plasmon mechanism for superconductivity becomes important when the ratio between ω_{ph} and typical energy scale of the frequency dependence of W is not negligibly small. In H_3S , for instance it has been shown that the plasmon mechanism has a substantial effect. However, since λ is extremely large the plasmon effect does not dominate over the phonon mechanism [271, 247].

4. Computational methods for structural prediction

Since the pioneering ideas of Schön and Jansen [272] on global structure optimization, the solid state community has gathered considerable expertise on how to identify the stable phases of materials from numerical simulations. This has permitted to introduce in the last 25 years techniques and computational tools to efficiently explore the potential energy (or enthalpy) landscape of complex systems, including hydrides, often yielding accurate predictions and description of the experimental results. These tools have had a good repercussion in many field but particularly on the high pressure community on which had led to numerous successful predictions including high-temperature superconductors. In this section, we will briefly review the key concepts of the most widely-used methods currently at the forefront in crystal structure prediction (CSP) of materials.

4.1. Ab-initio crystal structure prediction

The determination of the correct atomic structure of a material is fundamental to determine its physical properties. In particular, one normally seeks the thermodynamically most stable structure at a given temperature and pressure, although low-energy metastable structures are also of interest. It is often necessary to search over structures with many different stoichiometries to determine the most stable ones. In practice, only a finite number of stoichiometries can be searched and only a finite number of structures with a particular stoichiometry can be calculated, whereas both the number of stoichiometries and number of structures are in principle infinite.

Stable and metastable structures of a given system correspond to global and local minima of its potential energy surface (PES). Locating the global minimum of the PES of a complex system is a central problem in physics, chemistry and biology. Finding the most stable structures for a given composition is a challenging task that quickly becomes computationally prohibitive as the number of atoms under consideration increases. In the case of high-pressure hydrides, like in other materials, the number of local minima increases exponentially with the

number of atoms in the system [273] and the unconstrained structure prediction based solely on the chemical composition is considered a NP-hard problem (non-deterministic polynomial-time hard) in computer science. For a periodic system of N atoms, the number of degrees of freedom is $3N$ for the atomic coordinates, plus nine degrees of freedom accounting for the translational vectors that define the unit cell of the periodic system. If one considers that six degrees of freedom account for the translational invariance of the crystal and the rotational invariance of the cell, the remaining degrees of freedom define a $3N + 3$ dimensional optimization problem.

4.1.1. Potential energy surface

The Born-Oppenheimer energy surface $E(\mathbf{R}_i)$, in short the potential energy surface (PES), is the function that associates the total energy of a set of atoms to their positions: note that $E(\mathbf{R}_i)$ is formally the ground state eigenvalue of the Hamiltonian 2. In a non-periodic system the coordinates \mathbf{R}_i are a finite set, whereas in periodic crystals the PES depends on 3 angles and 3 lattice vectors $(a, b, c, \alpha, \beta, \gamma)$ that describe the unit cell plus the internal coordinates of the atom in the cell. The free energy is thus represented by a function of the internal degrees of freedom of the system and this is what is modeled with computational methods; its study is fundamental for the characterization of a material at given external conditions.

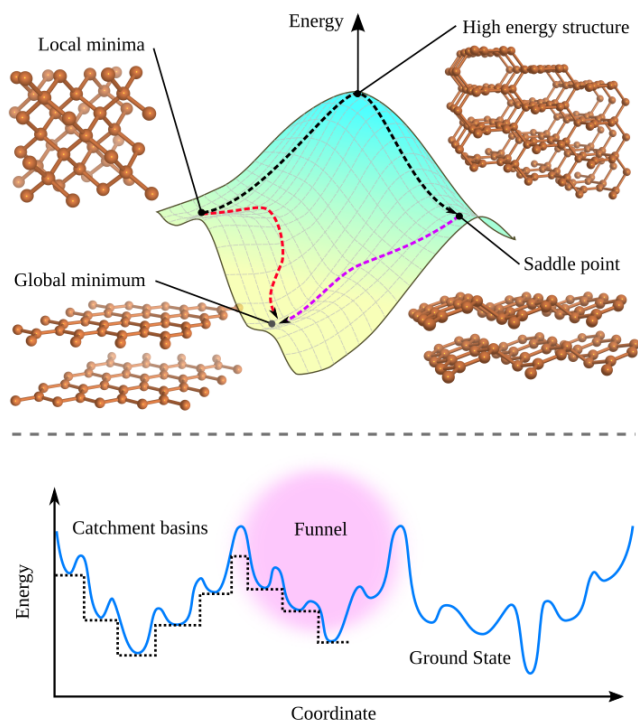


Figure 17: Top: Conceptual illustration of a potential energy surface and hypothetical structures ranked in energy in different areas of it. Bottom: a one-dimensional energy plot as function of reaction coordinate.

A schematic view of a potential energy surface with the hypothetical energy ranking of different crystalline structures is illustrated in the top panel of Fig. 17. We recall that each point on the PES represents a single atomic configuration $\{\mathbf{R}_i\}$. The

stationary points on the PES, which correspond to a set of stable atomic and cell configurations for which all forces vanish, are of utmost importance to predict the (meta)stable structures and the thermodynamics of a compound. These stationary points can be minima, where the system is locally stable, maxima or saddle points. The latter divide the PES into regions each uniquely related to a local minimum [274]. These regions are called *basins of attraction* or catchment basin and are defined as the set of configurations from which a steepest-descent relaxation converges to the basin minimum. The bottom panel of Fig. 17 shows a schematic one-dimensional energy profile on which a set of neighboring basins form a super-basins structure, called a *funnel*. Funnels are defined as collections of basins in which the global minimum of the set can be reached without crossing barriers that are very high. This means that the barrier to be crossed should not be larger than the average difference in energy between neighboring basins within the funnel.

Energy landscapes can be characterized by analyzing the energetic distribution of local minima and transition states connecting them. In systems described by PESs with staircase-like forms, where only one funnel exists and very few local minima have competitively similar energies separated by low barriers, the ground state can be easily found with any crystal structure prediction scheme. On the other hand, systems with characteristic energy landscapes that contain multiple funnels are a great challenge for global optimization algorithms.

4.1.2. Methods to explore structures

In structural prediction methods the goal is primarily to find the correct energetic ordering of dynamically stable local minima on the PES (a dynamically stable energy minimum is one in which the Hessian is positive definite). This is equivalent to minimizing the Gibbs free energy $G = UTS + pV$, whose components are the internal energy, temperature, entropy, pressure and volume of the system $-U, T, S, p$ and V respectively. The stable configuration with the lowest Gibbs free energy corresponds to the ground state structure and represents the most likely structure that a system will acquire at equilibrium conditions.

The main task of a global optimization method is thus to find the lowest-energy structure among all local minima. As mentioned above, the number of such local minima on a high-dimensional PES increases exponentially with the system size [273]. This makes it impossible to identify the global minimum even for moderately-sized systems with simple enumerative search methods. Limited computational time restricts all global optimization algorithms to perform a search on a (small) fraction of the total number of local minima based on assumptions on the characteristics of the PES. The lowest-energy structure found after a throughout search is then identified as the putative ground state (although in general there is no fundamental reason to identify it as a global minimum). Global optimization methods can be divided into two main groups: those based on thermodynamic (Boltzmann) approaches and metaheuristics ones, which include evolutionary and stochastic global optimizers. Simulated annealing, metadynamics and basin hopping are based on thermodynamic principles; genetic algorithms and

particle swarm optimization, for example, belong to the class of evolutionary methods; random search, database searching and data mining schemes are stochastic approaches which rely primarily on chemical intuition and structure-chemistry correlation models. We will briefly describe the main characteristics of those methods and how these have been used for searching for new high-pressure hydrides.

Random sampling

This method is based on the premise that a large part of the PES of a reasonably large assembly of atoms corresponds to very high-energy structures in which some atoms are much closer or far apart than their equilibrium bond length. Indeed, for most cases the empirical evidence suggests that large portions of the PES correspond to fragmented structures, while local minima correspond to niches -localized areas- around basins of attraction [275]. All these undesired portions can be avoided by imposing *a priori* constraints on the configuration space.

Random structure searching requires very few external parameters and is relatively easy to implement. The biases are largely controllable, understandable and based on physical principles. It is also possible to condition/steer the search by adding information from experiments, chemical and structural hypothetical candidates for the system in question, as well as information generated by previous searches.

Technically, a random search starts by generating a set of random atomic arrangements based on educated guesses of bond lengths. A random set of lattice parameters and angles between lattice vectors of the unit cell is generated and the cell volume is re-normalized to yield a random value within 50% of a chosen mean volume. Together with this initial random guess, an important step in these algorithms is the *shake*, in which one performs a random displacement of the atoms and if appropriate, a random adjustment of the unit cell. These atomic displacements (shakes) of a fraction of a bond length have a non-negligible chance of pushing the system into a nearby basin of attraction. This methodology has been proven to be robust and highly reliable for finding (in an unbiased way) the global minima of systems with up to ≈ 12 atoms unit cell, before the price for combinatorial complexity becomes too high to be acceptable. Imposing suitable constraints, however, searches have been successfully conducted on larger systems.

When the method was first proposed, the searches were conducted mostly at DFT level, but nowadays force-fields and other methods are coupled with random searches to improve the final efficiency. The most successful implementation of the random search methodology is the *Ab initio* Random Structure Searching (AIRSS) by Pickard-Needs [276, 277]. In the context of high pressure has been largely used to propose and uncover new stable phases of hydrogen [278], aluminum [279], ammonia [280] and in many other materials [281]. The corresponding code is released under the GPL2 licence and is tightly integrated in the CASTEP first-principles total energy code [282]. However, it is relatively straightforward to modify the scripts provided to adapt the method to other codes to obtain the core functionality.

Particle swarm optimization

Particle swarm optimization (PSO) is a methodology inspired by the choreography of a bird flock and can be viewed as a distributed-behavior algorithm that performs multidimensional searches [283]. PSO belongs to the class of metaheuristic methods, as it makes few or no assumptions about the solutions. The algorithm works by moving particles in the search-space based on efficient algorithms that use the particle's position and velocity (structures). Therefore, all the individuals in the swarm can quickly converge to the global position and near-optimal geographical position by the behavior of the flock and their flying histories.

Essentially in PSO, the behavior of each individual, which in the case of structural search is a structure, is affected by either the best local or the best global individual to help it fly through a hyperspace (i.e. PES). An individual (structure) can be optimized by a feedback mechanism and learn from its past experiences to adjust its flying speed and direction (search areas). This methodology exploits symmetry constraints during structure generation which tend to reduce the searching space and enhance the structural diversity. In the searches, a certain percentage of new structures are introduced in each generation to enhance structural diversity. PSO also uses structural characterization techniques to eliminate similar structures from the swarm. Which guarantee that all the individuals in the swarm can quickly converge to the global position and near-optimal geographical position. This algorithm when used for structure prediction it exploits local structural optimization, which reduce the noise of the energy surfaces and assures the generation of physically justified structures.

Particle Swarm Optimization exists in two variants, based on global and local PSO algorithms, which have both been successfully used in many applications [284]. The global PSO has the advantage of fast convergence, while the local PSO is good at avoiding premature convergence and thus enhances the capability of dealing with more complex systems. CALYPSO, which stands from Crystal structure AnaLYsis by Particle Swarm Optimization, is the main implementation of this methodology. It is an efficient structure prediction method which is available as a free package that can be used to predict/determine the crystal structure and design multi-functional materials [285]. This package is extremely popular and has been interfaced to a number of local structural optimization codes (VASP, QE, GULP, SIESTA, CP2K CASTEP) varying from highly accurate DFT methods to fast semiempirical approaches that can deal with large systems. Notably this PSO-based algorithm [286, 287, 288, 289] combined with a fingerprint and matrix bond analysis has been successfully used in solving numerous structural problems [290, 291, 292, 293, 294], including prediction of new high-pressure superconducting hydrides [295, 182, 296, 297].

Evolutionary algorithms

Evolutionary methods are a modern class of algorithms that rely on operations or principles inherited from genetic algorithms. In evolutionary algorithms a population of candidate

structures is evolved over successive iterations of random variation and selection operations (as in genetic algorithms). Random variation provides the mechanism for discovering new solutions. Selection determines which individuals will be retained for further evolution. Solids are represented through 6 lattice parameters (3 unit cell vectors and 3 angles), which are encoded as the lengths of the three lattice vectors and fractions of 2π , respectively. Each atom is represented by three coordinates, expressed as a fraction of the corresponding lattice vector. In modern evolutionary algorithms a given set of values defines one structure and a locally optimized structure is referred to as an individual. A set of individuals is called a population or depending on the context, a generation. The comparison between different individuals is based on the corresponding *fitness* values (in our case the fitness is the free energy or enthalpy). The simulation technically starts with individuals (structures) generated by some educated guess or in a completely random fashion. These structures then undergo evolution through a series of different genetic operations. New candidate individuals are obtained applying one or more variation operators to selected individuals. For every operation one or two individuals, depending on the type of operation are chosen stochastically from the population. The probability of a given individual being chosen for a given operation is a function of the individual's fitness rank; a predefined number of worst individuals has a probability of zero. The selected individual is not removed from the pool and can thus be selected multiple times. The candidates generated are then scaled to a given unit cell volume and those which do not fulfill some hard constraints are discarded. The rest gets locally optimized (technically at DFT level) and hereby new individuals are created. Each operation is repeated until the user-requested number of new individuals for this operation are produced. The total number of new individuals equals the population size. After the calculation of the fitness value for each new individual, a new population is obtained taking the best individuals from the combination of offspring and a user-defined number of best individuals from the parental population.

USPEX, which stands for Universal Structure Predictor: Evolutionary Xtallography, is perhaps the most popular and by far the most exploited method among all presented in this section. This methodology was originally described in Ref. [298, 299] by Glass et al. USPEX introduces a unique number of features or variation operators: heredity, mutation and permutation [300, 301, 302]. In heredity, two individuals are selected and used to produce one new candidate. This is simply achieved taking a fraction of each individual and combining these fractions to create new individuals. The fraction of each individual should be chosen as to contain as much information as possible. The main information in a crystal structure is the relative position of the nearby atoms. Thus, in order to conserve information, the fraction of an individual is selected taking a spatially-coherent slab. The two slabs, one of each individual, are then fitted together, and the resulting structure is then rearranged by adjusting the number of atoms of each type to the requirements. In mutation an individual is selected and used to produce a single new candidate: technically this is done transforming the lattice vectors to new vec-

tors applying a strain matrix. Permutation is used to produce a single new candidate; in this operation, two atoms of different types are interchanged. This operation, which is of course only possible for systems with different types of atoms, facilitates finding the correct atomic ordering. Another interesting feature is volume scaling; according to this operation, every produced candidate is scaled to a certain unit cell volume, prior to testing it against hard constraints and to local optimization. This enhances the performance for systems where the initial value of the volume is not sufficiently accurate. For each new generation, the new volume is obtained as a weighted average between the old and the average volume of the best individuals of the previous generation. A fundamental step, as in other methodologies is to perform an efficient local optimization which increases the cost of each individual, but reduces the search space to the local optima, enhances comparability between different structures and provides locally optimal structures for further usage [303, 304, 305]. This software is free of charge and is provided as a simple and robust method to use as a black-box and find the stable crystal structure of systems with up to several dozen atoms/cell. Due to local optimization and the process of exploiting promising regions, many highly competitive metastable structures are found during the search. This method is interfaced with several *ab initio* codes, such as VASP, SIESTA, GULP, Quantum Espresso, CP2K, CASTEP, LAMMPS, etc. and has been used in the context of materials discovery [306] and high-pressure materials for superconductivity [307, 308, 309, 310].

Another implementation of evolutionary algorithms is XTALOPT, An Open-Source Evolutionary Algorithm for Crystal Structure Prediction, by Lonie et al. [311, 312, 313]. XTALOPT features a periodic displacement (ripple) operator which is ideally suited for extended systems. It features hybrid operators, which combine two pure operators reducing the number of duplicate structures in the search. This allows for better exploration of the potential energy surface of a given system. This software has been applied to explore hydrides under pressure [314, 315] and is available under the GNU Public License. One main advantage for beginners is that it possesses an intuitive graphical interface and is interfaced to force-fields and various DFT codes.

Although is rarely used, a genetic algorithm that can in principle explore novel structures for a given stoichiometry is implemented in the geometry optimization routines of ABINIT [316].

Minima Hopping method

The minima hopping algorithm was especially conceived to quickly climb out of wrong funnels in a potential energy surface with a multifunnel structure. This was achieved by abandoning the standard Markov-based Monte Carlo methods and introducing a feedback mechanism that based on the whole simulation history, enforces the exploration of new regions of the configuration space.

The minima hopping method (MHM) [317, 318] consists of an inner part, which performs jumps to the local minimum of another basin, and an outer part, which will accept or reject

this new local minimum. Fig. 18 shows the flowchart of this method. The acceptance/rejection is performed setting an energy threshold, which means that a step will be accepted if the energy of the new local minimum E_{new} will be less than a given E_{diff} higher than the current energy E_{cur} . The threshold on the energy difference is continuously adjusted during the simulation, so that half of the moves are accepted and half are rejected. This condition, which is implemented in the outer part, introduces a preference for steps that go down in energy. However, if the inner part proposes only steps that go up in energy, in the end these steps will also be accepted, because after many rejections E_{diff} will have become sufficiently large. The inner part consists of a more complex escape mechanism that aims to move from the current local minimum, followed by a geometry relaxation which will bring the system into another neighbouring local minimum or will make it escape to another basin. The geometry relaxation is performed by a combination of standard steepest-descent and conjugate-gradient methods or more involved methods [319]. Initially a random velocity direction with Gaussian distributed magnitudes is chosen for atoms. A generalized version of the algorithm of minima hopping to periodic systems using variable cell shape molecular dynamics for the escape step was implemented by Amsler and Goedecker [320] in 2010. The escape mechanism in this case is represented by a short molecular dynamics simulation that starts from the current minimum. To optimize the escape steps the initial atomic and cell velocities are aligned to low-curvature directions of the current local minimum. This means that the system will have enough energy to overcome energy barriers which are lower than the kinetic energy measured relative to the current minimum. If the kinetic energy is small, the system will arguably fall back into the current minimum, otherwise, if it is sufficiently large, the system will most likely be ejected from the current basin and end up in a different minimum. Softening, works by aligning velocities towards soft directions, therefore biasing the MD simulation to efficient escape trials [321].

Another important feature that MHM exploits, is the Bell-EvansPolanyi principle [322] that states "highly exothermic chemical reactions have a low activation energy". This can be translated as "is more likely to find a low-energy local minimum if one goes from the current basin into a new basin crossing a low barrier than if one has to overcome a high barrier" [323]. Since stages of its development, MHM has been proven not only to provide reliable solutions for the global minimum but also for nearby local minima, which can be of interest for many applications. It has been tested on a large set of materials classes [324, 325], including superconducting hydrides at high pressure [159, 326]. Although this package is not as popular as previously described algorithms, it is extremely powerful and reliable for large variety of situation and systems, including ternaries [327], Heusler-systems [328], etc. It is currently interfaced with a number of local structural optimization codes such as ABINIT, VASP, QE, GULP, SIESTA, LAMMPS, etc.

Another method, similar at least in the name, is basin hopping [274], which exploits powerful Monte Carlo methods for the determination of the global minimum. This methodology

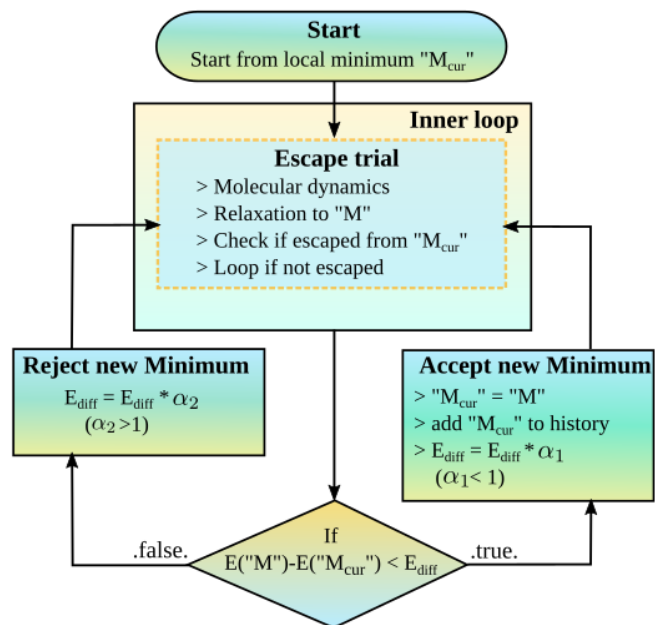


Figure 18: Flowchart of the minima hopping algorithm.

transforms the potential energy surface in an advantageous way: the value of the potential energy surface within one basin is replaced by the value of the potential energy at the associated minimum. The basin hopping method essentially eliminates the barriers between the basins of different minima, making it easy to connect them or to jump from one to the other. It is important to note that the basin hopping method does not eliminate the barriers between super-basins or funnels. On the other hand, the transformed piece-wise constant potential energy surface of the basin hopping method still exhibits barriers that have to be overcome by Monte Carlo steps. This methodology has not been used in the context of solids periodic systems or hydrides to explore potential superconducting structures at high pressure.

Simulated annealing

Stochastic simulated annealing-type algorithms to optimize global and local problems were introduced more than 35 years ago. Being based on Boltzmann statistics, from a purely historical perspective it is understandable that they were the first methods developed to tackle optimization problems. Nevertheless, it was not until 90's that these techniques started to be used to help structure determination and to predict solid phases of elements. As a side note, the early development of these methods matches almost perfectly in parallel with the availability of commercial diamond anvil cells (see Sect. 2, which gave access to high pressure to many laboratories, essentially opening the era of characterization of solid-phase transformation under pressure. At the time, although addressing theoretically solid-phase transformations was a great, if not unsolvable, problem. There were a few brave attempts in this direction, see for example Refs. [329, 330, 331]. We refer in this context to the famous 1988 editorial note in Nature by John Maddox: "one

of the continuing scandals in the physical sciences is that it remains in general impossible to predict the structure of even the simplest crystalline solids from a knowledge of their chemical composition” [37].

Coming back to our original story line, simulated annealing algorithms were first introduced by Kirkpatrick et al. [332] and Černý et al. [333]. The great advantage of these methods lies in the relative ease of implementation and the very general applicability, regardless of the specific optimization problem [334].

In general, the simulated annealing algorithm employs random walker(s) to explore energy landscapes based on a few fundamental features that make it stochastic: First, a set of walkers that may or not interact with each other and learn from each other’s steps. Second, a configuration space with an energy cost function which may remain unchanged or evolve as the algorithm proceeds. Third, a moveclass, which for each state gives returns a neighbouring structure which may or not be accessed with a certain probability (also this probability can evolve along with the algorithm or stay unchanged). Fourth, an acceptance criterion according to which the walker makes moves to the selected neighbor.

In principle the algorithm starts from a current configuration i (random structure or well-educated guess). A neighboring configuration $i + 1$ is chosen randomly according to a set of rules (defined in “moveclass”). If the energy E_{i+1} is below or equal to E_i , the move is always accepted, that is, $i + 1$ becomes the new current configuration. Otherwise, the move is accepted with a probability $e^{-(E_{i+1}-E_i)/C}$, where C is a control parameter of the random walk. Thus during a sequence of such Monte Carlo steps, the system can climb over barriers of the energy surface. It can be shown that in the long-time limit ($t \rightarrow \infty$) for an ergodic system the probability $p(i)$ of visiting the configuration i is given by the Boltzmann distribution for the system at a temperature given by $T = C/kB$.

The general prototype of this type of algorithms is the so-called Monte Carlo Metropolis algorithm which describes a single walker at a constant temperature T . These algorithms explore ergodic regions especially if T is varied or if the landscape evolves during the simulation. The generalization of the Metropolis algorithm consists in varying the temperature during the run, i.e. what is called simulated annealing. Simulated annealing works by slowly lowering the temperature, which implies that the walker will move from average states (ergodic regions) to states with lower and lower energy. The premises of this algorithm is that if ones proceed slowly enough, at the end of the simulation the walker will have found global minimum of the energy landscape. Of the methodologies introduced before, this is the only one for which one can be sure to obtain or guarantee a solution -global minimum- (structure) at the end of the run.

Although relatively easy to implement, the method is computationally very demanding especially for large systems. Applications in predicting solid compounds using simulated annealing are lead by Schön, Doll, and Jansen [335, 336], with important successful cases like the prediction for lead sulfide structure at standard and elevated pressures [337].

Data mining and high-dimensional correlations. A frequently applied approach to reveal hidden correlations is the use of data-mining methods on large databases of computational [338] or experimental [339] data. This is justified, since compounds which are chemically similar also tend to exhibit similar crystal structures. Simply by examining the behaviour of neighboring elements in the periodic tables, one may derive hints on stable compositions and crystal structures for hypothetical systems. Properties like electronegativity, atomic radii, number of valence electrons, valence electron energy or electron configuration could be exploited to discern trends in the search space.

In this context, starting from the experimental data contained in the inorganic crystal structure database, Glawe et al. [340] used a statistical analysis to determine the likelihood that a chemical element A can be replaced by another B in a given structure. This information can be stored in matrix form in which the each entry (A,B) measures its likelihood. Ordering the rows and columns of this matrix to reduce its bandwidth, a one-dimension scale can be used to sort analogous chemical elements, i.e. the Pettifor scale. Alternatively, Goldschmidt’s rules of substitution describes for example simple recipes to exchange atomic species in ionic crystals.

The Materials Project initiated by Ceder et al. [341] has been pioneering attempts in this direction. Ceder’s group developed several approaches based on data mining combining high-throughput with *ab initio* calculations to predict ground-state structures of novel compounds [342]. This Data Mining Structure Predictor (DMSP) scheme relies on the idea that in alloys a strong structure-structure correlation exists among different compositions due to underlying physical properties. Therefore, it is possible to obtain a probability distribution for the crystal structures of an unknown composition of an alloy based on the already known crystal structures at other compositions. The data-mining techniques are limited only to structures in the underlying database, limiting their use in crystal structure predictions. For example, applicability to high-pressure or high-temperature phases for example is restricted due to limited available data from theory and experiments. We expect, however, that in near future thanks to new and rapid developments in the field, it will be possible to study high-pressure materials databases specifically in the case of hydrides.

An interesting methodology that aims to decrease the expensive computational need for the creation of large-scale databases, for instance in materials under pressure, was proposed by Amsler [343]. Although simple in spirit, this framework approximates the enthalpy of stable compounds at ambient conditions with a linear approximation to the enthalpy (at high pressure limit) of compounds based in data from databases of calculated materials properties. This work has successfully demonstrated that is possible to explain the occurrence in nature of phases which are not ground states at ambient conditions and to estimate the pressures at which such ambient-metastable phases become thermodynamically accessible.

4.2. Convex hull and phase diagrams

As previously mentioned, the prediction of computer-designed material is a formidable task, since it requires a thor-

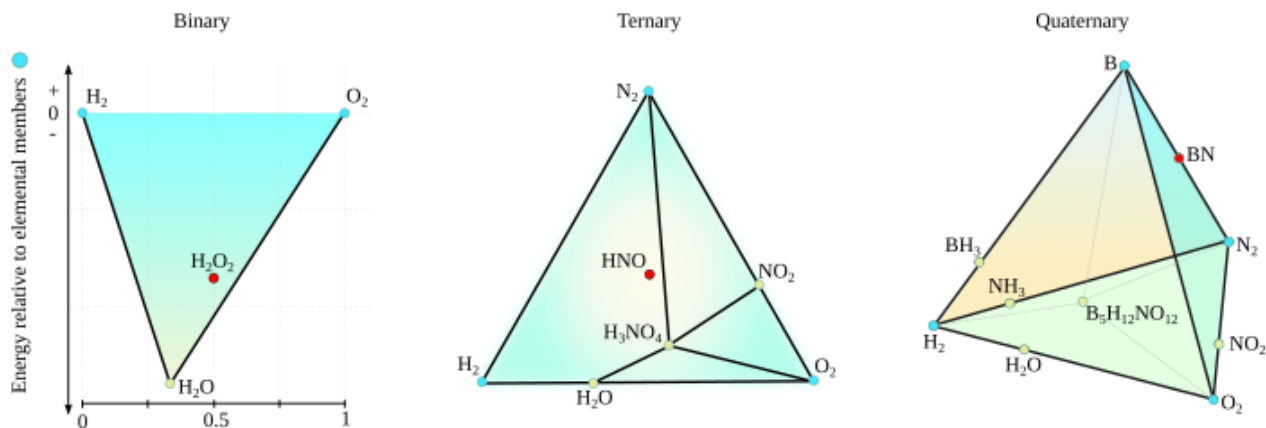


Figure 19: Examples of binary, ternary and quaternary construction of convex hull type diagram, for H-O, H-O-N, and H-O-N-B, respectively. Blue nodes on the phase diagrams represent elemental phases, green nodes are compositions that are calculated to be stable and red phases that are not stable. The chemical space becomes quickly challenging to explore, adding a one-dimension (another element) the complexity in compositions is evident: $B_5H_{12}NO_{12}$.

ough structure exploration, computation of enthalpy and entropy functions and barriers to phase transformations between all competing phases under given conditions. The convex hull is used as a guide to estimate the formation energy (or enthalpy) and to determine the thermodynamic stability for a given composition with respect to its forming elements. Fig. 19 shows examples of binary, ternary and quaternary systems. To determine the ground states of a system at a given composition one needs to find, the ordered compounds that have an energy lower than any other structure or any linear combination of structures corresponding to that composition. Mathematically, the convex hull of a set of x points, in the Euclidean plane or in a Euclidean space, is the smallest convex set that contains x .

In our example, the set of points represents a set of ground-state structures and in particular those forming a convex hull, while other structures (points) having an energy above the set of tie lines connecting the energy of the ground states are not stable. The convex hull thus reflects the Gibbs free energy of the compounds at zero temperature.

The convex hull construction permits to visualize very valuable information, i.e. it can be used to derive a "phase diagram" of the compositions that in principle have the lowest energy and hence are accessible to experiments. Thus, a convex hull of the enthalpy in materials science represents a rudimentary compositional phase diagram, in which the boundaries and eutectic points are not displayed. Fig. 19 shows real systems represented as convex hull phase diagram; an example of binary compositional phase diagrams shown for H_2O , in which the y-axis represents the formation energy per atom and the x-axis the composition. The stable composition obtained by combining H_2 and O_2 , represented by a green dot, is one of the most stable molecules in the universe, H_2O . The black line shows the convex hull construction, which connects stable phases (H_2 to H_2O to O_2). The line drawn between these points is also called the line of stability. The H_2O_2 composition, which has a negative formation enthalpy with respect to elemental constituents but lies above the line of stability, is not stable. Thus, the convex hull suggests that likely the only composition that will sponta-

neously form is H_2O .

In the ternary case, one dimension is added; the energy axis is removed so that the entire compositional space can be represented. The ternary system (H,N,O) is now represented by an equilateral triangle, with three elements at its vertices and the nodes represent compositions for which the decomposition energies are zero (see middle panel in Fig.19). Adding another element (quaternary), the chemical space becomes extremely challenging to explore and even to represent, we now use a pyramid to represent the B,N,O,H system. The complexity in compositions is evident: we have indicated on the plot an interesting stable point: $B_5H_{12}NO_{12}$. While the black lines in the ternary phase diagrams are projections of the convex hull construction into compositional space. The lines form Gibbs triangles, which can be used to find stable phases at arbitrary compositions. At any point in the phase diagram other than the stable nodes, the equilibrium phases are given by vertices of the triangle bounding that composition. For example, the equilibrium phases for a composition with H:N:O ratio of 3:1:4, is predicted to be H_2O , O_2 , NO_2 and N_2 . We will revisit the implications that this has for hydrides and superconductivity in a subsequent section.

To calculate the convex hull of the formation of energy of a given system with respect to its forming elements, the following expression is used for binaries, $\Delta^{sys} = (E^{sys} - (E^a + E^b))/N$, and for ternaries $\Delta^{sys} = (E^{sys} - (E^a + E^b + E^c))/N$, where E^{sys} represent the energy for a given structure N number of atoms and $E^a, E^b, \dots E^n$ the energy of elemental decomposition in their lowest-energy structure. For multi-components systems, as evidenced in Fig. 19, above 4 dimension is not longer convenient to try and visualize the system graphically, although one may in principle employ mathematical reduction of dimensions or explore fixed compositions by mapping via function composition to lower dimensions. In practice, this has never been attempted in the case of hydrides.

Furthermore, it is of course reasonable to ask, what is the accuracy of a prediction based on convex hull formation energies? For points (structures) which correspond to clear minima of the

formation energy, like H_2O , which has a formation energy of a few eV/atom, it is arguable that this composition is the most stable. However, when one deals with challenging compositions and complex structures under high pressure, where configurations are energetically very close, it is much more problematic to discern whether or not a structure will form based on its formation enthalpy. What is the limit where we could consider stability or metastability for secondary phase structures or compositions?

Sun et al. [344] were the first to address this question and suggested an order of energy differences of 100 meV/atom among polymorphs of the same stoichiometry. This criterion is based on differences in properties such as entropy, volume, or surface energy and convoluted information from pressure, temperature, or surface area between two systems. An energy difference of 100 meV/atom is sufficient to overcome a ΔS of 10 J/mol K, a ΔV of $2 \text{ \AA}^3/\text{mol}$, or a $\Delta \gamma$ of 2 J/m^2 . More recently, Aykol et al. [345] also evidenced the lack of a rigorous metric to identify which compounds may or may not be synthesized and suggested a thermodynamic upper limit on the energy scale, above which the laboratory synthesis of a polymorph is highly unlikely. They defined this limit on the basis of the amorphous state and validated its applicability by effectively classifying more than 700 polymorphs in 41 common inorganic material systems of the *Materials Project* for synthesizability.

Note, however that while these estimates are relatively safe to draw conclusions at zero pressure and for cases analogous to those contained in the original dataset, could be highly risky and obsolete for the case of high pressure. In fact, both works reported that these values are highly chemistry-dependent. In particular, the data sets of studied materials do not contain hydrides under pressure. In hydrides under pressure the existence of polymorphs stabilized via quantum effects (via vibrational entropy) and the anharmonic effects of the hydrogen-related modes, prove predictions to be further challenging.

4.3. First principles calculations

Quantum mechanical modelling using density functional theory [197] allows to investigate the electronic structure of many-body systems, in particular of atoms, molecules, and the condensed phases at relatively cheap computational cost and high accuracy. DFT is perhaps the main computational tool used by force of sheer numbers world-wide and represents the driving force behind physics, chemistry and materials science. More than 20,000 publications using results based on DFT are published every year.

DFT is increasingly used in an automated fashion to build large databases or repositories of *ab initio* calculations or combined with multiscale techniques, limiting the direct human intervention. On average more than 100,000 calculations are executed every day world-wide, producing more than 36 million DFT total energies a year. This has been possible thanks to licensed and free-to-use codes developed by large communities, which are easy and efficient to use, spurring to thousands of users. A large number of DFT computer codes are available and many of them differ considerably in the implementation

details; this means that each of them attains a different "precision" relative to each codes. Reproducibility of these DFT results was recently addressed on the basis of different benchmarks by a large world-wide collaboration, involving the developers of several codes. Studies of this type are extremely important to reassure the scientific community on the credibility of DFT results [346]. The study convincingly showed that despite the large number of codes, basis sets and different implementations solving the same set of equations: all codes lead to the same results, of course within an threshold error. Thus the community has a large array of many first-principles DFT codes available (see for instance Ref. [347]). Irrespective of the code, the main information from a DFT calculation used in crystal structure prediction is the total energy (sum of different contributions) and forces acting ions, together with stresses on the unit cell for the case of periodic crystals.

Other methods. Structure prediction for condensed matter systems containing a large number of atoms (more than hundreds) is at present out-of-reach at the DFT level even with the most efficient basis sets. It is preferable to decrease the computational cost of estimating energies and forces by an order of magnitude or more, if a many-atoms system have to be explored. There are packages such as GULP [348] and LAMMPS [349, 350] (commonly used in the solid state community) that implement accurate force-fields (FF) which permit to reach these goals. Force-fields refers to the functional form of interatomic potentials used to calculate the potential energy of a system of atoms. The parameters of the energy functions may be derived from experiments in physics or chemistry, *ab initio* quantum mechanical calculations, or both. The obvious downside is the availability of transferable interatomic potentials for all atomic species under consideration. Density functional based tight binding (DFTB) method represents an alternative method which combine the accuracy of DFT with scalability of force-fields. It is based on a second-order expansion of the Kohn-Sham total energy in DFT with respect to charge density fluctuations. The zeroth order approach is equivalent to a common standard non-self-consistent (TB) scheme, while at second order a transparent, parameter-free, and readily calculable expression for generalized Hamiltonian matrix elements can be derived [351]. However, also in this case one needs parameters, the so called Slater-Koster files. Codes available with DFTB are c2PK, DFTB+, AMBER, GAUSSIAN etc.

Basis sets. In Hartree-Fock or DFT methods the electronic wavefunction is expanded on a basis set to turn the partial differential equations (see Sec. 3) of the model into algebraic equations suitable for efficient implementation on a computer. The basis set used in a DFT code will largely determine its use and applicability to a certain class of problems and hence target a scientific community. Historically, Slater-type orbitals (STO) were the first type of basis sets available; however, they proved to be extremely inefficient, because they required the cumbersome numerical calculation of integrals. These were followed by Numerical Atomic Orbitals (NAO) and the Linear Combination of Atomic Orbitals LCAO ansatz which provided a much

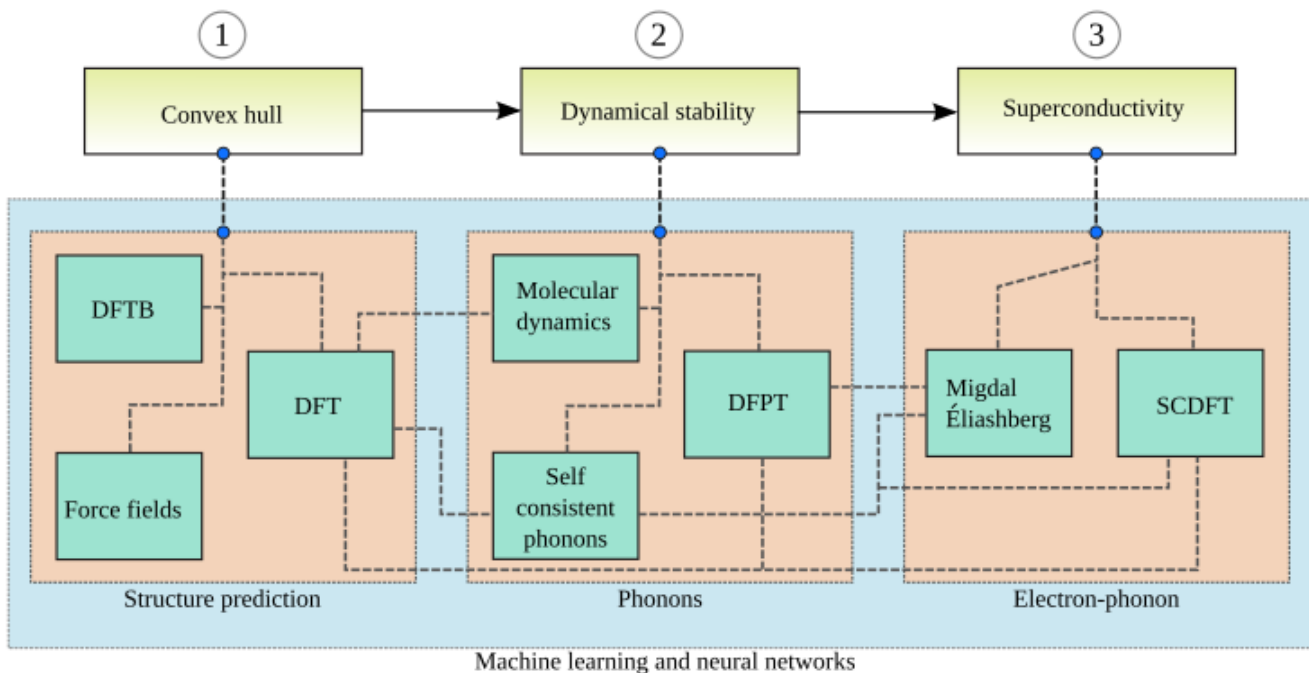


Figure 20: Summary of computational steps to predict superconductors at high pressure. First step is to explore the configurational space of selected compositions and build the convex hull. Many structure prediction algorithm are available and can be used at distinct level of accuracy from classical to quantum mechanical. The second step is verification and consists in characterizing the vibrational properties of the thermodynamically-stable compositions. Available methodologies include among other MD, DFPT, and self-consistent phonons. Third step is accessing the superconducting properties for candidates. The great effort by the community has made possible to predict room-temperature superconductors without prior experimental knowledge. The large palette of available methods reflects the maturity of the field and further development of these methodologies will guarantee many more interesting discoveries.

better trade-off and ease of implementation. Gaussian-type orbitals (GTO) are by far the most often used in terms of numbers of codes and users, especially in the quantum-chemistry community. This type of basis set allows efficient implementations by exploiting the property that the product of two GTOs can be written as the linear combination of GTOs. Thus integrals with Gaussian basis functions can be written in closed form and this leads to a huge save of computational time. In addition to localized basis sets, plane-wave basis sets can also be used in quantum-chemical simulations. Plane waves are in principle a complete basis set; however, in practical implementation the Hilbert space is truncated and only plane-waves up to a kinetic energy cut-off are included in the basis. Increasing the number of plane waves, the solution is guaranteed to converge variationally to the exact one. In order to obtain convergence with a reasonable number of basis functions, in plane-wave codes the full electron-ion Coulomb potential is usually replaced by a pseudopotential, which cuts all small-scale oscillations of the nuclear wave function close to the nuclei – see next section. Analogously to the plane wave basis sets, where the basis functions are eigenfunctions of the momentum operator, there are basis sets based on eigenfunctions of the position operator, that is, points on a uniform mesh in real-space. Actual implementations of this idea may use finite differences, finite elements or Lagrange sine-functions or wavelets [352]. Other mixed-basis sets, such (linear) augmented plane waves, have proven to be able to achieve rigorous accuracy in solids and are used as standard benchmark providing reference val-

ues [353, 354, 355]. All-electron, full-potential (opposed to pseudopotential) approaches are in principle the most suitable to be used in high pressure calculations. However, due to the required expertise necessary to conduct these calculation, together with their elevated computational cost, they are rarely, if not used at all.

Pseudopotentials and benchmarks. As alluded before, the scientific community has tight on efforts to improve on efficiency and reliability DFT codes. Plane-wave codes, which are very often used in the solid-state community, employ a pseudopotential approximation in which the full Coulomb potential between nuclei and electrons is replaced by an effective potential, which reproduces the correct behavior of the wavefunctions of the valence electrons in the regions between the nuclei, where chemical bonds are formed, but smooths all short-range oscillations in a region close to the nuclei, i.e. below a suitably-chosen cutoff radius. Core electrons are not included explicitly in the calculation permitting to reduce the size of the plane-wave basis functions used to represent the density and potential in the Kohn-Sham equations but this introduces an additional source of inaccuracy when compared to all-electron approaches. However, most of the currently employed pseudopotentials have an impressive accuracy, practically comparable to that of all-electron calculations. This has been possible in part by the intense development of website platforms that are in charge of producing standardized pseudopotentials, intensively tested and open to public scrutiny. First, in this effort was the

PseudoDojo.org website that gives access to the latest released version of pseudopotentials [356]. Another standard protocol was proposed later on to verify publicly available pseudopotential libraries, based on several independent criteria including verification against the all-electron equations of state, as well as plane-wave convergence tests for several properties, including phonon frequencies, band structure, cohesive energy and pressure. All these tests have been performed to give rise to the Standard Solid State Pseudopotential (SSSP) efficiency and precision libraries [357].

k-point sampling and other sensitive parameters of DFT calculations. A good method for Brillouin zone sampling which allows for fast, yet accurate estimates of the total energy, is particularly crucial when dealing with structural exploration. It has been demonstrated that non-converged DFT calculations can lead to strong biases in the structure searches, since the quality of the *k*-sampling determines the final accuracy of forces.

The community largely uses MonkhorstPack (MP) [358] meshes of *k*-points; a criterion that can be used to compare different structures is to choose for all of them the MP mesh for which the smallest separation among *k*-points is less than a given distance. A rule-of-thumb, based on empirical experience, is to use a grid spacing of $2\pi \times 0.07 \text{ \AA}^{-1}$ for structure searching and preliminary results, and $2\pi \times 0.04 \text{ \AA}^{-1}$ for refining structures and obtaining good energies. These rules apply to systems with a gap in the electronic spectrum (insulators and semiconductors), while metals may require typically denser grids, $2\pi \times 0.05 \text{ \AA}^{-1}$ for searching and preliminary results, and $2\pi \times 0.02 \text{ \AA}^{-1}$ to refine the structures and obtain good estimate of total energy. For the cut-off energy in the planewave expansions, preliminary tests have to be carried out at the beginning of the investigation, although, if one works with pseudopotential libraries where benchmark tests have been carried out before, it is advisable to start from these recommended values.

The nitty-gritty of predicting superconductors at HP. Finally we would like to summarize in Fig. 20 the computational steps which are regularly followed to uncover new hydride superconductors. One usually starts by picking a composition or set of compositions. Either based on chemical intuition or in the case of hydrides, stable molecules (binaries) that exist at ambient conditions are for example a good starting point.

The first step is to explore the configurational space of selected compositions and build the convex hull. As described in previous sections, one can choose from a large array of methods available. Despite the claims, in reality all the methods are equally good and there is not really a method/software that is superior to others; difference arises more from the tools that certain packages have in order to process the data. Mainstream packages are robust and users can certainly use it as black-box. While other less developed software provide basic functions, perhaps less efficient implementations and one has to write their own scripts for post-processing. Essentially all the software available for structure prediction are interfaced to DFT, DFT tight-binding or force-fields. Once the PES has been sampled thoroughly with your favorite method, the main aim in this

step is to build a phase diagram (convex hull) to identify low-enthalpy compositions.

The second step is a verification one, which consists in characterizing the vibrational properties of the thermodynamically-stable compositions. This step in most cases is performed using linear-repose theory at DFT level which assumes harmonic vibrations. Conversely, molecular dynamics or other methods to estimate anharmonic inter-atomic force constants are available. If phonon frequencies are real in the entire Brillouin zone, i.e. the predicted compound is dynamically stable, one can estimate the vibrational free energy and the zero-point energy contribution. Especially in hydrides, these terms have proved to have significant impact on the energy ranking of configurations.

The third step consists in characterizing the superconducting properties of top candidates. For this, one needs to estimate the electron-phonon coupling spectral function ($\alpha^2 F(\mathbf{k}, \mathbf{k}', \omega)$), the electron-electron Coulomb repulsion and solve the superconductivity equations. Electron-phonon coupling constant (λ) is obtained by integrating the spectral function and the logarithmic-averaged phonon frequency (Ω_{\log}) as well. As a first glance, it is sufficient to have a rough estimate of the transition temperature using empirical models such as the McMillan-Allen-Dynes, Eq. 100. However, as described in Sec. 3, this model become less accurate in the limit of large coupling or electronic anisotropic systems. In this case, it is more appropriate to use other methods based on a perturbative Green's function approach such as Migdal-Eliashberg (see Sec. 3.2.2 or advanced methods as SCDFT (see Sec. 3.3)).

To conduct DFT calculations for superconductors in practice, the most common choice are the two largely and popular free-to-use plane-wave basis set codes: ABINIT [359] and QUANTUM ESPRESSO [360] which can also calculate higher order derivatives (i.e. electron-phonon coupling). A licensed code that is very popular and features good scaling together with a robust structural optimization routines is VASP [361] which also provides its own well-tested pseudopotential libraries. Recently the use of graphics processing unit (GPU) in conjunction with DFT calculations, has been proven feasible resulting in speed up of calculation time for up to a thousand atoms [362]. However, this requires state-of-the-art supercomputers (CPU+GPU) that are still not available in most supercomputer centers. Moreover, force-field codes such as GULP or *ab initio* molecular dynamics methods are popular and accurate, while being computationally efficient and are often used to perform preliminary scans of the PES.

In addition to the steps alluded above, in Fig. 20 one can distinguish an additional box that encloses the three steps: it refers to methodologies such as machine learning (ML) and neural networks, both belonging to artificial intelligence. The recent progress in the field of machine learning for molecular and materials science is evidenced in the Review of Butler et al. [363]. Scientists seem to embrace the inclusion of these methods in their research and the number of reported applications in material science is growing at an extraordinary rate (see References [364, 365, 366]). In hydrides under pressure this approach is still largely under development, but we will certainly witness a tremendous progress in future years thanks to these

methodologies.

In structure prediction these methods can be used at two fronts: I) crystal structure prediction via deep learning [367]: neural-network models can be trained to effectively distinguish chemical elements based on the topology of their crystallographic environment/properties [368]. This approach has been used to effectively guide the synthetic efforts in the discovery of new materials, especially in the case of systems composed of three or more chemical elements [369]. II) Machine learning can also be employed at the level of structural exploration to speed-up the searches by learning inter-atomic model potentials [370, 371]. In principle, the construction of a generalized convex hull is a type of problem perfectly accessible for machine learning [372] and neural networks [373]. Forces are relatively straightforward to machine-learn and in the chemistry community there is ample evidence that this is possible for molecular systems. Once accurate forces are learned, also vibrational properties (phonons) are accessible. The transfer of these technologies to the solid-state community is underway and it is very likely that progress in the field of periodic solids at high pressures will soon occur. Other extraordinary examples in the solid-state community is the one led by Curtarolo and his team that exploits repository for *ab initio* calculations combined with Quantitative Materials Structure-Property Relationship models to predict properties such as metal/insulator classification, band gap energy, bulk/shear moduli, Debye temperature and heat capacities [374].

Finally, in the field of superconductivity there has been recent efforts to tackle this puzzling problem irrespective of the underlying mechanism of superconductivity [375, 376, 377], for instance to machine learn models of superconducting critical temperatures [378]. In the field of hydrides under pressure a recent work correlated structural fingerprint, major characteristics in the energy landscape of H_3S and H_3Se with superconducting properties. This type of correlations between of crystal structure to electronic structure serve as fundamental steps to further explore with machine learning and neural network material design [379, 174]. Generally, we see the field of hydrides under pressure as a green and vast terrain ready to flourish, on which modern computational techniques such as deep learning and statistical models can play a major role (see Sec. 6, perspectives).

5. Trends on hydrides under pressure

Historically, the first hints on the metallization of hydrogen dates back to 1926 [380], when J. D. Bernal suggested that any element becomes a metal at high enough pressures. Particularly, for a diatomic molecule such as hydrogen, the intermolecular distance decreases with pressure, until an individual atom cannot be assigned clearly to one molecule or another, and the material becomes metallic, with all atoms approximately equidistant and all electrons uniformly distributed. Years later in 1935, Eugene Wigner and Hillard Bell Huntington published the first paper in which they predicted that for pressure in excess of 25 GPa hydrogen would become an alkali metal-like solid [6]. Decades later in 1968 Ashcroft and independently

Ginzburg in 1969 [8], evidenced the implications of metallic hydrogen by predicting the possibility of high- T_c superconductivity [7, 8] based on arguments of BCS theory [30].

Ashcroft's prediction can be readily understood using the McMillan expression for T_c (Eq. 66),

$$T_c = \frac{\omega}{1.2} \exp \left[-\frac{1.04(1 + \lambda)}{\lambda - \mu_c^*(1 + 0.62\lambda)} \right] \quad (100)$$

together with the simplified Hopfield's expression [250, 381] for the e - p coupling parameter:

$$\lambda = \frac{N_{E_F} I^2}{M\omega^2}, \quad (101)$$

obtained from Eq. 54, Eq. 61 and Eq. 15 for an Einstein mode of effective mass M and frequency ω . N_{E_F} is the density of states at the Fermi level and $I = g\sqrt{M\omega}$, with g the average e - p matrix element in Eq. 15, the deformation potential.

Indeed, the metallic phase of hydrogen would optimize several factors appearing in McMillan's expression:

- The average phonon frequency, which appears as a prefactor in Eq. (100), would be high due to the light hydrogen mass.
- The matrix element I would also be large, since hydrogen does not have core electrons that screen the Coulomb electron-ion potential.
- Assuming that hydrogen at HP crystallizes in a densely-packed structure, as initially postulated by Wigner and Huntington, then electronic density and the density of states at the Fermi level, N_{E_F} , would be large. The latter would imply a large e - p coupling (λ), which appears in the exponent of Eq. 100.

Although the suggested pressure to metallize hydrogen at that time was merely 25 GPa (1935), it was far beyond reach for the technology of the epoch (see Fig. 3). As more accurate calculations and experiments were performed, this estimate was quickly outdated and replaced by higher values, i.e. first to 1 megabar and subsequently to 3 megabar (300 GPa). In fact, as discussed in the experimental section, the search for metallic hydrogen was one of the main motivations to develop high-pressure techniques. The pressure to transform H to a solid metallic substance is nowadays unambiguously set to be above 450 GPa.

In the 70's, the idea that hydrogen could achieve high critical temperatures (read contextual history in Introduction section) was simply too attractive and stimulated the study of superconductivity in metal hydrides throughout the whole decade. One can clearly identify that the field of superconducting hydrides was born at the beginning of the 70's after Ashcroft's bold prediction on high- T_c in elemental hydrogen. The rationale of the epoch was to focus on hydrogenated intermetallic compounds [382] in hopes for evidences that could point towards the exciting idea of metallizing hydrogen. As a side note, we recommend the reader to read the Review of Maksimov and Pankratov of 1975 [383], which is an excellent piece of work

that provides a deeper detail on the development of metallic hydrides during the 70's. The first metal-hydride ever synthesized and confirmed to be superconductor was Th_4H_{15} in 1970, which at atmospheric pressures had a non-negligible T_c of 7.6 K [384]. This compound is also special historically because, according to our bibliographic investigation, it was also the first metal-hydride to be a subject of high pressure studies, back in 1974. An increase in T_c to 8.5 K was meticulously measured upon compression [385].

The discovery of high superconducting transition temperatures in palladium [386, 387] and other noble metal-hydrogen systems further fueled the interest in this problem [388] (see Fig. 3, max T_c at that time was ~ 19 K for NbGe). As a matter of fact, the highest T_c ever measured and thoroughly confirmed for a hydride material at zero pressure is 16.6 K, measured in 1974 for PdCuH_x [389]. Other hydrides subject of studies were HfV_xH_x (T_c 4.8 K) [390], niobium-hydrogen (T_c 9.4 K) [391] and hydrides of vanadium, zirconium, titanium and lanthanum, for which superconductivity was not reported, at least in the temperature range explored [392, 393].

One can trace back important developments and predictions which also took place during this *first hydride rush* [383]. Indeed, we believe the origins of 'chemical precompression' dates back to 1971 and can be coined to J. J. Gilman when he studied the possibility of making a new form of hydrogen in a metallic state through preparation of a covalent compound, LiH_2F , under pressure [13]. In his very instructive work, Gilman described how the reduction of distance between molecules under pressure could be reached in lithium dihydrogen fluoride.

The *second hydride rush* was triggered in 2004 by Ashcroft [12], who proposed to look for new superconductors in molecular hydrides such as SiH_4 and SnH_4 . Although the idea was clearly not new, Ashcroft's paper provided novel perspectives and revived the field. Important concepts to guide the search for superconducting materials were re-introduced: First, in order to obtain an effective metallization of the hydrogen sublattice, it would be more convenient to start from an existing hydrogen-rich molecule, since in this case hydrogen does not have to be incorporated into a host metal lattice, as it was done in the 70's. Second, a chemical precompression (as Gilman suggested in 1971) mechanism can be exploited: in molecular hydrides the characteristic distances among hydrogen atoms is reduced, as compared to large values found in metal hydrides: thus, covalent systems are of interest (as LiH_2F). Third, the chemical precompression further reduces the necessary pressure for metallization and more importantly this pressure is accessible by experiments.

The successful proof-of-concept of this ideas was given by Eremets in 2008. His team reported the metallization of silane (SiH_4) at 50 GPa and the subsequent appearance of a superconducting phase with a maximum T_c of 17 K at 120 GPa [153]. Despite this initial success, the field was not yet ready to wake up. It was only until 2015, when Eremets' team reported convincing evidences of high-temperature ($T_c \approx 203$ K) superconductivity at HP ($P \approx 170$ GPa) in H_xS [1] that the field truly erupted [394].

The field has evolved at such an incredible pace that in less

than three years a 250 K superconducting transition in LaH_x was reported by two independent teams [181, 3]. A central role behind this great success in discovering high- T_c materials was played by computational and theoretical predictions. As shown in Fig. 2, the number of works published in the field increased dramatically during the last years, notably computational studies. It is clear that this field is flourishing and entering a new era, the *third hydride rush*. We expect that by the end of the next decade the number of publications in this field will double to reach 10,000.

5.1. Periodic table of binary hydrides

As mentioned before, the number of studies involving hydrides on the field of superconductivity has considerably increased. In little less than 5 years (2014-2019), the community has conducted computational explorations on practically all binary hydrides. A convenient form to summarize these results is to show the corresponding periodic table of superconducting hydrides. The following sections describe superconducting hydrides, as well as binary hydrides that do not show superconductivity.

5.1.1. Superconducting hydrides

In order to disentangle the relatively large and uncorrelated information that the community has published on hydride superconductors under pressure, we would like to distinguish conveniently two regimes of pressure: from 10 to 100 GPa (relatively low pressure) and above 100 up to 300 GPa (megabar pressures). The collected data is shown by Fig. 21 in the form of two periodic tables, reporting for each element the predicted T_c and chemical composition. The numbers below the element symbols indicate the value of T_c , while the color of the box refers to the chemical composition -the lighter the color, the higher H value. Top periodic table in Fig. 21 reports T_c for the thermodynamically stable composition (lowest energy structure and composition in convex hull) in the 10-100 GPa range. The bottom periodic table in Fig. 21 shows the highest T_c in the 100-300 GPa range, independently of whether the composition and structure are stable in the convex hull. See Appendix for references used to construct these tables (Sec. 7).

Let us first focus on the low-pressure regime. The highest T_c reported in this range of pressure is 50 K for H_2S . We observe that at low pressures the hydrogen to guest-atom ratio is dictated by the valence of the guest atom and superconductivity is found in three categories: hydrides that show temperatures of the order of 40 K or higher are, besides H_2S , the ones formed by Sc, Y and Li. These compositions are thermodynamically stable and in principle should be also accessible to experiments. The hydrides formed by I, La and Pt show superconductivity below 20 K. Interestingly, there are not some many stable compositions in the low pressure range as one could expect and the total number of stable hydrides is merely 19. The absence of superconducting hydrides formed with group I (alkali), II (alkaline earth metals), post-transition metals groups XI, XII, XIII and group XIV is noticeable. On the other hand, most of the transition metals tend to form hydrides that are stable in the

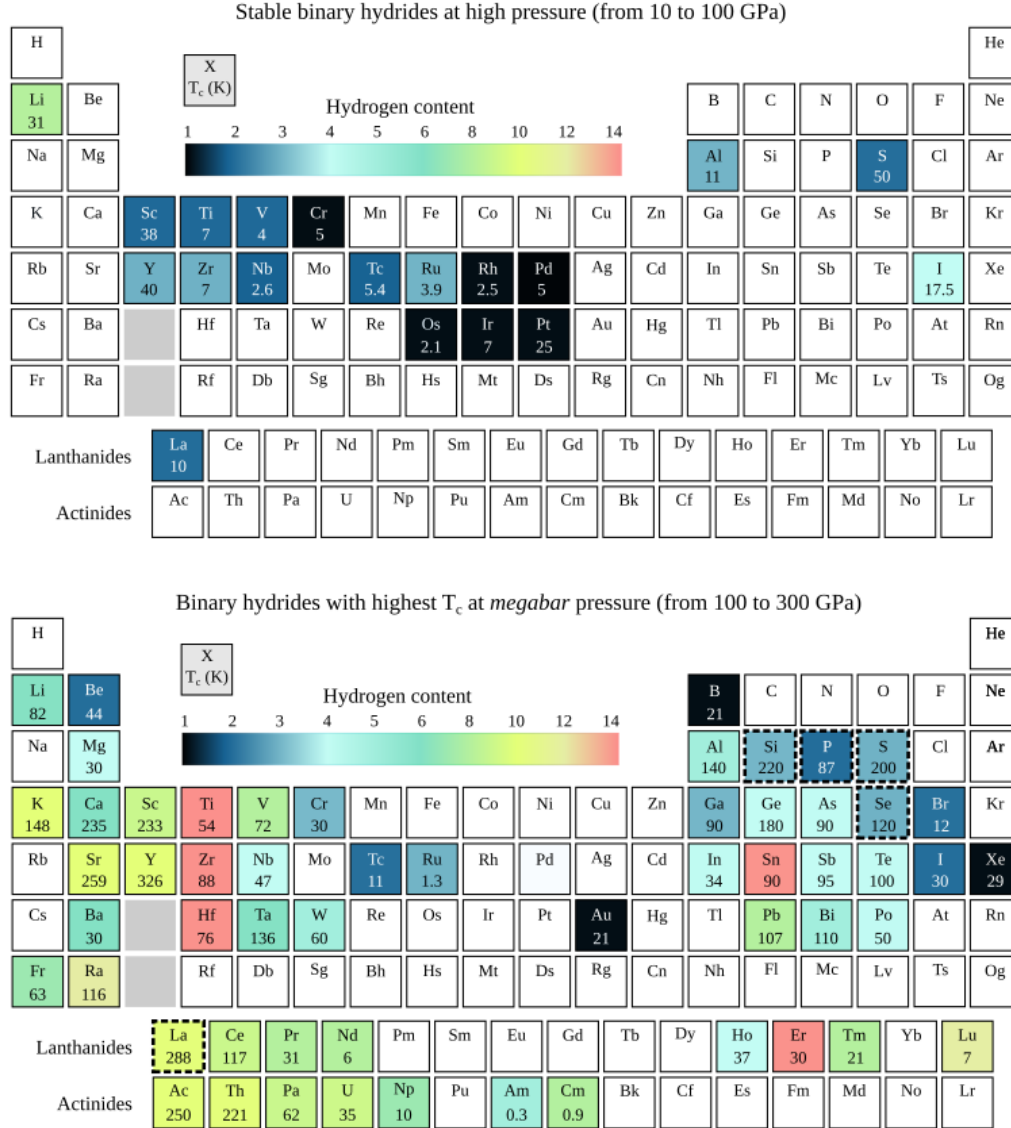


Figure 21: Summary of computational predictions reported in literature on binary hydrides. Top periodic chart prioritize stability: T_c is reported for the most stable configuration (lowest energy structure and composition in convex hull) in the 10-100 GPa. Bottom periodic chart highlights highest T_c , independently of whether composition and structure are stable in convex hull. In both panels, the number below the symbol element displays T_c and the color scale correlates to hydrogen content. A dash-dotted in some elements indicates that the compound has been subject of experimental work.

low-pressure range. Clearly, the stability of hydrides is dominated by compositions with *low* H-content at low pressure. In fact, one can notice that darker colors dominate over the whole periodic table in top panel.

Let's now examine the HP limit. The bottom periodic table in Fig. 21 shows the highest T_c in the 100-300 GPa range. The most noticeable features are: compared to low pressures, 1) there are many more hydrides reported with considerable higher T_c and 2) the table is colorful, indicating that at high pressure hydrides tend to form with *high* H-content. The highest T_c reported in this range of pressure is for YH_{10} with 326 K. Note that, due to our choice to restrict our table to chemically-accessible pressures some high- T_c predictions such as Mg-hydrides are not included in this table. It is fascinating that

there are also many more hydrides predicted with astonishingly high- T_c , including the whole La-series and group II. On the opposite, transition metals seem doomed in the HP range and neither T_c or H-content increase compared to low pressures. This evidences that the original idea followed during the decade of the 70s was probably not the best strategy to maximize T_c .

A word of caution should also be added at this point: these tables contain predictions extracted from a large array of published articles from many groups. Not all of these articles were conducted with the same level of accuracy, convergence, etc. By no means the number given here is guaranteed to represent the final conclusion for a given compound (see for instance Ref. [395]). Therefore, we cannot guarantee specific predictions and the use of these table should be restricted to

discuss major trends among the elements. Circumstances or cases on which theory/computation fail are well documented and the reader can find them elsewhere. Specifically, rare-earth-metals and actinides are challenging to describe theoretically and one can easily obtain wrong results applying standard density-functional theory.

Moreover, we can observe that the megabar range of pressure is substantially richer, superconductivity appears in most regions of the periodic table, including noble gases (Xe) and elements belonging to groups XIV, XV and XVI. There is a large spread of critical temperatures from low to high, as well as in chemical compositions, from low to high H content. It is evident that the high pressure allows to overcome enthalpy barriers to form bonds and stabilize several *superhydrides*, i.e. systems with a high-H content (> 6).

5.1.2. Non-superconducting hydrides

Materials that either do not metallize or else do not show superconductivity at high pressure, but that form stable compositions are eclipsed by their counterparts, the superconducting ones. There is a clear trend in this sense, as second period elements such as C, N, O, F and 3d transition metals as Mn, Fe, Co, Ni and Zn do not form metallic systems under pressure. Notably, H_2O , which is perhaps the most abundant and best studied hydride, remains insulating up to the terapascal range of pressures [396, 397, 398, 399, 400]. Furthermore, noble metals (Cu, Ag, and Au) show an outstanding resilience to hydride formation at ambient pressure.

Experimentally there are no reports of a stable compound with a hydrogen molar ratio > 1 at room temperature [401]. Through high pressure and *in situ* laser heating H can eventually be incorporated in ratios higher than 1, but these compounds usually remain either magnetic or/and insulating at HP.

Studies of hydrides at HP date back to 2003, when Eremets et al. studied $\text{B}_{10}\text{H}_{14}$ [402] and its transformation under pressure. Other systems studied for their potential transformation to a metallic substance include: He-H [403], Li-H [404], Na-H [405], H-O [406, 407], AlH_3 [408], Fe-H [409, 410, 411, 412, 413], Co-H [414], Ni-H [415, 416], Si-H [417, 418, 36], Cu-H [419], SeH_3 [420], Nb-H [421], Rh-H [422], I-H [423], Ta-H [424], Ce-H [425], Eu-H [426], La-Ni-H [427] and other rare earth trihydrides under high pressure [428]. These systems were subject to pressure and phase transformation occurred, but no clear evidence of either metallicity or superconductivity was given, and transport measurements are not reported. This does not rule out the possibility that under other thermodynamic conditions some of these systems may show superconductivity.

5.2. Overview of selected hydrides

Within the broad classes of low and high-pressure hydride superconductors, several classification schemes have been proposed in literature, among others we would like to mention studies based on structural motifs [429], inter-atomic distances, guest to host atom ratio [430], valence band analysis [431], ELF, etc [432, 433, 44, 434, 41, 39, 40, 435]. The main scope of these analyses has been to identify general trends to devise

material' optimization strategies. It is of course desirable to reach a general classification of hydrides but it turns out that these types of global perspectives may oversimplify reality and be eventually misleading [395].

In fact, one may realize that even two important theoretical arguments, such as the Ashcroft-Ginzburg (metallic hydrogen) and the Gilman-Ashcroft (chemical precompression) offer a picture of hydrides which is quite oversimplified, although it may be used as a general guideline. The precompression paradigm assumes that the guest atom would only be exerting "pressure" on the hydrogen sublattice but not alter bonding or chemical properties. In this perfect scenario, superconductivity would be dominated by H states raising to very high- T_c (as it was predicted for solid metallic hydrogen). In practice, hydrides are imperfect realizations of this concept: each guest atom affects the *chemistry* of hydrogen and provides additional electronic and vibrational states tangled with those of hydrogen, ultimately plying a role in superconductivity.

In this Review, we do not attempt to discern a general trend for hydrides or propose any classification scheme. Instead, we identified four binary hydrides that cover a spectrum of pressure and hydrogen contents and clearly exemplify the increasing role that H plays in superconductivity with pressure. In the following, these are treated as representatives of hydride classes. In addition to these systems, we consider metallic hydrogen: the so called atomic (non-molecular) phase. Crystal structures of the representative systems are shown in Fig. 22, and are discussed in order of *increasing* hydrogen content:

- I) PdH, representing metal hydrides at ambient pressure (0 GPa).
- II) PH_2 , example of molecular crystals of metallic hydrides at intermediate pressures (120 GPa).
- III) H_3S , to represent covalently-bonded hydrides at high pressure (200 GPa).
- IV) LaH_{10} , example of superhydrides at very high pressures (300 GPa).
- V) Solid metallic hydrogen, a non-molecular structure stable above 500 GPa.

For the representative compound in each class, we will address the following questions: How does these materials form? What are their structural features? how good superconductors are? What is the connection between high or low T_c to aspects of its electronic structure, such as bonding, electronic and band dispersions? What is the role of hydrogen?

To address these questions we will analyze for each material the basics of its electronic structure, bonding properties, phonons and *e-p* coupling and electron-phonon spectral functions that have been extracted from best existing literature.

Superconductivity is discussed with the help of the McMillan-Allen-Dynes Eq. 100 using $\mu^* = 0.1$. Such approach avoids the complexity of a full-scale theory (Sec. 3) and while not quantitatively excellent, is still sufficiently reliable to highlight trends and capture physical effects. The *e-p* coupling λ is

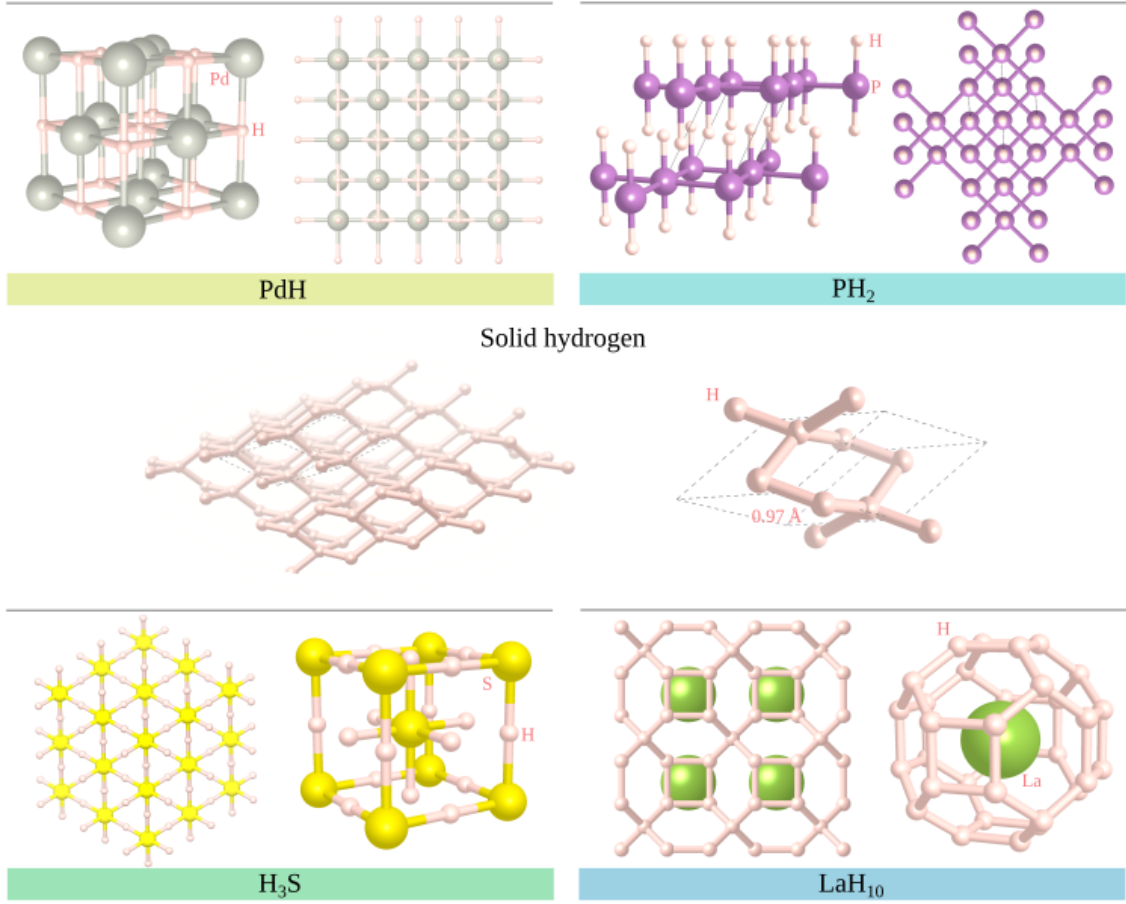


Figure 22: Crystal structures of representative binary-hydrides and elemental hydrogen. PdH: Metal hydride at ambient pressure (0 GPa). PH₂: a molecular crystal hydride at intermediate pressure (120 GPa). H₃S: a covalent bonded hydride at high pressure (200 GPa). LaH₁₀: a superhydride at very high pressure (300 GPa) and H₂: solid metallic hydrogen at megabar pressure (500 GPa).

decomposed with the help of the Hopfield formula Eq. 101 used for $\omega = \omega_{log}$.

For our analysis, it is crucial to have an understanding of the chemical bonding. We studied it based on the Crystal Orbital Hamilton Population (COHP) introduced by Dronskowki and Bloechl in 1993 [436].² This type of analysis is extremely useful because it permits to decompose the complicated energy-dependent electronic structure of a material into a sum of pairwise interactions between atoms, in a tight-binding like local framework, and hence identify which atom pairs participate in a given bond and whether their contribution is of bonding, anti-bonding or non-bonding nature. In addition, the COHP encodes information on the band dispersion, not included in other types

²The COHP method permits to decompose the complicated energy-dependent electronic structure of a material into a sum of pairwise interactions between atoms, in a local basis framework, like tight-binding. The interaction between two atom-centered orbitals (say $|\phi_\mu\rangle$ and $|\phi_\nu\rangle$) is described by the Hamiltonian matrix element $H_{\mu,\nu} = \langle \phi_\mu | \hat{H} | \phi_\nu \rangle$, which when multiplied by the density-of-states matrix, measures the bonding, anti-bonding or non-bonding character if it lowers, rises or does not change the band-structure energy, respectively. This *simple* real-space interpretation of otherwise abstract reciprocal space information contained in the band structure, can result in a useful descriptor to understand the physical and chemical mechanisms through which (high- T_c) superconductivity is realized in different hydrides.

of real-space bond analysis, and hence can be easily connected to the two electronic factors in the Hopfield formula (101).

To understand the role of phonons in the coupling, we will rely on the Éliashberg spectral function – Eq. 54 – and its two moments ω_{log} and λ – Eqs. 67- 61. The Éliashberg function is essentially a phonon density of states weighted by electron-phonon matrix elements and its peaks identify regions of the phonon spectrum where the coupling to electrons is stronger.

5.2.1. Palladium hydride

Background. After Ashcroft's suggestion of possible high temperature superconductivity in metallic hydrogen [7], the hope to induce or rise the superconducting critical temperature of metals by means of hydrogen alloying lead to the discovery of superconductivity in Th [384] and Pd [386, 387] metal hydrides. Hydrogen in these systems is at a relatively high concentration, so that these hydrides can be thought of as alloys in which hydrogen (guest) and metal (host) atoms are both embedded in a common metallic environment.

Elemental palladium is a transition metal which is not superconducting at ambient pressure. Interestingly, its moderate e - p interaction ($\lambda = 0.36$) and characteristic frequencies ($\omega_{log} = 180K$), would lead to a small, but non-zero supercon-

ducting T_c however, superconductivity is suppressed by paramagnetic spin fluctuations, with a coupling constant λ_{SF} comparable to the e - p one [261, 437].

Hydrogen incorporation results in T_c as high as 9 K for PdH [387, 386], indicating a low or intermediate e - p coupling. Indeed, the phase diagram of PdH $_x$ is quite complicated: the crystal is stable for $x > 0.03$ and superconductivity appears at $x \approx 0.7$ with $T_c \approx 5$ K and further increases up to 9 K with a seemingly linear dependence on the H content. The proper determination of the structure of the crystalline phase of PdH $_x$ at various concentrations is a crucial question. In Pd-*fcc* lattice there are two inequivalent interstitial sites, the octahedral site (*O*) and the tetrahedral site (*T*). While at $x=1$ both neutron experiments and first-principles calculations indicate that the *O* site is stable [438, 439, 440], a substantial *T* occupation is likely to occur at lower H concentrations.

The existence of two different *tetra*- or *octa*-hedral absorption sites for hydrogen may be related to old [441] and more recent [442] reports of superconducting phases in PdH with very high- T_c (300 and 62 K, respectively). In view of metastable superconducting phases recently observed for other hydrides, it is possible that given the small energy difference between *O* and *T* site occupations, slow or rapid quenching from the high- T phase may stabilize different a phase with substantial *T* occupations, with improved superconducting properties. However, recent first-principles calculations [443] indicate that a full occupation of *tetra*-sites is detrimental for superconductivity, since it decreases the electron-phonon coupling with H-derived modes, which is at odds with previous studies.

A quite peculiar aspect of PdH is the existence of an *inverse isotope effect*: isotope substitution of H with deuterium results in an increase of T_c up to 11 K in PdD [387]. The inverse isotope effect has been related to a strong anharmonicity of the phonon modes, which is also suggested by resistivity, photoemission, inelastic neutron scattering and tunneling experiments [444, 445, 446, 447, 448].

Only recently the complicated physics of PdH was put on firm grounds by first-principle calculations of phonon frequencies and electron-phonon coupling which include the anharmonic phonon contributions non-perturbatively. These calculations which permitted to reconcile severe discrepancies between theory and experiments in the structural stability and the superconducting properties [208]. In particular, the inclusion of anharmonic corrections on the phonon spectrum strongly renormalizes frequencies of optical branches, yielding a much better qualitative agreement with experiments and stabilizes the lowest acoustical branch, which is predicted to be unstable at the harmonic level. More importantly, anharmonic corrections correct the severe overestimation of the superconducting T_c found by harmonic calculations – T_c is reduced from 47 K (harmonic) to 5.0 K for PdH and 6.5 K for PdD (anharmonic). Calculations including phonon anharmonicity correctly reproduce the anomalous inverse isotope effect observed by experiments, although the calculated value of the isotope coefficient, $\alpha=0.38$, is about 50% lower than the experimental one [208]. The remaining quantitative differences may be related to Coulomb effects, which in Ref. [208] were treated with an empirical pseu-

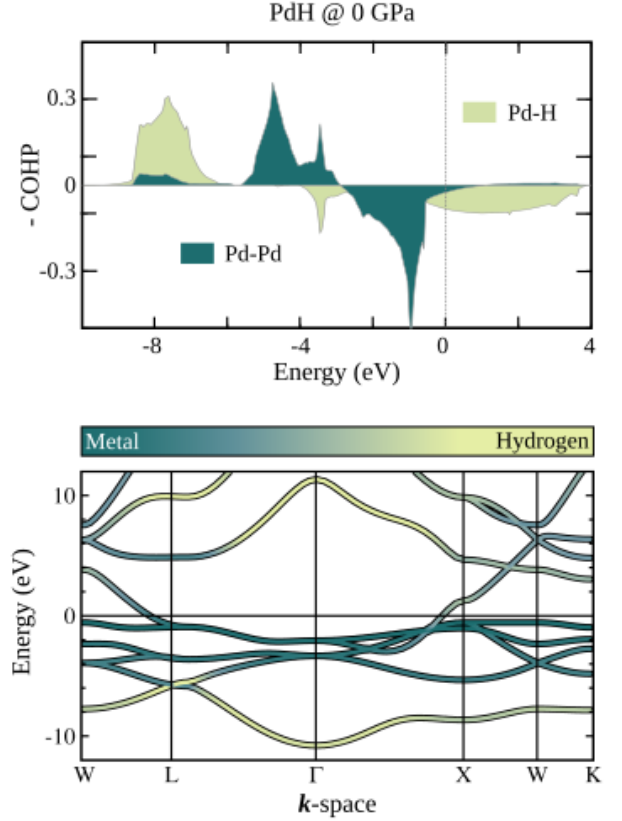


Figure 23: Electronic structure of PdH at 0 GPa. Top: COHP bonding analysis. Bottom: Kohn-Sham band structure, where H projection of the electronic states are shown by a color-code scale: from green (low) to yellow (high).

dopotential and not on a first-principles ground or from anharmonic effects on the deformation potential, which was also disregarded. Both types of effects may be relevant also in other hydrides.

Electronic structure and superconductivity. For the following discussion, we consider PdH with hydrogen in the *O*-sites which according to first-principles calculations and experiments, should be the ground-state structure for $x \sim 1$. The crystal structure is shown in top left corner of Fig. 22: Pd and hydrogen atoms form two interpenetrating *fcc* lattices, with a lattice constant of 4.04 Å, which is around 5% larger with respect to elemental Pd.

In Fig. 23 we report the atom-projected DFT band structure and COHP. As shown, palladium-derived bands dominate the region near the Fermi level. These are *d*-states octahedrally split into e_g and t_{2g} manifolds; the latter can form σ -type bonds with hydrogen in the rocksalt structure. Indeed, we observe a clear splitting of Pd-H hybridized states into a bonding (≈ -10 eV at the Γ -point) and an antibonding (≈ 10 eV at the Γ -point) manifold. Compared to pure Pd, in which they sit at the Fermi level, in Pd-H due to the presence of an additional H electron the Pd-*d* states are completely full and hence the Fermi surface consists on a single Pd-H band, which also has additional Pd-*sp* character. Note that the filling of the *d*-bands compared to pure Pd has the additional effect of reducing the spin fluctu-

ations, which in Pd suppress superconductivity [437]. In top panel of Fig.23 we present the COHP as a function of energy for two different types of interactions (Pd-Pd and Pd-H). In this plot, as well as in all COHP figures below, the convention chosen is to plot the negative of the COHP, so that positive and negative peaks indicate bonding and antibonding interactions, respectively.

The bonding Pd-Pd interaction is evident from the (positive) peak at ≈ -4.5 eV, while the antibonding (negative) peak at ≈ -0.4 eV is filled due to electrons donated by hydrogen. The first dispersing band (from -10 to -6 eV) has Pd-H bonding character and the corresponding antibonding region is located from -2 to 3 eV. Bands crossing at the Fermi energy are responsible for electron-phonon interaction and superconductivity and are antibonding states of both Pd-H (the largest contribution), and Pd-Pd interactions. The hydrogenic fraction at the Fermi level is estimated to be of the order of 5%, a rather small but non negligible value.

The presence of hydrogenic states crossing the Fermi level qualitatively implies that those modes should provide to some extent, a sizable deformation potential. This seems to be the case (see Table in Fig. 28), the Hopfield ratio $I^2/M = 0.08$ that accounts for the part of the coupling that is independent from the phonon energy and from the electronic DOS N_{E_F} , is three times larger than that of niobium ($T_c=9.3$ K). That hydrogenic modes are responsible for a significant part of the coupling can be also seen from the Éliashberg function (Fig. 28) as it is clearly weighted towards high energies with $\omega_{log}=53$ meV. However the total electron phonon coupling has a very small value $\lambda = 0.4$ and the computed critical temperature is very low (2.7 K³). This highlights a small drawback of hydrogenic superconductivity: high phonon modes provide a potential large scale for the phonon to provide scattering (prefactor of Eq. 100). However, since the same phonon energies also affect the coupling strength (λ), according to Eq. 101, unless the deformation potential I is strong enough, superconductivity is killed by the sublinear dependence of T_c at weak coupling (Fig. 14). One could also make a step further and use Eq. 101 to compute the optimal phonon energy to maximize T_c . The optimal T_c for PdH would be as high as 40 K if ω_{log} could be reduced down to 20 meV. The computed critical temperature of 2.7 K is however quite off with respect to the experimental value of 9 K. This inaccuracy can be ascribed in part to the $\mu^* = 0.1$ assumption and to the sensitivity of T_c to the phonon energies and their strong anharmonicity. It is in fact possible that anharmonic corrections to the phonon frequencies [208] have been overestimated resulting in modes that are too stiff, or that corrections to the deformation potential, not included in the calculation of the Éliashberg function are also relevant. As mentioned in the previous section this suggests that more accurate calculations of anharmonic phonon and Coulomb terms would be necessary to obtain quantitative agreement.

To summarize, the presence of hydrogen in PdH is crucial

for superconductivity for several reasons: i) It is efficiently incorporated in the original *fcc* Pd matrix at large stoichiometry ($x \approx 1$). ii) The hybridization between H and Pd states is sufficiently large to promote an anti-bonding Pd-H band at the Fermi energy. iii) This band couples with H-derived phonon modes showing large anharmonic effects. iv) The additional electrons donated by hydrogen fill the Pd-*d* bands suppressing spin fluctuations that would otherwise kill superconductivity. However, the coupling provided by hydrogen is relatively weak (λ is in fact comparable to the one in elemental Pd) thus, the large (anharmonic) phonon energies limit the coupling strength.

5.2.2. Phosphorus hydride

Background. After less than one year from the H₃S discovery, the same group reported the discovery of high-temperature superconductivity in phosphines under pressure [169]. PH₃ molecules (phosphine) have already the same hydrogen to host-atom ratio as H₃S. Experiments report that a mixture of this gas and hydrogen loaded in a diamond anvil cell becomes metallic at 40 GPa and eventually superconducting at 80 GPa, with a maximum T_c of 103 K at 207 GPa (see Sec. 2). At the time of the experiments there were no indications on the possible crystalline phases of phosphine under pressure and without available diffraction experiments, first-principles methods could give hints about what phases could become stable at high pressure. Independently, two groups reported a complete high pressure phase diagram of PH_x with $x = 1, 2, 3, 4, 5, 6$ compositions [449, 168]. Quite surprisingly, both studies found a thermodynamical instability of all the compositions upon dissociation towards pure phosphorus and pure H. The only *metastable* phases sufficiently close to the convex hull in the range 100-200 GPa had PH, PH₂, and PH₃ compositions. The ground-state structures at a pressure of 120 GPa have a *I4/mmm* space group for both PH and PH₂ and *C2/m* for PH₃. At this pressure, the P-H bond length is 1.4 Å (of the same order of the S-H bond length in the superconducting H₃S), while the P-P bonds are ≈ 2.1 Å long in all three structures. In addition and at variance with other hydrides, it was found that P atoms tend to form 1D polymeric structures or 2D layers, connected by weak interactions among them (see structural sketch in top right panel of Fig. 22).

Assuming that, *metastable* phases may actually be stabilized in experiments, the authors on Refs. [449, 168] found that PH, PH₂, PH₃ are dynamically stable and their calculated critical temperatures and evolution with pressure are in such a good agreement with the experimental results (see Fig. 11) that the hypothesis of metastability is probably valid [168].

Electronic structure and superconductivity. The structural motif of PH₂ at 120 GPa (shown in Fig.22) is characterized by a two dimensional square lattice of linear PH₂ molecules linked together by P-P bonds. The two-dimensional layers are stacked in a AB fashion along the direction perpendicular to the layers. This layered crystalline phase is quite unique in the realm of high-pressure hydrides and it is probably at the origin of its metastability.

³Our estimation is lower than that in Ref. [208] because we have opted for a conventional value $\mu^*=0.1$. This choice was made to allow a same ground comparison between the selected hydrides.

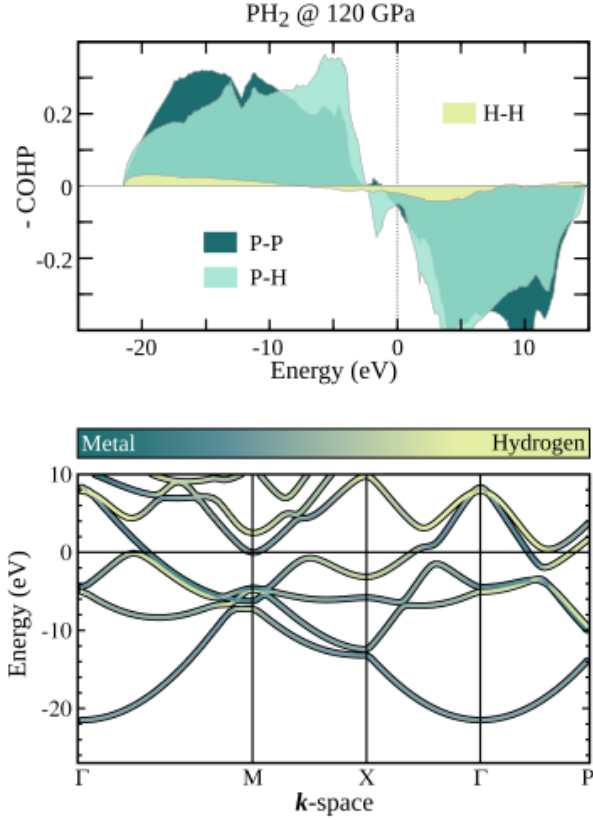


Figure 24: Electronic structure of PH_2 at 120 GPa. Top: COHP bonding analysis. Bottom: Kohn-Sham band structure on which H-projected electronic states are shown by a color-code scale: from green (low) to yellow (high).

The projected band structure of PH_2 at 120 GPa, reported in Fig. 24 shows that occupied bands and in particular the states at the Fermi level, have a strong P-H hybridization. The integrated H projection at the Fermi level accounts for about 50% of the DOS (see Table in Fig. 28).

The bonding properties of the 2D network can be analyzed in terms of the COHP, also shown in Fig. 24. The P-H interaction shows well separated bonding and antibonding regions (roughly below and above the Fermi level, respectively). However, antibonding states are partially occupied with a Fermi surface formed by antibonding states which extends 2 eV below Fermi energy. These states originate from molecular orbitals of the PH_2 units extending within the layer linked together by P-P bonds, which shows clear occupied bonding states. A key aspect is that the system is made of layered units that are weakly bound, clearly seen from the low values of H-H COHP. The difference with the bonding character in H_3S (see next section) is evident: in the latter the covalent metallic bond is stronger and extends to the entire solid.

The vibrational spectrum is characterized by a large energy scale dictated by hydrogenic modes: a scale that is about 3 times that of PdH. In addition to this, the hydrogen contribution to the Fermi DOS is estimated to be much larger ($\approx 55\%$). The electron phonon coupling is distributed homogeneously over all the modes [168].

A predicted T_c of 53 K indicates that the Gilman-Ashcroft mechanism is at play, but not acting at its full potential. In fact the total electron phonon coupling ($\lambda = 1$) is in the mid-coupling regime and the ω_{\log} of 59 meV is quite low, not much higher than in PdH (53 meV). The rationale for this is that, while both hydrogenic phonons and especially hydrogen-related electronic states at the Fermi level are available, the latter are not efficiently scattered by the former. This aspect can be traced back to the layered nature of the compound, in which the distortion in the electronic potential caused by H modes is shifted outside the conductive network of the P-layer.

5.2.3. Sulfur hydride

Background: At ambient pressure, sulfur hydride is a molecular solid formed by H_2S molecules, with a relatively complex phase diagram [160]. When placed in a hydrogen-rich atmosphere, H_2S easily absorbs hydrogen. In 2015, experiments showed that at pressure higher than 90 GPa the $\text{H}_2\text{S} + \text{H}_2$ mixture becomes metallic and at about 100 GPa, superconducting, with a critical temperature of ≈ 8 K at $P \approx 150$ GPa [1] (see Sec. 2 for details). Upon further increasing pressure and measuring the resistance up to room temperature to obtain reliable results, experiments showed a rapid increase of the critical temperature up to ≈ 200 K for pressures $\gtrsim 170$ GPa, indicating a new (and in part unexpected) superconducting phase. The measured shift of the critical temperature with applied magnetic field from 0 to 7 Tesla certified the superconducting nature of the phase transition and the measure of an isotope coefficient of $\alpha = 0.3$ upon H/D substitution, its conventional (electron-phonon) origin.

The initial interest in the sulfur-hydrogen system was motivated by a key theoretical prediction by Li and coworkers [160] of a possible metallization and superconductivity of H_2S . While this work opened the field, it was later discovered that the phase experimentally formed had the H_3S stoichiometry. A correct and complete prediction of stability and superconductivity in H_3S under pressure was given by Duan and coworkers [161] independently and shortly before the publication of the experimental results [162]. For contextual history readers are urged to see *Serendipity of the discovery of superconducting H_xS* in Sec. 2.

In their work, which can certainly be considered a milestone for *ab initio* superconductivity, Duan et al. [161], performed a study of the phase stability of the $(\text{H}_2\text{S})_2\text{H}_2$ system under pressure. Their study was motivated by a previous prediction and observation of hydrogen-rich $\text{SiH}_4(\text{H}_2)$; SH_2 , analogously to silane, had been shown to easily incorporate hydrogen under pressure. According to DFT calculations, H_2 molecules start to incorporate into the H_2S molecular crystal already at around 10 GPa, forming structures in which, at the lowest pressures, where they are stable, the two molecular species are still clearly recognizable. However upon increasing pressure, H_2S and H_2 molecules are pushed closer until, at around 90 GPa, intramolecular bonds break and new bonds start to form between sulfur and hydrogen, giving rise to distinct H_3S stoichiometric units.

The first predicted H_3S phase, which is stable from 111 GPa up to 180 GPa, has an $R3m$ symmetry. In this phase, sul-

fur atoms occupy the lattice points of a (rhombohedrally distorted) conventional *bcc* cell, each of them is surrounded by three hydrogens, forming isolated units [161]. The formation of an H_3S phase is supported experimentally because the predicted superconducting critical temperature for this phase is ≈ 160 K at 130 GPa and rapidly increases with pressure, exactly in line with experimental evidences. Starting at 180 GPa another structural transition is predicted towards an $Im\bar{3}m$ (*bcc*) phase, characterized by a symmetrization of the bonds between sulfur and H atoms, thus not forming isolated H_3S units anymore. In this structure, shown in Fig.22, the H atoms are symmetrically placed between two S atoms resulting in the formation of hydrogen-shared SH_6 unit. Interestingly the calculated [161, 309, 173, 209] T_c for the $Im\bar{3}m$ structure at 200 GPa is ≈ 200 K, making it a strong candidate to be the high- T_c phase observed in the experiments.

The final confirmation of the crystal structure of the superconducting phase was given by synchrotron X-ray diffraction measurements [167], which showed the H_3S units sit on a *bcc* lattice, as theoretically predicted. In addition, infrared optical spectroscopy measurements observed optically active phonons at 160 meV with a dramatically enhanced oscillator strength [450] as well as evidences of superconducting gap at 76 meV, interpreted with the Éliashberg theory of electron-phonon driven superconductivity. As in PdH, however the proper theoretical interpretation of all the experimental results require the inclusion of anharmonic and quantum effects of hydrogen. Indeed, a proper treatment of these effects [209] is fundamental to predict the correct critical pressure for the $R3m \rightarrow Im\bar{3}m$ phase transition, the anharmonic phonon frequencies of the hydrogen-dominated phonon modes and the shift of T_c upon isotope H/D substitution [451].

In addition to the high- T_c phase, experiments clearly identify one or more low-pressure phases. For these, many structural models have been proposed theoretically, based on thermodynamic stability consideration and estimation of T_c [161, 452, 173]. In particular, a modulated structure model with long periods of alternating slab-like H_2S and H_3S regions forming a sequence of “*Magnéli phase*” was proposed [175]. Even though the pressure trend of a comparatively low- T_c phase may be reproduced, the calculated XRD patterns of these Magnéli phases do not match the experimental data [453, 454].

Electronic structure and superconductivity. Rather than a dense hydrogen sublattice, high- T_c *bcc* H_3S should be more accurately described as a dense solid of covalently-bonded hydrogen and sulfur. In this structure, shown in left bottom panel in Fig. 22, sulfur sits on a *bcc* lattice with lattice constant $a = 2.96\text{\AA}$ (at 220 GPa), while hydrogen fills the positions in the middle of the edges and faces. Thus, each hydrogen has two sulfur and four hydrogen nearest neighbors, at an equal distance of 1.48\AA .

Electronic band structure and COHP analysis for H_3S are shown in Fig. 25. The relevant bandwidth extends 25 eV below the Fermi energy, with the lower band originating from S-3s orbitals with a (small) H-1s contribution. The hybridization between H and S states is strongly enhanced in the region

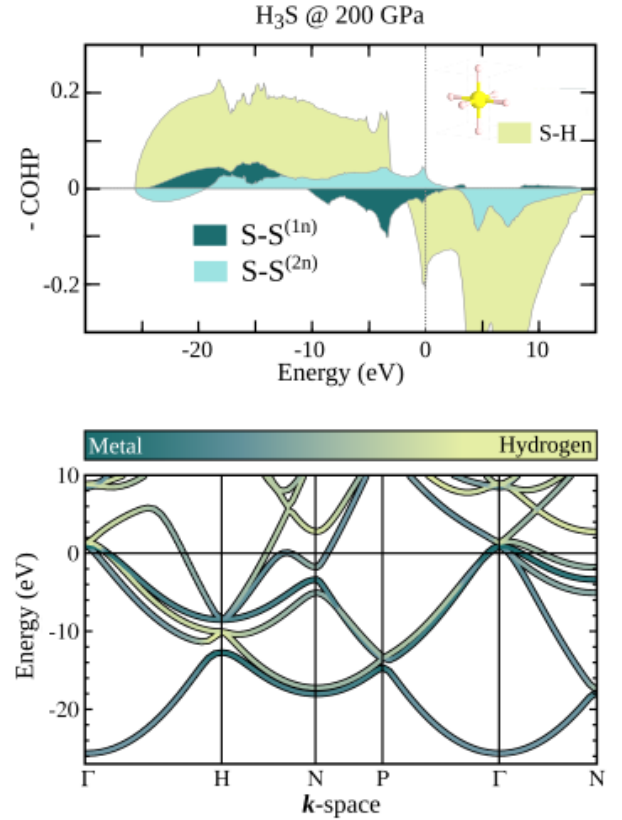


Figure 25: Electronic structure of H_3S at 200 GPa. Top: COHP bonding analysis. Bottom: Kohn-Sham band structure on which H-projected electronic states are shown by a color-code scale: from green (low) to yellow (high).

around the Fermi energy ($-5 - 5$ eV), where the S-3p and H-1s interaction dominates. The origin of one of the van Hove singularities [455] can be traced back to the maximum of the band dispersion along the H-N direction of the Brillouin zone which is below the Fermi energy [247, 456, 457, 458]. The presence of van Hove singularities close to the Fermi level has stimulated discussions of new and alternative superconducting mechanisms or refinements of the conventional electron-phonon theory of superconductivity [459, 247, 456, 457, 458]. Hydrogen contribution is predominant on the higher energy part of the spectrum.

The COHP, shown in top panel in Fig.25, permits to interpret the same electronic structure in terms of real-space interactions. The majority of the valence region is dominated by a bonding S-H interaction; the corresponding energy states are fully occupied indicating a strong stability of the S-H network. The Fermi level falls into the region of antibonding (negative COHP) S-H orbitals with the van Hove singularity clearly visible close to the Fermi energy. Sulfur-Sulfur interactions give a lower but non negligible contribution considering that they extend up to the next nearest neighbour, while direct H-H interactions, on the other hand, do not contribute to the bonding. In PdH, the strong Pd-Pd bonding/antibonding levels were fully occupied due to the additional electrons donated by H, so that the states Fermi level were eventually of Pd-H antibonding charac-

ter. Also in H_3S , the dominant contribution to the states at the Fermi level is of antibonding H-host character, but the S-S interaction is strongly reduced; the much larger electron-phonon coupling and phonon frequencies in H_3S result from the fact that the metal-H distances are sensibly shorter ($d_{\text{S-H}}=1.4 \text{ \AA}$, $d_{\text{Pd-H}}=2.02 \text{ \AA}$).

The vibrational properties of H_3S are characterized by low-energy ($\lesssim 75 \text{ meV}$) S-derived modes separated by H-derived modes which extend up to $\approx 250 \text{ meV}$, once anharmonic corrections are included [209]. The latter show a clear separation into bending modes, ranging from ≈ 100 to $\approx 200 \text{ meV}$, and high-energy stretching modes from ≈ 200 to $\approx 250 \text{ meV}$, which are the modes most coupled to electrons at the Fermi energy [209]. Calculation including anharmonic corrections predict an isotope effect $\alpha=0.35$, sensibly reduced with respect to the BCS value and in good agreement with experiments [209].

The total electron-phonon coupling parameter (see Fig. 28) is $\lambda=1.84$, which results in a critical temperature of 194 K (using $\mu^*=0.1$) at 200 GPa which agrees with the experimental reported critical temperature of 190 K [1].

The large T_c comes from the key role of hydrogen vibrational modes and electronic states. Hydrogen contributes to about 45% of the states at the Fermi level, slightly less than in PH_2 , but still quite significantly. The Fermi level is pinned at a peak in the density of states, although the Fermi DOS is similar to that of other hydrides and not significantly higher. Hydrogen related modes spread to high energies ($\approx 250 \text{ meV}$) yet, in spite to these large scales, high energy modes show up in the Éliashberg function as a broad and high peak (Fig. 28) overcoming the ω^{-1} factor carried by the electron-phonon coupling (Eq. 15). One can disentangle the effect of phonon frequencies in the electron-phonon coupling considering the I^2/M factor in Hopfield formula Eq. 101: for H_3S one gets $I^2/M = 1.46$ a very large value, one order of magnitude larger than in PH_2 and about 40% of that computed for pure hydrogen (See Table below Fig. 28). In short, H_3S is exceptionally because while hydrogen only accounts for 50% of the Fermi DOS, these hydrogens are fully covalently bound together with sulfur belong to a full 3D network of conductive bonds. In addition, one should also consider that sulphur itself provides and extra coupling, and S modes significantly enhance λ . In fact elemental sulphur is a superconductor at the high pressure regime.

5.2.4. Lanthanum hydride

Background: LaH_{10} currently holds (2019) the record for highest T_c measured among all known superconductors ($\approx 260 \text{ K}$). It is a *superhydride*, which forms upon laser heating of lanthanum in a hydrogen-rich atmosphere and belongs to a large class of sodalite-like clathrates, which includes hydrides of other elements, such as Mg, Ca, Y, La, with predicted T_c 's close to or exceeding room temperature, between 200 and 400 GPa [460, 177].

In 2017, the Argonne group reported the synthesis of lanthanum superhydrides under pressure, through laser heating of lanthanum in a hydrogen-rich atmosphere [191]. The hydrogen to lanthanum ratio was estimated to be $x \in [9, 12]$, based on the

unit cell volume. Due to the small X-ray cross section of hydrogen, it is not possible to resolve directly the H sublattice but only the La one. This was indexed as an $Fm\bar{3}m$ lattice (*fcc*). The high- T_c *fcc* phase of LaH_{10} , for which Li et al. predicted a T_c of 280 K at 210 GPa was thus suggested as the most likely candidate for the observed phase [182]. The main structural motif of the structure is the cage of H's in which La atoms are located, linked together by direct H-H bonds, see Fig. 22.

In 2018, two groups reported superconductivity measurements on lanthanum hydrides under pressure. The first group reported a maximum T_c of 215 K , around 200 GPa [183]. The second set of measurements reported T_c 's as high as 260 K , in samples heated up to 1000 K at 180 GPa [3]. Finally, the same authors as in Ref. [181] confirmed a few months later a T_c as high as 250 K in LaH_x samples, but also reported the existence of several phases with lower and distinct T_c 's, depending on the synthesis conditions [181].

The same study contains other measurements, which are crucial to establish superconductivity and its conventional nature in LaH_{10} : isotope effect (hydrogen vs deuterium substitution) and measurements of T_c under magnetic field. Due to the difficult synthesis conditions, the linear dimensions of the current samples of LaH_{10} ($10\text{-}20 \text{ }\mu\text{m}$) are much smaller than those of H_3S (up to $100 \text{ }\mu\text{m}$); this does not allow a proper measurement of the Meissner effect, but the authors show that indeed magnetic field suppresses superconductivity.

The dependence of the critical temperatures on pressure reported by the two studies are also conflicting: while the Argonne measurements report an abrupt increase in T_c up to 290 K [3] Ref. [181] report a dome-like shape of the T_c vs P curves. All the observations above suggest that, depending on the synthesis conditions, different phases with different stoichiometries and/or crystal structures may be stabilized by laser heating.

Electronic structure and superconductivity. The high- T_c *fcc* phase of LaH_{10} , shown in the right panel of the lower row of Fig. 22, can be considered one of the closest realization of the Ashcroft-Gillan-Ginzburg chemically-precompressed hydrogen sublattice in hydrides. The main structural motif is a highly symmetric cage formed by 32 hydrogens, with 12 hexagonal and 6 square faces, which surround a central La atom. These large cages are interconnected forming a dense hydrogen sublattice, with two different bond lengths – $d_{\text{HH}} = 1.07(1.15)$ for a square (hexagonal) edge.

The electronic band structure of LaH_{10} in the high- T_c *fcc* phase at 300 GPa is shown in the lower panel of Fig. 26. As a confirmation of the general trend, the states at the Fermi level derive from both the H sublattice and the La sublattice, even if in this case there is a clearer separation of La- and H- derived Fermi surfaces.

The Fermi surface comprises six distinct pockets, centered around the BZ center and boundaries, formed by H $1s$ and La states bands, which hybridize along some directions of the BZ. The hybridization is mainly due to the presence of low-lying *f*-states of La, centered around 5 eV above the Fermi level. The surprising presence of a non-negligible contribution of *f*

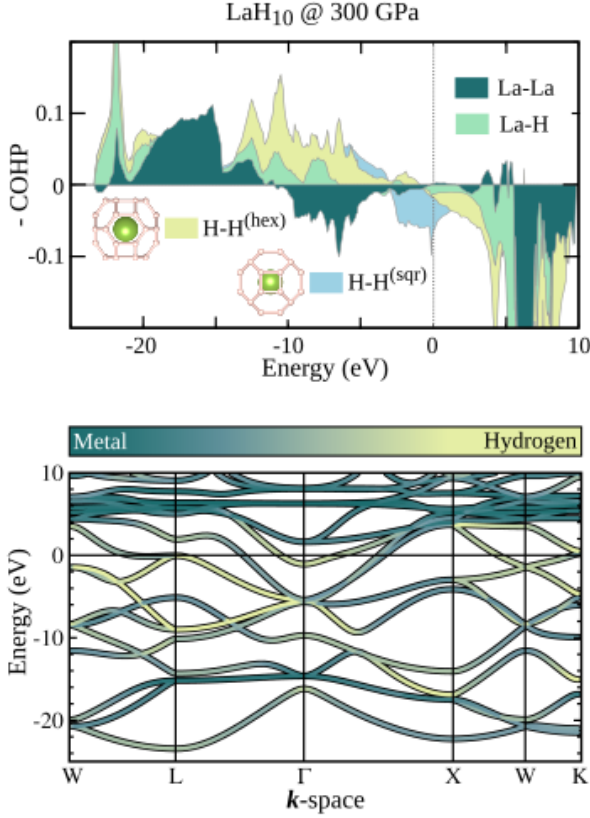


Figure 26: Electronic structure of LaH_{10} at 300 GPa. Top: COHP bonding analysis. Bottom: Kohn-Sham band structure on which H-projected electronic of states are shown by a color-code scale: from green (low) to yellow (high).

electrons to the Fermi level was already pointed out by Liu et al. [182], who observed that in LaH_{10} not only s and p La electrons contribute to the DOS at E_F , but also the f electrons. We remark that these states, being strongly localized, are usually not well described by DFT-like methods, and hence this seems to cast doubts about the reliability of the DFT results on this system. On the other hand, the fact that the high- T_c properties computed in this system are very similar to other hydrides which do not contain f electrons indirectly confirms the reliability of existing predictions. As evident from the band structure, at the Γ -point an electron-like H-derived band crosses E_F and two other bands, of mixed La and H character, form electron pockets. Hole pockets at the zone boundary are formed by states with dominant La character. At the L-point of the BZ we observe a Van Hove singularity very close to the Fermi level which, similarly to what we discussed for H_3S , may be partially responsible for enhancing the superconducting properties [461].

In this case the COHP analysis (see Fig. 26) turns out to be fundamental to analyze the bonding properties of the system, which is quite complex. First we consider the H-H interactions. In the system there are two nonequivalent H-H bonds, the nearest - neighbour H-H (1.06 \AA) connecting H atoms forming the hexagons and the next-nearest neighbours H-H bonds (1.15 \AA) among H atoms forming the squares (see Figure 22). The for-

mer interaction is clearly covalent with occupied bonding states well separated from the unoccupied antibonding states (brown curve). The next-nearest neighbours (1.15 \AA , squares bonds) H-H interaction is different, showing that the antibonding states are populated (this feature is similar to what observed in other hydrides). The bonding states between La and H (averaged between nearest and next-nearest neighbours) are located at a very low energy (they extend only up to -10 eV), while at the Fermi level the (hybridized) states are mainly of non-bonding character (COHP is ≈ 0.0). The states derived by direct La - La interaction have non-bonding character at E_F , with populated bonding and antibonding states.

Phonons and electron-phonon coupling. The phonon dispersion of LaH_{10} extend up to $\approx 3000 \text{ cm}^{-1}$. Due to the very different phonon mass of La and hydrogen, La and H modes split into low-energy modes with distinct La character, and high-energy modes with H character. The e - p coupling is quite uniformly spread over all phonon modes, resulting in $\lambda = 1.8$ and $\omega_{\log} = 1490 \text{ K}$ (values at 300 GPa from Ref. [182]). This yields a T_c of 215 K using the modified McMillan-Allen-Dynes formula or higher values solving Migdal-Éliashberg equations, assuming a standard values of μ^* (0.1-0.13). In principle anisotropic effects and anomalous Coulomb screening could strongly modify the calculated T_c values. Although no direct calculations of these effects for LaH_{10} exist in literature, a recent first-principles study on the closely-related YH_{10} system seems to rule out both possibilities [460].

An interesting issue is the dynamical stability of the high- T_c fcc structure. According to harmonic DFPT calculations the sodalite-like structure, which is the likeliest candidate for its stability above 200 GPa, while experiments measure a T_c already at 170 GPa. The most likely explanation is that anharmonic effects stabilize the structure to lower pressures or it represents a metastable phase stabilized by peculiar thermodynamical conditions [462]. Currently, there are no calculations addressing these points.

Electron phonon coupling calculations [182] are available for $P=300 \text{ GPa}$. Éliashberg spectral function and coupling parameters are reported in Fig. 28, this picture a system that is similar to H_3S . As for H_3S λ is in the strong-coupling regime and relevant lattice modes are significantly contributed by hydrogen. The scenario drawn by the Hopfield decomposition of λ and use of the McMillan-Allen-Dyes equation for T_c as shown in Fig. 28, indicates that LaH_{10} is similar to H_3S : Fermi DOS, similar hydrogenic fraction and almost identical deformation potential. The only difference is that the coupling is slightly shifted towards lower energies, so the coupling constant λ is larger, leading to an improvement of T_c to 234 K. From this argument, one is tempted to draw the conclusion that the reason behind for LaH_{10} to be a better superconductor than H_3S is in a slightly better tuning of the phonon energy to coupling ratio. The calculation of the optimal ω_{\log} using the Hopfield formula in the McMillan equation would, in fact indicate for both H_3S and LaH_{10} a value of about 100 meV.

However one has to be careful because existing calculations refer to a pressure (300 GPa) that is way higher than the pres-

sure at which the system is experimentally measured ≈ 200 GPa. At this pressure, LaH_{10} results to be neither thermodynamically nor dynamically stable (harmonic phonons). It is safe to say that, unlike for H_3S the physics of LaH_{10} is not fully unveiled. The disagreement with experiments could be possibly ascribed to a different structural phase, with respect to the theoretical model or to large anharmonic effects (as compared to H_3S).

5.2.5. Elemental hydrogen at HP

Background. The metalization of hydrogen has been seen as a compelling subject of study by many scientists, ranging from experimental chemists and physicists [134, 135, 136, 137, 10, 463, 9], to theoreticians [139, 140, 141]. However, despite the great advancement in high pressure-techniques and tools, the metalization of hydrogen in its solid phase has proven to be very challenging, and still debated [142, 143, 144, 145, 146, 147, 148, 149, 150, 151, 152]. The $P - T$ phase diagram of hydrogen comprises many structures, including solid and molecular crystals and is so complex that it could be subject of a Review by itself [463].

Here, we study the first predicted *atomic* metal phase of hydrogen, the $\beta - \text{Sn}$ structure, which, according to first-principles calculations, should be stable between 500 GPa and 1 TPa [278, 10]. All molecular phases of hydrogen are characterized by the presence of H_2 molecules with a 0.7 \AA bond. In atomic phases this bond is broken. However, both the $\beta - \text{Sn}$ and the next stable structure, the $R\bar{3}m$ one, are relatively open, and H forms bonds of different types. Only at very high pressures ($\geq 3.0 \text{ TPa}$) hydrogen is predicted to form genuinely close-packed (*bcc* or *hcp*) phases.

Electronic structure and superconductivity. The $I4_1/amd$ structure, commonly known as $\beta - \text{Sn}$ or $Cs - IV$ structure, comprises two nonequivalent H atom in a *bct* unit cell, each of which forms four short (0.98 \AA) and four long (1.21 \AA) bonds. The typical 0.7 \AA H_2 bonds characterizing the molecular phases at lower pressures are not present.

The electronic structure at 500 GPa is shown in Fig. 27. Hydrogen in the $\beta - \text{Sn}$ structure has a very large bandwidth ($\sim 40 \text{ eV}$), reflecting electron large kinetic energy. The band dispersion is very close to the free-electron one, except for $\sim 5 \text{ eV}$ gaps opening close to the zone boundaries due to the strong unscreened electron-ion potential, responsible for the $e-p$ interaction. The corresponding Fermi surface is an almost perfect Fermi sphere, refolded into the Brillouin zone, with strong H-s electronic character and tubular deformations around the zone boundary. The COHP function is shown in Fig. 27, resolved in into 1st and 2nd nearest neighbours H-H contributions. The plot clearly shows that the bonding is characterized by filled bonding states for nearest neighbours H-H neighbours interactions, clearly separated at E_F from the antibonding states. Antibonding states from next-nearest interactions, are on the contrary occupied starting from -10 eV , the 3rd n.n. contribution is essentially non-bonding (not shown).

At 500 GPa, the phonon dispersion (from Ref. [464]) extends up to 370 meV , a range comparable to the frequencies calculated for clathrate hydrides at similar pressures. The Éliashberg

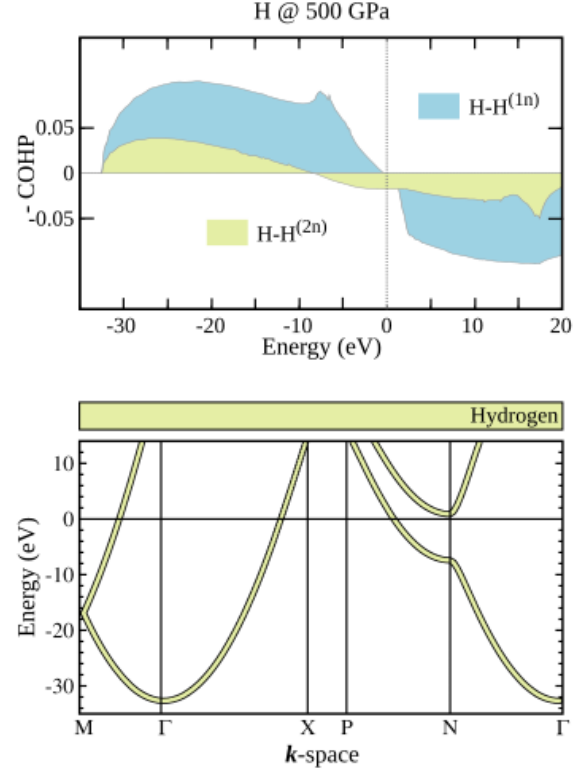


Figure 27: Electronic structure of H at 500 GPa. Top: COHP bonding analysis. Bottom: Kohn-Sham electronic band structure.

function reported in Fig. 28, shows that the coupling is spread quite homogeneously over the entire frequency range. The average energy $\omega_{\log} = 166 \text{ meV}$ is larger than in other hydrides, partially reflecting stronger bonds and the larger applied pressure. In spite of this, coupling λ is the same as in H_3S , clearly leading to a larger $T_c = 282 \text{ K}$. The reason why λ can be high in spite of the large phonon energy lies in the larger I^2/M ratio. An analysis of the optimal ω_{\log} , as done for PdH and other hydrides, indicates a maximum achievable T_c of 300 K for if ω_{\log} could be softened down to 140 meV (see Table 1).

Even for this case, T_c of metallic-solid hydrogen would remain in the same ball-park as those predicted for the best clathrate hydrides. In order to increase T_c further, the only possible way would be to increase pressure. Indeed, McMahon and Ceperley extended the study of superconductivity of hydrogen in its $\beta - \text{Sn}$ structure up to 1.5 TPa ($1,500 \text{ GPa}$) [137]. At those pressures T_c is predicted to increase up to 500 K at $\approx 700 \text{ GPa}$ and then experience a sharp drop. T_c 's up to 750 K (at 2 TPa) have been predicted for the next stable H polymorph: the $R\bar{3}m$ phase, which is not discussed here.

5.3. Summary

We have shown in previous sections that *ab initio* calculations closely reproduce the superconducting properties of the five representative hydrides that we have chosen as examples. These compounds are in many ways all realizations of the Aschcroft-Ginzburg-Gilman's arguments, but with very different outcomes. In fact, the actual superconducting properties

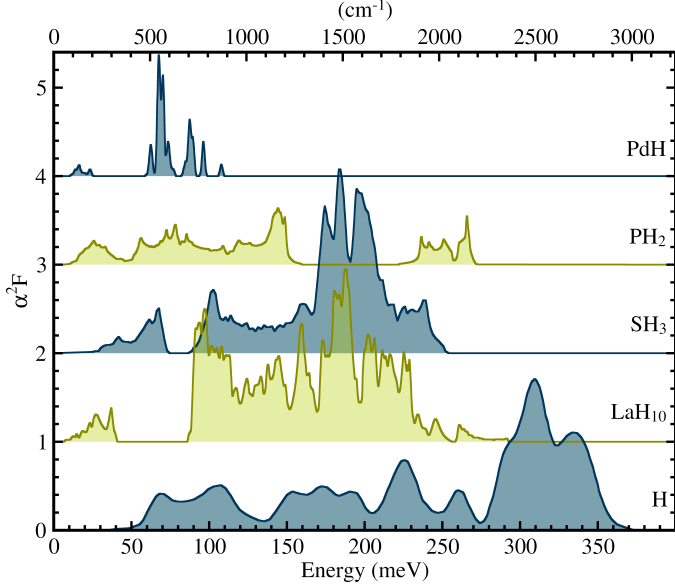


Figure 28: Éliashberg α^2F function computed for selected hydrides: PdH (0 GPa) [208], PH₂ (120 GPa) [168], H₃S (200 GPa) [173], LaH₁₀ (300 GPa) [461] and H₂ (500 GPa) [464]. A vertical shift is applied for plotting the functions. The value of the integrated coupling constant λ is indicated for each material.

vary from being marginal (as in PdH) to astonishing, as in H₃S or LaH₁₀, depending on specific aspects of electronic structure and coupling – see table 1.

PdH, our first example, is a prototypical metallic hydride, where H is incorporated in the original *fcc*-Pd matrix at a small stoichiometry ($x \approx 1$). This amount of hydrogen is sufficient to promote an antibonding Pd-H band at the Fermi energy, yielding a small and non-negligible fraction of H states at the Fermi level. These states are coupled with H-derived phonon modes showing large anharmonic effects. However, the hydrogen contribution is not large enough to lead to a substantial *e-p* coupling. In fact, the Hopfield factor I^2/M , which gives an estimate of the *e-p* coupling fraction independent of the electronic DOS and phonon spectrum, is merely 0.08, as opposed to ~ 1.5 in H₃S and LaH₁₀. The resulting *e-p* coupling constant is relatively weak ($\lambda = 0.4$), comparable to that of elemental Pd ($\lambda = 0.36$). Compared to elemental Pd, the presence of hydrogen increases the phonon energy scale, and yields a finite T_c . However, due to a substantial anharmonic hardening, the interplay between phonon frequencies and electron-phonon matrix elements is not optimal, therefore T_c is substantially reduced with respect to the optimal value $T_c = 40$ K.

Hydrogen incorporation in a metal framework is clearly very far from the idea of chemical precompression, which implies a rearrangement of bonds into a dense hydrogen sublattice and overcoming energy barriers in the megabar range. PH₂ represents an intermediate step towards this idea. With respect to phosphine, which at ambient pressure forms an open crystal of PH₃ pyramidal molecules, a major rearrangement of bonds occur. At high pressure, the new structural motif is characterized by a two-dimensional square lattice of linear PH₂ molecules

Table 1: Collected electron-phonon parameters computed for the same set of materials. We tabulated: Pressure (p), N_{E_F} that is the density of states at the Fermi level and $N_{E_F}^H$ the fraction of it that projects on the H site. ω_{log} and λ are electron phonon coupling parameters defined in Eq. 67 and Eq. 61. I^2/M is computed from Eq. 101 for $\omega = \omega_{log}$. T_c^{McM} is the McMillan critical temperature (Eq. 66) at $\mu^* = 0.1$; T_c^{AD} is the more accurate Allen-Dynes critical temperature (Eq. 70), also computed for $\mu^* = 0.1$.

	PdH	PH ₂	H ₃ S	LaH ₁₀	H
p (GPa)	0	120	200	300	500
N_{E_F} (eV ⁻¹ sp. ⁻¹)	0.014	0.021	0.019	0.016	0.011
$N_{E_F}^H$ (%)	5	55	45	50	100
ω_{log} (meV)	53	59	129	104	166
λ	0.4	1.0	1.6	2.2	1.63
I^2/M (eV ³ A ³)	0.08	0.16	1.46	1.48	4.30
T_c^{McM} (K)	2.6	48	182	183	237
T_c^{AD} (K)	2.7	53	214	234	282

linked together by P-P bonds, but no H-H bonds. Due to the relatively high concentration of hydrogen, H contributes around half of the electronic states at the Fermi level. However, the open 2D structure is very inefficient in terms of *e-p* coupling, and the Hopfield factor, although twice as large as in PdH, is almost one order of magnitude smaller than in the two other high-pressure hydrides, H₃S and LaH₁₀.

In the high- T_c phases of H₃S and LaH₁₀, the effect of megabar pressure on the crystal structure is dramatic. In both structures, hydrogen is embedded in a closely-packed metallic network, held together by strong covalent bonds. The superconducting properties are comparable to those of solid hydrogen. The COHP analysis shows that the states at E_F have essentially an antibonding character. In H₃S, where sulfur is incorporated in the hydrogen lattice, the dominant interaction is of S-H type, while in LaH₁₀ the geometry favors direct H-H interactions. One may argue that LaH₁₀, where only hydrogen is involved in covalent bonding, is a better realization of the Aschcroft-Ginzburg-Gilman concept than H₃S, and hence should exhibit a higher T_c . However, the presence of another atom involved in the bonding seems to be marginal in this sense. In both compounds, in fact hydrogen contributes roughly 50% of the total DOS at E_F and dominates the phonon spectrum. This yields very similar values for the Hopfield factor and ω_{log} . A $\sim 10\%$ difference in the superconducting properties comes from a better optimization of the phonon spectrum. Differences in T_c of this order can be easily be compensated by other effects, such as doping or pressure.

It is interesting to compare *e-p* coupling values of H₃S and LaH₁₀ with those of atomic hydrogen at 500 GPa –see Table 1. Indeed, in the latter, the Hopfield factor is about a factor of three larger, but since the shape of the phonon spectrum is not optimized and the electronic DOS is low, the superconducting properties do not improve appreciably. Significantly higher T_c is found in hydrogen only at much higher pressures, where the H lattice is denser and fully symmetric.

Our analysis confirms that many of the empirical parameters

that are used to identify promising hydrides, such as H-H distances and hydrogenic fraction, do not simply correlate with T_c . For instance, once hydrogen is embedded in a covalent metallic structure, T_c can only be predicted by a detailed analysis that takes into account all full aspects of electronic structure.

On one hand, this means that it is probably very hard, if not impossible, to formulate general rules. On the other hand, this implies that hydride superconductivity is of highly tunable nature: by acting on the bonding and on the density of charge carriers by doping, for example, it could be easy to optimize the superconducting properties within a given material class.

Rather than a set of precise rules, our analysis suggest a modern set of *necessary* conditions to maximize T_c in hydrides and similar materials:

- Electronic states originating from hydrogen or light-elements should cross the Fermi level.
- Hydrogen or light elements should form covalent bonds among them or with the host, preferably forming an extended (non-molecular) bonding structure.
- Phonon energies should be optimally tuned to the strength of this coupling: A stronger coupling requires higher energy phonon modes.

Arguably, the above requirements are likely to be fulfilled at extreme pressures, where thermodynamic conditions permit to stabilize structures in metallic phases. It could also be that expanding the search space to multinary hydrides or devising suitable thermodynamical conditions, one could overcome the issue of stabilizing these metallic phases at substantially lower pressures.

6. Discussion and Perspectives

Over the course of the last five years, we witnessed two practical realizations of conventional high- T_c , in H_3S (2015) and LaH_{10} (2018), both compositions stabilized at HP and with critical temperatures above 200 K. This hints to an imminent possibility of reaching room temperature (300 K) superconductivity in coming years. However, the main hindrance to any practical application of these materials is the high pressure needed to stabilize their crystal structure and stoichiometry. The main and most challenging question becomes: how can we lower pressure and retain high-temperature superconductivity? and ultimately how can we find a superconductor at *ambient conditions* of pressure and temperature?

In this section we will discuss possible strategies to realize these goals based on the present understanding of superconductivity and on currently available materials and synthesis techniques. In the first two parts (Sec. 6.1 and 6.2) we will maintain the focus on hydrides, which at the moment represent an excellent hunting ground for room temperature superconductivity and which we expect will continue to yield exciting results in the coming years. In the third part (Sec. 6.3) we will go beyond hydrides and briefly discuss a more general perspective involving other possible superconducting materials of conventional type.

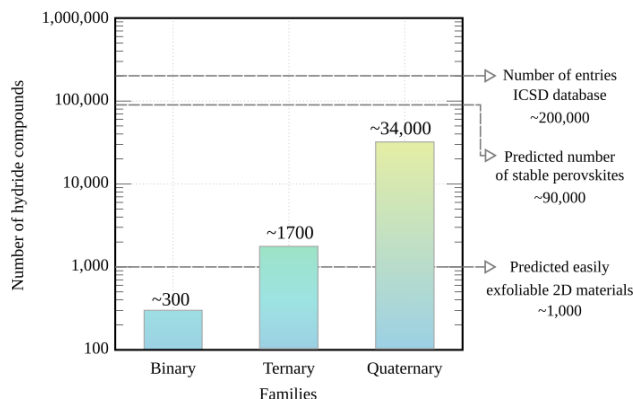


Figure 29: Rough estimates of the size of hydrides chemical space for different families. For comparison the number of entries in the Inorganic Crystal Structure Database (ICSD) is over 200,000 structures and the estimated chemical space for drug discovery spans to 10 millions (structures and compositions).

6.1. Chemical space of hydrides

The first question to ask is how big is the chemical abundance of hydrides, since the answer to this question may give an order of magnitude on the number of potential candidates for superconductivity. Let us start with binary hydrides (XH) which have been studied extensively. A reasonable estimate is to consider that for each element X, in a pressure range between 50 and 300 GPa at least five compositions would lie in the convex hull of stability. Assuming that 60 elements could form a stable hydride and show superconductivity (a generous estimate), this gives a safe upper limit of 300 binary hydrides that exist and are thermodynamically stable.

Providing an equally meaningful estimate for ternaries is quite difficult, because at the moment the available knowledge of the phase stability and energy landscape is very limited. As the number of elements increases, in fact, the number of possible configurations rapidly grows and at the same time, the number of channels for structural decomposition also increases. In addition, it is also plausible that the role of metastability will become more crucial, i.e. metastable phases will prone in some regions of the phase diagram, as decomposition paths will become more complex.

An extremely rough estimate can be obtained (at a single pressure) by a simple combinatorial argument: similarly to binaries, we assume that ternaries can be formed with 60 elements of the periodic table. At a single pressure, not considering alloying, the number of possible stable compounds is 1,770. However there is no sufficient data to estimate how many structures will be on the hull in the 50 to 300 GPa range. It is even harder to provide a good estimate for quaternary compounds, but the same analysis yields to 34,220 combinatorial compounds at a single pressure, ignoring alloying, metastability and configurational disorder. Clearly, the number of conceivable structures in complex hydrides is vast and grows even rapidly with the number of elements involved. Arguably, any experimental attempt without prior knowledge from computation/theory is bound to fail.

We report our estimated numbers in Fig. 29 where, to give

a perspective on the size of this chemical landscape, we compare them with other families of materials: *Perovskites*, one of the most versatile and chemically diverse family [465]. Currently there are approximately 2,000 compositions known, but the number of perovskites predicted to be stable is close to 90,000 [466, 467] at ambient pressure; Yet this number of accessible structures could potentially be much larger, especially if we include hybrid metal-organic perovskites under pressure [468]. *Two-dimensional* (2D) materials, have emerged as promising candidates for next-generation electronic applications. Although only a few dozens 2D materials have been successfully synthesized [469] or exfoliated [470], a recent study identified $\sim 1,000$ easily exfoliable compounds [471]. *Inorganic 3D lattices* as contained in the ICSD are above 200,000; The AFLOW database (<http://aflowlib.org/>) lists $\approx 1,600$ binary systems, $\approx 30,000$ ternaries and 150,000 quaternaries. The estimated chemical space for *drug discovery* is quantitatively of the order of several millions of structures and compositions [472].

6.2. Optimizing T_c and pressure in hydrides

Having observed that the hypothetical chemical space available in hydrides is ridiculously vast. Computational explorations are and will be at the forefront to help to navigate to promising directions. We now describe pragmatic strategies targeted at increasing T_c and reducing pressure to stabilize hydrides.

- **Selected Ternary phases:** Due to the vast chemical space available for ternary hydrides a systematic search can hardly be afforded and thus only few studies, in literature, explore selected phases and compositions on ternary hydrides. For example, one can focus on ternary compositions stable at ambient pressure or attempt for substitutions in binary hydride based on concepts as chemical substitubility [473, 340], or electronic structure arguments.

A good starting point is to consider ternary doping of existing high- T_c binary hydrides, as exploited by several authors which investigated different strategies of doping of H_3S . Heil and Boeri [474], studied *isovalent* substitution of sulfur in H_3S , with chalcogens (O, S, Se, Te) using the virtual crystal approximation to identify trends which would increase the T_c . They evidenced that isovalent substitution of sulfur with oxygen or selenium for example, modifies the superconducting properties by acting on the bonding rather than on the Fermi level position, which hints towards a general trend in hydrides under pressure. Recently (2018), Liu et al. [475] performed crystal structure prediction calculations at a fixed composition of $S_{0.5}Se_{0.5}H_3$ and found that the lowest enthalpy structures indeed correspond to different decorations of the cubic SH_3 lattice. Based on their electron-phonon calculations, the superconducting temperature decreases when S is replaced by Se, which the authors attribute to a decreasing strength of the covalent H-S or H-Se bonds. More recent calculation of thermodynamical stability of $H_3S_{1-x}Se_x$ compound by Amsler [326] revealed that, when stable the mixed S/Se compositions does not show improved superconducting properties.

A similar strategy applied in superhydrides, this time inspired by the discovery of LaH_{10} brought to the prediction

of superconductivity at 258 K in $CaYH_{12}$ under pressure [476, 477].

The renaissance of hydrides as energy materials could also have deep implications in the field of superconductivity. In fact, the field of energy materials is much more mature than high-pressure superconductivity and the phase diagram and thermodynamics of many hydrides at ambient pressure are known in great detail. This knowledge can be used in the near future to design new superconductors. Large families such as borohydrides, amides, alanates, gallates, transition metal-hydrides and possibly active materials for lithium-ion storage are potential candidates for high-pressure studies. The evolution of ternary hydrides as energy materials in a broader context was recently reviewed in an excellent work by Mohtadi-Orimo [478].

Two examples of high-pressure studies in hydrogen-storage materials are discussed by Kokail et al. [479], who studied lithium borohydrides, or the studies on H-O-N at high pressure [480, 481].

- **Doping under pressure:** The study of ternary phases discussed above still focuses on searching for thermodynamical stability, which however is a (likely) sufficient but not necessary condition for a material to be physically synthesizable and practically stable. One could abandon the pursuit for thermodynamic stability and directly address the search for long-lived metastable structures, especially if a synthesis path can be easily conceived. This is the case of doping into a stable crystal, inserting (substitutionally or interstitially) extra atoms, at low concentration.

An obvious starting point is to perform charge doping of existing metallic phases at high pressure through partial replacement of guest atoms. This can be used, for example, to optimally position the Fermi level in a region of high density of states, modify the shape of Fermi surfaces or promote structural or electronic phase transitions which increase the electron-phonon coupling. However, high-pressure doping presents inherent experimental difficulties and thus this possibility has been explored so far only by computational studies. For example, it has been shown that hole doping of H_3S with 6.25% of phosphorus at 200 GPa, increases T_c from 189 to 212 K [482] due to the positive effect of the van Hove singularity. On the other hand, electron doping achieved by 6.25% of chlorine doping, reduces T_c to 160 K but has a positive impact in the pressure, lowering the stabilization threshold for the $Im\bar{3}m$ phase. In a similar spirit, Ge et al. [483] proposed doping H_3S with elements from neighboring groups in the periodic table and concluded that a T_c as high as 280 K could be reached at 250 GPa in $S_{0.925}P_{0.075}H_3$. However, the stability of other phases on the ternary convex hull could hinder doping of binary phases, a still unexplored possibility.

A very promising way to use doping in searching for new superconducting hydrides is to induce metallicity in insulating crystals. It is well known that by introducing enough electron or hole-donating impurities one can render a semiconducting system metallic and even superconducting [484, 485, 486]. As a matter of fact the class of molecular crystals containing light elements like carbon and hydrogen is immense and full of potential. Following this idea, Flores-Livas et al. [487, 488]

studied H₂O and polyethylene, identifying promising substitution/dopant and showing that for realistic levels of doping at high pressure, these covalent phases may exhibit superconductivity with critical temperature of about 60 K at moderate pressures. In view of the vast number of hydrides that are covalent bonded but remain insulating up to rather large pressures, this venue represent a promising route for hunting high-T_c hydrides.

In spite of a few promising theoretical hints, this strategy of use doping at high pressure is at early stages of development both experimentally and computationally: Experimentally one faces with the problem that methods for doping under pressure have not being developed, thus it still remains a challenge in the field of semiconductors [489]. Computationally, one faces with the problem of accessing the "doping space" of materials which requires to apply systematic and well-converged protocols to scan for suitable dopants [490], establishing properties and stability of dopants. At zero pressure and for semiconducting systems accurate estimations [491, 492] can be obtained but are intrinsically difficult to compute.

- **Mechanical precompression: nanoscaffolds.**

Recently, Xia et al. [493] predicted that it is possible to obtain high-density hydrogen confining it in a (8,0) single-wall carbon nanotube. Their simulations showed evidence of metalization at moderate pressures. The so-called "physical compression effect", which together with chemical pre-compression, extends the possibilities to study materials at reduced pressures. Nanoscaffold structures such as nanotubes or fullerenes are ideal systems that could exert further pressure on tiny molecules confined at their interior. A word of caution, is of course that the stability of nano-scale systems and encapsulation of molecules may be experimentally very challenging.

- **Non-hydrostatic pressure:** Although non-hydrostatic conditions are preferably avoided in high pressure experiments, if controlled, these effects may represent a promising route to tune electronic and vibrational properties in hydrides. However, controlling hydrostatic conditions experimentally is very challenging: while it is known that the lack of pressure-transmitting medium in the region of 100-200 GPa seems to lead to conditions of inhomogeneous pressure, it is very hard to control in a reproducible manner. In fact, non-hydrostatic conditions is highly material, and sample preparation dependent [494].

A recent computational work by Liu et al. [495] attempted to examine the effect of non-hydrostatic strain modulation in H₃S. This paper pointed out that applied strain can effectively modify electronic energy levels and the lattice vibrations, thereby exerting sensitive control over T_c.

Another attractive possibility is to use non-hydrostatic conditions to access metastable phases. This offers a unique possibility to enhance the electronic structure and consequently superconductivity of materials under pressure. For example, in the recent work on LaH_x non-hydrostaticity seem to play a role in favoring some metastable compositions and structures [3].

- **Metastability:** An ample number of examples have been recently reported, in which metastability adds an extra dimension in the phase diagram of several systems: elemental phosphorus [74]; barium [91] and gallium under pressure [496]; tin-nitrides under pressure [497]; PdH [442]; PH₂ [168]; LaH_x [3,

181]; metastable charge-density-wave superconductors [498] as well as oxides [499, 500]. These works showed that controlled heating and cooling cycles or pressure-hysteresis cycles permit to selectively stabilize different metastable phases.

It is likely that at least some of the high-T_c phases observed in high-pressure hydrides are also metastable at lower pressures. Refining the experimental techniques that control the pressure-hysteresis cycles may hopefully allow, in near future, to stabilize some of the *inaccessible* high-T_c phases at moderate pressures.

6.3. Searches on other superconductors

Presently the main candidate materials for room temperature and pressure superconductivity are unconventional superconductors such as cuprates or iron pnictides, which currently hold the record for the highest T_c at zero pressure. These are still heavily investigated and keep giving surprises. However, a clear advantage of the field of conventional superconductors is that theory/computational methods can help and guide the experimental discovery. The same is hardly transferred to exotic pairing superconductors where a bridging between methods is still under development and *ab initio* computational approaches are extremely challenging [238].

Listed below, we address what we believe are the most promising strategies that are/can be followed in searching for new superconducting materials, non necessarily restricted to hydrides nor to conventional superconductivity. Yet some of these strategies still may benefit of the use of light elements, where the same arguments as discussed for hydrogen (low mass and strong covalent bonding) also hold.

- **Reduced dimensionality: synthetic materials.** A modern achievement in condensed matter research is the design of materials at the atomic scale by means of techniques such as controlled sputtering deposition [501], growth of hetero-structures atom-by-atom, exfoliation and strain engineering with molecular beam epitaxy [502]. These methods allow to create completely artificial materials (FeSe/FeTe on graphene, STO) in which is possible to induce or tune superconductivity [503]. The realization of low-dimension 1D/2D metallic structures with light covalent bonded elements (carbon, boron, nitrogen, etc...) represents an attractive possibility to discover high-T_c superconductors at ambient pressure. Nonetheless, conceptually these approaches are orthogonal to those used at high pressure, where very little can be controlled and synthesis is dictated unwittingly by thermodynamic conditions.

Interestingly one of the most interesting predictions that have been made within this class is that of doped graphane [504] the hydrogenated graphite (see below), indicating that hydrogen can be a main player searching for superconducting low dimensional materials. Along the same line, the prediction of a superconducting phase in lithium doped graphene[505] and its subsequent experimental confirmation[506], further testify the accuracy of first-principles computational methods for superconductivity.

- **Indirect role of hydrogen:** Due to its strong ionic potential and high mobility, it is difficult for hydrogen at ambient

pressure to be stable in any other chemical configuration than a fully saturated covalent bond. However, due to its small atomic size it may be incorporated into existing materials and act indirectly to induce superconductivity. This is for example what is seen in the case of palladium hydride, where hydrogen improves the superconducting properties of elemental palladium suppressing spin fluctuations [507]. This approach, may not fully benefit from low-mass/high-phonon frequency argument, however, may be key to high temperature conventional superconductivity. This is particularly evident in the prediction of high- T_c in doped graphane, where hydrogen saturates π states of graphene and in turn a non-negligible electron-phonon coupling arises promoting states with large e - p coupling close to the Fermi level. When hole doped, superconductivity has been predicted to occur as high as 100 K [508]. Combining these ideas and using MgB_2 monolayer as template material, Bekaert et al. [509] report an increased critical temperature in MgB_2 of up to 67 K.

- **Chemical doping:** Charge doping by means of alkali metal incorporation had led to the discovery of a superconducting phase in fullerenes (C_{60}) [510] for which the current record is 40 K in Cs_3C_{60} . Endohedral doping of the cages is often regarded as the most efficient approach to induce superconductivity, but exohedral doping of fullerenes could also be an attractive alternative [511]. In the same spirit, stable cages of sodalite-type structure have shown the possibility to be doped with elements of the V, VI, and VII columns of the periodic table [512]. More recently theoretical calculation have also shown the possibility to induce superconductivity in doped cages of ZnO [513]. Doping graphite layers leads to the discovery of intercalated graphite superconductors, notably CaC_6 [514]. Since 2010, alkali metal intercalation in polycyclic aromatic hydrocarbons (PAH), has been investigated and guided to promising results. Another example of intercalated systems showing superconductivity are layered binary silicides [515], where it has been show through a high-pressure synthesis procedure, the stabilization of metastable sheets of silicon that lead to an enhancement of almost 30% in T_c [516]. Estimates of superconductivity in the high-doping limit were given for generic families of intercalated group-IV honeycomb structures [517]. Other examples include potassium-doping of polycyclic aromatic hydrocarbons molecular crystals like picene [518], phenanthrene [519], dibenzopentacene [520] and terphenyl [521, 522], which have been reported to exhibit critical temperature as high as 100 K [521, 522].

- **Doping by field-effect:** Modern techniques based on liquid electrolytes permit to achieve doping levels as high as 10^{15} carriers/ cm^3 , corresponding to tenths of electrons, roughly three orders of magnitude larger than standard solid-state techniques. At the same time, field gating does not act by simply charging the system but, due to the intense fields involved, it can also lead to permanent or long-lived chemical or structural transformations in the region near to the surface of 2D systems. A very interesting possibility to speculate is that since electrolytes are usually hydrogen or light-elements, field gating may induce a sizable migration of H^+ ions onto the gated system, leading to a metallic transition and possibly to superconductivity.

Such an insulator-to-metal transition has been unequivocally seen in hydrogen-doped WO_3 [523], for which there were reported claims of induced superconductivity at 120 K [524].

Moreover, the possibility to induce surface metallic states in insulators by means of an intense electric field and turn two dimensional materials into superconductors [525] have opened a new avenue of research. The successful synthesis of a plethora of two-dimensional systems over the last years such as transition metal dichalcogenides [526], layered transition metal oxides [527, 528], hexagonal-boron nitride [529], topological insulators [530], 2D-cuprates [531], ferromagnetic 2D systems [532], phosphorene [533], bismuthene[534], silicene, germanene [535, 536] and borophene [537] have fuelled the field opening the possibility to investigate doping and induced superconductivity in a large array of different systems.

6.4. Theoretical and experimental outlook

As discussed in Sec. 6.2, there is still a long path to walk on conventional superconductors. Specifically on hydrides under pressure, we have show how computational methods help and guide experimental search to undercover novel conventional superconductors.

Yet, there are several theoretical aspects and computational flaws that are left for future development. Before concluding we would like to point out some (not ordered by importance):

Theoretically: I) the Coulomb interaction is often treated within a crude Morel-Anderson approximation, but this is not guaranteed to hold generally; II) Electronic self-energy corrections beyond the Migdal approximation are usually neglected but it has been proved to play a role in hydrogen-rich materials and generally for systems where phonon frequencies are large and the e - p interaction is sizable [538, 539]. III) Phononic non-adiabatic effects [540] and implications on superconductors are practically unknown;

IV) Non-linear electron-phonon and its repercussions on T_c , are largely overlooked.

V) Plasmon and polaron effects have been shown to play an important role for some materials under pressure but are usually disregarded.

VI) Currently there is not a KS-DFT functional constructed for the extreme compression limit and essentially all studies conducted so far rely on functionals derived/based on the standard electron-gas and tuned to reproduce ambient pressure properties.

VII) Phonon anharmonicity has been conclusively shown to be of tremendous importance, specifically at HP and for hydrogen rich materials [209]. Presently simulation requires an extreme computational cost and efficiency improvement in computational schemes, algorithms and implementations would be desirable.

Computationally most of the future research effort will certainly be directed towards automation and the inclusion of computational informatics (machine learning, artificial intelligence, etc). The automatic prediction of phase diagrams is a realistic goal to be reached within the next few years. In this context, the exploration of binary hydrides (computationally) is almost

completed and the next venue for searching are ternaries. Other aspects that have to be addressed by means of computations are reaction paths between structures and stoichiometries, rare events and nucleation [541] are practically unexplored issues in hydrides under pressure.

Experimentally, the future in high pressure foresees many more developments, as mentioned before in two fronts: first, focus ion beam techniques will play a fundamental role in DACs, sculpting futuristic micro-anvils that will extend the range of pressure well above the 400 GPa (the ceiling pressure for one-stage DAC) and second, thanks to the advancement in new X-ray sources (synchrotron and X-ray free electron laser) bringing down to sub-micro beams, brighter and more intense with shorted pulses, will enable the study compression volumes of only tens of picolitres. Another experimental areas of high pressure that will increase substantially in terms of research is the one related to magnetism at the megabar.

7. Conclusions

In this Review we offered an up-to-date perspective on the field of conventional superconductivity at high pressures. Recently, the field has been fueled by the experimental discovery of two record-breaking hydrides, H_3S (2015, 200 K) and LaH_{10} (2018, 250 K). These materials, which currently hold the record for the highest and second-highest T_c , are different in almost every respect from what would have been considered an ideal superconductor few years ago. They have a rather simple stoichiometry, highly-symmetric structures and are standard metals that obey a conventional mechanism for superconductivity. Given the extremely rapid progress over the last three years, it is a safe bet to predict that hydrides will be the first materials to achieve room temperature superconductivity (300 K) in coming years.

Hydrides, despite their apparent modesty when compared to more complex unconventional (cuprates, Fe-based, etc) superconductors, do possess one aspect which makes them unusual: these materials require pressures more than one million higher than ambient pressure in order to exist and superconduct. Currently, only a handful number of groups world-wide are able to perform the complex characterization needed to detect superconductivity at these pressures. It is important to realize, however, that this rather small number of groups able to perform these experiments should not be confused with how expensive or sophisticate the set-up are. Counter-intuitively, HP set-up such as diamond anvil cells are considerably more accessible than even the cheapest scanning electronic microscope or ultra-high-vacuum deposition chambers. In fact, many groups have access to commercial diamond anvil cells and can routinely reach megabar pressures. The difference resides in mastering of techniques needed to detect the properties of superconductors under pressure. The very specific set of skills and instruments have been developed only by a few groups through many years of involved experimentation.

Furthermore, the excitement produced by the discovery of warm-superconductors is only one aspect of the even more exciting paradigm shift that is taking place in material research.

The discovery of high- T_c superconductivity in hydrides is in fact a spectacular demonstration of the extraordinary symbiosis between experimental research, theoretical methods and computational tools that has taken place over the last years.

Currently, the main drawback of superconducting hydrides lies in the impossibility for any practical application, remaining (near future) at the level of basic research. Nevertheless, it is reasonable to expect that this field will increase considerable in size. This assure it will flourish to new endeavours, promising perhaps futuristic applications. To push this field forward, it is highly desirable to determine whether high-temperature conventional superconductivity can be extended to other hydrides which exist in the solid state and, in the long term, whether pressure can be drastically decreased. Indeed, the large portfolio of existing hydrides, which includes energy storage and active materials for lithiumion storage, contains many promising materials for achieving this task. Another route to explore and to find better superconductors is, that the same concepts and methods that lead to the discovery of high- T_c superconductivity in hydrides may be applied to other compounds.

In previous sections, we have reviewed the main aspects of the extraordinary machinery used to discover new materials under high pressure, which aided the ground-breaking discoveries of H_3S and LaH_{10} , and elucidated the underlying physics in these materials. We provided a fresh update on experimental techniques and reviewed the key points on the theoretical understanding of superconductors. Other important active areas of research and future direction are also discussed in this Review.

Finally, due to the rapid progress of the field, we are certain that some parts of the Review will become obsolete in a short time. Interestingly, over the last five years (2015-2019), the goal of superconducting research in hydrides has shifted from an unseeingly impossible room-temperature superconductivity to find ways to achieve the same phenomenon at ambient conditions, both of pressure and temperature. It is our hope, that the methodological framework described and commutable knowledge from experiments, theory and computation serve as a reference work and help to lead many more exciting discoveries in years to follow.

Acknowledgements: J.A.F.-L. acknowledges Stefan Goedecker for willingness to support and the NCCR MARVEL funded by the Swiss National Science Foundation. Computational resources from the Swiss National Supercomputing Center (CSCS) in Lugano are gratefully acknowledged. L.B. acknowledges support from Fondo Ateneo Sapienza 2017-18. R.A. was supported by a Grant-in-Aid for Scientific Research (No.16H06345) from Ministry of Education, Culture, Sports, Science and Technology, Japan. M.E. is thankful to the Max Planck community for the invaluable support, and U. Pöschl for the constant encouragement. Authors acknowledges the hospitality of the *cini-Sardegna* meeting where parts of this work were written.

Appendix

Periodic Tables: Information shown in the periodic table of superconducting elements (Fig. 1) has been collected from references [53, 54, 52, 55]. The following works refer to studies of binary hydrides under pressure for which some of the information was taken Fig. 21: Li [542], K [543], Fr [434], Be [544], Mg [545], Ca [176], Sr [546, 547] Ba [548], Ra [434], Sc [549], Y [182], La [182, 177], (Ce, Pr, Nd, Ho, Er, Tm, and Lu) [434], Ac [550], Th [551], Pa [434, 552], U [553], (Np, Cm) [434], (Ti,Zr,Hf) [434], V [554], Nb [555, 556], Ta [557], Cr [558], W [559], Tc [560], Ru [561], Os [562], (Rh,Ir) [563], Pd [440, 564], Pt [565, 566, 563, 567], Au [563], B [568], Al [569], Ga [570], In [571], Si [159, 572], Ge [573, 574, 575, 576, 577, 578, 573, 578], Sn [579], Pb [580], P [168, 449, 581, 582, 583], As [584], Sb [585], Bi [586], S [173], Se [173, 587], Te [588], Po [589], Br [590], I [591, 592], and Xe [593].

Definition of hydrides and superhydrides: Note, that the term hydride is an old concept and could have several definitions. For example, Gibb used it to describe a compound in which there is a metal-to-hydrogen bond. Along this Review we treated hydride simply as a combination of hydrogen and any other element. Under this definition, hydrides can be generally classified into four categories based on the nature of their hydrogen bonding: ionic or saline (i.e., hydrides of alkali and alkaline earth metals), covalent or volatile (i.e., hydrides of group IIIA–VIIA elements), metallic (i.e., hydrides of transition metals), or vdW (i.e., hydrides of rare gas elements). It is clear that this classification does not offer a complete vision of hydrides as the nature of the hydrogen bond can be significantly altered by pressure. As such, for simplicity in the construction of periodic tables (Fig. 21 and Fig. 1) we omit the naming of compounds accordingly to chemistry conventions. For example note that in the periodic table H_3S appears as SH_3 . It also neglects further distinctions such as superhydrides, which have unusually high hydrogen contents (e.g., LaH_{10}).

Statistics on publications: In order to track the number of publications on the field (see Fig. 2) we used GOOGLE SCHOLAR engine together with searches and key words such as –hydrides– followed by filtering options with –superconducting– over the selected period of time. Needless to mention that these numbers are approximate and that can vary over time, specially on decades when hydrides started to be explored on other domains such energy materials.

References

- [1] A. P. Drozdov, M. I. Erements, I. A. Troyan, V. Ksenofontov, S. I. Shylin, Conventional superconductivity at 203 kelvin at high pressures in the sulfur hydride system, *Nature* 525 (2015) 2015/08/17/online. doi:doi:10.1038/nature14964.
- [2] A. P. Drozdov, P. Kong, et al. **UPDATE**, Superconductivity at 250 k in lanthanum hydride under high pressures, *Nature*.
- [3] M. Somayazulu, M. Ahart, A. K. Mishra, Z. M. Geballe, M. Baldini, Y. Meng, V. V. Struzhkin, R. J. Hemley, Evidence for superconductivity above 260 k in lanthanum superhydride at megabar pressures, *Phys. Rev. Lett.* 122 (2019) 027001. doi:10.1103/PhysRevLett.122.027001. URL <https://link.aps.org/doi/10.1103/PhysRevLett.122.027001>
- [4] V. L. Ginzburg, What problems of physics and astrophysics seem now to be especially important and interesting (thirty years later, already on the verge of xxi century)?, *Physics-Uspekhi* 42 (4) (1999) 353.
- [5] K. N. Mukhin, A. F. Sustavov, V. N. Tikhonov, On the centenary of the nobel prize: Russian laureates in physics, *Physics-Uspekhi* 46 (5) (2003) 493.
- [6] E. Wigner, H. á. Huntington, On the possibility of a metallic modification of hydrogen, *The Journal of Chemical Physics* 3 (12) (1935) 764–770.
- [7] N. Ashcroft, Metallic hydrogen: A high-temperature superconductor?, *Phys. Rev. Lett.* 21 (1968) 1748–1749. doi:10.1103/PhysRevLett.21.1748. URL <http://link.aps.org/doi/10.1103/PhysRevLett.21.1748>
- [8] V. L. Ginzburg, Superfluidity and superconductivity in the universe, *Journal of Statistical Physics* 1 (1) (1969) 3–24.
- [9] R. P. Dias, I. F. Silvera, Observation of the wigner-huntington transition to metallic hydrogen, *Science* doi:10.1126/science.aal1579.
- [10] J. M. McMahon, M. A. Morales, C. Pierleoni, D. M. Ceperley, The properties of hydrogen and helium under extreme conditions, *Reviews of modern physics* 84 (4) (2012) 1607.
- [11] B. Militzer, F. Soubiran, S. M. Wahl, W. Hubbard, Understanding jupiter's interior, *Journal of Geophysical Research: Planets* 121 (9) (2016) 1552–1572. arXiv:<https://agupubs.onlinelibrary.wiley.com/doi/pdf/10.1002/2016JE005080>, doi:10.1002/2016JE005080. URL <https://agupubs.onlinelibrary.wiley.com/doi/abs/10.1002/2016JE005080>
- [12] N. W. Ashcroft, Hydrogen dominant metallic alloys: High temperature superconductors?, *Phys. Rev. Lett.* 92 (2004) 187002. doi:10.1103/PhysRevLett.92.187002. URL <http://link.aps.org/doi/10.1103/PhysRevLett.92.187002>
- [13] J. J. Gilman, Lithium dihydrogen fluoride—an approach to metallic hydrogen, *Phys. Rev. Lett.* 26 (1971) 546–548. doi:10.1103/PhysRevLett.26.546. URL <https://link.aps.org/doi/10.1103/PhysRevLett.26.546>
- [14] D. Alfè, M. Gillan, G. Price, Composition and temperature of the earths core constrained by combining ab initio calculations and seismic data, *Earth and Planetary Science Letters* 195 (1-2) (2002) 91–98.
- [15] A. Molodets, Scaling law for high pressure isotherms of solids, *High Pressure Research* 25 (4) (2005) 267–276.
- [16] P. Loubeyre, R. LeToullec, D. Hausermann, M. Hanfland, R. Hemley, H. Mao, L. Finger, X-ray diffraction and equation of state of hydrogen at megabar pressures, *Nature* 383 (6602) (1996) 702.
- [17] R. J. Hemley, Effects of high pressure on molecules, *Annual Review of Physical Chemistry* 51 (1) (2000) 763–800.
- [18] A. Hermann, Chemical bonding at high pressure, *Reviews in Computational Chemistry* 30 (2017) 1–41.
- [19] C.-S. Yoo, Physical and chemical transformations of highly compressed carbon dioxide at bond energies, *Physical Chemistry Chemical Physics* 15 (21) (2013) 7949–7966.
- [20] H. K. Onnes, Further experiments with liquid helium. h. on the electrical resistance of pure metals etc. vii. the potential difference necessary for the electric current through mercury below 4 19k, in: *KNAW, Proceedings*, Vol. 15, 1913, pp. 1406–1430.

- [21] B. T. Matthias, T. H. Geballe, R. H. Willens, E. Corenzwit, G. W. Hull, Superconductivity of Nb_3Ge , *Phys. Rev.* 139 (1965) A1501–A1503. doi:10.1103/PhysRev.139.A1501. URL <https://link.aps.org/doi/10.1103/PhysRev.139.A1501>
- [22] M. Cohen, P. Anderson, Superconductivity in d - and f - band Metals, American Inst. of Physics, 1972.
- [23] J. Nagamatsu, N. Nakagawa, T. Muranaka, Y. Zenitani, J. Akimitsu, Superconductivity at 39 K in magnesium diboride, *Nature (London)* 410 (2001) 63.
- [24] A. Schilling, M. Cantoni, J. D. Guo, H. R. Ott, Superconductivity above 130 K in the Hg-Ba-Ca-Cu-O system, *Nature* 363 (6424) (1993) 56–58. doi:10.1038/363056a0. URL <https://doi.org/10.1038/363056a0>
- [25] Y. Kamihara, H. Hiramatsu, M. Hirano, R. Kawamura, H. Yanagi, T. Kamiya, H. Hosono, Iron-based layered superconductor: LaOFeP , *Journal of the American Chemical Society* 128 (31) (2006) 10012–10013. doi:10.1021/ja063355c. URL <https://doi.org/10.1021/ja063355c>
- [26] Y. Kamihara, T. Watanabe, M. Hirano, H. Hosono, Iron-based layered superconductor LaOFeAs , *Journal of the American Chemical Society* 130 (11) (2008) 32963297. doi:10.1021/ja800073m. URL <http://dx.doi.org/10.1021/ja800073m>
- [27] B. Matthias, Chapter v superconductivity in the periodic system, in: *Progress in low temperature physics*, Vol. 2, Elsevier, 1957, pp. 138–150.
- [28] S. Y. Savrasov, D. Y. Savrasov, Electron-phonon interactions and related physical properties of metals from linear-response theory, *Phys. Rev. B* 54 (1996) 16487.
- [29] T. H. Geballe, The never-ending search for high-temperature superconductivity, *Journal of superconductivity and novel magnetism* 19 (3–5) (2006) 261–276.
- [30] J. Bardeen, L. N. Cooper, J. R. Schrieffer, Theory of superconductivity, *Phys. Rev.* 108 (1957) 1175–1204. doi:10.1103/PhysRev.108.1175. URL <http://link.aps.org/doi/10.1103/PhysRev.108.1175>
- [31] G. Eliashberg, Eliashberg Equations of Strong Coupling Theory, *Teor. Fiz* 38, 966 (1960)[*Sov. Phys. FETP* 38].
- [32] L. N. Oliveira, E. K. U. Gross, W. Kohn, Density-functional theory for superconductors, *Phys. Rev. Lett.* 60 (1988) 2430–2433. doi:10.1103/PhysRevLett.60.2430. URL <http://link.aps.org/doi/10.1103/PhysRevLett.60.2430>
- [33] M. Lüdgers, M. A. L. Marques, N. N. Lathiotakis, A. Floris, G. Profeta, L. Fast, A. Continenza, S. Massidda, E. K. U. Gross, Ab initio theory of superconductivity. i. density functional formalism and approximate functionals, *Phys. Rev. B* 72 (2005) 024545. doi:10.1103/PhysRevB.72.024545. URL <http://link.aps.org/doi/10.1103/PhysRevB.72.024545>
- [34] M. A. L. Marques, M. Lüdgers, N. N. Lathiotakis, G. Profeta, A. Floris, L. Fast, A. Continenza, E. K. U. Gross, S. Massidda, Ab initio theory of superconductivity. ii. application to elemental metals, *Phys. Rev. B* 72 (2005) 024546. doi:10.1103/PhysRevB.72.024546. URL <http://link.aps.org/doi/10.1103/PhysRevB.72.024546>
- [35] J. M. An, W. E. Pickett, Superconductivity of MgB_2 : Covalent bonds driven metallic, *Phys. Rev. Lett.* 86 (2001) 4366–4369. doi:10.1103/PhysRevLett.86.4366. URL <http://link.aps.org/doi/10.1103/PhysRevLett.86.4366>
- [36] M. I. Erements, I. A. Trojan, S. A. Medvedev, J. S. Tse, Y. Yao, Superconductivity in hydrogen dominant materials: Silane, *Science* 319 (5869) (2008) 1506–1509. arXiv:<http://science.sciencemag.org/content/319/5869/1506.full.pdf>, doi:10.1126/science.1153282. URL <http://science.sciencemag.org/content/319/5869/1506>
- [37] J. Maddox, Crystals from first principles, *Nature* 335 (6187) (1988) 201.
- [38] J. G. Bednorz, K. A. Müller, Possible high T_c superconductivity in the BaLaCuO system, *Zeitschrift für Physik B Condensed Matter* 64 (189–193). doi:10.1007/BF01303701.
- [39] A. Oganovich, C. Pickard, Q. Zhu, R. Needs, Structure prediction drives materials discovery, *Nature Reviews Materials* X (X) (2019) XX–XX.
- [40] D. Duan, H. Yu, H. Xie, T. Cui, Ab initio approach and its impact on superconductivity, *Journal of Superconductivity and Novel Magnetism* 32 (1) (2019) 53–60.
- [41] H. Wang, X. Li, G. Gao, Y. Li, Y. Ma, Hydrogen-rich superconductors at high pressures, *Wiley Interdisciplinary Reviews: Computational Molecular Science* 8 (1) (2018) e1330.
- [42] L. Zhang, Y. Wang, J. Lv, Y. Ma, Materials discovery at high pressures, *Nature Reviews Materials* 2 (4) (2017) 17005.
- [43] Y. Wang, Y. Ma, Perspective: Crystal structure prediction at high pressures, *The Journal of chemical physics* 140 (4) (2014) 040901.
- [44] T. Bi, N. Zarifi, T. Terpstra, E. Zurek, The search for superconductivity in high pressure hydrides, arXiv preprint arXiv:1806.00163.
- [45] L. P. Gor'kov, V. Z. Kresin, Colloquium: High pressure and road to room temperature superconductivity, *Rev. Mod. Phys.* 90 (2018) 011001. doi:10.1103/RevModPhys.90.011001. URL <https://link.aps.org/doi/10.1103/RevModPhys.90.011001>
- [46] P. W. Bridgman, The way things are, *The Nobel Prize in Physics* 1946 – (–) (1946) –.
- [47] C. Weir, E. Lippincott, A. Van Valkenburg, E. Bunting, Infrared studies in the 1-to 15-micron region to 30,000 atmospheres, *J. Res. Natl. Bur. Stand. A* 63 (1959) 55–62.
- [48] R. M. Hazen, The new alchemists: Breaking through the barriers of high pressure, Crown Publishing Group (NY), 1993.
- [49] H. Mao, High-pressure physics: sustained static generation of 1.36 to 1.72 megabars, *Science* 200 (4346) (1978) 1145–1147.
- [50] W. J. Nellis, *Ultracondensed matter by dynamic compression*, Cambridge University Press, 2017.
- [51] T. Dornheim, S. Groth, M. Bonitz, The uniform electron gas at warm dense matter conditions, *Physics Reports*.
- [52] J. Hamlin, Superconductivity in the metallic elements at high pressures, *Physica C: Superconductivity and its Applications* 514 (2015) 59 – 76, superconducting Materials: Conventional, Unconventional and Undetermined. doi:<https://doi.org/10.1016/j.physc.2015.02.032>. URL <http://www.sciencedirect.com/science/article/pii/S0921453415000593>
- [53] C. Buzza, K. Robbie, Assembling the puzzle of superconducting elements: a review, *Superconductor Science and Technology* 18 (1) (2004) R1.
- [54] K. Shimizu, K. Amaya, N. Suzuki, Pressure-induced superconductivity in elemental materials, *Journal of the Physical Society of Japan* 74 (5) (2005) 1345–1357. arXiv:<http://dx.doi.org/10.1143/JPSJ.74.1345>, doi:10.1143/JPSJ.74.1345. URL <http://dx.doi.org/10.1143/JPSJ.74.1345>
- [55] K. Shimizu, Superconductivity from insulating elements under high pressure, *Physica C: Superconductivity and its Applications* 514 (2015) 46–49.
- [56] Y. Akahama, H. Kawamura, D. Häusermann, M. Hanfland, O. Shimomura, New high-pressure structural transition of oxygen at 96 gpa associated with metallization in a molecular solid, *Physical review letters* 74 (23) (1995) 4690.
- [57] K. Shimizu, K. Suhara, M. Ikumo, M. Erements, K. Amaya, Superconductivity in oxygen, *Nature* 393 (6687) (1998) 767.
- [58] J. S. Schilling, Superconductivity in the alkali metals, *High Pressure Research* 26 (3) (2006) 145–163.
- [59] J. Wittig, Pressure-induced superconductivity in cesium and yttrium, *Physical Review Letters* 24 (15) (1970) 812.
- [60] J. Neaton, N. Ashcroft, Pairing in dense lithium, *Nature* 400 (6740) (1999) 141.
- [61] K. Shimizu, H. Ishikawa, D. Takao, T. Yagi, K. Amaya, Superconductivity in compressed lithium at 20 K, *Nature* 419 (6907) (2002) 597–599.
- [62] S. Deemyad, J. S. Schilling, Superconducting phase diagram of Li metal in nearly hydrostatic pressures up to 67 GPa, *Physical review letters* 91 (16) (2003) 167001.
- [63] V. V. Struzhkin, M. I. Erements, W. Gan, H.-k. Mao, R. J. Hemley, Superconductivity in dense lithium, *Science* 298 (5596) (2002) 1213–1215.
- [64] J. Tuoriniemi, K. Juntunen-Nurmilaikas, J. Uusvuori, E. Pentti, A. Salmela, A. Sebedash, Superconductivity in lithium below 0.4 mil-

- likelvin at ambient pressure, *Nature* 447 (7141) (2007) 187.
- [65] L. Lundegaard, E. Gregoryanz, M. McMahon, C. Guillaume, I. Loa, R. Nelves, Single-crystal studies of incommensurate na to 1.5 mbar, *Physical Review B* 79 (6) (2009) 064105.
- [66] E. Gregoryanz, O. Degtyareva, M. Somayazulu, R. J. Hemley, H.-k. Mao, Melting of dense sodium, *Physical review letters* 94 (18) (2005) 185502.
- [67] C. Richardson, N. Ashcroft, Effective electron-electron interactions and the theory of superconductivity, *Physical Review B* 55 (22) (1997) 15130.
- [68] M. I. Eremets, V. V. Struzhkin, H.-k. Mao, R. J. Hemley, Superconductivity in boron, *Science* 293 (5528) (2001) 272–274.
- [69] M. Sakata, Y. Nakamoto, K. Shimizu, T. Matsuoka, Y. Ohishi, Superconducting state of ca-vii below a critical temperature of 29 k at a pressure of 216 gpa, *Physical Review B* 83 (22) (2011) 220512.
- [70] H. Fujihisa, Y. Nakamoto, M. Sakata, K. Shimizu, T. Matsuoka, Y. Ohishi, H. Yamawaki, S. Takeya, Y. Gotoh, Ca-vii: A chain ordered host-guest structure of calcium above 210 gpa, *Phys. Rev. Lett.* 110 (2013) 235501. doi:10.1103/PhysRevLett.110.235501. URL <https://link.aps.org/doi/10.1103/PhysRevLett.110.235501>
- [71] J. Hamlin, V. Tissen, J. Schilling, Superconductivity at 17 k in yttrium metal under nearly hydrostatic pressures up to 89 gpa, *Physical Review B* 73 (9) (2006) 094522.
- [72] H. Kawamura, I. Shirokuni, K. Tachikawa, Anomalous superconductivity and pressure induced phase transitions in black phosphorus, *Solid state communications* 54 (9) (1985) 775–778.
- [73] M. Karuzawa, M. Ishizuka, S. Endo, The pressure effect on the superconducting transition temperature of black phosphorus, *Journal of Physics: Condensed Matter* 14 (44) (2002) 10759.
- [74] J. A. Flores-Livas, A. Sanna, A. P. Drozdov, L. Boeri, G. Profeta, M. Eremets, S. Goedecker, Interplay between structure and superconductivity: Metastable phases of phosphorus under pressure, *Physical Review Materials* 1 (2) (2017) 024802.
- [75] Y. Akahama, M. Kobayashi, H. Kawamura, Simple-cubic-simple-hexagonal transition in phosphorus under pressure, *Phys. Rev. B* 59 (1999) 8520–8525. doi:10.1103/PhysRevB.59.8520. URL <http://link.aps.org/doi/10.1103/PhysRevB.59.8520>
- [76] T. Ishikawa, H. Nagara, K. Kusakabe, N. Suzuki, Determining the structure of phosphorus in phase iv, *Phys. Rev. Lett.* 96 (2006) 095502. doi:10.1103/PhysRevLett.96.095502. URL <http://link.aps.org/doi/10.1103/PhysRevLett.96.095502>
- [77] H. Fujihisa, Y. Akahama, H. Kawamura, Y. Ohishi, Y. Gotoh, H. Yamawaki, M. Sakashita, S. Takeya, K. Honda, Incommensurate structure of phosphorus phase iv, *Phys. Rev. Lett.* 98 (2007) 175501. doi:10.1103/PhysRevLett.98.175501. URL <http://link.aps.org/doi/10.1103/PhysRevLett.98.175501>
- [78] M. Marqués, G. J. Ackland, L. F. Lundegaard, S. Falconi, C. Hejny, M. I. McMahon, J. Contreras-García, M. Hanfland, Origin of incommensurate modulations in the high-pressure phosphorus iv phase, *Phys. Rev. B* 78 (2008) 054120. doi:10.1103/PhysRevB.78.054120. URL <http://link.aps.org/doi/10.1103/PhysRevB.78.054120>
- [79] H. Katze, P. Tolédano, Displacive mechanisms and order-parameter symmetries for the a7-incommensurate-bcc sequences of high-pressure reconstructive phase transitions in group va elements, *Phys. Rev. B* 77 (2008) 024109. doi:10.1103/PhysRevB.77.024109. URL <http://link.aps.org/doi/10.1103/PhysRevB.77.024109>
- [80] T. Sugimoto, Y. Akahama, H. Fujihisa, Y. Ozawa, H. Fukui, N. Hirao, Y. Ohishi, Identification of superlattice structure *cil6* in the p-vi phase of phosphorus at 340 gpa and room temperature via x-ray diffraction, *Phys. Rev. B* 86 (2012) 024109. doi:10.1103/PhysRevB.86.024109. URL <http://link.aps.org/doi/10.1103/PhysRevB.86.024109>
- [81] E. Gregoryanz, V. V. Struzhkin, R. J. Hemley, M. I. Eremets, H.-k. Mao, Y. A. Timofeev, Superconductivity in the chalcogens up to multimegabar pressures, *Physical Review B* 65 (6) (2002) 064504.
- [82] Y. Akahama, M. Kobayashi, H. Kawamura, Structural studies of pressure-induced phase transitions in selenium up to 150 gpa, *Phys. Rev. B* 47 (1993) 20–26. doi:10.1103/PhysRevB.47.20. URL <http://link.aps.org/doi/10.1103/PhysRevB.47.20>
- [83] Y. Akahama, M. Kobayashi, H. Kawamura, Pressure-induced structural phase transition in sulfur at 83 gpa, *Phys. Rev. B* 48 (1993) 6862–6864. doi:10.1103/PhysRevB.48.6862. URL <http://link.aps.org/doi/10.1103/PhysRevB.48.6862>
- [84] V. V. Struzhkin, R. J. Hemley, H.-k. Mao, Y. A. Timofeev, Superconductivity at 10–17 k in compressed sulphur, *Nature* 390 (6658) (1997) 382–384.
- [85] Y. Akahama, M. Kobayashi, H. Kawamura, Pressure-induced metallization and structural transition of α -monoclinic and amorphous se, *Phys. Rev. B* 56 (1997) 5027–5031. doi:10.1103/PhysRevB.56.5027. URL <http://link.aps.org/doi/10.1103/PhysRevB.56.5027>
- [86] S. Kometani, M. I. Eremets, K. Shimizu, M. Kobayashi, K. Amaya, Observation of pressure-induced superconductivity of sulfur, *Journal of the Physical Society of Japan* 66 (9) (1997) 2564–2565.
- [87] W. L. Mao, H.-k. Mao, P. J. Eng, T. P. Trainor, M. Newville, C.-c. Kao, D. L. Heinz, J. Shu, Y. Meng, R. J. Hemley, Bonding changes in compressed superhard graphite, *Science* 302 (5644) (2003) 425–427.
- [88] M. Amsler, J. A. Flores-Livas, L. Lehtovaara, F. Balima, S. A. Ghasemi, D. Machon, S. Pailhes, A. Willand, D. Caliste, S. Botti, et al., Crystal structure of cold compressed graphite, *Physical review letters* 108 (6) (2012) 065501.
- [89] U. Schwarz, A. Grzechnik, K. Syassen, I. Loa, M. Hanfland, Rubidium-iv: A high pressure phase with complex crystal structure, *Phys. Rev. Lett.* 83 (1999) 4085–4088. doi:10.1103/PhysRevLett.83.4085. URL <https://link.aps.org/doi/10.1103/PhysRevLett.83.4085>
- [90] F. J. H. Ehlers, N. E. Christensen, Phosphorus under pressure: Ba-iv-type structure as a candidate for p-iv, *Phys. Rev. B* 69 (2004) 214112. doi:10.1103/PhysRevB.69.214112. URL <http://link.aps.org/doi/10.1103/PhysRevB.69.214112>
- [91] D. E. Jackson, D. VanGennep, Y. K. Vohra, S. T. Weir, J. J. Hamlin, Superconductivity of barium-vi synthesized via compression at low temperatures, *Phys. Rev. B* 96 (2017) 184514. doi:10.1103/PhysRevB.96.184514. URL <https://link.aps.org/doi/10.1103/PhysRevB.96.184514>
- [92] Y. K. Vohra, S. J. Duclos, A. L. Ruoff, High-pressure x-ray diffraction studies on rhenium up to 216 gpa (2.16 mbar), *Phys. Rev. B* 36 (1987) 9790–9792. doi:10.1103/PhysRevB.36.9790. URL <https://link.aps.org/doi/10.1103/PhysRevB.36.9790>
- [93] W. Holzappel, Physics of solids under strong compression, *Reports on Progress in Physics* 59 (1) (1996) 29.
- [94] E. Y. Tonkov, E. Ponyatovsky, Phase transformations of elements under high pressure, CRC press, 2004.
- [95] A. Jayaraman, Diamond anvil cell and high-pressure physical investigations, *Reviews of Modern Physics* 55 (1) (1983) 65.
- [96] W. A. Bassett, Diamond anvil cell, 50th birthday, *High Pressure Research* 29 (2) (2009) 163–186.
- [97] X. Wang, K. Kamenev, Review of modern instrumentation for magnetic measurements at high pressure and low temperature, *Low Temperature Physics* 40 (8) (2014) 735–746.
- [98] G. Shen, H. K. Mao, High-pressure studies with x-rays using diamond anvil cells, *Reports on Progress in Physics* 80 (1) (2016) 016101.
- [99] P. F. McMillan, Pressing on: the legacy of percy w. bridgman, *Nature materials* 4 (10) (2005) 715.
- [100] H.-K. Mao, X.-J. Chen, Y. Ding, B. Li, L. Wang, Solids, liquids, and gases under high pressure, *Reviews of Modern Physics* 90 (1) (2018) 015007.
- [101] A. F. Goncharov, Raman spectroscopy at high pressures, *International Journal of Spectroscopy* 2012.
- [102] A. F. Goncharov, J. A. Montoya, N. Subramanian, V. V. Struzhkin, A. Kolesnikov, M. Somayazulu, R. J. Hemley, Laser heating in diamond anvil cells: developments in pulsed and continuous techniques, *Journal of synchrotron radiation* 16 (6) (2009) 769–772.
- [103] T. Meier, At its extremes: Nmr at giga-pascal pressures, in: *Annual Reports on NMR Spectroscopy*, Vol. 93, Elsevier, 2018, pp. 1–74.
- [104] T. Meier, N. Wang, D. Mager, J. G. Korvink, S. Petitgirard, L. Dubrovinn

- sky, Magnetic flux tailoring through lenz lenses for ultrasmall samples: A new pathway to high-pressure nuclear magnetic resonance, *Science advances* 3 (12) (2017) eaao5242.
- [105] M. Eremets, High pressure experimental methods, Oxford University Press, 1996.
- [106] S. Mozaffari, D. Sun, V. S. Minkov, D. Knyazev, J. B. Betts, M. Einaga, K. Shimizu, M. I. Eremets, L. Balicas, F. F. Balakirev, Superconducting phase-diagram of h3s under high magnetic fields, *arXiv preprint arXiv:1901.11208*.
- [107] T. Kobayashi, H. Hidaka, H. Kotegawa, K. Fujiwara, M. Eremets, Non-magnetic indenter-type high-pressure cell for magnetic measurements, *Review of scientific instruments* 78 (2) (2007) 023909.
- [108] T. Meier, S. Khandarkhaeva, S. Petitgirard, T. Körber, A. Lauerer, E. Rössler, L. Dubrovinsky, Nmr close to mega-bar pressures, *arXiv preprint arXiv:1803.05472*.
- [109] R. Boehler, Laser heating in the diamond cell: techniques and applications, *Hyperfine Interactions* 128 (1-3) (2000) 307–321.
- [110] A. F. Goncharov, V. B. Prakapenka, V. V. Struzhkin, I. Kantor, M. L. Rivers, D. A. Dalton, X-ray diffraction in the pulsed laser heated diamond anvil cell, *Review of Scientific Instruments* 81 (11) (2010) 113902.
- [111] R. Boehler, K. De Hantsetters, New anvil designs in diamond-cells, *High Pressure Research* 24 (3) (2004) 391–396.
- [112] N. Dubrovinskaia, L. Dubrovinsky, N. A. Solopova, A. Abakumov, S. Turner, M. Hanfland, E. Bykova, M. Bykov, C. Prescher, V. B. Prakapenka, et al., Terapascal static pressure generation with ultrahigh yield strength nanodiamond, *Science advances* 2 (7) (2016) e1600341.
- [113] Y. K. Vohra, G. K. Samudrala, S. L. Moore, J. M. Montgomery, G. M. Tsoi, N. Velisavljevic, High pressure studies using two-stage diamond micro-anvils grown by chemical vapor deposition, *High Pressure Research* 35 (3) (2015) 282–288.
- [114] S. S. Lobanov, V. B. Prakapenka, C. Prescher, Z. Konôpková, H.-P. Liermann, K. L. Crispin, C. Zhang, A. F. Goncharov, Pressure, stress, and strain distribution in the double-stage diamond anvil cell, *Journal of Applied Physics* 118 (3) (2015) 035905.
- [115] T. Sakai, T. Yagi, H. Ohfuji, T. Irifune, Y. Ohishi, N. Hirao, Y. Suzuki, Y. Kuroda, T. Asakawa, T. Kanemura, High-pressure generation using double stage micro-paired diamond anvils shaped by focused ion beam, *Review of Scientific Instruments* 86 (3) (2015) 033905.
- [116] M. McMahon, Diamond sculpting pushes extremes, *Nature materials* 17 (2018) 858–859.
- [117] Z. Jenei, E. OBannon, S. Weir, H. Cynn, M. Lipp, W. Evans, Single crystal toroidal diamond anvils for high pressure experiments beyond 5 megabar, *Nature communications* 9 (1) (2018) 3563.
- [118] A. Dewaele, P. Loubeyre, F. Occelli, O. Marie, M. Mezouar, Toroidal diamond anvil cell for detailed measurements under extreme static pressures, *Nature communications* 9.
- [119] E. F. OBannon III, Z. Jenei, H. Cynn, M. J. Lipp, J. R. Jeffries, Contributed review: Culet diameter and the achievable pressure of a diamond anvil cell: Implications for the upper pressure limit of a diamond anvil cell, *Review of Scientific Instruments* 89 (11) (2018) 111501.
- [120] H. Mao, P. Bell, Electrical resistivity measurements of conductors in the diamond-window, high-pressure cell, *Review of Scientific Instruments* 52 (4) (1981) 615–616.
- [121] M. I. Eremets, R. J. Hemley, H.-k. Mao, E. Gregoryanz, Semiconducting non-molecular nitrogen up to 240 gpa and its low-pressure stability, *Nature* 411 (6834) (2001) 170.
- [122] C. Rotundu, T. Čuk, R. Greene, Z.-X. Shen, R. J. Hemley, V. Struzhkin, High-pressure resistivity technique for quasi-hydrostatic compression experiments, *Review of Scientific Instruments* 84 (6) (2013) 063903.
- [123] K. Das, V. Venkatesan, K. Miyata, D. Dreifus, J. Glass, A review of the electrical characteristics of metal contacts on diamond, *Thin Solid Films* 212 (1-2) (1992) 19–24.
- [124] D. Evans, O. Roberts, G. Williams, A. Vearey-Roberts, F. Bain, S. Evans, D. Langstaff, D. Twitchen, Diamond-metal contacts: interface barriers and real-time characterization, *Journal of Physics: Condensed Matter* 21 (36) (2009) 364223.
- [125] M. Werner, O. Dorsch, H.-U. Baerwind, E. Obermeier, C. Johnston, P. R. Chalki, S. Romani, The effect of metallization on the ohmic contact resistivity to heavily b-doped polycrystalline diamond films, *IEEE Transactions on Electron Devices* 42 (7) (1995) 1344–1351.
- [126] R. A. Forman, G. J. Piermarini, J. D. Barnett, S. Block, Pressure measurement made by the utilization of ruby sharp-line luminescence, *Science* 176 (4032) (1972) 284–285.
- [127] J. A. Flores-Livas, L. Lehtovaara, M. Amsler, S. Goedecker, S. Pailhes, S. Botti, A. San Miguel, M. A. Marques, Raman activity of s p 3 carbon allotropes under pressure: A density functional theory study, *Physical Review B* 85 (15) (2012) 155428.
- [128] M. Hanfland, K. Syassen, A raman study of diamond anvils under stress, *Journal of applied physics* 57 (8) (1985) 2752–2756.
- [129] M. Eremets, Megabar high-pressure cells for raman measurements, *Journal of Raman Spectroscopy* 34 (7-8) (2003) 515–518.
- [130] Y. Akahama, H. Kawamura, Pressure calibration of diamond anvil raman gauge to 310 gpa, *Journal of Applied Physics* 100 (4) (2006) 043516.
- [131] Y. Akahama, H. Kawamura, Pressure calibration of diamond anvil raman gauge to 410 gpa, in: *Journal of Physics: Conference Series*, Vol. 215, IOP Publishing, 2010, p. 012195.
- [132] Y. Akahama, H. Kawamura, Diamond anvil raman gauge in multi-megabar pressure range, *High Pressure Research* 27 (4) (2007) 473–482.
- [133] H.-k. Mao, R. J. Hemley, Ultrahigh-pressure transitions in solid hydrogen, *Reviews of modern physics* 66 (2) (1994) 671.
- [134] P. Loubeyre, F. Occelli, R. LeToullec, Optical studies of solid hydrogen to 320 GPa and evidence for black hydrogen, *Nature* 416 (6681) (2002) 13–17. doi:10.1038/416613a. URL <http://dx.doi.org/10.1038/416613a>
- [135] M. I. Eremets, I. A. Troyan, Conductive dense hydrogen, *Nat. Mat.* 10 (2011) 927–931. doi:<http://dx.doi.org/10.1038/nmat3175>.
- [136] M. Eremets, I. Troyan, A. Drozdov, Low temperature phase diagram of hydrogen at pressures up to 380 gpa. a possible metallic phase at 360 gpa and 200 k, *arXiv preprint arXiv:1601.04479*.
- [137] J. M. McMahon, D. M. Ceperley, High-temperature superconductivity in atomic metallic hydrogen, *Phys. Rev. B* 84 (2011) 144515. doi:10.1103/PhysRevB.84.144515. URL <http://link.aps.org/doi/10.1103/PhysRevB.84.144515>
- [138] B. Monserrat, N. D. Drummond, P. Dalladay-Simpson, R. T. Howie, P. L. Ríos, E. Gregoryanz, C. J. Pickard, R. J. Needs, Structure and metallicity of phase v of hydrogen, *Physical Review Letters* 120 (25) (2018) 255701.
- [139] J. Carbotte, E. Nicol, T. Timusk, Detecting superconductivity in the high pressure hydrides and metallic hydrogen from optical properties, *Physical review letters* 121 (4) (2018) 047002.
- [140] M. Borinaga, J. Ibañez-Azpiroz, A. Bergara, I. Errea, Strong electron-phonon and band structure effects in the optical properties of high pressure metallic hydrogen, *Physical review letters* 120 (5) (2018) 057402.
- [141] C. Cazorla, J. Boronat, Simulation and understanding of atomic and molecular quantum crystals, *Reviews of Modern Physics* 89 (3) (2017) 035003.
- [142] C.-S. Zha, Z. Liu, R. Hemley, Synchrotron infrared measurements of dense hydrogen to 360 gpa, *Phys. Rev. Lett.* 108 (2012) 146402. doi:10.1103/PhysRevLett.108.146402. URL <http://link.aps.org/doi/10.1103/PhysRevLett.108.146402>
- [143] I. I. Naumov, R. J. Hemley, Aromaticity, closed-shell effects, and metallization of hydrogen, *Accounts of Chemical Research* 47 (12) (2014) 3551–3559, PMID: 25369180. arXiv:<http://dx.doi.org/10.1021/ar5002654>, doi:10.1021/ar5002654. URL <http://dx.doi.org/10.1021/ar5002654>
- [144] M. Zaghoo, A. Salamat, I. F. Silvera, Evidence of a first-order phase transition to metallic hydrogen, *Physical Review B* 93 (15) (2016) 155128.
- [145] M. Eremets, A. Drozdov, P. P. Kong, H. Wang, Molecular semimetallic hydrogen, *arXiv preprint arXiv:1708.05217*.
- [146] S. Azadi, G. J. Ackland, The role of van der waals and exchange interactions in high-pressure solid hydrogen, *Physical Chemistry Chemical Physics* 19 (32) (2017) 21829–21839.
- [147] I. B. Magdău, M. Marqués, B. Borgulya, G. J. Ackland, Simple thermodynamic model for the hydrogen phase diagram, *Physical Review B* 95 (9) (2017) 094107.
- [148] X.-D. Liu, P. Dalladay-Simpson, R. T. Howie, B. Li, E. Gregoryanz, Comment on observation of the wigner-huntington transition to metallic hydrogen, *Science* 357 (6353) (2017) eaan2286.

- [149] A. F. Goncharov, V. V. Struzhkin, Comment on observation of the wigner-huntington transition to metallic hydrogen, *Science* 357 (6353) (2017) eaam9736.
- [150] C.-s. Zha, H. Liu, S. T. John, R. J. Hemley, Melting and high p- t transitions of hydrogen up to 300 gpa, *Physical review letters* 119 (7) (2017) 075302.
- [151] M. Zaghoo, I. F. Silvera, Conductivity and dissociation in liquid metallic hydrogen and implications for planetary interiors, *Proceedings of the National Academy of Sciences* (2017) 201707918.
- [152] G. Rillo, M. A. Morales, D. M. Ceperley, C. Pierleoni, Coupled electron-ion monte carlo simulation of hydrogen molecular crystals, *The Journal of chemical physics* 148 (10) (2018) 102314.
- [153] M. I. Eremets, I. A. Trojan, S. A. Medvedev, J. S. Tse, Y. Yao, Superconductivity in hydrogen dominant materials: Silane, *Science* 319 (5869) (2008) 1506–1509. doi:10.1126/science.1153282. URL <http://www.sciencemag.org/content/319/5869/1506.abstract>
- [154] X.-J. Chen, V. V. Struzhkin, Y. Song, A. F. Goncharov, M. Ahart, Z. Liu, H.-k. Mao, R. J. Hemley, Pressure-induced metallization of silane, *Proceedings of the National Academy of Sciences* 105 (1) (2008) 20–23. doi:10.1073/pnas.0710473105. URL <http://www.pnas.org/content/105/1/20.abstract>
- [155] S. Wang, H.-k. Mao, X.-J. Chen, W. L. Mao, High pressure chemistry in the h₂-sih₄ system, *Proceedings of the National Academy of Sciences* 106 (35) (2009) 14763–14767. doi:10.1073/pnas.0907729106. URL <http://www.pnas.org/content/106/35/14763.abstract>
- [156] M. Hanfland, J. E. Proctor, C. L. Guillaume, O. Degtyareva, E. Gregoryanz, High-pressure synthesis, amorphization, and decomposition of silane, *Phys. Rev. Lett.* 106 (9) (2011) 095503. doi:10.1103/PhysRevLett.106.095503. URL <http://link.aps.org/doi/10.1103/PhysRevLett.106.095503>
- [157] D. Y. Kim, R. H. Scheicher, C. J. Pickard, R. J. Needs, R. Ahuja, Predicted formation of superconducting platinum-hydride crystals under pressure in the presence of molecular hydrogen, *Phys. Rev. Lett.* 107 (2011) 117002. doi:10.1103/PhysRevLett.107.117002. URL <http://link.aps.org/doi/10.1103/PhysRevLett.107.117002>
- [158] G. Liu, Z. Yu, S. Li, H. Wang, The experimental compression behavior of platinum hydride to 128 gpa, *Materials Letters*.
- [159] J. A. Flores-Livas, M. Amsler, T. J. Lenosky, L. Lehtovaara, S. Botti, M. A. L. Marques, S. Goedecker, High-pressure structures of disilane and their superconducting properties, *Phys. Rev. Lett.* 108 (2012) 117004. doi:10.1103/PhysRevLett.108.117004. URL <http://link.aps.org/doi/10.1103/PhysRevLett.108.117004>
- [160] Y. Li, J. Hao, H. Liu, Y. Li, Y. Ma, The metallization and superconductivity of dense hydrogen sulfide, *The Journal of chemical physics* 140 (17) (2014) 174712.
- [161] D. Duan, Y. Liu, F. Tian, D. Li, X. Huang, Z. Zhao, H. Yu, B. Liu, W. Tian, T. Cui, Pressure-induced metallization of dense (h₂s)₂h₂ with high-tc superconductivity, *Sci. Rep.* 4. doi:http://dx.doi.org/10.1038/srep06968.
- [162] A. Drozdov, M. Eremets, I. Troyan, Conventional superconductivity at 190 k at high pressures, *arXiv preprint arXiv:1412.0460*.
- [163] H. Shimizu, H. Yamaguchi, S. Sasaki, A. Honda, S. Endo, M. Kobayashi, Pressure-temperature phase diagram of solid hydrogen sulfide determined by raman spectroscopy, *Physical Review B* 51 (14) (1995) 9391.
- [164] M. Sakashita, H. Yamawaki, H. Fujihisa, K. Aoki, S. Sasaki, H. Shimizu, Pressure-induced molecular dissociation and metallization in hydrogen-bonded h₂ s solid, *Physical review letters* 79 (6) (1997) 1082.
- [165] H. Fujihisa, H. Yamawaki, M. Sakashita, A. Nakayama, T. Yamada, K. Aoki, Molecular dissociation and two low-temperature high-pressure phases of h₂ s, *Physical Review B* 69 (21) (2004) 214102.
- [166] A. Drozdov, Superconductivity in hydrogen-rich materials at high pressures, Ph.D. thesis, Johannes Gutenberg-Universitat Mainz (2016).
- [167] M. Einaga, M. Sakata, T. Ishikawa, K. Shimizu, M. I. Eremets, A. P. Drozdov, I. A. Troyan, N. Hirao, Y. Ohishi, Crystal structure of the superconducting phase of sulfur hydride, *Nature Physics*.
- [168] J. A. Flores-Livas, M. Amsler, C. Heil, A. Sanna, L. Boeri, G. Profeta, C. Wolverton, S. Goedecker, E. K. U. Gross, Superconductivity in metastable phases of phosphorus-hydride compounds under high pressure, *Phys. Rev. B* 93 (2016) 020508. doi:10.1103/PhysRevB.93.020508. URL <http://link.aps.org/doi/10.1103/PhysRevB.93.020508>
- [169] A. Drozdov, M. Eremets, I. Troyan, Superconductivity above 100 k in ph₃ at high pressures, *arXiv preprint arXiv:1508.06224*.
- [170] I. Troyan, A. Gavriluk, R. Rüffer, A. Chumakov, A. Mironovich, I. Lyubutin, D. Perekalin, A. P. Drozdov, M. I. Eremets, Observation of superconductivity in hydrogen sulfide from nuclear resonant scattering, *Science* 351 (6279) (2016) 1303–1306.
- [171] I. Errea, M. Calandra, C. J. Pickard, J. Nelson, R. J. Needs, Y. Li, H. Liu, Y. Zhang, Y. Ma, F. Mauri, High-pressure hydrogen sulfide from first principles: A strongly anharmonic phonon-mediated superconductor, *Phys. Rev. Lett.* 114 (2015) 157004. doi:10.1103/PhysRevLett.114.157004. URL <http://link.aps.org/doi/10.1103/PhysRevLett.114.157004>
- [172] C. Heil, L. Boeri, Influence of bonding on superconductivity in high-pressure hydrides, *Phys. Rev. B* 92 (2015) 060508. doi:10.1103/PhysRevB.92.060508. URL <http://link.aps.org/doi/10.1103/PhysRevB.92.060508>
- [173] A. J. Flores-Livas, A. Sanna, E. Gross, High temperature superconductivity in sulfur and selenium hydrides at high pressure, *Eur. Phys. J. B* 89 (3) (2016) 1–6. doi:10.1140/epjb/e2016-70020-0. URL <http://dx.doi.org/10.1140/epjb/e2016-70020-0>
- [174] J. A. Flores-Livas, A. Sanna, S. Goedecker, Accelerated materials design approaches based on structural classification: application to low enthalpy high pressure phases of sh₃ and seh₃, *Novel Superconducting Materials* 3 (1) (2017) 6–13.
- [175] R. Akashi, W. Sano, R. Arita, S. Tsuneyuki, Possible “magnéli” phases and self-alloying in the superconducting sulfur hydride, *Phys. Rev. Lett.* 117 (2016) 075503. doi:10.1103/PhysRevLett.117.075503. URL <http://link.aps.org/doi/10.1103/PhysRevLett.117.075503>
- [176] H. Wang, S. T. John, K. Tanaka, T. Iitaka, Y. Ma, Superconductive sodalite-like clathrate calcium hydride at high pressures, *Proceedings of the National Academy of Sciences* 109 (17) (2012) 6463–6466.
- [177] F. Peng, Y. Sun, C. J. Pickard, R. J. Needs, Q. Wu, Y. Ma, Hydrogen clathrate structures in rare earth hydrides at high pressure s: Possible route to room-temperature superconductivity, *Phys. Rev. Lett.* 119 (2017) 107001. doi:10.1103/PhysRevLett.119.107001. URL <https://link.aps.org/doi/10.1103/PhysRevLett.119.107001>
- [178] Y. Li, G. Gao, Y. Xie, Y. Ma, T. Cui, G. Zou, Superconductivity at 100 k in dense sih₄(h₂)₂ predicted by first principles, *Proceedings of the National Academy of Sciences* 107 (36) (2010) 15708–15711. doi:10.1073/pnas.1007354107. URL <http://www.pnas.org/content/107/36/15708.abstract>
- [179] G. Profeta, C. Franchini, N. Lathiotakis, A. Floris, A. Sanna, M. A. L. Marques, M. Lüders, S. Massidda, E. K. U. Gross, A. Continenza, Superconductivity in lithium, potassium, and aluminum under extreme pressure: A first-principles study, *Phys. Rev. Lett.* 96 (2006) 047003. doi:10.1103/PhysRevLett.96.047003. URL <http://link.aps.org/doi/10.1103/PhysRevLett.96.047003>
- [180] T. Muramatsu, W. K. Wanene, M. Somayazulu, E. Vinitsky, D. Chandra, T. A. Strobel, V. V. Struzhkin, R. J. Hemley, Metallization and superconductivity in the hydrogen-rich ionic salt bareh₉, *The Journal of Physical Chemistry C* 119 (32) (2015) 18007–18013. *arXiv*:<http://dx.doi.org/10.1021/acs.jpcc.5b03709>, doi:10.1021/acs.jpcc.5b03709. URL <http://dx.doi.org/10.1021/acs.jpcc.5b03709>
- [181] A. Drozdov, P. Kong, V. Minkov, S. Besedin, M. Kuzovnikov, S. Mozafari, L. Balicas, F. Balakirev, D. Graf, V. Prakapenka, et al., Superconductivity at 250 k in lanthanum hydride under high pressures, *arXiv preprint arXiv:1812.01561*.
- [182] H. Liu, I. I. Naumov, R. Hoffmann, N. Ashcroft, R. J. Hemley, Potential high-tc superconducting lanthanum and yttrium hydrides at high pres-

- sure, *Proceedings of the National Academy of Sciences* 114 (27) (2017) 6990–6995.
- [183] A. Drozdov, V. Minkov, S. Besedin, P. Kong, M. Kuzovnikov, D. Knyazev, M. Erements, Superconductivity at 215 K in lanthanum hydride at high pressures, arXiv preprint arXiv:1808.07039.
- [184] I. J. e. a. Errea-Flores, Superconductivity in lanthanum hydride under high pressures, arXiv preprint arXiv:SOON.
- [185] J. Flores Livas, Computational and experimental studies of sp³-materials at high pressure, Ph.D. thesis, University of Lyon 1 (2012).
- [186] W. Grochala, R. Hoffmann, J. Feng, N. W. Ashcroft, The chemical imagination at work in very tight places, *Angewandte Chemie International Edition* 46 (20) (2007) 3620–3642.
- [187] J. H. Nguyen, D. Orlikowski, F. H. Streitz, J. A. Moriarty, N. C. Holmes, High-pressure tailored compression: Controlled thermodynamic paths, *Journal of applied physics* 100 (2) (2006) 023508.
- [188] O. Degtyareva, J. E. Proctor, C. L. Guillaume, E. Gregoryanz, M. Hanfland, Formation of transition metal hydrides at high pressures, *Solid State Communications* 149 (39–40) (2009) 1583–1586. doi:10.1016/j.ssc.2009.07.022. URL <http://www.sciencedirect.com/science/article/pii/S0038109809004414>
- [189] T. Strobel, P. Ganesh, M. Somayazulu, P. Kent, R. Hemley, Novel cooperative interactions and structural ordering in H₂S-H₂, *Phys. Rev. Lett.* 107 (2011) 255503. doi:10.1103/PhysRevLett.107.255503. URL <http://link.aps.org/doi/10.1103/PhysRevLett.107.255503>
- [190] V. I. Levitas, High pressure phase transformations revisited, *Journal of Physics: Condensed Matter* 30 (16) (2018) 163001.
- [191] Z. M. Geballe, H. Liu, A. K. Mishra, M. Ahart, M. Somayazulu, Y. Meng, M. Baldini, R. J. Hemley, Synthesis and stability of lanthanum superhydrides, *Angewandte Chemie International Edition* 57 (3) (2018) 688–692.
- [192] E. R. Margine, F. Giustino, Anisotropic migdal-eliasberg theory using wannier functions, *Phys. Rev. B* 87 (2013) 024505. doi:10.1103/PhysRevB.87.024505. URL <http://link.aps.org/doi/10.1103/PhysRevB.87.024505>
- [193] A. Sanna, J. A. Flores-Livas, A. Davydov, G. Profeta, K. Dewhurst, S. Sharma, E. Gross, Ab initio eliasberg theory: Making genuine predictions of superconducting features, *Journal of the Physical Society of Japan* 87 (4) (2018) 041012.
- [194] J. P. Carbotte, Properties of boson-exchange superconductors, *Rev. Mod. Phys.* 62 (1990) 1027–1157. doi:10.1103/RevModPhys.62.1027. URL <http://link.aps.org/doi/10.1103/RevModPhys.62.1027>
- [195] S. Baroni, S. de Gironcoli, A. Dal Corso, P. Giannozzi, Phonons and related crystal properties from density-functional perturbation theory, *Rev. Mod. Phys.* 73 (2001) 515–562. doi:10.1103/RevModPhys.73.515. URL <http://link.aps.org/doi/10.1103/RevModPhys.73.515>
- [196] R. M. Dreizler, E. Gross, *Density Functional Theory*, Springer-Verlag Berlin Heidelberg, 1990.
- [197] W. Kohn, L. J. Sham, Self-consistent equations including exchange and correlation effects, *Phys. Rev.* 140 (1965) A1133–A1138. doi:10.1103/PhysRev.140.A1133. URL <http://link.aps.org/doi/10.1103/PhysRev.140.A1133>
- [198] J. P. Perdew, K. Burke, M. Ernzerhof, Generalized gradient approximation made simple, *Phys. Rev. Lett.* 77 (1996) 3865–3868. doi:10.1103/PhysRevLett.77.3865. URL <https://link.aps.org/doi/10.1103/PhysRevLett.77.3865>
- [199] J. P. Perdew, A. Zunger, Self-interaction correction to density-functional approximations for many-electron systems, *Phys. Rev. B* 23 (1981) 5048–5079. doi:10.1103/PhysRevB.23.5048. URL <https://link.aps.org/doi/10.1103/PhysRevB.23.5048>
- [200] J. Sun, A. Ruzsinszky, J. P. Perdew, Strongly constrained and appropriately normed semilocal density functional, *Phys. Rev. Lett.* 115 (2015) 036402. doi:10.1103/PhysRevLett.115.036402. URL <https://link.aps.org/doi/10.1103/PhysRevLett.115.036402>
- [201] S. Baroni, P. Giannozzi, A. Testa, Green’s-function approach to linear response in solids, *Phys. Rev. Lett.* 58 (1987) 1861–1864. doi:10.1103/PhysRevLett.58.1861. URL <http://link.aps.org/doi/10.1103/PhysRevLett.58.1861>
- [202] S. de Gironcoli, Lattice dynamics of metals from density-functional perturbation theory, *Phys. Rev. B* 51 (1995) 6773–6776. doi:10.1103/PhysRevB.51.6773. URL <http://link.aps.org/doi/10.1103/PhysRevB.51.6773>
- [203] A. Marini, S. Poncé, X. Gonze, Many-body perturbation theory approach to the electron-phonon interaction with density-functional theory as a starting point, *Phys. Rev. B* 91 (2015) 224310. doi:10.1103/PhysRevB.91.224310. URL <https://link.aps.org/doi/10.1103/PhysRevB.91.224310>
- [204] M. Born, K. Huang, *Dynamical theory of crystal lattices*, Clarendon press, 1954.
- [205] M. Born, D. J. Hooton, Statistische dynamik mehrfach periodischer systeme, *Zeitschrift für Physik* 142 (2) (1955) 201–218. doi:10.1007/BF01329422. URL <https://doi.org/10.1007/BF01329422>
- [206] A. Maradudin, A. Fein, Scattering of neutrons by an anharmonic crystal, *Physical Review* 128 (6) (1962) 2589.
- [207] T. R. Koehler, Theory of the self-consistent harmonic approximation with application to solid neon, *Physical Review Letters* 17 (2) (1966) 89.
- [208] I. Errea, M. Calandra, F. Mauri, First-principles theory of anharmonicity and the inverse isotope effect in superconducting palladium-hydride compounds, *Phys. Rev. Lett.* 111 (2013) 177002. doi:10.1103/PhysRevLett.111.177002. URL <https://link.aps.org/doi/10.1103/PhysRevLett.111.177002>
- [209] I. Errea, M. Calandra, C. J. Pickard, J. R. Nelson, R. J. Needs, Y. Li, H. Liu, Y. Zhang, Y. Ma, F. Mauri, Quantum hydrogen-bond symmetrization in the superconducting hydrogen sulfide system, *Nature* 532 (7597) (2016) 81.
- [210] C. Wang, C. Chan, K. Ho, Tight-binding molecular-dynamics study of phonon anharmonic effects in silicon and diamond, *Physical Review B* 42 (17) (1990) 11276.
- [211] O. Hellman, I. Abrikosov, S. Simak, Lattice dynamics of anharmonic solids from first principles, *Physical Review B* 84 (18) (2011) 180301.
- [212] O. Hellman, P. Steneteg, I. A. Abrikosov, S. I. Simak, Temperature dependent effective potential method for accurate free energy calculations of solids, *Physical Review B* 87 (10) (2013) 104111.
- [213] O. Hellman, I. A. Abrikosov, Temperature-dependent effective third-order interatomic force constants from first principles, *Physical Review B* 88 (14) (2013) 144301.
- [214] D. M. Ceperley, Path integrals in the theory of condensed helium, *Reviews of Modern Physics* 67 (2) (1995) 279.
- [215] J. M. Bowman, Self-consistent field energies and wavefunctions for coupled oscillators, *The Journal of Chemical Physics* 68 (2) (1978) 608–610.
- [216] B. Monserrat, N. Drummond, R. Needs, Anharmonic vibrational properties in periodic systems: energy, electron-phonon coupling, and stress, *Physical Review B* 87 (14) (2013) 144302.
- [217] D. Hooton, Lviii. some vibrational properties of solid helium, *The London, Edinburgh, and Dublin Philosophical Magazine and Journal of Science* 46 (376) (1955) 485–498.
- [218] D. Hooton, The use of a model in anharmonic lattice dynamics, *Philosophical Magazine* 3 (25) (1958) 49–54.
- [219] N. R. Werthamer, Self-consistent phonon formulation of anharmonic lattice dynamics, *Phys. Rev. B* 1 (1970) 572–581. doi:10.1103/PhysRevB.1.572. URL <https://link.aps.org/doi/10.1103/PhysRevB.1.572>
- [220] R. A. Cochran, W. and Cowley, *Phonons in Perfect Crystals*, Springer Berlin Heidelberg, Berlin, Heidelberg, 1967. doi:10.1007/978-3-642-46074-6. URL <https://doi.org/10.1007/978-3-642-46074-6>
- [221] J. Menéndez, M. Cardona, Temperature dependence of the first-order raman scattering by phonons in Si, Ge, and α -Sn: Anharmonic effects, *Phys. Rev. B* 29 (1984) 2051–2059. doi:10.1103/PhysRevB.29.2051. URL <https://link.aps.org/doi/10.1103/PhysRevB.29.2051>

- [222] P. Souvatzis, O. Eriksson, M. Katsnelson, S. Rudin, Entropy driven stabilization of energetically unstable crystal structures explained from first principles theory, *Physical review letters* 100 (9) (2008) 095901.
- [223] I. Errea, M. Calandra, F. Mauri, Anharmonic free energies and phonon dispersions from the stochastic self-consistent harmonic approximation: Application to platinum and palladium hydrides, *Phys. Rev. B* 89 (2014) 064302. doi:10.1103/PhysRevB.89.064302. URL <https://link.aps.org/doi/10.1103/PhysRevB.89.064302>
- [224] T. Tadano, S. Tsuneyuki, Self-consistent phonon calculations of lattice dynamical properties in cubic SrTiO_3 with first-principles anharmonic force constants, *Phys. Rev. B* 92 (2015) 054301. doi:10.1103/PhysRevB.92.054301. URL <https://link.aps.org/doi/10.1103/PhysRevB.92.054301>
- [225] A. A. Maradudin, A. E. Fein, Scattering of neutrons by an anharmonic crystal, *Phys. Rev.* 128 (1962) 2589–2608. doi:10.1103/PhysRev.128.2589. URL <https://link.aps.org/doi/10.1103/PhysRev.128.2589>
- [226] M. Lazzeri, M. Calandra, F. Mauri, Anharmonic phonon frequency shift in MgB_2 , *Phys. Rev. B* 68 (2003) 220509. doi:10.1103/PhysRevB.68.220509. URL <https://link.aps.org/doi/10.1103/PhysRevB.68.220509>
- [227] F. Zhou, W. Nielson, Y. Xia, V. Ozoliņš, et al., Lattice anharmonicity and thermal conductivity from compressive sensing of first-principles calculations, *Physical review letters* 113 (18) (2014) 185501.
- [228] T. Tadano, S. Tsuneyuki, First-principles lattice dynamics method for strongly anharmonic crystals, *Journal of the Physical Society of Japan* 87 (4) (2018) 041015.
- [229] T. Tadano, S. Tsuneyuki, Quartic anharmonicity of rattlers and its effect on lattice thermal conductivity of clathrates from first principles, *Physical review letters* 120 (10) (2018) 105901.
- [230] L. Hedin, New method for calculating the one-particle green's function with application to the electron-gas problem, *Phys. Rev.* 139 (1965) A796–A823. doi:10.1103/PhysRev.139.A796. URL <http://link.aps.org/doi/10.1103/PhysRev.139.A796>
- [231] F. Aryasetiawan, O. Gunnarsson, The gw method, *Reports on Progress in Physics* 61 (3) (1998) 237. URL <http://stacks.iop.org/0034-4885/61/i=3/a=002>
- [232] S. Vonsovsky, Y. Izyumov, E. Kurmaev, E. Brandt, A. Zavaritsyn, *Superconductivity of Transition Metals: Their Alloys and Compounds*, Springer Series in Solid-State Sciences Series, Springer London, Limited, 1982. URL <http://books.google.de/books?id=ANOAMQEACAAJ>
- [233] E. Runge, E. K. U. Gross, Density-functional theory for time-dependent systems, *Phys. Rev. Lett.* 52 (1984) 997–1000. doi:10.1103/PhysRevLett.52.997. URL <https://link.aps.org/doi/10.1103/PhysRevLett.52.997>
- [234] P. Morel, P. W. Anderson, Calculation of the superconducting state parameters with retarded electron-phonon interaction, *Phys. Rev.* 125 (1962) 1263–1271. doi:10.1103/PhysRev.125.1263. URL <http://link.aps.org/doi/10.1103/PhysRev.125.1263>
- [235] R. Akashi, R. Arita, Development of density-functional theory for a plasmon-assisted superconducting state: Application to lithium under high pressures, *Phys. Rev. Lett.* 111 (2013) 057006. doi:10.1103/PhysRevLett.111.057006. URL <http://link.aps.org/doi/10.1103/PhysRevLett.111.057006>
- [236] G. R. Stewart, Unconventional superconductivity, *Advances in Physics* 66 (2) (2017) 75–196. arXiv:<https://doi.org/10.1080/00018732.2017.1331615>, doi:10.1080/00018732.2017.1331615. URL <https://doi.org/10.1080/00018732.2017.1331615>
- [237] D. J. Scalapino, A common thread: The pairing interaction for unconventional superconductors, *Rev. Mod. Phys.* 84 (2012) 1383–1417. doi:10.1103/RevModPhys.84.1383. URL <https://link.aps.org/doi/10.1103/RevModPhys.84.1383>
- [238] F. Essenberg, A. Sanna, A. Linscheid, F. Tandetzky, G. Profeta, P. Cudazzo, E. K. U. Gross, Superconducting pairing mediated by spin fluctuations from first principles, *Phys. Rev. B* 90 (2014) 214504. doi:10.1103/PhysRevB.90.214504. URL <http://link.aps.org/doi/10.1103/PhysRevB.90.214504>
- [239] L. P. Gor'kov, On the energy spectrum of superconductors, *Sov. Phys. JETP* 7 (3) (1958) 505.
- [240] P. B. Allen, B. Mitrović, *Theory of Superconducting T_c* , Vol. 37 of *Solid State Physics*, Academic Press, 1983. doi:[http://dx.doi.org/10.1016/S0081-1947\(08\)60665-7](http://dx.doi.org/10.1016/S0081-1947(08)60665-7).
- [241] A. A. Abrikosov, I. Dzyaloshinskii, L. P. Gor'kov, *Methods of quantum field theory in statistical physics*, Dover, New York, NY, 1975. URL <https://cds.cern.ch/record/107441>
- [242] A. Fetter, J. D. Walecka, *Quantum Theory of Many-Particle Systems*, Dover, New York, 1971, 2003.
- [243] P. G. de Gennes, *Superconductivity of Metals and Alloys*, Westview Press, 1966.
- [244] A. B. Migdal, Interaction between electrons and lattice vibrations in a normal metal, *Sov. Phys. JETP* 7 (6) (1958) 996–1001.
- [245] C. C. Tsuei, J. R. Kirtley, C. C. Chi, L. S. Yu-Jahnes, A. Gupta, T. Shaw, J. Z. Sun, M. B. Ketchen, Pairing symmetry and flux quantization in a tricrystal superconducting ring of $\text{YBa}_2\text{Cu}_3\text{O}_{7-\delta}$, *Phys. Rev. Lett.* 73 (1994) 593–596. doi:10.1103/PhysRevLett.73.593. URL <https://link.aps.org/doi/10.1103/PhysRevLett.73.593>
- [246] G. A. C. Ummarino, Eliashberg theory, in: Pavarini, Eva and Koch, Erik and Schollwöck, Ulrich (Ed.), *Emergent Phenomena in Correlated Matter*, Verlag des Forschungszentrum Jülich, Jülich, 2013, Ch. 13, p. 395.
- [247] W. Sano, T. Koretsune, T. Tadano, R. Akashi, R. Arita, Effect of van Hove singularities on high- T_c superconductivity in h_3S , *Phys. Rev. B* 93 (2016) 094525. doi:10.1103/PhysRevB.93.094525. URL <https://link.aps.org/doi/10.1103/PhysRevB.93.094525>
- [248] W. L. McMillan, Transition temperature of strong-coupled superconductors, *Phys. Rev.* 167 (1968) 331–344. doi:10.1103/PhysRev.167.331. URL <https://link.aps.org/doi/10.1103/PhysRev.167.331>
- [249] R. Dynes, Mcmillan's equation and the T_c of superconductors, *Solid State Communications* 10 (7) (1972) 615–618.
- [250] P. B. Allen, R. C. Dynes, Transition temperature of strong-coupled superconductors reanalyzed, *Phys. Rev. B* 12 (1975) 905–922. doi:10.1103/PhysRevB.12.905. URL <http://link.aps.org/doi/10.1103/PhysRevB.12.905>
- [251] S. Kurth Ph.D. thesis, *Exchange-Correlation Functionals for Inhomogeneous Superconductors*, Bayerische Julius-Maximilians Universität Würzburg, 1995. URL http://users.physik.fu-berlin.de/~ag-gross/theses/kurth_phd.pdf
- [252] T. Kreibich, E. K. U. Gross, Multicomponent density-functional theory for electrons and nuclei, *Phys. Rev. Lett.* 86 (2001) 2984–2987. doi:10.1103/PhysRevLett.86.2984. URL <https://link.aps.org/doi/10.1103/PhysRevLett.86.2984>
- [253] J. A. Flores-Livas, A. Sanna, Superconductivity in intercalated group-iv honeycomb structures, *Phys. Rev. B* 91 (2015) 054508. doi:10.1103/PhysRevB.91.054508. URL <http://link.aps.org/doi/10.1103/PhysRevB.91.054508>
- [254] A. Sanna, A. Davydov, J. K. Dewhurst, S. Sharma, J. A. Flores-Livas, Superconductivity in hydrogenated carbon nanostructures, *The European Physical Journal B* 91 (8) (2018) 177.
- [255] P. Hohenberg, W. Kohn, Inhomogeneous electron gas, *Phys. Rev.* 136 (1964) B864–B871. doi:10.1103/PhysRev.136.B864. URL <http://link.aps.org/doi/10.1103/PhysRev.136.B864>
- [256] J. Schmidt, C. L. Benavides-Riveros, M. A. Marques, Representability problem of density functional theory for superconductors, *Physical Review B* 99 (2) (2019) 024502.
- [257] J. Schmidt, C. L. Benavides-Riveros, M. A. Marques, Reduced density matrix functional theory for superconductors, arXiv preprint arXiv:1903.01516.
- [258] N. D. Mermin, Thermal properties of the inhomogeneous

- electron gas, *Phys. Rev.* 137 (1965) A1441–A1443. doi:10.1103/PhysRev.137.A1441.
URL <https://link.aps.org/doi/10.1103/PhysRev.137.A1441>
- [259] N. N. Bogoljubov, V. V. Tolmachev, D. V. Åirkov, A new method in the theory of superconductivity, *Fortschritte der Physik* 6 (11-12) (1958) 605–682. doi:10.1002/prop.19580061102.
URL <http://dx.doi.org/10.1002/prop.19580061102>
- [260] F. Giustino, Electron-phonon interactions from first principles, *Rev. Mod. Phys.* 89 (2017) 015003. doi:10.1103/RevModPhys.89.015003.
URL <https://link.aps.org/doi/10.1103/RevModPhys.89.015003>
- [261] S. Y. Savrasov, D. Y. Savrasov, O. K. Andersen, Linear-response calculations of electron-phonon interactions, *Phys. Rev. Lett.* 72 (1994) 372–375. doi:10.1103/PhysRevLett.72.372.
URL <http://link.aps.org/doi/10.1103/PhysRevLett.72.372>
- [262] M. Lüders Ph.D. thesis, Density Functional Theory for Superconductors, A first Principles Approach to the SC Phase, Bayerische Julius-Maximilians Universität Würzburg, 1998.
URL www.physik.fu-berlin.de/~ag-gross/theses/lueders_phd.pdf
- [263] M. Marques Ph.D. thesis, Density Functional Theory for Superconductors, Exchange and Correlation Potentials for Inhomogeneous Systems, Bayerische Julius-Maximilians Universität Würzburg, 2000.
URL http://www.tddft.org/bmg/files/marques/marques_phd.pdf
- [264] A. Sanna, E. K. U. Gross, to be published.
- [265] R. Akashi, R. Arita, Density Functional Theory for Plasmon-Assisted Superconductivity, *Journal of the Physical Society of Japan* 83 (6) (2014) 061016. doi:10.7566/JPSJ.83.061016.
URL <http://journals.jps.jp/doi/abs/10.7566/JPSJ.83.061016>
- [266] F. Essenerberger, A. Sanna, P. Buczek, A. Ernst, L. Sandratskii, E. K. U. Gross, Ab initio, *Phys. Rev. B* 94 (2016) 014503. doi:10.1103/PhysRevB.94.014503.
URL <http://link.aps.org/doi/10.1103/PhysRevB.94.014503>
- [267] Y. Takada, Plasmon mechanism of superconductivity in two- and three-dimensional electron systems, *Journal of the Physical Society of Japan* 45 (3) (1978) 786–794. arXiv:<http://dx.doi.org/10.1143/JPSJ.45.786>. doi:10.1143/JPSJ.45.786.
URL <http://dx.doi.org/10.1143/JPSJ.45.786>
- [268] V. Radhakrishnan, Superconductivity in transition elements, *Physics Letters* 16 (1965) 247–248.
- [269] H. Rietschel, L. J. Sham, Role of electron Coulomb interaction in superconductivity, *Physical Review B* 28 (9) (1983) 5100–5108. doi:10.1103/PhysRevB.28.5100.
URL <http://link.aps.org/doi/10.1103/PhysRevB.28.5100>
- [270] H. Fröhlich, Superconductivity in metals with incomplete inner shells, *Journal of Physics C: Solid State Physics* 1 (2) (1968) 544.
- [271] R. Akashi, M. Kawamura, S. Tsuneyuki, Y. Nomura, R. Arita, First-principles study of the pressure and crystal-structure dependences of the superconducting transition temperature in compressed sulfur hydrides, *Phys. Rev. B* 91 (2015) 224513. doi:10.1103/PhysRevB.91.224513.
URL <https://link.aps.org/doi/10.1103/PhysRevB.91.224513>
- [272] J. C. Schön, M. Jansen, First step towards planning of syntheses in solid-state chemistry: determination of promising structure candidates by global optimization, *Angewandte Chemie International Edition in English* 35 (12) (1996) 1286–1304.
- [273] F. H. Stillinger, Exponential multiplicity of inherent structures, *Physical Review E* 59 (1) (1999) 48.
- [274] D. Wales, Energy landscapes: Applications to clusters, biomolecules and glasses, Cambridge University Press, 2003.
- [275] C. J. Pickard, Hyperspatial optimization of structures, *Physical Review B* 99 (5) (2019) 054102.
- [276] C. J. Pickard, R. J. Needs, High-pressure phases of silane, *Phys. Rev. Lett.* 97 (2006) 045504. doi:10.1103/PhysRevLett.97.045504.
URL <https://link.aps.org/doi/10.1103/PhysRevLett.97.045504>
- [277] C. J. Pickard, R. Needs, Ab initio random structure searching, *Journal of Physics: Condensed Matter* 23 (5) (2011) 053201.
- [278] C. J. Pickard, R. J. Needs, Structure of phase iii of solid hydrogen, *Nature Physics* 3 (7) (2007) 473.
- [279] C. J. Pickard, R. Needs, Aluminium at terapascal pressures, *Nature materials* 9 (8) (2010) 624.
- [280] C. J. Pickard, R. Needs, Highly compressed ammonia forms an ionic crystal, *Nature materials* 7 (10) (2008) 775.
- [281] R. J. Needs, C. J. Pickard, Perspective: Role of structure prediction in materials discovery and design, *APL Materials* 4 (5) (2016) 053210.
- [282] M. Segall, P. J. Lindan, M. a. Probert, C. J. Pickard, P. J. Hasnip, S. Clark, M. Payne, First-principles simulation: ideas, illustrations and the castep code, *Journal of Physics: Condensed Matter* 14 (11) (2002) 2717.
- [283] R. Eberhart, J. Kennedy, A new optimizer using particle swarm theory, in: *Micro Machine and Human Science, 1995. MHS'95., Proceedings of the Sixth International Symposium on*, IEEE, 1995, pp. 39–43.
- [284] Y. Wang, J. Lv, L. Zhu, Y. Ma, Calypso: A method for crystal structure prediction, *Computer Physics Communications* 183 (10) (2012) 2063–2070.
- [285] Y. Wang, J. Lv, L. Zhu, Y. Ma, Crystal structure prediction via particle-swarm optimization, *Physical Review B* 82 (9) (2010) 094116.
- [286] J. Lv, Y. Wang, L. Zhu, Y. Ma, Particle-swarm structure prediction on clusters, *The Journal of Chemical Physics* 137 (8) (2012) 084104.
- [287] X. Zhang, Y. Wang, J. Lv, C. Zhu, Q. Li, M. Zhang, Q. Li, Y. Ma, First-principles structural design of superhard materials, *The Journal of chemical physics* 138 (11) (2013) 114101.
- [288] S. Lu, Y. Wang, H. Liu, M.-s. Miao, Y. Ma, Self-assembled ultrathin nanotubes on diamond (100) surface, *Nature communications* 5 (2014) 3666.
- [289] P. Gao, Q. Tong, J. Lv, Y. Wang, Y. Ma, X-ray diffraction data-assisted structure searches, *Computer Physics Communications* 213 (2017) 40–45.
- [290] J. Shi, W. Cui, J. A. Flores-Livas, A. San-Miguel, S. Botti, M. A. Marques, Investigation of new phases in the ba–si phase diagram under high pressure using ab initio structural search, *Physical Chemistry Chemical Physics* 18 (11) (2016) 8108–8114.
- [291] C. Su, J. Lv, Q. Li, H. Wang, L. Zhang, Y. Wang, Y. Ma, Construction of crystal structure prototype database: methods and applications, *Journal of Physics: Condensed Matter* 29 (16) (2017) 165901.
- [292] Q. Tong, L. Xue, J. Lv, Y. Wang, Y. Ma, Accelerating calypso structure prediction by data-driven learning of potential energy surface, *Faraday Discussions*.
- [293] L. Zhu, Z. Wang, Y. Wang, G. Zou, H.-k. Mao, Y. Ma, Spiral chain o4 form of dense oxygen, *Proceedings of the National Academy of Sciences* 109 (3) (2012) 751–753.
- [294] V. N. Robinson, Y. Wang, Y. Ma, A. Hermann, Stabilization of ammonia-rich hydrate inside icy planets, *Proceedings of the National Academy of Sciences* 114 (34) (2017) 9003–9008.
- [295] H. Wang, S. T. John, K. Tanaka, T. Iitaka, Y. Ma, Superconductive sodalite-like clathrate calcium hydride at high pressures, *Proceedings of the National Academy of Sciences* 109 (17) (2012) 6463–6466.
- [296] X. Ye, N. Zarifi, E. Zurek, R. Hoffmann, N. W. Ashcroft, High hydrides of scandium under pressure: Potential superconductors, *The Journal of Physical Chemistry C* 122 (11) (2018) 6298–6309.
- [297] S. Zhang, J. Lin, Y. Wang, G. Yang, A. Bergara, Y. Ma, Nonmetallic feh6 under high pressure, *The Journal of Physical Chemistry C*.
- [298] C. W. Glass, A. R. Oganov, N. Hansen, Uspexevolutionary crystal structure prediction, *Computer physics communications* 175 (11-12) (2006) 713–720.
- [299] A. R. Oganov, Modern methods of crystal structure prediction, John Wiley & Sons, 2011.
- [300] A. R. Oganov, C. W. Glass, Crystal structure prediction using ab initio evolutionary techniques: Principles and applications, *The Journal of chemical physics* 124 (24) (2006) 244704.
- [301] A. R. Oganov, C. W. Glass, Evolutionary crystal structure prediction as a tool in materials design, *Journal of Physics: Condensed Matter* 20 (6) (2008) 064210.
- [302] I. Kruglov, R. Akashi, S. Yoshikawa, A. R. Oganov, M. M. D. Esfahani,

- Refined phase diagram of the Hf system with high- T_c superconductivity, *Physical Review B* 96 (22) (2017) 220101.
- [303] Y. Ma, A. R. Oganov, Y. Xie, High-pressure structures of lithium, potassium, and rubidium predicted by an *ab initio* evolutionary algorithm, *Physical Review B* 78 (1) (2008) 014102.
- [304] P. Zaleski-Ejgierd, R. Hoffmann, N. Ashcroft, High pressure stabilization and emergent forms of PbH_4 , *Physical review letters* 107 (3) (2011) 037002.
- [305] A. O. Lyakhov, A. R. Oganov, H. T. Stokes, Q. Zhu, New developments in evolutionary structure prediction algorithm uspx, *Computer Physics Communications* 184 (4) (2013) 1172–1182.
- [306] A. Oganov, G. Saleh, A. Kvashnin, *Computational Materials Discovery*, Royal Society of Chemistry, 2018.
- [307] M. Martinez-Canales, A. R. Oganov, Y. Ma, Y. Yan, A. O. Lyakhov, A. Bergara, Novel structures and superconductivity of silane under pressure, *Physical review letters* 102 (8) (2009) 087005.
- [308] Y. Ma, M. Eremets, A. R. Oganov, Y. Xie, I. Trojan, S. Medvedev, A. O. Lyakhov, M. Valle, V. Prakapenka, Transparent dense sodium, *Nature* 458 (7235) (2009) 182.
- [309] D. Duan, X. Huang, F. Tian, D. Li, H. Yu, Y. Liu, Y. Ma, B. Liu, T. Cui, Pressure-induced decomposition of solid hydrogen sulfide, *Physical Review B* 91 (18) (2015) 180502.
- [310] I. A. Kruglov, e. a. Semenok, Superconductivity in LaH_{10} : a new twist of the story, *arXiv preprint arXiv:1810.01113*.
- [311] D. C. Lonie, E. Zurek, Identifying duplicate crystal structures: Xtalcomp, an open-source solution, *Computer Physics Communications* 183 (3) (2012) 690–697.
- [312] D. C. Lonie, E. Zurek, Xtalopt: An open-source evolutionary algorithm for crystal structure prediction, *Computer Physics Communications* 182 (2) (2011) 372–387.
- [313] P. Avery, Z. Falls, E. Zurek, Xtalopt version r10: An open-source evolutionary algorithm for crystal structure prediction, *Computer Physics Communications* 217 (2017) 210–211.
- [314] N. Zarifi, T. Bi, H. Liu, E. Zurek, Crystal structures and properties of iron hydrides at high pressure, *The Journal of Physical Chemistry C* 122 (42) (2018) 24262–24269.
- [315] A. K. Mishra, T. Muramatsu, H. Liu, Z. M. Geballe, M. Somayazulu, M. Ahart, M. Baldini, Y. Meng, E. Zurek, R. J. Hemley, New calcium hydrides with mixed atomic and molecular hydrogen, *The Journal of Physical Chemistry C* 122 (34) (2018) 19370–19378.
- [316] X. Gonze, B. Amadon, P.-M. Anglade, J.-M. Beuken, F. Bottin, P. Boulanger, F. Bruneval, D. Caliste, R. Caracas, M. Côté, et al., Abinit: First-principles approach to material and nanosystem properties, *Computer Physics Communications* 180 (12) (2009) 2582–2615.
- [317] S. Goedecker, Minima hopping: An efficient search method for the global minimum of the potential energy surface of complex molecular systems, *The Journal of Chemical Physics* 120 (21) (2004) 9911.
- [318] S. Goedecker, W. Hellmann, T. Lenosky, Global Minimum Determination of the Born-Oppenheimer Surface within Density Functional Theory, *Phys. Rev. Lett.* 95 (5) (2005) 055501.
- [319] E. Bitzek, P. Koskinen, F. Gähler, M. Moseler, P. Gumbsch, Structural relaxation made simple, *Phys. Rev. Lett.* 97 (2006) 170201. doi:10.1103/PhysRevLett.97.170201. URL <http://link.aps.org/doi/10.1103/PhysRevLett.97.170201>
- [320] M. Amsler, S. Goedecker, Crystal structure prediction using the minima hopping method, *The Journal of Chemical Physics* 133 (22) (2010) 224104.
- [321] M. Amsler, Crystal structure prediction based on density functional theory, Ph.D. thesis, University of Basel (2012).
- [322] F. Jensen, *Introduction to computational chemistry*, John Wiley & sons, 2017.
- [323] M. Amsler, Minima hopping method for predicting complex structures and chemical reaction pathways, *Handbook of Materials Modeling: Applications: Current and Emerging Materials* (2018) 1–20.
- [324] M. Amsler, S. S. Naghavi, C. Wolverton, Prediction of superconducting iron-bismuth intermetallic compounds at high pressure, *Chemical science* 8 (3) (2017) 2226–2234.
- [325] S. M. Clarke, M. Amsler, J. P. Walsh, T. Yu, Y. Wang, Y. Meng, S. D. Jacobsen, C. Wolverton, D. E. Freedman, Creating binary Cu-Bi compounds via high-pressure synthesis: a combined experimental and theoretical study, *Chemistry of Materials* 29 (12) (2017) 5276–5285.
- [326] M. Amsler, Thermodynamics and superconductivity of SxSe1-xH3 , *Physical Review B* 99 (6) (2019) 060102.
- [327] M. Amsler, L. Ward, V. I. Hegde, M. G. Goesten, X. Yi, C. Wolverton, Ternary mixed-anion semiconductors with tunable band gaps from machine-learning and crystal structure prediction, *arXiv preprint arXiv:1812.02708*.
- [328] J. He, S. S. Naghavi, V. I. Hegde, M. Amsler, C. Wolverton, Designing and discovering a new family of semiconducting quaternary heusler compounds based on the 18-electron rule, *Chemistry of Materials* 30 (15) (2018) 4978–4985.
- [329] A. Y. Liu, M. L. Cohen, Structural properties and electronic structure of low-compressibility materials: $\beta\text{-Si}_3\text{N}_4$ and hypothetical $\beta\text{-C}_3\text{N}_4$, *Phys. Rev. B* 41 (1990) 10727–10734. doi:10.1103/PhysRevB.41.10727. URL <https://link.aps.org/doi/10.1103/PhysRevB.41.10727>
- [330] J. Pannetier, J. Bassas-Alsina, J. Rodriguez-Carvajal, V. Caignaert, Prediction of crystal structures from crystal chemistry rules by simulated annealing, *Nature* 346 (6282) (1990) 343.
- [331] S. Tsuneyuki, M. Tsukada, H. Aoki, Y. Matsui, First-principles interatomic potential of silica applied to molecular dynamics, *Phys. Rev. Lett.* 61 (1988) 869–872. doi:10.1103/PhysRevLett.61.869. URL <https://link.aps.org/doi/10.1103/PhysRevLett.61.869>
- [332] S. Kirkpatrick, C. D. Gelatt, M. P. Vecchi, Optimization by simulated annealing, *science* 220 (4598) (1983) 671–680.
- [333] V. Černý, Thermodynamical approach to the traveling salesman problem: An efficient simulation algorithm, *Journal of optimization theory and applications* 45 (1) (1985) 41–51.
- [334] P. Van Laarhoven, *Simulated annealing*/pjm van laarhoven, ehl aarts, Theory and Applications.—Dordrecht.—Springer.
- [335] K. Doll, J. Schön, M. Jansen, Global exploration of the energy landscape of solids on the *ab initio* level, *Physical Chemistry Chemical Physics* 9 (46) (2007) 6128–6133.
- [336] J. C. Schön, K. Doll, M. Jansen, Predicting solid compounds via global exploration of the energy landscape of solids on the *ab initio* level without recourse to experimental information, *physica status solidi (b)* 247 (1) (2010) 23–39.
- [337] D. Zagorac, K. Doll, J. Schön, M. Jansen, *Ab initio* structure prediction for lead sulfide at standard and elevated pressures, *Physical Review B* 84 (4) (2011) 045206.
- [338] S. Curtarolo, G. L. Hart, M. B. Nardelli, N. Mingo, S. Sanvito, O. Levy, The high-throughput highway to computational materials design, *Nature materials* 12 (3) (2013) 191.
- [339] J. R. Hatrick-Simpers, J. M. Gregoire, A. G. Kusne, Perspective: Composition–structure–property mapping in high-throughput experiments: Turning data into knowledge, *APL Materials* 4 (5) (2016) 053211.
- [340] H. Glawe, A. Sanna, E. Gross, M. A. Marques, The optimal one dimensional periodic table: a modified pettifor chemical scale from data mining, *New Journal of Physics* 18 (9) (2016) 093011.
- [341] S. P. Ong, W. D. Richards, A. Jain, G. Hautier, M. Kocher, S. Cholia, D. Gunter, V. L. Chevrier, K. A. Persson, G. Ceder, Python materials genomics (pymatgen): A robust, open-source python library for materials analysis, *Computational Materials Science* 68 (2013) 314–319.
- [342] C. C. Fischer, K. J. Tibbetts, D. Morgan, G. Ceder, Predicting crystal structure by merging data mining with quantum mechanics, *Nature materials* 5 (8) (2006) 641.
- [343] M. Amsler, V. I. Hegde, S. D. Jacobsen, C. Wolverton, Exploring the high-pressure materials genome, *Phys. Rev. X* 8 (2018) 041021. doi:10.1103/PhysRevX.8.041021. URL <https://link.aps.org/doi/10.1103/PhysRevX.8.041021>
- [344] W. Sun, S. T. Dacek, S. P. Ong, G. Hautier, A. Jain, W. D. Richards, A. C. Gamst, K. A. Persson, G. Ceder, The thermodynamic scale of inorganic crystalline metastability, *Science advances* 2 (11) (2016) e1600225.
- [345] M. Aykol, S. S. Dwaraknath, W. Sun, K. A. Persson, Thermodynamic limit for synthesis of metastable inorganic materials, *Science advances* 4 (4) (2018) eaq0148.
- [346] K. Lejaeghere, G. Bihlmayer, T. Björkman, P. Blaha, S. Blügel, V. Blum, D. Caliste, I. E. Castelli, S. J. Clark, A. Dal Corso, et al., Reproducibility

- in density functional theory calculations of solids, *Science* 351 (6280) (2016) aad3000.
- [347] List of quantum chemistry and solid-state physics software, https://en.wikipedia.org/wiki/List_of_quantum_chemistry_and_solid-state_physics_software, accessed: 2019-02-21.
- [348] J. D. Gale, A. L. Rohl, The general utility lattice program (gulp), *Molecular Simulation* 29 (5) (2003) 291–341.
- [349] J. D. Gale, Gulp: A computer program for the symmetry-adapted simulation of solids, *J. Chem. Soc., Faraday Trans. 93* (1997) 629–637. doi:10.1039/A606455H. URL <http://dx.doi.org/10.1039/A606455H>
- [350] S. Plimpton, Fast parallel algorithms for short-range molecular dynamics, *Journal of Computational Physics* 117 (1) (1995) 1 – 19. doi: <https://doi.org/10.1006/jcph.1995.1039>. URL <http://www.sciencedirect.com/science/article/pii/S002199918571039X>
- [351] M. Elstner, D. Porezag, G. Jungnickel, J. Elsner, M. Haugk, T. Frauenheim, S. Suhai, G. Seifert, Self-consistent-charge density-functional tight-binding method for simulations of complex materials properties, *Phys. Rev. B* 58 (1998) 7260–7268. doi:10.1103/PhysRevB.58.7260. URL <https://link.aps.org/doi/10.1103/PhysRevB.58.7260>
- [352] L. Genovese, A. Neelov, S. Goedecker, T. Deutsch, S. A. Ghasemi, A. Willand, D. Caliste, O. Zilberberg, M. Rayson, A. Bergman, et al., Daubechies wavelets as a basis set for density functional pseudopotential calculations, *The Journal of chemical physics* 129 (1) (2008) 014109.
- [353] O. K. Andersen, Linear methods in band theory, *Phys. Rev. B* 12 (1975) 3060–3083. doi:10.1103/PhysRevB.12.3060. URL <https://link.aps.org/doi/10.1103/PhysRevB.12.3060>
- [354] A. Gulans, A. Kozhevnikov, C. Draxl, Microhartree precision in density functional theory calculations, *Phys. Rev. B* 97 (2018) 161105. doi:10.1103/PhysRevB.97.161105. URL <https://link.aps.org/doi/10.1103/PhysRevB.97.161105>
- [355] S. R. Jensen, S. Saha, J. A. Flores-Livas, W. Huhn, V. Blum, S. Goedecker, L. Frediani, The elephant in the room of density functional theory calculations, *The journal of physical chemistry letters* 8 (7) (2017) 1449–1457.
- [356] M. Van Setten, M. Giantomassi, E. Bousquet, M. J. Verstraete, D. R. Hamann, X. Gonze, G.-M. Rignanese, The pseudodojo: Training and grading a 85 element optimized norm-conserving pseudopotential table, *Computer Physics Communications* 226 (2018) 39–54.
- [357] G. Prandini, A. Marrazzo, I. E. Castelli, N. Mounet, N. Marzari, Precision and efficiency in solid-state pseudopotential calculations, *npj Computational Materials* 4 (1) (2018) 72.
- [358] H. J. Monkhorst, J. D. Pack, Special points for brillouin-zone integrations, *Phys. Rev. B* 13 (1976) 5188–5192. doi:10.1103/PhysRevB.13.5188. URL <https://link.aps.org/doi/10.1103/PhysRevB.13.5188>
- [359] X. Gonze, F. Jollet, F. A. Araujo, D. Adams, B. Amadon, T. Applencourt, C. Audouze, J.-M. Beuken, J. Bieder, A. Bokhanchuk, et al., Recent developments in the abinit software package, *Computer Physics Communications* 205 (2016) 106–131.
- [360] P. Giannozzi, O. Andreussi, T. Brumme, O. Bunau, M. B. Nardelli, M. Calandra, R. Car, C. Cavazzoni, D. Ceresoli, M. Cococcioni, et al., Advanced capabilities for materials modelling with quantum espresso, *Journal of Physics: Condensed Matter* 29 (46) (2017) 465901.
- [361] G. Kresse, J. Furthmüller, Efficiency of ab-initio total energy calculations for metals and semiconductors using a plane-wave basis set, *Comput. Mat. Sci.* 6 (1996) 15–50.
- [362] L. E. Ratcliff, A. Degomme, J. A. Flores-Livas, S. Goedecker, L. Genovese, Affordable and accurate large-scale hybrid-functional calculations on gpu-accelerated supercomputers, *Journal of Physics: Condensed Matter* 30 (9) (2018) 095901.
- [363] K. T. Butler, D. W. Davies, H. Cartwright, O. Isayev, A. Walsh, Machine learning for molecular and materials science, *Nature* 559 (7715) (2018) 547.
- [364] L. Ward, C. Wolverton, Atomistic calculations and materials informatics: A review, *Current Opinion in Solid State and Materials Science* 21 (3) (2017) 167–176.
- [365] T. Mueller, A. G. Kusne, R. Ramprasad, Machine learning in materials science: Recent progress and emerging applications, *Reviews in Computational Chemistry* 29 (2016) 186–273.
- [366] A. Seko, A. Togo, I. Tanaka, Descriptors for machine learning of materials data, in: *Nanoinformatics*, Springer, Singapore, 2018, pp. 3–23.
- [367] Y. LeCun, Y. Bengio, G. Hinton, Deep learning, *nature* 521 (7553) (2015) 436.
- [368] T. Xie, J. C. Grossman, Crystal graph convolutional neural networks for an accurate and interpretable prediction of material properties, *Physical review letters* 120 (14) (2018) 145301.
- [369] K. Ryan, J. Lengyel, M. Shatruk, Crystal structure prediction via deep learning, *Journal of the American Chemical Society* 140 (32) (2018) 10158–10168.
- [370] J. Behler, Perspective: Machine learning potentials for atomistic simulations, *The Journal of chemical physics* 145 (17) (2016) 170901.
- [371] E. V. Podryabinkin, E. V. Tikhonov, A. V. Shapeev, A. R. Oganov, Accelerating crystal structure prediction by machine-learning interatomic potentials with active learning, *Physical Review B* 99 (6) (2019) 064114.
- [372] F. Faber, A. Lindmaa, O. A. von Lilienfeld, R. Armiento, Crystal structure representations for machine learning models of formation energies, *International Journal of Quantum Chemistry* 115 (16) (2015) 1094–1101.
- [373] W. Ye, C. Chen, Z. Wang, I.-H. Chu, S. P. Ong, Deep neural networks for accurate predictions of crystal stability, *Nature communications* 9 (1) (2018) 3800.
- [374] O. Isayev, C. Oses, C. Toher, E. Gossett, S. Curtarolo, A. Tropsha, Universal fragment descriptors for predicting properties of inorganic crystals, *Nature Communications* 8 (2017) 15679 EP–. URL <https://doi.org/10.1038/ncomms15679>
- [375] M. Klintonberg, O. Eriksson, Possible high-temperature superconductors predicted from electronic structure and data-filtering algorithms, *Computational materials science* 67 (2013) 282–286.
- [376] T. O. Owolabi, K. O. Akande, S. O. Olatunji, Estimation of superconducting transition temperature T_c for superconductors of the doped mgb 2 system from the crystal lattice parameters using support vector regression, *Journal of Superconductivity and Novel Magnetism* 28 (1) (2015) 75–81.
- [377] M. Norman, Materials design for new superconductors, *Reports on Progress in Physics* 79 (7) (2016) 074502.
- [378] V. Stanev, C. Oses, A. G. Kusne, E. Rodriguez, J. Paglione, S. Curtarolo, I. Takeuchi, Machine learning modeling of superconducting critical temperature, *npj Computational Materials* 4 (1) (2018) 29.
- [379] P. Mehta, M. Bukov, C.-H. Wang, A. G. Day, C. Richardson, C. K. Fisher, D. J. Schwab, A high-bias, low-variance introduction to machine learning for physicists, *Physics Reports*.
- [380] P. Ball, Material witness: Metallic hydrogen in the spotlight, *Nature materials* 16 (3) (2017) 288.
- [381] J. Hopfield, Angular momentum and transition-metal superconductivity, *Phys. Rev.* 186 (1969) 443.
- [382] W. M. Mueller, J. P. Blackledge, G. G. Libowitz, Metal hydrides, Academic Press, N. Y., 1968.
- [383] E. G. Maksimov, O. A. Pankratov, Hydrogen in metals, *Soviet Physics Uspekhi* 18 (7) (1975) 481–495. doi:10.1070/pu1975v018n07abeh004890. URL <https://doi.org/10.1070/pu1975v018n07abeh004890>
- [384] C. B. Satterthwaite, I. L. Toepke, Superconductivity of hydrides and deuterides of thorium, *Phys. Rev. Lett.* 25 (1970) 741–743. doi:10.1103/PhysRevLett.25.741. URL <https://link.aps.org/doi/10.1103/PhysRevLett.25.741>
- [385] M. Dietrich, W. Gey, H. Rietschel, C. Satterthwaite, Pressure dependence of the superconducting transition temperature of th4h15, *Solid State Communications* 15 (5) (1974) 941–943.
- [386] T. Skoskiewicz, Superconductivity in the palladium-hydrogen and palladium-nickel-hydrogen systems, *physica status solidi (a)* 11 (2) (1972) K123–K126. arXiv:<https://onlinelibrary.wiley.com/doi/pdf/10.1002/pssa.2210110253>, doi:10.1002/pssa.2210110253. URL <https://onlinelibrary.wiley.com/doi/abs/10.1002/pssa.2210110253>
- [387] B. Stritzker, W. Buckel, Superconductivity in the palladium-hydrogen

- and the palladium-deuterium systems, *Zeitschrift für Physik A Hadrons and nuclei* 257 (1) (1972) 1–8. doi:10.1007/BF01398191. URL <https://doi.org/10.1007/BF01398191>
- [388] H. Oesterreicher, J. Clinton, H. Bittner, Studies of hydride formation and superconductivity in hydrides of th and pd compounds, *Journal of Solid State Chemistry France* 16 (1976) 209–210.
- [389] B. Stritzker, High superconducting transition temperatures in the palladium-noble metal-hydrogen system, *Zeitschrift für Physik* 268 (2) (1974) 261–264. doi:10.1007/BF01669889. URL <https://doi.org/10.1007/BF01669889>
- [390] P. Duffer, D. M. Gualtieri, V. U. S. Rao, Pronounced isotope effect in the superconductivity of hfv₂ containing hydrogen (deuterium), *Phys. Rev. Lett.* 37 (1976) 1410–1413. doi:10.1103/PhysRevLett.37.1410. URL <https://link.aps.org/doi/10.1103/PhysRevLett.37.1410>
- [391] J. M. Welter, F. J. Johnen, Superconducting transition temperature and low temperature resistivity in the niobium-hydrogen system, *Zeitschrift für Physik B Condensed Matter* 27 (3) (1977) 227–232. doi:10.1007/BF01325532. URL <https://doi.org/10.1007/BF01325532>
- [392] E. Ponyatovskii, I. Bashkin, New phase transitions in hydrides of the ia, iii-a, and iv-a group metals, *Zeitschrift für Physikalische Chemie* 146 (2) (1985) 137–157.
- [393] E. Y. Tonkov, *Compounds and alloys under high pressure: a handbook*, CRC Press, 1998.
- [394] I. I. Mazin, Superconductivity: Extraordinarily conventional, *Nature* 525 (7567) (2015) 40–41.
- [395] A. Zunger, Beware of plausible predictions of fantasy materials (2019).
- [396] B. Militzer, H. F. Wilson, New phases of water ice predicted at megabar pressures, *Phys. Rev. Lett.* 105 (2010) 195701. doi:10.1103/PhysRevLett.105.195701. URL <https://link.aps.org/doi/10.1103/PhysRevLett.105.195701>
- [397] J. M. McMahon, Ground-state structures of ice at high pressures from ab initio random structure searching, *Phys. Rev. B* 84 (2011) 220104. doi:10.1103/PhysRevB.84.220104. URL <https://link.aps.org/doi/10.1103/PhysRevB.84.220104>
- [398] S. Zhang, H. F. Wilson, K. P. Driver, B. Militzer, H₄O and other hydrogen-oxygen compounds at giant-planet core pressures, *Phys. Rev. B* 87 (2013) 024112. doi:10.1103/PhysRevB.87.024112. URL <https://link.aps.org/doi/10.1103/PhysRevB.87.024112>
- [399] C. J. Pickard, M. Martinez-Canales, R. J. Needs, Decomposition and terapascal phases of water ice, *Phys. Rev. Lett.* 110 (2013) 245701. doi:10.1103/PhysRevLett.110.245701. URL <https://link.aps.org/doi/10.1103/PhysRevLett.110.245701>
- [400] T. Bartels-Rausch, V. Bergeron, J. H. E. Cartwright, R. Escribano, J. L. Finney, H. Grothe, P. J. Gutiérrez, J. Haapala, W. F. Kuhs, J. B. C. Pettersson, S. D. Price, C. I. Sainz-Díaz, D. J. Stokes, G. Strazzulla, E. S. Thomson, H. Trinks, N. Uras-Aytemiz, Ice structures, patterns, and processes: A view across the icefields, *Rev. Mod. Phys.* 84 (2012) 885–944. doi:10.1103/RevModPhys.84.885. URL <https://link.aps.org/doi/10.1103/RevModPhys.84.885>
- [401] C. Donnerer, T. Scheler, E. Gregoryanz, High-pressure synthesis of noble metal hydrides, *The Journal of chemical physics* 138 (13) (2013) 134507.
- [402] M. I. Erements, V. V. Struzhkin, H.-k. Mao, R. J. Hemley, Exploring superconductivity in low-z materials at megabar pressures, *Physica B: Condensed Matter* 329 (2003) 1312–1316.
- [403] Y. Wang, X. Zhang, S. Jiang, Z. M. Geballe, T. Pakornchote, M. Somayazulu, V. B. Prakapenka, E. Greenberg, A. F. Goncharov, Helium-hydrogen immiscibility at high pressures, *The Journal of Chemical Physics* 150 (11) (2019) 114504. doi:10.1063/1.5086270. URL <https://doi.org/10.1063/1.5086270>
- [404] C. Pépin, P. Loubeyre, F. Occelli, P. Dumas, Synthesis of lithium polyhydrides above 130 gpa at 300 k, *Proceedings of the National Academy of Sciences* 112 (25) (2015) 7673–7676. arXiv:<http://www.pnas.org/content/112/25/7673.full.pdf>, doi:10.1073/pnas.1507508112. URL <http://www.pnas.org/content/112/25/7673>
- [405] V. V. Struzhkin, D. Y. Kim, E. Stavrou, T. Muramatsu, H.-k. Mao, C. J. Pickard, R. J. Needs, V. B. Prakapenka, A. F. Goncharov, Synthesis of sodium polyhydrides at high pressures, *Nature Communications* 7 (2016) 12267 EP–, article. URL <http://dx.doi.org/10.1038/ncomms12267>
- [406] E. Ponyatovsky, O. Barkalov, Pressureinduced amorphous phases, *Materials Science Reports* 8 (4) (1992) 147–191.
- [407] A. Goncharov, V. Struzhkin, M. Somayazulu, R. Hemley, H. Mao, Compression of ice to 210 gigapascals: Infrared evidence for a symmetric hydrogen-bonded phase, *Science* 273 (5272) (1996) 218–220.
- [408] I. Goncharenko, M. I. Erements, M. Hanfland, J. S. Tse, M. Amboage, Y. Yao, I. A. Trojan, Pressure-induced hydrogen-dominant metallic state in aluminum hydride, *Phys. Rev. Lett.* 100 (2008) 045504. doi:10.1103/PhysRevLett.100.045504. URL <https://link.aps.org/doi/10.1103/PhysRevLett.100.045504>
- [409] C. M. Pépin, A. Dewaele, G. Geneste, P. Loubeyre, M. Mezouar, New iron hydrides under high pressure, *Phys. Rev. Lett.* 113 (2014) 265504. doi:10.1103/PhysRevLett.113.265504. URL <https://link.aps.org/doi/10.1103/PhysRevLett.113.265504>
- [410] C. M. Pépin, G. Geneste, A. Dewaele, M. Mezouar, P. Loubeyre, Synthesis of feh5: A layered structure with atomic hydrogen slabs, *Science* 357 (6349) (2017) 382–385. doi:10.1126/science.aan0961. URL <http://science.sciencemag.org/content/357/6349/382>
- [411] L. B. Christoph Heil, Giovanni B. Bachelet, No superconductivity in iron polyhydrides at high pressures, arXiv preprint, arXiv:1804.03572. URL arXiv:1804.03572
- [412] T. Meier, F. Trybel, S. Khandarkhaeva, G. Steinle-Neumann, S. Chariton, T. Fedotenko, S. Petitgirard, M. Hanfland, K. Glazyrin, N. Dubrovinskaia, et al., Pressure induced hydrogen-hydrogen interaction in metallic feh revealed by nmr, arXiv preprint arXiv:1902.03182.
- [413] C. Heil, G. B. Bachelet, L. Boeri, Absence of superconductivity in iron polyhydrides at high pressures, *Phys. Rev. B* 97 (2018) 214510. doi:10.1103/PhysRevB.97.214510. URL <https://link.aps.org/doi/10.1103/PhysRevB.97.214510>
- [414] M. Wang, J. Binns, M.-E. Donnelly, M. Peña-Alvarez, P. Dalladay-Simpson, R. T. Howie, High pressure synthesis and stability of cobalt hydrides, *The Journal of chemical physics* 148 (14) (2018) 144310.
- [415] J. Binns, M.-E. Donnelly, M. Wang, A. Hermann, E. Gregoryanz, P. Dalladay-Simpson, R. T. Howie, Synthesis of ni₂h₃ at high temperatures and pressures, *Phys. Rev. B* 98 (2018) 140101. doi:10.1103/PhysRevB.98.140101. URL <https://link.aps.org/doi/10.1103/PhysRevB.98.140101>
- [416] J. Ying, H. Liu, E. Greenberg, V. B. Prakapenka, V. V. Struzhkin, Synthesis of new nickel hydrides at high pressure, *Phys. Rev. Materials* 2 (2018) 085409. doi:10.1103/PhysRevMaterials.2.085409. URL <https://link.aps.org/doi/10.1103/PhysRevMaterials.2.085409>
- [417] X.-J. Chen, J.-L. Wang, V. V. Struzhkin, H.-k. Mao, R. J. Hemley, H.-Q. Lin, Superconducting behavior in compressed solid sih₄ with a layered structure, *Phys. Rev. Lett.* 101 (2008) 077002. doi:10.1103/PhysRevLett.101.077002. URL <https://link.aps.org/doi/10.1103/PhysRevLett.101.077002>
- [418] T. A. Strobel, A. F. Goncharov, C. T. Seagle, Z. Liu, M. Somayazulu, V. V. Struzhkin, R. J. Hemley, High-pressure study of silane to 150 gpa, *Phys. Rev. B* 83 (2011) 144102. doi:10.1103/PhysRevB.83.144102. URL <https://link.aps.org/doi/10.1103/PhysRevB.83.144102>
- [419] J. Binns, M. Peña-Alvarez, M.-E. Donnelly, E. Gregoryanz, R. T. Howie, P. Dalladay-Simpson, Structural studies on the cu-h system under compression, *Engineering*.
- [420] X. Zhang, W. Xu, Y. Wang, S. Jiang, F. A. Gorelli, E. Greenberg, V. B. Prakapenka, A. F. Goncharov, Synthesis and properties of

- selenium trihydride at high pressures, *Phys. Rev. B* 97 (2018) 064107. doi:10.1103/PhysRevB.97.064107. URL <https://link.aps.org/doi/10.1103/PhysRevB.97.064107>
- [421] G. Liu, S. Besedin, A. Irodova, H. Liu, G. Gao, M. Eremets, X. Wang, Y. Ma, Nb-h system at high pressures and temperatures, *Phys. Rev. B* 95 (2017) 104110. doi:10.1103/PhysRevB.95.104110. URL <https://link.aps.org/doi/10.1103/PhysRevB.95.104110>
- [422] B. Li, Y. Ding, D. Y. Kim, R. Ahuja, G. Zou, H.-K. Mao, Rhodium dihydride (rh2) with high volumetric hydrogen density, *Proceedings of the National Academy of Sciences* 108 (46) (2011) 18618–18621.
- [423] J. Binns, P. Dalladay-Simpson, M. Wang, G. J. Ackland, E. Gregoryanz, R. T. Howie, Formation of h₂-rich iodine-hydrogen compounds at high pressure, *Phys. Rev. B* 97 (2018) 024111. doi:10.1103/PhysRevB.97.024111. URL <https://link.aps.org/doi/10.1103/PhysRevB.97.024111>
- [424] M. A. Kuzovnikov, M. Tkacz, H. Meng, D. I. Kapustin, V. I. Kulakov, High-pressure synthesis of tantalum dihydride, *Phys. Rev. B* 96 (2017) 134120. doi:10.1103/PhysRevB.96.134120. URL <https://link.aps.org/doi/10.1103/PhysRevB.96.134120>
- [425] N. P. Salke, M. Esfahani, Y. Zhang, I. A. Kruglov, J. Zhou, Y. Wang, E. Greenberg, V. B. Prakapenka, A. R. Oganov, J.-F. Lin, Synthesis of clathrate cerium superhydride ceh9 at 80 gpa with anomalously short hh distance, *arXiv preprint arXiv:1805.02060*.
- [426] T. Matsuoka, H. Fujihisa, N. Hirao, Y. Ohishi, T. Mitsui, R. Masuda, M. Seto, Y. Yoda, K. Shimizu, A. Machida, K. Aoki, Structural and valence changes of europium hydride induced by application of high-pressure h₂, *Phys. Rev. Lett.* 107 (2011) 025501. doi:10.1103/PhysRevLett.107.025501. URL <https://link.aps.org/doi/10.1103/PhysRevLett.107.025501>
- [427] H. Oesterreicher, J. Clinton, H. Bittner, Hydrides of la-ni compounds, *Materials Research Bulletin* 11 (10) (1976) 1241–1247.
- [428] H. Meng, M. Kuzovnikov, M. Tkacz, Phase stability of some rare earth trihydrides under high pressure, *International Journal of Hydrogen Energy* 42 (49) (2017) 29344 – 29349. doi:<https://doi.org/10.1016/j.ijhydene.2017.10.067>. URL <http://www.sciencedirect.com/science/article/pii/S0360319917340442>
- [429] P.-H. Chang, S. Silayi, D. Papaconstantopoulos, M. Mehl, Pressure-induced high temperature superconductivity in h3x (x= as, se, br, sb, te and i), *arXiv preprint arXiv:1903.03255*.
- [430] P. Sennikov, Weak hydrogen-bonding by second-row (ph3, h2s) and third-row (ash3, h2se) hydrides, *The Journal of Physical Chemistry* 98 (19) (1994) 4973–4981.
- [431] K. Abe, N. W. Ashcroft, Stabilization and highly metallic properties of heavy group-v hydrides at high pressures, *Phys. Rev. B* 92 (2015) 224109. doi:10.1103/PhysRevB.92.224109. URL <https://link.aps.org/doi/10.1103/PhysRevB.92.224109>
- [432] M. Gupta, J. Burger, Trends in the electron-phonon coupling parameter in some metallic hydrides, *Physical Review B* 24 (12) (1981) 7099.
- [433] J. Burger, Electron-phonon coupling and superconductivity in metal-hydrogen systems, *Journal of the Less Common Metals* 101 (1984) 53–67.
- [434] D. V. Semenov, I. A. Kruglov, A. G. Kvashnin, A. R. Oganov, On distribution of superconductivity in metal hydrides, *arXiv preprint arXiv:1806.00865*.
- [435] D. Y. Kim, R. H. Scheicher, H.-k. Mao, T. W. Kang, R. Ahuja, General trend for pressurized superconducting hydrogen-dense materials, *PNAS* 107 (7) (2010) 2793–2796. doi:10.1073/pnas.0914462107. URL <http://www.pnas.org/content/107/7/2793>
- [436] R. Dronskowski, P. E. Bloechl, Crystal orbital hamilton populations (cohp): energy-resolved visualization of chemical bonding in solids based on density-functional calculations, *The Journal of Physical Chemistry* 97 (33) (1993) 8617–8624. doi:10.1021/j100135a014. URL <https://doi.org/10.1021/j100135a014>
- [437] N. F. Berk, J. R. Schrieffer, Effect of ferromagnetic spin correlations on superconductivity, *Phys. Rev. Lett.* 17 (1966) 433–435. doi:10.1103/PhysRevLett.17.433. URL <https://link.aps.org/doi/10.1103/PhysRevLett.17.433>
- [438] K. G. McLennan, E. M. Gray, J. F. Dobson, Deuterium occupation of tetrahedral sites in palladium, *Phys. Rev. B* 78 (2008) 014104. doi:10.1103/PhysRevB.78.014104. URL <https://link.aps.org/doi/10.1103/PhysRevB.78.014104>
- [439] R. CAPUTO, A. ALAVI, Where do the h atoms reside in pdh x systems?, *Molecular Physics* 101 (11) (2003) 1781–1787. arXiv:<https://doi.org/10.1080/0026897031000094489>, doi:10.1080/0026897031000094489. URL <https://doi.org/10.1080/0026897031000094489>
- [440] A. Houari, S. F. Matar, V. Eyert, Electronic structure and crystal phase stability of palladium hydrides, *Journal of Applied Physics* 116 (17) (2014) 173706. arXiv:<https://doi.org/10.1063/1.4901004>, doi:10.1063/1.4901004. URL <https://doi.org/10.1063/1.4901004>
- [441] P. Tripodi, D. Di Gioacchino, R. Borelli, J. D. Vinko, Possibility of high temperature superconducting phases in pdh, *Physica C: Superconductivity* 388 (2003) 571–572.
- [442] H. Syed, T. Gould, C. Webb, E. Gray, Superconductivity in palladium hydride and deuteride at 52-61 kelvin, *arXiv preprint arXiv:1608.01774*.
- [443] S. Ostanin, V. Borisov, D. Fedorov, E. Salamatov, A. Ernst, I. Mertig, Role of tetrahedrally coordinated dopants in palladium hydrides on their superconductivity and inverse isotope effect, *Journal of Physics: Condensed Matter*.
- [444] J. Burger, S. Senoussi, B. Soufach, Electrical and magnetic properties of palladium hydrides compared with those of pure palladium, *Journal of the Less Common Metals* 49 (1976) 213 – 222, hydrogen in metals. doi:[https://doi.org/10.1016/0022-5088\(76\)90036-9](https://doi.org/10.1016/0022-5088(76)90036-9). URL <http://www.sciencedirect.com/science/article/pii/0022508876900369>
- [445] D. E. Eastman, J. K. Cashion, A. C. Switendick, Photoemission studies of energy levels in the palladium-hydrogen system, *Phys. Rev. Lett.* 27 (1971) 35–38. doi:10.1103/PhysRevLett.27.35. URL <https://link.aps.org/doi/10.1103/PhysRevLett.27.35>
- [446] J. M. Rowe, J. J. Rush, H. G. Smith, M. Mostoller, H. E. Flotow, Lattice dynamics of a single crystal of pdd_{0.63}, *Phys. Rev. Lett.* 33 (1974) 1297–1300. doi:10.1103/PhysRevLett.33.1297. URL <https://link.aps.org/doi/10.1103/PhysRevLett.33.1297>
- [447] O. Blaschko, R. Klemencic, P. Weinzierl, L. Pintschovius, Lattice dynamics of β -pdd_{0.78} at 85 k and ordering effects at 75 k, *Phys. Rev. B* 24 (1981) 1552–1555. doi:10.1103/PhysRevB.24.1552. URL <https://link.aps.org/doi/10.1103/PhysRevB.24.1552>
- [448] J. Burger, Electron-phonon coupling and superconductivity in palladium hydrides and deuterides, in: *Metal Hydrides*, Springer, 1981, pp. 243–253.
- [449] A. Shamp, T. Terpstra, T. Bi, Z. Falls, P. Avery, E. Zurek, Decomposition products of phosphine under pressure: Ph2 stable and superconducting?, *J. Am. Chem. Soc.* 138 (6) (2016) 1884–1892, pMID: 26777416. doi:10.1021/jacs.5b10180. URL <http://dx.doi.org/10.1021/jacs.5b10180>
- [450] F. Capitani, B. Langerome, J.-B. Brubach, P. Roy, A. Drozdov, M. I. Eremets, E. J. Nicol, J. P. Carbotte, T. Timusk, Spectroscopic evidence of a new energy scale for superconductivity in h3s, *Nature Physics* 13 (2017) 859 EP –, article. URL <http://dx.doi.org/10.1038/nphys4156>
- [451] R. Bianco, I. Errea, M. Calandra, F. Mauri, High-pressure phase diagram of hydrogen and deuterium sulfides from first principles: Structural and vibrational properties including quantum and anharmonic effects, *Phys. Rev. B* 97 (2018) 214101. doi:10.1103/PhysRevB.97.214101. URL <https://link.aps.org/doi/10.1103/PhysRevB.97.214101>
- [452] Y. Wang, Y. Ma, Perspective: Crystal structure prediction at high pressures, *The Journal of Chemical Physics* 140 (4) (2014) –. doi:<http://dx.doi.org/10.1063/1.4861966>. URL <http://scitation.aip.org/content/aip/journal/jcp/>

- 140/4/10.1063/1.4861966
- [453] Y. Yao, J. S. Tse, Superconducting hydrogen sulfide, *Chemistry A European Journal* 24 (8) (2018) 1769–1778. arXiv: <https://onlinelibrary.wiley.com/doi/pdf/10.1002/chem.201705321>, doi:10.1002/chem.201705321. URL <https://onlinelibrary.wiley.com/doi/abs/10.1002/chem.201705321>
- [454] A. Majumdar, S. T. John, Y. Yao, Mechanism for the structural transformation to the modulated superconducting phase of compressed hydrogen sulfide, *Scientific reports* 9 (1) (2019) 5023.
- [455] L. Van Hove, The occurrence of singularities in the elastic frequency distribution of a crystal, *Phys. Rev.* 89 (1953) 1189–1193. doi:10.1103/PhysRev.89.1189. URL <https://link.aps.org/doi/10.1103/PhysRev.89.1189>
- [456] Y. Quan, W. E. Pickett, Van hove singularities and spectral smearing in high-temperature superconducting H_3S , *Phys. Rev. B* 93 (2016) 104526. doi:10.1103/PhysRevB.93.104526. URL <https://link.aps.org/doi/10.1103/PhysRevB.93.104526>
- [457] T. X. R. Souza, F. Marsiglio, The possible role of van hove singularities in the high T_c of superconducting H_3S , *International Journal of Modern Physics B* 31 (25) (2017) 1745003. arXiv: <https://doi.org/10.1142/S0217979217450035>, doi:10.1142/S0217979217450035. URL <https://doi.org/10.1142/S0217979217450035>
- [458] T. Jarlborg, A. Bianconi, Breakdown of the migdal approximation at lifshitz transitions with giant zero-point motion in the H_3S superconductor, *Scientific Reports* 6 (2016) 24816 EP –.
- [459] L. Ortenzi, E. Cappelluti, L. Pietronero, Band Structure and electron-phonon coupling in H_3S : a tight-binding model, *ArXiv e-prints* arXiv:1511.04304.
- [460] C. Heil, S. Di Cataldo, G. B. Bachelet, L. Boeri, S. U. di Roma, et al., Superconductivity in sodalite-like yttrium hydride clathrates, *arXiv preprint arXiv:1901.04001*.
- [461] L. Liu, C. Wang, S. Yi, K. W. Kim, J. Kim, J.-H. Cho, Microscopic mechanism of room-temperature superconductivity in compressed LaH_{10} , *Phys. Rev. B* 99 (2019) 140501. doi:10.1103/PhysRevB.99.140501. URL <https://link.aps.org/doi/10.1103/PhysRevB.99.140501>
- [462] H. Liu, I. I. Naumov, Z. M. Geballe, M. Somayazulu, S. T. John, R. J. Hemley, Dynamics and superconductivity in compressed lanthanum superhydride, *Physical Review B* 98 (10) (2018) 100102.
- [463] P. Dalladay-Simpson, R. T. Howie, E. Gregoryanz, Evidence for a new phase of dense hydrogen above 325 gigapascals, *Nature* 529 (7584) (2016) 63–67.
- [464] M. Borinaga, I. Errea, M. Calandra, F. Mauri, A. Bergara, Anharmonic effects in atomic hydrogen: Superconductivity and lattice dynamical stability, *Phys. Rev. B* 93 (2016) 174308. doi:10.1103/PhysRevB.93.174308. URL <http://link.aps.org/doi/10.1103/PhysRevB.93.174308>
- [465] J. Flores-Livas, R. Sarmiento-Perez, S. Botti, S. Goedecker, M. A. Marques, Rare-earth magnetic nitride perovskites, *Journal of Physics: Materials*.
- [466] M. R. Filip, F. Giustino, The geometric blueprint of perovskites, *Proceedings of the National Academy of Sciences* 115 (21) (2018) 5397–5402.
- [467] Q. Xu, Z. Li, M. Liu, W.-J. Yin, Rationalizing perovskite data for machine learning and materials design, *The journal of physical chemistry letters* 9 (24) (2018) 6948–6954.
- [468] J. A. Flores-Livas, D. Tomerini, M. Amsler, A. Boziki, U. Rothlisberger, S. Goedecker, Emergence of hidden phases of methylammonium lead iodide ($\text{CH}_3\text{NH}_3\text{PbI}_3$) upon compression, *Phys. Rev. Materials* 2 (2018) 085201. doi:10.1103/PhysRevMaterials.2.085201. URL <https://link.aps.org/doi/10.1103/PhysRevMaterials.2.085201>
- [469] C. Gong, L. Li, Z. Li, H. Ji, A. Stern, Y. Xia, T. Cao, W. Bao, C. Wang, Y. Wang, et al., Discovery of intrinsic ferromagnetism in two-dimensional van der waals crystals, *Nature* 546 (7657) (2017) 265.
- [470] K. S. Novoselov, A. K. Geim, S. V. Morozov, D. Jiang, Y. Zhang, S. V. Dubonos, I. V. Grigorieva, A. A. Firsov, Electric field effect in atomically thin carbon films, *science* 306 (5696) (2004) 666–669.
- [471] N. Mounet, M. Gibertini, P. Schwaller, D. Campi, A. Merkys, A. Marrazzo, T. Sohier, I. E. Castelli, A. Cepellotti, G. Pizzi, et al., Two-dimensional materials from high-throughput computational exfoliation of experimentally known compounds, *Nature nanotechnology* 13 (3) (2018) 246.
- [472] J.-L. Reymond, M. Awale, Exploring chemical space for drug discovery using the chemical universe database, *ACS chemical neuroscience* 3 (9) (2012) 649–657.
- [473] V. M. Goldschmidt, Die gesetze der krystallochemie, *Naturwissenschaften* 14 (21) (1926) 477–485. doi:10.1007/BF01507527. URL <https://doi.org/10.1007/BF01507527>
- [474] C. Heil, L. Boeri, Influence of bonding on superconductivity in high-pressure hydrides, *Phys. Rev. B* 92 (2015) 060508. doi:10.1103/PhysRevB.92.060508. URL <https://link.aps.org/doi/10.1103/PhysRevB.92.060508>
- [475] B. Liu, W. Cui, J. Shi, L. Zhu, J. Chen, S. Lin, R. Su, J. Ma, K. Yang, M. Xu, J. Hao, A. P. Durajski, J. Qi, Y. Li, Y. Li, Effect of covalent bonding on the superconducting critical temperature of the h-s-se system, *Phys. Rev. B* 98 (2018) 174101. doi:10.1103/PhysRevB.98.174101. URL <https://link.aps.org/doi/10.1103/PhysRevB.98.174101>
- [476] X. Liang, A. Bergara, L. Wang, B. Wen, Z. Zhao, X.-F. Zhou, J. He, G. Gao, Y. Tian, Potential high- T_c superconductivity in CaH_{12} under pressure, *Phys. Rev. B* 99 (2019) 100505. doi:10.1103/PhysRevB.99.100505. URL <https://link.aps.org/doi/10.1103/PhysRevB.99.100505>
- [477] H. Xie, D. Duan, Z. Shao, H. Song, Y. Wang, X. Xiao, D. Li, F. Tian, B. Liu, T. Cui, High-temperature superconductivity in ternary clathrate CaH_{12} under high pressures, *Journal of Physics: Condensed Matter*.
- [478] R. Mohtadi, S.-i. Orimo, The renaissance of hydrides as energy materials, *Nature Reviews Materials* 2 (3) (2017) 16091.
- [479] C. Kokail, W. von der Linden, L. Boeri, Prediction of high- T_c conventional superconductivity in the ternary lithium borohydride system, *Phys. Rev. Materials* 1 (2017) 074803. doi:10.1103/PhysRevMaterials.1.074803. URL <https://link.aps.org/doi/10.1103/PhysRevMaterials.1.074803>
- [480] V. Naden Robinson, M. Marqués, Y. Wang, Y. Ma, A. Hermann, Novel phases in ammonia-water mixtures under pressure, *The Journal of chemical physics* 149 (23) (2018) 234501.
- [481] V. N. Robinson, Y. Wang, Y. Ma, A. Hermann, Stabilization of ammonia-rich hydrate inside icy planets, *Proceedings of the National Academy of Sciences* 114 (34) (2017) 9003–9008.
- [482] A. Nakanishi, T. Ishikawa, K. Shimizu, First-principles study on superconductivity of p- and cl-doped H_3S , *Journal of the Physical Society of Japan* 87 (12) (2018) 124711.
- [483] Y. Ge, F. Zhang, Y. Yao, First-principles demonstration of superconductivity at 280 K in hydrogen sulfide with low phosphorus substitution, *Phys. Rev. B* 93 (2016) 224513. doi:10.1103/PhysRevB.93.224513. URL <https://link.aps.org/doi/10.1103/PhysRevB.93.224513>
- [484] E. A. Ekimov, V. A. Sidorov, E. D. Bauer, N. N. Mel'nik, N. J. Curro, J. D. Thompson, S. M. Stishov, Superconductivity in diamond, *Nature* 428 (6982) (2004) 542–545. doi:10.1038/nature02449. URL <http://www.nature.com/nature/journal/v428/n6982/abs/nature02449.html>
- [485] L. Boeri, J. Kortus, O. K. Andersen, Three-dimensional MgB_2 -type superconductivity in hole-doped diamond, *Phys. Rev. Lett.* 93 (2004) 237002. doi:10.1103/PhysRevLett.93.237002. URL <https://link.aps.org/doi/10.1103/PhysRevLett.93.237002>
- [486] E. Bustarret, C. Marcatat, P. Achatz, J. Kačmarčík, F. Lévy, A. Huxley, L. Ortégua, E. Bourgeois, X. Blase, D. Débarre, et al., Superconductivity in doped cubic silicon, *Nature* 444 (7118) (2006) 465–468.
- [487] J. A. Flores-Livas, A. Sanna, M. Grauzinyte, A. Davydov, S. Goedecker, M. A. L. Marques, Emergence of superconductivity in doped H_2O ice

- at high pressure, *Scientific Reports* 7 (1) (2017) 6825. doi:10.1038/s41598-017-07145-4.
URL <https://doi.org/10.1038/s41598-017-07145-4>
- [488] Flores-Livas, José A., Grauzinyte, Migle, Boeri, Lilia, Profeta, Gianni, Sanna, Antonio, Superconductivity in doped polyethylene at high pressure, *Eur. Phys. J. B* 91 (8) (2018) 176.
- [489] R. K. Willardson, E. R. Weber, W. Paul, T. Suski, High pressure semiconductor physics I, Vol. 54, Academic Press, 1998.
- [490] M. Grauzinyte, S. Goedecker, J. A. Flores-Livas, Computational screening of useful hole-electron dopants in SnO_2 , *Chemistry of Materials* 29 (23) (2017) 10095–10103.
- [491] C. Freysoldt, B. Grabowski, T. Hickel, J. Neugebauer, G. Kresse, A. Janotti, C. G. Van de Walle, First-principles calculations for point defects in solids, *Rev. Mod. Phys.* 86 (2014) 253–305. doi:10.1103/RevModPhys.86.253.
URL <https://link.aps.org/doi/10.1103/RevModPhys.86.253>
- [492] F. Bruneval, J.-P. Crocombette, Ab initio formation volume of charged defects, *Phys. Rev. B* 86 (2012) 140103. doi:10.1103/PhysRevB.86.140103.
URL <https://link.aps.org/doi/10.1103/PhysRevB.86.140103>
- [493] Y. Xia, B. Yang, F. Jin, Y. Ma, X. Liu, M. Zhao, Hydrogen confined in a single wall carbon nanotube becomes a metallic and superconductive nanowire under high pressure, *Nano letters*.
- [494] S. Klotz, J. Chervin, P. Munsch, G. Le Marchand, Hydrostatic limits of 11 pressure transmitting media, *Journal of Physics D: Applied Physics* 42 (7) (2009) 075413.
- [495] C. Liu, H. Zhai, Y. Sun, W. Gong, Y. Yan, Q. Li, W. Zheng, Strain-induced modulations of electronic structure and electron-phonon coupling in dense h^3s , *Physical Chemistry Chemical Physics* 20 (8) (2018) 5952–5957.
- [496] D. Campanini, Z. Diao, A. Rydh, Raising the superconducting T_c of gallium: In situ characterization of the transformation of α -Ga into β -Ga, *Phys. Rev. B* 97 (2018) 184517. doi:10.1103/PhysRevB.97.184517.
URL <https://link.aps.org/doi/10.1103/PhysRevB.97.184517>
- [497] J. S. Kearney, M. Grauzinyte, D. Smith, D. Sneed, C. Childs, J. Hinton, C. Park, J. S. Smith, E. Kim, S. D. Fitch, et al., Pressure-tuneable visible-range band gap in the ionic spinel tin nitride, *Angewandte Chemie International Edition* 57 (36) (2018) 11623–11628.
- [498] C. Shang, Y. Q. Fang, Q. Zhang, N. Z. Wang, Y. F. Wang, Z. Liu, B. Lei, F. B. Meng, L. K. Ma, T. Wu, Z. F. Wang, C. G. Zeng, F. Q. Huang, Z. Sun, X. H. Chen, Superconductivity in the metastable $1'$ and $1''$ phases of MoS_2 crystals, *Phys. Rev. B* 98 (2018) 184513. doi:10.1103/PhysRevB.98.184513.
URL <https://link.aps.org/doi/10.1103/PhysRevB.98.184513>
- [499] A. Palnichenko, O. Vyaselev, A. Mazilkin, I. Zverkova, S. Khasanov, Metastable superconductivity of w/wO_3 interface, *Physica C: Superconductivity and its Applications* 534 (2017) 61 – 67. doi:https://doi.org/10.1016/j.physc.2017.02.002.
URL <http://www.sciencedirect.com/science/article/pii/S0921453416302830>
- [500] A. Palnichenko, I. Zverkova, D. Shakhrai, O. Vyaselev, Metastable superconductivity of $\text{mo}/\text{moo}_3\text{x}$ interface, *Physica C: Superconductivity and its Applications* 558 (2019) 25 – 29. doi:https://doi.org/10.1016/j.physc.2019.01.006.
URL <http://www.sciencedirect.com/science/article/pii/S0921453419300231>
- [501] E. Rucavado, M. Grauzinyte, J. A. Flores-Livas, Q. Jeangros, F. Landucci, Y. Lee, T. Koida, S. Goedecker, A. Hessler-Wyser, C. Ballif, et al., New route for cold-passivation of defects in tin-based oxides, *The Journal of Physical Chemistry C* 122 (31) (2018) 17612–17620.
- [502] A. Ignatiev, A. Freundlich, O. Pchelyakov, A. Nikiforov, L. Sokolov, D. Pridachin, V. Blinov, Molecular beam epitaxy in the ultravacuum of space: Present and near future, in: *Molecular Beam Epitaxy*, Elsevier, 2018, pp. 741–749.
- [503] C.-L. Song, Y.-L. Wang, Y.-P. Jiang, Z. Li, L. Wang, K. He, X. Chen, X.-C. Ma, Q.-K. Xue, Molecular-beam epitaxy and robust superconductivity of stoichiometric fese crystalline films on bilayer graphene, *Phys. Rev. B* 84 (2011) 020503. doi:10.1103/PhysRevB.84.020503.
URL <https://link.aps.org/doi/10.1103/PhysRevB.84.020503>
- [504] G. Savini, A. C. Ferrari, F. Giustino, First-principles prediction of doped graphane as a high-temperature electron-phonon superconductor, *Phys. Rev. Lett.* 105 (2010) 037002. doi:10.1103/PhysRevLett.105.037002.
URL <http://link.aps.org/doi/10.1103/PhysRevLett.105.037002>
- [505] G. Profeta, M. Calandra, F. Mauri, Phonon-mediated superconductivity in graphene by lithium deposition, *Nature Phys.* 8 (2012) 131–134.
- [506] B. M. Ludbrook, G. Levy, P. Nigge, M. Zonno, M. Schneider, D. J. Dvorak, C. N. Veenstra, S. Zhdanovich, D. Wong, P. Dosanjh, C. Straßer, A. Stöhr, S. Forti, C. R. Ast, U. Starke, A. Damascelli, Evidence for superconductivity in li-decorated monolayer graphene, *Proceedings of the National Academy of Sciences* 112 (38) (2015) 11795–11799. arXiv: <http://www.pnas.org/content/112/38/11795.full.pdf>, doi:10.1073/pnas.1510435112.
URL <http://www.pnas.org/content/112/38/11795>
- [507] A. Bouffelfel, Hydrogen effect on electron-phonon interactions in HfO_2 , *Journal of Superconductivity and Novel Magnetism* (2019) 1–9.
- [508] G. Savini, A. C. Ferrari, F. Giustino, First-principles prediction of doped graphane as a high-temperature electron-phonon superconductor, *Phys. Rev. Lett.* 105 (2010) 037002. doi:10.1103/PhysRevLett.105.037002.
URL <https://link.aps.org/doi/10.1103/PhysRevLett.105.037002>
- [509] J. Bekaert, M. Petrov, A. Aperis, P. M. Oppeneer, M. V. Milošević, Hydrogen-induced high-temperature superconductivity in two-dimensional materials: Example of hydrogenated monolayer MgB_2 , arXiv preprint arXiv:1902.03818.
- [510] S. Margadonna, K. Prassides, Recent advances in fullerene superconductivity, *Journal of Solid State Chemistry* 168 (2) (2002) 639–652.
- [511] D. S. De, J. A. Flores-Livas, S. Saha, L. Genovese, S. Goedecker, Stable structures of exohedrally decorated C_{60} -fullerenes, *Carbon* 129 (2018) 847–853.
- [512] D. Hapiuk, M. A. L. Marques, P. Melinon, J. A. Flores-Livas, S. Botti, B. Masenelli, p doping in expanded phases of ZnO : An ab initio study, *Phys. Rev. Lett.* 108 (2012) 115903. doi:10.1103/PhysRevLett.108.115903.
URL <https://link.aps.org/doi/10.1103/PhysRevLett.108.115903>
- [513] D. Hapiuk, M. Marques, P. Melinon, S. Botti, B. Masenelli, J. Flores-Livas, Superconductivity in an expanded phase of ZnO : an ab initio study, *New Journal of Physics* 17 (4) (2015) 043034.
- [514] T. E. Weller, M. Ellerby, S. S. Saxena, R. P. Smith, N. T. Skipper, Superconductivity in the intercalated graphite compounds CC_6Yb and C_6Ca , *Nat. Phys.* 1 (39–41).
URL <http://dx.doi.org/10.1038/nphys0010>
- [515] J. A. Flores-Livas, R. Debord, S. Botti, A. San Miguel, S. Pailhès, M. A. L. Marques, Superconductivity in layered binary silicides: A density functional theory study, *Phys. Rev. B* 84 (2011) 184503. doi:10.1103/PhysRevB.84.184503.
URL <https://link.aps.org/doi/10.1103/PhysRevB.84.184503>
- [516] J. A. Flores-Livas, R. Debord, S. Botti, A. San Miguel, M. A. L. Marques, S. Pailhès, Enhancing the superconducting transition temperature of BaSi_2 by structural tuning, *Phys. Rev. Lett.* 106 (2011) 087002. doi:10.1103/PhysRevLett.106.087002.
URL <https://link.aps.org/doi/10.1103/PhysRevLett.106.087002>
- [517] J. A. Flores-Livas, A. Sanna, Superconductivity in intercalated group-iv honeycomb structures, *Phys. Rev. B* 91 (2015) 054508. doi:10.1103/PhysRevB.91.054508.
URL <https://link.aps.org/doi/10.1103/PhysRevB.91.054508>
- [518] R. Mitsuhashi, Y. Suzuki, Y. Yamanari, H. Mitamura, T. Kambe, N. Ikeda, H. Okamoto, A. Fujiwara, M. Yamaji, N. Kawasaki, Y. Maniwa, Y. Kubozono, Superconductivity in alkali-metal-doped picene, *Nature* 464 (2010) 76 EP –.

- [519] X. F. Wang, R. H. Liu, Z. Gui, Y. L. Xie, Y. J. Yan, J. J. Ying, X. G. Luo, X. H. Chen, Superconductivity at 5 k in alkali-metal-doped phenanthrene, *Nature Communications* 2 (2011) 507 EP –.
- [520] M. Xue, T. Cao, D. Wang, Y. Wu, H. Yang, X. Dong, J. He, F. Li, G. F. Chen, Superconductivity above 30 k in alkali-metal-doped hydrocarbon, *Scientific Reports* 2 (2012) 389 EP –.
- [521] R.-S. Wang, Y. Gao, Z.-B. Huang, X.-J. Chen, Superconductivity above 120 kelvin in a chain link molecule, *arXiv e-prints* (2017) arXiv:1703.06641arXiv:1703.06641.
- [522] W. Liu, H. Lin, R. Kang, X. Zhu, Y. Zhang, S. Zheng, H.-H. Wen, Magnetization of potassium-doped *p*-terphenyl and *p*-quaterphenyl by high-pressure synthesis, *Phys. Rev. B* 96 (2017) 224501. doi:10.1103/PhysRevB.96.224501. URL <https://link.aps.org/doi/10.1103/PhysRevB.96.224501>
- [523] X. Leng, J. Pereiro, J. Strle, G. Dubuis, A. T. Bollinger, A. Gozar, J. Wu, N. Litombe, C. Panagopoulos, D. Pavuna, I. Božović, Insulator to metal transition in wo_3 induced by electrolyte gating, *npj Quantum Materials* 2 (1) (2017) 35.
- [524] S. Reich, G. Leitus, R. Popovitz-Biro, A. Goldbourt, S. Vega, A possible $2d \times 1 \times 1$ superconductor with a T_c of 120 K, *Journal of Superconductivity and Novel Magnetism - J SUPERCOND NOV MAGN* 22 (2009) 343–346.
- [525] Y. Saito, T. Nojima, Y. Iwasa, Gate-induced superconductivity in two-dimensional atomic crystals, *Superconductor Science and Technology* 29 (9) (2016) 093001.
- [526] K. F. Mak, C. Lee, J. Hone, J. Shan, T. F. Heinz, Atomically thin MoS_2 : A new direct-gap semiconductor, *Phys. Rev. Lett.* 105 (2010) 136805. doi:10.1103/PhysRevLett.105.136805. URL <https://link.aps.org/doi/10.1103/PhysRevLett.105.136805>
- [527] A. J. Molina-Mendoza, J. L. Lado, J. O. Island, M. A. Niño, L. Aballe, M. Foerster, F. Y. Bruno, A. López-Moreno, L. Vaquero-Garzon, H. S. J. van der Zant, G. Rubio-Bollinger, N. Agrait, E. M. Pérez, J. Fernández-Rossier, A. Castellanos-Gomez, Centimeter-scale synthesis of ultrathin layered MoO_3 by van der Waals epitaxy, *Chemistry of Materials* 28 (11) (2016) 4042–4051.
- [528] M. P. M. Dean, R. S. Springell, C. Monney, K. J. Zhou, J. Pereiro, I. Božović, B. Dalla Piazza, H. M. Rønnow, E. Morenzoni, J. van den Brink, T. Schmitt, J. P. Hill, Spin excitations in a single La_2CuO_4 layer, *Nature Materials* 11 (2012) 850 EP –.
- [529] D. Golberg, Y. Bando, Y. Huang, T. Terao, M. Mitome, C. Tang, C. Zhi, Boron nitride nanotubes and nanosheets, *ACS Nano* 4 (6) (2010) 2979–2993.
- [530] H. Tang, D. Liang, R. L. J. Qiu, X. P. A. Gao, Two-dimensional transport-induced linear magneto-resistance in topological insulator Bi_2Se_3 nanoribbons, *ACS Nano* 5 (9) (2011) 7510–7516.
- [531] D. Jiang, T. Hu, L. You, Q. Li, A. Li, H. Wang, G. Mu, Z. Chen, H. Zhang, G. Yu, J. Zhu, Q. Sun, C. Lin, H. Xiao, X. Xie, M. Jiang, High- T_c superconductivity in ultrathin $\text{Bi}_2\text{Sr}_2\text{CaCu}_2\text{O}_{8+x}$ down to half-unit-cell thickness by protection with graphene, *Nature Communications* 5 (2014) 5708 EP –.
- [532] B. Huang, G. Clark, E. Navarro-Moratalla, D. R. Klein, R. Cheng, K. L. Seyler, D. Zhong, E. Scherrigall, M. A. McGuire, D. H. Cobden, W. Yao, D. Xiao, P. Jarillo-Herrero, X. Xu, Layer-dependent ferromagnetism in a van der Waals crystal down to the monolayer limit, *Nature* 546 (2017) 270 EP –.
- [533] L. Li, Y. Yu, G. J. Ye, Q. Ge, X. Ou, H. Wu, D. Feng, X. H. Chen, Y. Zhang, Black phosphorus field-effect transistors, *Nature Nanotechnology* 9 (2014) 372 EP –.
- [534] F. Reis, G. Li, L. Dudy, M. Bauernfeind, S. Glass, W. Hanke, R. Thomale, J. Schäfer, R. Claessen, Bismuthene on a SiC substrate: A candidate for a high-temperature quantum spin Hall material, *Science* 357 (6348) (2017) 287–290.
- [535] B. Aufray, A. Kara, S. Vizzini, H. Oughaddou, C. Landri, B. Ealet, G. Le Lay, Graphene-like silicon nanoribbons on $\text{Ag}(110)$: A possible formation of silicene, *Applied Physics Letters* 96 (18) (2010) 183102. arXiv:https://doi.org/10.1063/1.3419932, doi:10.1063/1.3419932. URL <https://doi.org/10.1063/1.3419932>
- [536] J. Yuhara, H. Shimazu, K. Ito, A. Ohta, M. Aradai, M. Kurosawa, M. Nakatake, G. Le Lay, Germanene epitaxial growth by segregation through $\text{Ag}(111)$ thin films on $\text{Ge}(111)$, *ACS Nano* 12 (11) (2018) 11632–11637.
- [537] Z. Zhang, Y. Yang, G. Gao, B. I. Yakobson, Two-dimensional boron monolayers mediated by metal substrates, *Angewandte Chemie International Edition* 54 (44) (2015) 13022–13026. arXiv:https://onlinelibrary.wiley.com/doi/pdf/10.1002/anie.201505425, doi:10.1002/anie.201505425. URL <https://onlinelibrary.wiley.com/doi/abs/10.1002/anie.201505425>
- [538] C. Grimaldi, L. Pietronero, S. Straessler, Nonadiabatic superconductivity: electron-phonon interaction beyond Migdal's theorem, *Phys. Rev. Lett.* 75 (1995) 1158.
- [539] L. Boeri, E. Cappelluti, L. Pietronero, Small Fermi energy, zero-point fluctuations, and nonadiabaticity in MgB_2 , *Phys. Rev. B* 71 (2005) 012501. doi:10.1103/PhysRevB.71.012501. URL <http://link.aps.org/doi/10.1103/PhysRevB.71.012501>
- [540] Y. Yang, I. Kylänpää, N. M. Tubman, J. T. Krogel, S. Hammes-Schiffer, D. M. Ceperley, How large are nonadiabatic effects in atomic and diatomic systems?, *The Journal of chemical physics* 143 (12) (2015) 124308.
- [541] L. Bonati, M. Parrinello, Silicon liquid structure and crystal nucleation from ab initio deep metadynamics, *Phys. Rev. Lett.* 121 (2018) 265701. doi:10.1103/PhysRevLett.121.265701. URL <https://link.aps.org/doi/10.1103/PhysRevLett.121.265701>
- [542] Y. Xie, Q. Li, A. R. Oganov, H. Wang, Superconductivity of lithium-doped hydrogen under high pressure, *Acta Crystallographica Section C: Structural Chemistry* 70 (2) (2014) 104–111.
- [543] D. Zhou, X. Jin, X. Meng, G. Bao, Y. Ma, B. Liu, T. Cui, Ab initio study revealing a layered structure in hydrogen-rich KH_6 under high pressure, *Physical Review B* 86 (1) (2012) 014118.
- [544] S. Yu, Q. Zeng, A. R. Oganov, C. Hu, G. Frapper, L. Zhang, Exploration of stable compounds, crystal structures, and superconductivity in the Be-H system, *AIP Advances* 4 (10) (2014) 107118.
- [545] X. Feng, J. Zhang, G. Gao, H. Liu, H. Wang, Compressed sodalite-like MgH_6 as a potential high-temperature superconductor, *RSC Advances* 5 (73) (2015) 59292–59296.
- [546] J. Hooper, T. Terpstra, A. Shamp, E. Zurek, Composition and constitution of compressed strontium polyhydrides, *The Journal of Physical Chemistry C* 118 (12) (2014) 6433–6447.
- [547] Y. Wang, H. Wang, S. T. John, T. Itaka, Y. Ma, Structural morphologies of high-pressure polymorphs of strontium hydrides, *Physical Chemistry Chemical Physics* 17 (29) (2015) 19379–19385.
- [548] J. Hooper, B. Altintas, A. Shamp, E. Zurek, Polyhydrides of the alkaline earth metals: a look at the extremes under pressure, *The Journal of Physical Chemistry C* 117 (6) (2013) 2982–2992.
- [549] X. Ye, N. Zarifi, E. Zurek, R. Hoffmann, N. W. Ashcroft, High hydrides of scandium under pressure: potential superconductors, *The Journal of Physical Chemistry C* 122 (11) (2018) 6298–6309.
- [550] D. V. Semenok, A. G. Kvashnin, I. A. Kruglov, A. R. Oganov, Actinium hydrides AcH_{10} , AcH_{12} , and AcH_{16} as high-temperature conventional superconductors, *The journal of physical chemistry letters* 9 (8) (2018) 1920–1926.
- [551] A. G. Kvashnin, D. V. Semenok, I. A. Kruglov, I. A. Wrona, A. R. Oganov, High-temperature superconductivity in a Th-H system under pressure conditions, *ACS applied materials & interfaces* 10 (50) (2018) 43809–43816.
- [552] X. Xiao, D. Duan, H. Xie, Z. Shao, D. Li, F. Tian, H. Song, H. Yu, K. Bao, T. Cui, Structure and superconductivity of protactinium hydrides under high pressure, *Journal of Physics: Condensed Matter*. URL <http://iopscience.iop.org/10.1088/1361-648X/ab1d03>
- [553] I. A. Kruglov, A. G. Kvashnin, A. F. Goncharov, A. R. Oganov, S. S. Lobanov, N. Holtgrewe, S. Jiang, V. B. Prakapenka, E. Greenberg, A. V. Yanilkin, Uranium polyhydrides at moderate pressures: Prediction, synthesis, and expected superconductivity, *Science advances* 4 (10) (2018) eaat9776.
- [554] X. Li, F. Peng, Superconductivity of pressure-stabilized vanadium hydrides, *Inorganic chemistry* 56 (22) (2017) 13759–13765.

- [555] G. Gao, R. Hoffmann, N. W. Ashcroft, H. Liu, A. Bergara, Y. Ma, Theoretical study of the ground-state structures and properties of niobium hydrides under pressure, *Physical Review B* 88 (18) (2013) 184104.
- [556] A. P. Durajski, Phonon-mediated superconductivity in compressed nbh₄ compound, *The European Physical Journal B* 87 (9) (2014) 210.
- [557] Q. Zhuang, X. Jin, T. Cui, Y. Ma, Q. Lv, Y. Li, H. Zhang, X. Meng, K. Bao, Pressure-stabilized superconductive ionic tantalum hydrides, *Inorganic chemistry* 56 (7) (2017) 3901–3908.
- [558] S. Yu, X. Jia, G. Frapper, D. Li, A. R. Oganov, Q. Zeng, L. Zhang, Pressure-driven formation and stabilization of superconductive chromium hydrides, *Scientific reports* 5 (2015) 17764.
- [559] S. Zheng, S. Zhang, Y. Sun, J. Zhang, J. Lin, G. Yang, A. Bergara, Structural and superconducting properties of tungsten hydrides under high pressure, *Frontiers in Physics* 6 (2018) 101.
- [560] X. Li, H. Liu, F. Peng, Crystal structures and superconductivity of technetium hydrides under pressure, *Physical Chemistry Chemical Physics* 18 (41) (2016) 28791–28796.
- [561] Y. Liu, D. Duan, F. Tian, C. Wang, Y. Ma, D. Li, X. Huang, B. Liu, T. Cui, Stability and properties of the ru–h system at high pressure, *Physical Chemistry Chemical Physics* 18 (3) (2016) 1516–1520.
- [562] Y. Liu, D. Duan, X. Huang, F. Tian, D. Li, X. Sha, C. Wang, H. Zhang, T. Yang, B. Liu, et al., Structures and properties of osmium hydrides under pressure from first principle calculation, *The Journal of Physical Chemistry C* 119 (28) (2015) 15905–15911.
- [563] D. Y. Kim, R. H. Scheicher, C. J. Pickard, R. Needs, R. Ahuja, Predicted formation of superconducting platinum-hydride crystals under pressure in the presence of molecular hydrogen, *Physical review letters* 107 (11) (2011) 117002.
- [564] H. Hemmes, A. Driessen, R. Griessen, M. Gupta, Isotope effects and pressure dependence of the T_c of superconducting stoichiometric pdh and pdd synthesized and measured in a diamond anvil cell, *Physical Review B* 39 (7) (1989) 4110.
- [565] I. Errea, M. Calandra, F. Mauri, Anharmonic free energies and phonon dispersions from the stochastic self-consistent harmonic approximation: Application to platinum and palladium hydrides, *Physical Review B* 89 (6) (2014) 064302.
- [566] X.-F. Zhou, A. R. Oganov, X. Dong, L. Zhang, Y. Tian, H.-T. Wang, et al., Superconducting high-pressure phase of platinum hydride from first principles, *Physical Review B* 84 (5) (2011) 054543.
- [567] T. Matsuoka, M. Hishida, K. Kuno, N. Hirao, Y. Ohishi, S. Sasaki, K. Takahama, K. Shimizu, Superconductivity of platinum hydride, *Phys. Rev. B* 99 (2019) 144511. doi:10.1103/PhysRevB.99.144511. URL <https://link.aps.org/doi/10.1103/PhysRevB.99.144511>
- [568] K. Abe, N. Ashcroft, Crystalline diborane at high pressures, *Physical Review B* 84 (10) (2011) 104118.
- [569] P. Hou, X. Zhao, F. Tian, D. Li, D. Duan, Z. Zhao, B. Chu, B. Liu, T. Cui, High pressure structures and superconductivity of alh₃ (h₂) predicted by first principles, *RSC Advances* 5 (7) (2015) 5096–5101.
- [570] R. Szcześniak, A. Durajski, Superconducting state above the boiling point of liquid nitrogen in the gah₃ compound, *Superconductor Science and Technology* 27 (1) (2013) 015003.
- [571] Y. Liu, D. Duan, F. Tian, H. Liu, C. Wang, X. Huang, D. Li, Y. Ma, B. Liu, T. Cui, Pressure-induced structures and properties in indium hydrides, *Inorganic chemistry* 54 (20) (2015) 9924–9928.
- [572] X. Jin, X. Meng, Z. He, Y. Ma, B. Liu, T. Cui, G. Zou, H.-k. Mao, Superconducting high-pressure phases of disilane, *Proceedings of the National Academy of Sciences* 107 (22) (2010) 9969–9973.
- [573] K. Abe, N. Ashcroft, Quantum disproportionation: The high hydrides at elevated pressures, *Physical Review B* 88 (17) (2013) 174110.
- [574] T. A. Strobel, X.-J. Chen, M. Somayazulu, R. J. Hemley, Vibrational dynamics, intermolecular interactions, and compound formation in geh₄ (h₂) under pressure, *The Journal of chemical physics* 133 (16) (2010) 164512.
- [575] R. Szcze, D. Szcze, A. Durajski, et al., Thermodynamics of the superconducting phase in compressed geh₄ (h₂)₂, *Solid State Communications* 184 (2014) 6–11.
- [576] G. Zhong, C. Zhang, G. Wu, J. Song, Z. Liu, C. Yang, Superconductivity in geh₄ (h₂)₂ above 220 gpa high-pressure, *Physica B: Condensed Matter* 410 (2013) 90–92.
- [577] P. Hou, F. Tian, D. Li, Z. Zhao, D. Duan, H. Zhang, X. Sha, B. Liu, T. Cui, Ab initio study of germanium-hydride compounds under high pressure, *RSC Advances* 5 (25) (2015) 19432–19438.
- [578] M. M. D. Esfahani, A. R. Oganov, H. Niu, J. Zhang, Superconductivity and unexpected chemistry of germanium hydrides under pressure, *Physical Review B* 95 (13) (2017) 134506.
- [579] M. M. D. Esfahani, Z. Wang, A. R. Oganov, H. Dong, Q. Zhu, S. Wang, M. S. Rakitin, X.-F. Zhou, Superconductivity of novel tin hydrides (sn n h m) under pressure, *Scientific reports* 6 (2016) 22873.
- [580] Y. Cheng, C. Zhang, T. Wang, G. Zhong, C. Yang, X.-J. Chen, H.-Q. Lin, Pressure-induced superconductivity in h₂-containing hydride pbh₄ (h₂)₂, *Scientific reports* 5 (2015) 16475.
- [581] H. Liu, Y. Li, G. Gao, J. S. Tse, I. I. Naumov, Crystal structure and superconductivity of ph₃ at high pressures, *The Journal of Physical Chemistry C* 120 (6) (2016) 3458–3461.
- [582] A. P. Durajski, Quantitative analysis of nonadiabatic effects in dense h₃s and ph₃ superconductors, *Scientific reports* 6 (2016) 38570.
- [583] T. Bi, D. P. Miller, A. Shamp, E. Zurek, Superconducting phases of phosphorus hydride under pressure: stabilization by mobile molecular hydrogen, *Angewandte Chemie* 129 (34) (2017) 10326–10329.
- [584] Y. Fu, X. Du, L. Zhang, F. Peng, M. Zhang, C. J. Pickard, R. J. Needs, D. J. Singh, W. Zheng, Y. Ma, High-pressure phase stability and superconductivity of pnictogen hydrides and chemical trends for compressed hydrides, *Chemistry of Materials* 28 (6) (2016) 1746–1755.
- [585] Y. Ma, D. Duan, D. Li, Y. Liu, F. Tian, X. Huang, Z. Zhao, H. Yu, B. Liu, T. Cui, The unexpected binding and superconductivity in sbh₄ at high pressure, *arXiv preprint arXiv:1506.03889*.
- [586] Y. Ma, D. Duan, D. Li, Y. Liu, F. Tian, H. Yu, C. Xu, Z. Shao, B. Liu, T. Cui, High-pressure structures and superconductivity of bismuth hydrides, *arXiv preprint arXiv:1511.05291*.
- [587] S. Zhang, Y. Wang, J. Zhang, H. Liu, X. Zhong, H.-F. Song, G. Yang, L. Zhang, Y. Ma, Phase diagram and high-temperature superconductivity of compressed selenium hydrides, *Scientific reports* 5 (2015) 15433.
- [588] X. Zhong, H. Wang, J. Zhang, H. Liu, S. Zhang, H.-F. Song, G. Yang, L. Zhang, Y. Ma, Tellurium hydrides at high pressures: High-temperature superconductors, *Phys. Rev. Lett.* 116 (2016) 057002. doi:10.1103/PhysRevLett.116.057002. URL <https://link.aps.org/doi/10.1103/PhysRevLett.116.057002>
- [589] Y. Liu, D. Duan, F. Tian, C. Wang, G. Wu, Y. Ma, H. Yu, D. Li, B. Liu, T. Cui, Prediction of stoichiometric pohn compounds: crystal structures and properties, *RSC Adv.* 5 (2015) 103445–103450. doi:10.1039/C5RA19223D. URL <http://dx.doi.org/10.1039/C5RA19223D>
- [590] D. Duan, F. Tian, Z. He, X. Meng, L. Wang, C. Chen, X. Zhao, B. Liu, T. Cui, Hydrogen bond symmetrization and superconducting phase of hbr and hcl under high pressure: An ab initio study, *The Journal of Chemical Physics* 133 (7) (2010) 074509. arXiv:https://doi.org/10.1063/1.3471446, doi:10.1063/1.3471446. URL <https://doi.org/10.1063/1.3471446>
- [591] D. Duan, F. Tian, Y. Liu, X. Huang, D. Li, H. Yu, Y. Ma, B. Liu, T. Cui, Enhancement of T_c in the atomic phase of iodine-doped hydrogen at high pressures, *Phys. Chem. Chem. Phys.* 17 (2015) 32335–32340. doi:10.1039/C5CP05218A. URL <http://dx.doi.org/10.1039/C5CP05218A>
- [592] A. Shamp, E. Zurek, Superconducting high-pressure phases composed of hydrogen and iodine, *The Journal of Physical Chemistry Letters* 6 (20) (2015) 4067–4072, pMID: 26722778. arXiv:https://doi.org/10.1021/acs.jpclett.5b01839, doi:10.1021/acs.jpclett.5b01839. URL <https://doi.org/10.1021/acs.jpclett.5b01839>
- [593] X. Yan, Y. Chen, X. Kuang, S. Xiang, Structure, stability, and superconductivity of new xeh compounds under high pressure, *The Journal of Chemical Physics* 143 (12) (2015) 124310. arXiv:https://doi.org/10.1063/1.4931931, doi:10.1063/1.4931931. URL <https://doi.org/10.1063/1.4931931>